Title

The role of CD4 T cells in the rhesus central nervous system during homeostasis and viral-induced neuroinflammation

Author

Elizaldi, Sonny Ramirez

Publication Date

2024

Peer reviewed|Thesis/dissertation

The role of CD4 T cells in the rhesus central nervous system during homeostasis and viral-induced neuroinflammation

By

Sonny R. Elizaldi

DISSERTATION

Submitted in partial satisfaction of the requirements for the degree of

DOCTOR OF PHILOSOPHY

in

Immunology

in the

OFFICE OF GRADUATE STUDIES

of the

UNIVERSITY OF CALIFORNIA,

DAVIS

Approved:

Smita S. Iyer, Chair

Stephen J. McSorley

Lillian Cruz-Orengo

Committee in Charge

2024

ACKNOWLEDGEMENTS

I wish to express my profound appreciation to Dr. Smita Iyer, my major professor and mentor, for her invaluable contributions to both my personal and professional growth. Her guidance, advice, and unwavering support have been instrumental in my growth and development as a scientist. I am grateful for her dedication to my success and that of her students. I could never pay back all of the knowledge and wisdom she has shared with me over the years. As I continue the next phase of my scientific career transitioning to the scientific industry, I hope I can make her proud.

Thank you to my dissertation committee members, Dr. Stephen McSorley and Dr. Lillian Cruz-Orengo. Your guidance and mentorship have been instrumental in shaping my research and helping me achieve my academic goals. I am grateful for the time and effort you have devoted to reviewing my work, providing constructive criticism, and challenging me to think critically. I am honored and privileged to have had the opportunity to work with such wonderful scientists, and I will always be grateful for your contributions to my academic development.

I am grateful for the funding I have received during my time as an immunology graduate student through the NIH T32 Animal models of Infectious disease training grant. Furthermore, I appreciate CNPRC staff/veterinarian staff for the excellent care of the non-human primates; CNPRC SAIDs for their assistance in many facets including, but not limited to infections and animal sampling; CNPRC pathology for their expertise in pathology and tissue collection.

Together this work would not have been possible without the help of my current and former lab mates: Anil Verma, Yashavanth Shann Lakshmanappa, Jamin Roh, Chase Hawes, Brian Schmidt, Nancy Nguyen. I sincerely appreciate your friendship, guidance, advice, and assistance in the labor-intensive primate studies over the years.

Finally, I would like to thank my Mother (Eva) and Father (Andrew). I want to express my deep appreciation for your unwavering support and encouragement throughout my educational journey. Your sacrifice and hard work have been a constant source of inspiration to me, and I am so grateful for everything that you have done for me. I know that your journey to this country was not easy, and that you both worked tirelessly in the fields as day laborers when you first arrived in this country in search of a better life. Despite the challenges you faced, you always instilled in me the importance of education and the value of hard work. I am so grateful for the sacrifices you made to ensure that I had the opportunity to pursue my educational goals. Your love, guidance, and unwavering support have been instrumental in helping me achieve my dreams. Without your encouragement, I would not have had the confidence to pursue my passions and the determination to overcome the obstacles that I encountered along the way. I hope you know how much your sacrifice and support mean to me. I will always be grateful for the values and lessons you have taught me and for the opportunities that you have provided me. Thank you for your unwavering support and for always believing in me. This Ph.D. would not be possible without you!

DISSERTATION ABSTRACT

Despite the advent and implementation of Anti-retroviral therapy (ART) in 1987, people living with HIV (PLWH) continue to experience a high incidence of age-associated comorbidities, particularly HIV associated neurocognitive disorders (HAND) which affect 40-70% of PLWH. Research over the past four decades has predominantly focused on the role of myeloid cells in the development of HAND due, in part, to the initial discovery of HIV-infected myeloid cells in the post-mortem brain tissue of AIDS patients.

My dissertation examines the understudied role of T lymphocytes in HAND, in light of three significant advancements in the fields of HIV and neuroimmunology. Firstly, ART treatment has not only stabilized disease progression but has also led to the reconstitution and stabilization of CD4 T cells, highlighting a newfound potential role for CD4 T cells in the neurological disease process. Secondly, we now recognize that T cells are an important immune population within the central nervous system (CNS) both during homeostasis and disease. Thirdly, data from neurodegenerative diseases such as Alzheimer's, Parkinson's, and Multiple Sclerosis highlight a critical role for T cells in contributing to neuroinflammation and disease progression.

Together, these advancements collectively provide a strong rationale for developing a more comprehensive understanding of the role of T cells in HAND. Given the early establishment of transmitted/founder (T/F) HIV in the CNS, the surveillance of the CNS by CCR5 (R5) + T helper 1 cells, which serve as primary HIV targets, and the influence of T-cell derived cytokines on microglial activation, we hypothesized that T cells are pivotal in acute CNS viral seeding and neuroinflammation. We tested this hypothesis in rhesus macaques (*Macaca mulatta*) - among the most robust models for studying the CNS and HIV pathogenesis. We employed models of both acute and chronic simian HIV (SHIV) infection using distinct strains: the R5/CD4 tropic T/F SHIV C.CH505, the virulent R5-T cell-tropic SIVmac251, and the macrophage-tropic SIVCL757, used

in studies of neuro-HIV. Together, our studies with these distinct viruses offer the following insights into the role of CD4 T cells in the brain during HIV infection.

In Chapter II, we presented RNA sequencing and viral load data across four synapse-dense regions of the brain susceptible to HIV infection (Prefrontal Cortex (PFC), Superior Temporal Sulcus, Caudate Nucleus, Hippocampus). First, our data demonstrated that these synapse-dense cognitive regions are rich in immune gene signatures at homeostasis. Following infection with T/F SHIV.C.CH505, our analysis showed activation of biological pathways consistent with T cell recruitment and microglial activation. Despite relatively low plasma and cerebrospinal fluid (CSF) viral loads, we observed viral (v)RNA and vDNA within these regions - an observation aligning with infiltration of SIV infected Th1 CD4 T cells into the PFC.

In Chapter III, we delved deeply into the phenotype of CD4 T cells within the CNS, including the brain and its associated border tissues. Our rationale for this comprehensive analysis was to delineate target cells in these regions to better understand susceptibility to viral establishment. We conducted single-cell analysis of CD45+ immune cells in brain parenchyma, comparing them to counterparts in the spleen of both uninfected macaques and those acutely infected with SIVmac251. The data demonstrated colocalization of viral transcripts within CD4 clusters and furthermore showed induction of antiviral responses during acute SIV infection. This supports the observations made in Chapter II that target cells for HIV populate the CNS, including the dura, choroid plexus stroma, and the skull bone marrow. Correspondingly, during the acute phase of SIVmac251 infection, we observed significant levels of viral RNA and DNA in these regions. In animals chronically infected with SIVmac251 (40 weeks) and treated with suboptimal ART, our data demonstrated that despite CSF viral suppression, there is incomplete reconstitution of CD4 T cells in the brain and surrounding CNS tissues underscoring their active engagement during acute and chronic phases of SIVmac251 infection.

In Chapter IV, we comprehensively assessed phenotypic and functional features of CCR7+ cells identified in Chapter III. Leveraging single-transcriptomic analysis, ATAC-seq, spatial transcriptomics and flow cytometry we show that CCR7+ CD4 T cells in the brain have T lymphocyte central memory-like features. Moreover, the skull bone marrow emerged as a potential niche for CCR7+ CD4 T cells. In a cohort of macaques chronically infected (112 weeks) with SIVCL757 and treated with suboptimal ART, we noted a decrease in CCR7+ CD4 T cells within the brain in parallel with evidence for microglial activation and induction of neurodegenerative pathways. These findings suggested that changes in CD4 T cell subsets within the CNS may drive neuroinflammation during chronic HIV infection.

In summary, the findings across my three chapters lead to three major conclusions. First, the presence of both CCR5 and CCR7 CD4 T cells in the parenchymal and border regions of the CNS, renders this organ susceptible to initial HIV infection and establishment of latent reservoirs. Second, our studies of acute infection with two viruses - SHIVC.CH505 and SIVmac251- suggests that CD4 T cells within the brain parenchyma are actively engaged during acute HIV infection serving as both viral targets and mediators of neuroinflammation. Third, our models of chronic infection under suboptimal ART with two viruses - SIVmac251 and SIVCL757 - demonstrate that inadequate CD4 T cell reconstitution together with reduction of CCR7+ CD4 T cells may underlie neuroimmune dysregulation in HIV-infected patients on ART.

Dissertation Table of Contents (TOC)

Dissertation

List of Figures/Tables

Chapter 1. Introduction: Overview of HIV and viral neuroimmunology

Chapter 2. Neuroinflammatory transcriptional programs induced in rhesus pre-frontal cortex white matter during acute SHIV infection

Chapter 3. Deep Analysis of CD4 T cells in the Rhesus CNS during SIV infection

Chapter 4. Chronic SIV-Induced neuroinflammation disrupts CCR7+ CD4+ T cell immunosurveillance in the rhesus macaque brain

Conclusions and Future Directions

CHAPTER 1: Introduction: Overview of HIV and viral neuroimmunology

Introduction

My introduction presents an extensive review of the current landscape of Human Immunodeficiency virus (HIV) research. I highlight that, despite the availability of Anti-retroviral therapy (ART), there are still prominent gaps in the field centered around our understanding of HIV and inflammation in the central nervous system (CNS). Given the interconnectedness of discoveries across various domains and their influence on our understanding of HIV-associated neurocognitive disorders (HAND), the introduction spans topics ranging from the immune composition of the CNS to immune dynamics in other models of neuroinflammation for a comprehensive understanding of the neuroimmune dynamics at play.

In section 4d, I will discuss the reasoning behind our focus on T cells in HAND by highlighting existing knowledge gaps in the HAND research field (**Figure 3**). I will emphasize lessons learned in HAND from the simian immunodeficiency virus (SIV) model and highlight outstanding questions in the current models utilized. In my statement of purpose, I outline our strategy for utilizing these advancements to enhance our knowledge of the immune makeup of the CNS at homeostasis, as well as the changes in CNS immune profiles, particularly T lymphocytes, during SIV infection and neuroinflammation. Altogether, this introduction will establish a strong foundational background for Chapters II-IV of my dissertation.

Introduction Table of Contents

Chapter 1. Introduction

List of Abbreviations (intro): **HIV**- Human Immunodeficiency virus, **ART** – antiretroviral therapy, **HAND** – HIV Associated neurocognitive disorders, **CNS** – Central nervous System, **SIV** – Simian Immunodeficiency virus, **AIDS** - acquired immunodeficiency syndrome, **CDC** - center for disease control and prevention, **RNA** - Ribonucleic acid, **Env** – envelope, **gp** – glycoprotein, **CCR** – chemokine receptor, **DNA** - Deoxyribonucleic acid, **DCs** - Dendritic cells, **PLWH** - people living with HIV, **AZT** – azidothymidine, **PrEP** - pre-exposure prophylaxis, **bNAbs** - Broadly-Neutralizing Antibodies, **dpi** – days post infection, **EIA** - enzyme immunoassays, **TLR** – toll-like receptor, **IFN** – interferon, **Th** – T helper, **TNF-α** – tumor necrosis alpha, **NK** – natural killer cell, **IL** – interleukin, **IP-10** - IFN-gamma-inducible protein 10, **MHC** – major histocompatibility complex, **Gag** – group specific antigen, **Nef** – negative factor, **GALT** - gut-associated lymphoid tissue, **TGF** – transforming growth factor, **MIP** – macrophage inflammatory protein, **RANTES** - regulated upon activation normal T cell expressed and secreted, **SIVmac** – Simian Immunodeficiency Virus of macaques, **ND** – neurodegeneration, **HAD** – HIV associated dementia, **BBB** – blood brain barrier, **ROS** – reactive oxygen species, **RNS** – reactive nitrogen species, **TNF** – tumor necrosis factor, **CSF** – cerebrospinal fluid, **ChP** – choroid plexus, **SAS** – subarachnoid space, **AD** – Alzheimer's disease, $\mathbf{T_{CM}}$ – Central memory T cell, $\mathbf{T_{EM}}$ – Effector memory T cell, **BCSFB** - blood-cerebrospinal fluid barrier, **VSV** - vesicular stomatitis, $\mathbf{T_{RM}}$ – tissue resident memory, **JHMV** - JHM strain of mouse hepatitis virus, LCMV - lymphocytic choriomeningitis virus, **TMEV** - Theiler's murine encephalitis virus, **HSV-1** - herpes simplex virus 1, **WNV** – West Nile virus, **CXCL** - C-X-C motif chemokine ligand, **CCL** – chemokine ligand, **PSGL1** - P-selectin glycoprotein ligand 1, **GPCR** - G protein-couple receptor, **ICAM-1** - Intercellular Adhesion Molecule 1, **V-CAM1** - Vascular cell adhesion protein 1, **LFA-1** – lymphocyte function-associated antigen 1, **MMP**- matrix metalloproteases, **Th1** - type 1 T helper, **VLA-4** – very late antigen 4, MS – multiple sclerosis, **EAE** - Experimental autoimmune encephalomyelitis, **APCs** – antigen presenting cells, $\mathbf{T_{reg}}$ – regulatory T cell, **SHIV** – simian-human immunodeficiency virus, **wpi** – weeks post infection, **PFC** – prefrontal cortex, **ANI** – asymptomatic neurocognitive impairment, **MND** – mild neurocognitive disorder, **Apoe4** - Apolipoprotein E4 allele, **NFL** – neurofilament light protein, **Tat** – transactivator of transcription, **ACTG** - the AIDS Clinical Trials Group, **Tau** - the microtubule-associated protein, **Hipp** – Hippocampus, **CPE**- CSF Penetration-Effectiveness, **NRTIs** – nucleoside/nucleotide reverse transcriptase inhibitors, **NNRTIs** - Non-nucleoside reverse transcriptase inhibitors, **PIs** – protease inhibitors

1. HIV

a) The discovery of HIV

On June 5, 1981, the first cases of unusual opportunistic infections caused by the fungal pathogen *Pneumocystis carinii (renamed Pneumocystis jirovecii)* were identified in five homosexual men in Los Angeles, California (1). These cases marked a new disease, what would later be known as the acquired immunodeficiency syndrome or AIDS. Per the CDC, one of the primary AIDS diagnostic criteria is a CD4 T cell count below 200 cells per ml. The virus responsible for AIDS, HIV, was identified in 1983 by French scientists, Barré-Sinoussi and Luc Montagnier, who later were awarded the Nobel prize in 2008 for their discovery.

b) HIV virology

Following the identification of AIDS and the discovery of HIV as the causative agent, scientists delved deeper into understanding how this virus operates on a cellular level, particularly its mechanisms of infecting the body's immune system. HIV is a single stranded, positive sense, enveloped RNA *lentivirus* that primarily targets CD4 T cells, but also has the capacity to infect other CD4-expressing cells such as monocytes and macrophages. The infection process begins when the envelope (Env) glycoprotein, gp120, on the viral membrane binds to the CD4 molecule on the surface of a CD4 T cell. This interaction induces a conformational change in the Env protein, enabling the chemokine receptor (CCR5 or CXCR4) on the cell to bind HIV. Next, the gp41 fusion peptide of Env is inserted into the target cell membrane, resulting in the formation of a six-helix bundle followed by complete membrane fusion and viral entry (2).

Once HIV enters a cell, its RNA genome is reverse transcribed into double-stranded DNA by the viral enzyme, reverse transcriptase (3). The newly formed viral DNA is then transported into the nucleus of the cell, where it integrates into the host DNA with the help of another viral enzyme, integrase, and additional host factors. Once integrated, the viral DNA can either remain

dormant or be transcribed into new HIV RNA genomes. These genomes are then packaged and released from the cell, ready to infect neighboring cells.

While CD4 T cells are the primary targets during the acute phase of HIV-1 infection, the virus also interacts with other immune cells throughout both acute and chronic stages of infection. During acute infection, dendritic cells (DCs) can enhance the spread of infection by carrying HIV to lymph nodes, facilitating its transmission to additional T cells. In the chronic phase of infection, especially after the depletion of CD4 T cells, monocytes and macrophages emerge as significant targets of infection (4, 5). It is important to note that while HIV can infect monocytes, efficient viral replication requires suppression of the anti-HIV factor β-catenin (6). This suppression occurs as monocytes differentiate into macrophages within tissues. Additionally, CD4-independent mechanisms of HIV entry have been identified. These include entry via receptor-mediated endocytosis and the spread of HIV via direct contact between cells. Such processes have been observed in cells that are atypical targets of HIV, such as astrocytes in the brain (7). However, the ability of HIV to replicate effectively in astrocytes is limited by the presence of viral restriction factors and the activation of β-catenin signaling. Together, this highlights the ability of HIV to exploit various components of the immune system to sustain infection and spread, underscoring the need for a comprehensive understanding of these interactions to devise effective treatments.

There are two distinct types of HIV: HIV-1 and HIV-2 (8). HIV-1 was the first to be identified and is the predominant HIV type worldwide. It is known to be more aggressive and pathogenic with a greater capacity to progress to AIDS without ART. In contrast, HIV-2 was identified after HIV-1 and is mostly confined to West Africa. HIV-2 is less virulent and consequently less pathogenic compared to HIV-1. Indeed, those infected with HIV-2 rarely progress to AIDS. The origins of these viral types trace back to distinct zoonotic events, with HIV-1 originating from chimpanzee SIV (SIVcpz) and HIV-2 from sooty mangabey SIV (SIVsmm) (9).

HIV-1 exhibits significant genetic heterogeneity, comprising a diverse array of mutant and recombinant genomes collectively referred to as quasi-species. It is hypothesized that in approximately 80% of heterosexual cases, 60% of cases involving men who have sex with men and 40% of injection drug users cases, HIV-1 transmission can be traced back to a single virus particle (10-15). Transmitted or founder HIV-1 proviruses (present at transmission) have been extensively phenotyped and are nearly always CD4 and CCR5 T-cell tropic variants (10-12). For the remainder of my dissertation, I will use 'HIV' to specifically refer to HIV-1.

c) Transmission, Epidemiology, and Treatment

Understanding the genetic diversity and transmission dynamics of HIV-1 sets the stage for a deeper exploration of its impact on global health and the advances in treatment that have transformed HIV from a terminal illness to a manageable condition. HIV can be transmitted via vaginal intercourse, rectal intercourse, needle sharing or via non-sexual transmission from mother to infant during pregnancy or during vaginal delivery. Despite the numerous modalities of transmission, it is estimated that approximately 80% of adults acquiring HIV-1 are infected via mucosal surfaces (vagina and rectum), while the remaining 20% are infected by percutaneous or intravenous transmission from intravenous drug use (16). According to the World Health Organization since the epidemic began in 1981, 85.6 million people have been infected with HIV and about 40.4 million people have died of HIV. At the end of 2022, it was projected that 39 million people were living with HIV. HIV disproportionately impacts people of color and gay/bisexual men. However, while many people today are affected by HIV, it is no longer the terminal illness it was back in 1981. Today, people living with HIV (PLWH) can expect a near average life expectancy with ART (17-20). In 1987, azidothymidine (AZT; now called zidovudine; a reverse transcriptase inhibitor) was the first HIV antiretroviral drug to become licensed, providing a reduction in plasma viral RNA and overall decreased morbidity/mortality. By 1996, highly effective combination ART marked a significant advancement, greatly improving patient health and halting the progression

of disease. Most importantly, ART-mediated suppression of systemic or plasma viral loads (to below 50 viral RNA copies/ml plasma) significantly decreased the risk of transmission to an uninfected sexual partner (21). Other treatments aimed at preventing HIV infection, like pre-exposure prophylaxis (PrEP)—a combination of antiviral drugs—have been pivotal in reducing HIV cases over the years. Experts in the HIV field, including the former director of the National Institute of Allergy and Infectious Diseases, Dr. Anthony Fauci, have endorsed PrEP, which has received significant support from government funding. A major emphasis on PrEP has been established in the US, “Ending the HIV Epidemic: A plan for America” is aimed to increase testing and treatment availability with the goal of reducing the number of new infections by 75% over 5 years and by 90% within 10 years (22).

In contrast to the advancements in ART and PrEP, progress in the development of HIV vaccines and broadly neutralizing antibodies (bnAbs) has been more gradual. Historically, vaccines have been one of societies best tools in preventing the spread of viral infections, however the search for an efficacious HIV vaccine has been elusive. To date, one of the best HIV vaccine trials is known as the RV144 trial. This trial was held in Thailand in both healthy at risk men and women (n = 16,395), consisting of four priming injections of canarypox vector vaccine and two boosters of recombinant gp120 subunit vaccine (23). At the end of the trial the vaccine was found to be 31.2% efficacious in preventing HIV acquisition. While the efficacy of the RV144 falls short compared to other efficacious vaccines such as the traditional measles vaccine (96%), the trial has had the best outcomes for all HIV vaccines in the last 4 decades. The challenge in HIV vaccine development lies behind the inadequate host immune response to HIV and the vast mutability/genetic diversity of HIV. bnAbs which can recognize and neutralize the entry of various strains of HIV could be an alternative approach for immunologists to neutralize the virus even as it mutates. However, bnAbs face their own challenges, as they are rarely generated in-vivo, are

difficult to induce, and their epitopes are conformationally masked, not primed and ready to participate in the immune response (24).

d) Stages of HIV infection

HIV infection is classified into seven recognized stages known as Fiebig stages (25). Immediately following exposure to HIV-1, an eclipse phase occurs where the virus replicates in the genital mucosa, submucosa, and draining lymphoreticular tissues without yet being detectable in the systemic circulation. This phase typically lasts between 7 to 21 days (10, 26-28). Fiebig stage I is characterized by the detection of HIV-1 RNA in the blood, occurring 13-28 days post infection (dpi) (25). Fiebig stage II is characterized by the detection of p24 antigen in the blood, 18-34 dpi. P24 antigen is a core viral protein necessary for capsid assembly, ramping up once HIV-1 RNA levels rise above 10,000 copies/mL and before detectable HIV antibodies. Acute HIV infection encompasses the first 2-4 weeks of exposure, corresponding to Fiebig stages I and II. During this period, plasma viral loads are significantly high (>100,000 copies/mL) and individuals may experience bouts of flu-like symptoms, fever, lymphadenopathy, headache, skin rash, and diarrhea (29-31). This critical period of high plasma viremia is attributed to infection of CD4 T cells, myeloid cells and subsequent viral replication. A sharp increase in peripheral viral loads is paired with a massive depletion of gastrointestinal lamina propria CD4 T cells within the first 3 to 6 weeks post infection (32, 33). Additionally, during the acute phase of infection there is an intense cytokine storm, characterized by high levels of chemokines and cytokines (34). Within approximately 5 days (22-37 dpi) after testing p24 antigen positive, Fiebig stage III begins, in which HIV-1 IgM antibodies can be detected with sensitive enzyme immunoassays (EIAs). Fiebig stage IV (27-43 dpi) is classified by the development of an indeterminant Western blot test due to the evolving antibody response. Fiebig stage V (71-154 dpi) is classified by a clearly positive Western blot test and a negative p31 antigen test, with p31 being an integrase antigen promoting the integration to the host DNA. Finally, Fiebig stage VI is classified by a clear positive western

blot test and a positive p31 antigen test. Thus, Fiebig stages mark the relationship between viral replication and evolution of the immune response to HIV.

e) Innate Immune Responses to HIV

The first sign of an immune response to HIV-1 infection is the acute phase response which includes the production of alpha$_1$-antitrypsin and serum amyloid A between 3 to 5 days post infection (35). Additionally, HIV, being a single-stranded RNA virus, triggers the activation of Toll-like receptors, TLR7 and TLR8 (TLR2, TLR4, and TLR 9 have also been implicated), in DCs resulting in the release of type I interferons (IFNs) and tumor necrosis factor α (TNF-α) (36-40). The earliest cytokines generated are derived from DCs, but as infection progresses multiple cell types including monocytes, macrophages, natural killer cells (NK) and T cells contribute (41). The presence of high viral loads stimulates the induction of inflammatory cytokines, including IFN-α and interleukin-15 (IL-15) (42). While this cytokine response is essential for ramping up the anti-viral response adaptive immune, the resulting cytokine storm generated can lead to excessive immune activation and a significant loss of CD4 T cells (34). The acute cytokine storm response is first followed by a rapid induction of IFN-α, IL-15, and IFN-gamma-inducible protein 10 (IP-10), followed by a slow increase in proinflammatory factors, and eventually a sustained increase in proinflammatory factors.

Among the innate immune cells involved in the anti-viral response to HIV, epidemiological evidence points to a strong role for NK cells in viral containment. Following the acute induction of IFN-α and IL-15, NK cells expand and become activated, specifically in the acute seronegative phase (34, 43-45). Specific killer immunoglobulin receptors, expressed on NK cells, and certain major histocompatibility complex I (MHC I) alleles are linked to slower HIV disease progression and early viral control (45-47). Due to the scope of this dissertation, the overview on NK cells is brief, however the interplay between HIV and NK cells is complex and HIV has developed multiple strategies to evade detection by NK cells.

f) Adaptive Immune Responses to HIV

Long lasting durable antibodies are key to establishing life-long protection to viral infections; unfortunately, the infection acquired antibody response to HIV falls short in many ways. An early antibody response targeting the viral Env is generated in response to infection, this response is non-neutralizing and does not account for viral escape (48). It isn't until 3 or more months post infection that neutralizing antibodies targeting gp120 Env are generated; these early antibody responses are focused on non-neutralizing sites of the gp41 envelope stalk (48, 49).

One overarching principle of HIV pathogenesis is the infection and depletion of CD4 T cells, which are responsible for coordinating the adaptive immune response against many pathogens. The CD4 T cells that survive viral mediated depletion can respond to HIV antigens, but they tend to expand and progress to exhaustion, comprising long-term memory populations (50). CD4 T cells can recognize viral epitopes across all viral proteins, however there is a preference for T cell responses to the immunodominant proteins - group specific antigen (Gag) and negative factor (Nef) (51). The percentage of HIV-specific T cells that are infected in presence of high viremia are typically only a few percent, suggesting that the majority of these cells escape infection by unknown mechanisms (52). Early studies in 1985 identified a relative lack of CD4 T cell responses to HIV-1 as assessed by antigen stimulation proliferation assays (53). However, a subsequent study in 1999 found that HIV-1 specific T cells were present in low numbers at all stages of infection (54). When PLWH are treated with ART very early after infection with HIV-1, strong CD4 T cell responses to HIV-1 can be observed by lymphocyte proliferation assays (55).

During HIV and ,experimental SIV infection of primates, CD4 T cells take on various roles. First, they can suppress viral replication by secreting cytotoxic molecules such as perforin and granzyme or release soluble anti-viral factors such as CCL3, CCL4, and CCL5 which block viral entry (56). Secondly, they can perform helper functions including Th2 and T follicular helper (Tfh) mediated development of HIV-specific B cell responses and Th1 mediated help of CD8 T cell

responses (57). Third, is the Th17 subset located within the genital mucosa that prevents opportunistic bacterial and fungal infections (58). Fourth, T_{regs} can play a role in suppressing HIV specific T cell responses resulting in increased viral replication and/or reducing chronic immune activation associated with HIV persistence (59). The interaction between HIV and CD4 T cells is complex and their depletion during HIV-1 infection has resulted in a poor understanding of these populations during both acute and chronic infection.

Studies in primate models support the hypothesis that CD4 T cells and a subset of DCs called Langerhans' cells are the first targets of HIV-1 infection, with DCs playing an accessory role (60-62). Irrespective of the route of infection, the gut-associated lymphoid tissue (GALT), which is rich in T cells, serves as a major site for viral replication, undergoing viral and bystander activation-induced cell death (32, 33, 63-65). In the GALT, the main targets of infection are resting CD4 CCR6+ Th17 cells, which lack activation markers, express low levels of the chemokine receptor CCR5, and express the α4β7 integrin (66-70). Within the GALT, there is a period of rapid viral replication which is then followed by systemic dissemination reflected by a sharp rise in plasma viral RNA (71, 72). This cascade of cellular death applies to all memory CD4 T cell populations, however there may be a preference for HIV-specific cells (73). Typically, only a small percentage of HIV-specific cells are infected, even in the presence of high plasma viremia. Without ART treatment, most individuals will progress to AIDS, denoted clinically by a CD4 count below 200/ml blood.

Despite the profound depletion of CD4 T cells during acute infection, the magnitude and breadth of the CD8 T cell response to HIV is robust. This response contributes to the control of peak viremia resulting in viral set-point (viral loads ranging from 100 to 100,000 copies/ml) during the chronic phases of infection (74-76). The CD8 T cell response, which emerges near the observed peak of viremia, typically targets between one and three distinct epitopes, commonly targeting HIV-1 proteins Nef and Gag, immunodominant proteins for CD8 T cell responses (77).

The importance of a CD8 T cell response in decreasing acute viral loads is established in primate studies, where depletion of CD8 T cells results in abrogation of viral control in both acute and chronic infection (78). Furthermore, evidence shows that individuals with specific HLA-1 polymorphisms, such as HLA-B*57 and HLA-B*27 - known as elite controllers, mount stronger CD8 T cell responses to Gag, leading to superior viral control (below 50 copies/ml) in the absence of therapy. This heightened CD8 T cell response correlates with better survival outcomes, even in the absence of ART (79).

g) Chronic complications in PLWH on ART: Beyond AIDS to Aging and Persistent Immune Challenges

Transitioning from the body's initial immune response to HIV, including both the limitations of antibody production and the complex dynamics involving CD4 and CD8 T cells, it is crucial to address how modern ART has shifted the landscape of HIV management. PLWH today who are ART compliant no longer face AIDS-related illnesses but are vulnerable to chronic HIV-associated complications. PLWH are at a higher risk of chronic inflammatory disorders including cardiovascular, liver, kidney, bone, and neurological disease compared to age-matched HIV-individuals (80). Some groups have hypothesized that HIV accelerates the aging process thereby contributing to the development of these disease outcomes (81). While ART inhibits HIV replication, the virus persists in long-lived infected myeloid and T cells which contain integrated, latent, HIV DNA (82). For example, during chronic SIV infection in non-human primates, there is an increase in activated T cells which is associated with the size of the HIV reservoir (83-85). While viral replication is linked to disease progression, several studies have demonstrated that immune activation is a better predictor of disease outcomes (86). Chronic immune activation is associated with elevated circulating proinflammatory cytokines and chemokines including type I IFNs, IL-6, Transforming growth factor-β (TGF-β), IL-8, IL-1α, IL-1β, macrophage inflammatory protein 1-α (MIP-1α), MIP-1β, and Regulated upon activation normal T cell expressed and

secreted (RANTES) (87, 88). The magnitude of the cytokine storm that is generated in response to infection predicts subsequent immune activation and CD4 T cell depletion. Additionally, persistent immune activation impedes the development of IL-2-producing memory CD4 T cells, which are vital for adaptive immunity and the establishment of set-point viral loads (89, 90). Indeed, up to 10% of HIV-infected patients who progress to AIDS within the first 2-3 years of infection – classified as rapid progressors – demonstrate high levels of inflammatory markers (91). While ART effectively prevents the progression to AIDS by controlling viral replication, a new obstacle has emerged where PLWH now confront chronic complications associated with the virus and its treatment.

2. CNS and HIV

a) Evolution of HAND: From Early discoveries to Today

In the early years of the HIV epidemic during the 1980s, most individuals experienced CD4 T cell depletion and rapidly progressed to what is now known as AIDS. Postmortem examinations of brain tissue from AIDS patients revealed two significant observations: (a) the presence of HIV colocalized with macrophages in the brain (92) and (b) the development of encephalitis typified by multinucleated giant cells (93). These early clinical findings set the stage for how the field approached HAND. As such, once animal models were established in rhesus macaques, HAND models aimed to recapitulate these salient aspects found in postmortem brain tissue of AIDS patients. Early HAND models were models of accelerated disease, often involved using strains such as SIVmac251, a viral swarm of distinct quasispecies, or SIVmac239, a molecular clone derived from SIVmac251, in conjunction with CD4 or CD8 T cell depletion. These immunosuppressive models, characterized by a high frequency of SIV encephalitis and significant infection rates among monocyte, macrophage, and microglia, provided valuable insights into the HAND of the pre-ART era, but may not as accurately reflect the milder forms of cognitive impairment that typify the current etiology of HAND.

Although the incidence of HAND remains high among PLWH today (~50%), the disease has transformed dramatically since its identification in 1981 (94, 95). Over the past four decades, an increase in life expectancy has led to a higher prevalence of neurodegenerative diseases (ND), as advanced age is considered the primary risk factor for ND (96). It is important to note that older age is associated with immune senescence and exhaustion, which could compromise viral control in organs, especially within the brain (97). Furthermore, co-factors such as cardiovascular disease, obesity, diabetes, tobacco, alcohol, and drug abuse accelerate disease progression (98). Despite the suppression of viral replication with ART, PLWH are still at a high risk for cognitive impairment (99, 100). Thanks to combination ART, the disease progression of HAND has slowed down, and milder forms of disease are much more common, occurring in approximately 50% of PLWH (99, 101-103). Severe encephalitis, once frequent in the pre-ART era, is now rare, with a recent study estimating the prevalence of asymptomatic neurological impairment to be 33%, mild neurocognitive impairment to be 12%, and HIV associated dementia (HAD) to be 2% (104). Altogether, the disease landscape of HAND has changed dramatically from its early characterization in the 1980s to the present day, we see a shift from widespread encephalitis and severe cognitive impairments towards a spectrum of milder neurocognitive disorders, reflecting a changing landscape of disease development and the key players involved.

b) HIV associated Dementia and HAND

Historically, the most severe form of neurological disease in PLWH is HIV associated dementia or HAD, commonly observed in immunocompromised individuals that develop AIDS. In the pre-ART era, impaired motor function emerged as a prominent symptom among PLWH and was more likely to worsen with age (105). A pivotal study by Dr. Richard Price's Lab in 1986, found that of 70 autopsied adult AIDS patients, 46 had clinical dementia and less than 10% of the brains were histologically normal, with abnormalities primarily attributed to the white matter and subcortical structures (106). Furthermore, within the brains of demented AIDS patients, a common

observation was mild to marked atrophy (28/37 brains) and inflammation consistent with perivascular and parenchymal lymphocyte and macrophage infiltrates. Encephalitis, characterized by multinucleated giant cells formed by infected macrophages and widespread CNS infiltration of lymphocytes and macrophages, was also frequently observed (107). The basal ganglia, a dopamine-rich region of the brain, proved to be highly susceptible to HIV-related neuropathological processes, with studies documenting a 25% loss of neurons in the substantial nigra of individuals with AIDS (106, 108, 109). Altogether, this overview underscores that, before the advent of ART, HIV's involvement in the CNS resulted in severe neuropathogenesis.

c) The role of myeloid cells in HAND

In 1913, microglia and oligodendrocytes were first described by Santiago Ramón y Cajal as the third element of the CNS (110). Microglia, the brain's most abundant mononuclear macrophages, comprise 5-10% of the brain's total cell population. These tissue-resident macrophages originate as early as embryonic day 8 (111-113). This resident population can be replenished from circulating monocytes recruited across the blood brain barrier or by dividing in situ, however turnover is rather slow compared to other peripheral tissues (111, 114-118). Initially, due to the dogma of the CNS being an immune privileged site, microglia were considered static bystanders with minimal function, largely limited to phagocytic scavenging and immune surveillance. Over the past few decades, the field has begun to understand that microglia are dynamic and active, constantly monitoring the brain, utilizing their highly ramified processes with the ability to interact with all CNS components to maintain tissue integrity (119-123). Furthermore, microglia are the main cells that express complement proteins in the brain – C1q, CR3 and CR5, which are essential for synaptic pruning during development, disease-associated synapse loss and cognitive decline in aging (124, 125). Another key role for microglia, is their ability to phagocytose live, dying, and dead cells in the developing and adult brain, in addition to interacting

with local cells to maintain homeostasis, mediate developmental programs, and contribute to disease pathology/assist in tissue repair (122, 126).

As previously outlined in section 2a and 2b, myeloid cells have been a primary focus in HAND during the pre-ART era. The prevailing hypothesis posits that HIV-infected CD14+ CD16+ circulating pro-inflammatory monocytes migrate across the blood brain barrier (BBB) into the CNS and differentiate into perivascular macrophages (127). Once myeloid cells seed the CNS, they are able to disseminate replication-competent virus to resident myeloid populations (e.g. macrophages and microglia) (128, 129). Once activated, microglia and perivascular macrophages contribute to oxidative stress by releasing reactive oxygen species (ROS) and reactive nitrogen species (RNS), exacerbating the inflammatory response (130). This oxidative environment fosters the proliferation of microglia and the secretion of pro-inflammatory cytokines (IFN-γ, tumor necrosis factor alpha [TNF-α], IL-1β, IL-6, IL-8, and IL-12) during HIV infection (131, 132). Altogether, microglia release a wide range of molecules in response to HIV infection, leading to neuronal dysfunction and possible neuron death. It is important to note that much of our understanding of the behavior of microglia and impact during HAND comes from observations in immunosuppressed states (e.g. AIDS) or during chronic, late-stage infection. This context is crucial, as it suggests that our current knowledge may not fully capture the dynamic roles and responses of microglia across different stages of HIV infection and in today's population of PLWH.

d) The CNS is a viral reservoir

HIV reservoirs have been well studied in the gut and bone marrow and more recently have garnered attention within the CNS. Evidence from non-human primate models of HAND and human autopsy brain samples have revealed the presence of HIV DNA in CNS myeloid populations, indicating a possible viral reservoir (133-137). Despite ART effectively suppressing HIV systemically, there are instances where the virus can continue to replicate within the CNS, a phenomenon known as CSF escape (138, 139). Historically, CNS macrophages and microglia

are attributed as sources of sustained HIV replication in the CNS due to their longevity. However, recent findings suggest that T cells may also persist in the CNS, raising questions about their potential role as CNS viral reservoirs (133, 140, 141).

3. Neuroimmunology

a) Immune composition of the CSF

The CSF is an ultrafiltrate of the plasma, produced and filtered by ependymal cells of the choroid plexus. Ependymal cells are a highly specialized type of glial cell with a ciliated simple columnar form that lines four cerebral ventricles (two lateral, third, and fourth) and central canal of the spinal cord (142, 143). Additionally, the CSF contains interstitial fluid (~20%) that drains from the brain parenchyma to aid in removal of waste products. Altogether, the composition of the CSF is a reflection of the systemic circulation, parenchymal space, and choroid plexus (144).

The CSF plays a pivotal role in maintaining a healthy brain, functioning much like the kidneys and liver of the CNS. Moreover, the CSF cushions the brain acting as a shock absorber and allowing the brain to become buoyant effectively reducing its weight 30-fold (145). It also serves a biological role – delivering essential nutrients to the brain and aiding in the removal of waste products (146). The waste removal function of the CSF necessitates frequent turnover (4-5 times/day) (147). Consequently, impairments in CSF turnover rates, often associated with aging, are believed to contribute to the accumulation of metabolic byproducts related to the cytochrome P450 system and mitochondrial function, among others. Accumulations of byproducts, such as misfolded amyloid β and hyperphosphorylated tau protein, are linked with onset of neurodegenerative diseases, highlighting the importance of CSF turnover and metabolites in brain health (147, 148).

In healthy individuals, the CSF contains between 1,000 to 3,000 cells per ml, amounting to a total of 150,000 to 750,000 cells within its typical volume of 150mL at homeostasis. The vast majority of the cells in the CSF are lymphocytes, with T lymphocytes making up approximately

90% of the cellular composition. Similar to their counterparts in the peripheral blood, the CD4 to CD8 ratio in the CSF is heavily skewed in favor of CD4 T cells (1.5-2.5:1 vs 2.3:1, respectively) (149, 150).

CD4 T cells in the CSF are predominantly memory T cells, with few naive cells, that are likely important for immune surveillance of the CNS. These memory cells predominately comprise of central memory T cells (T_{CM}), based on expression of CCR7 and CD28, and to some extent CD28- effector memory T cells (T_{EM}) (151). One key marker that delineates CSF T cells from those found in the periphery is the expression of the acute activation marker, CD69, which is expressed on 40% of CSF T cells (vs <5% in blood) (152). While the TCR specificities in these populations remain largely unexplored, a recent study of CSF from AD patients identified a unique specificity of CSF CD8 T cells to Epstein-Barr virus, perhaps reflective of viral reactivation (153).

Additionally, the CSF contains a small percentage (about 5%) of monocytes, which are notably enriched with the CCR5 receptor (approximately 75%) – a stark contrast to their counterparts in the peripheral blood (10-20%). The high frequency of CCR5 expression on CSF monocytes highlights a unique, activated phenotype, making them potential targets for HIV infection (154), a phenotype also observed in CSF CD4 and CD8 T cells.

Table 1 offers an overview of the components of the CSF, detailing their origins from systemic, brain parenchymal, and choroid plexus compartments under both baseline conditions and during HIV infection/inflammation/injury states.

b) Immune composition of the CNS

Having explored the lymphocyte populations that comprise the CSF, I now turn our focus to the CNS, where microglia and macrophages play significant roles. Immune cells in the brain parenchyma are largely comprised of microglia, as extensively reviewed in introduction section 2c. Macrophages are found within the meninges, choroid plexus, and the perivascular spaces of

the CNS parenchyma. Both microglia and CNS macrophages are maintained by circulating blood monocytes, to varying degrees (115, 186, 187). Other immune cells such as neutrophils, granulocytes, innate lymphocytes and resident DCs have not been documented in the healthy CNS.

c) CD4 T cell composition of the CNS

Historically, the CNS was considered an immune-privileged site, believed to be impenetrable by T cells. However, today we recognize that in the presence of an intact BBB, T cell trafficking to the CNS is possible. This migration occurs either through the BBB or the blood cerebrospinal fluid barrier (BCSFB) – reviewed in section 3e. Analysis of post-mortem human brain tissue has identified the presence of CD4 memory resting T cells, CD4 memory activated T cells, and CD8 T cells (188).

Once T cells enter the brain parenchyma (reviewed in section 3e), they can maintain residence with the CNS. For instance, mouse models of vesicular stomatitis virus (VSV) infection have demonstrated the presence of CD8+CD103+ tissue resident memory (T_{RM}) within the brain parenchyma after viral clearance (189). Additionally, CD8 T_{RM} lymphocyte populations have also been identified within the human brain, alluding to a role for protection against neurotropic virus reactivation (190). Despite these insights, our understanding of T cells within the brain parenchyma at homeostasis is limited, as most of our current knowledge comes from studying T cells in the CSF or in the CNS during neuroinflammation and various disease states – reviewed in section 3f.

d) Chemokines direct immune trafficking to the CNS

Our understanding of the CNS has evolved to recognize that T lymphocytes, among other immune cells, can migrate to and reside within the CNS. This migration is facilitated by chemokine gradients that not only promote the recruitment of these cells but also their retention within the

CNS. Chemokines are low-molecular weight proteins that are a part of the cytokine superfamily and participate in immune cell trafficking by binding to their corresponding receptors (191). These molecules are instrumental in both routine immune surveillance and in directing lymphocytes across the BBB toward sites of inflammation.

Astrocytes and microglia are the primary source of chemokines during a wide variety of CNS viral infections, including JHM strain of mouse hepatitis virus (JHMV), lymphocytic choriomeningitis virus (LCMV), Theiler's murine encephalitis virus (TMEV), herpes simplex virus 1 (HSV-1), and HIV (192-195). During HIV and West Nile virus (WNV) infection, neurons secrete chemokines such as IP-10 (also known as C-X-C motif chemokine ligand 10 - CXCL10) which can promote migration of inflammatory Th1 cells to the CNS (196, 197). Moreover, IP-10, which is chronically expressed in the brains of people with HAND, can also induce neuronal death, while proteolytically cleaved CXCL12 detectable in the brains of PLWH is capable of inducing neurotoxicity and apoptosis (198). Microglia and astrocytes produce MCP-1 (also known as chemokine ligand, CCL2), which promotes migration of PBMCs across the BBB (199). Moreover, CNS endothelial cells secrete chemokine ligand 3 (CCL3), CCL4, CCL5, CCL7, and CXCL10 during SIV encephalitis (200). Similarly, in the CSF of PLWH, MCP-1, CCL5 and IP-10 are increased and hypothesized as major players in the recruitment of monocytes and T cells to the CNS (201, 202). Furthermore, CCL19 and CCL20 are constitutively expressed by the epithelial cells of the choroid plexus and endothelial cells of the BBB, which may suggest a mechanism for preferential recruitment of CCR7+ T cells for immune surveillance (203-206). However, direct evidence linking the expression of endothelial/epithelial CCL19 to T cell trafficking to the CNS at homeostasis remains elusive.

In summary, these studies underscore the role of chemokines in mediating CNS toxicity and the migration of T cells and monocytes to the CNS during HIV infection. However, our

comprehension of the specific chemokines and T cell subsets within the brain at homeostasis remain incomplete.

e) T Lymphocyte trafficking to the CNS

Immune cells can traffic to the CNS via three different routes: the parenchymal and leptomeningeal blood vessels and the choroid plexus (207). Here I will first focus on the parenchymal and leptomeningeal blood vessels which together form the BBB (208). The BBB is a critical regulator of the influx and efflux of biological substances between the brain's capillaries and its parenchyma. It is significantly more selective than peripheral capillaries, a trait attributed to its complex tight junctions between endothelial cells, making it roughly 50 to 100 times more restrictive. Once neuroinflammation begins, the endothelium of the BBB undergoes various changes. These include increased expression of adhesion molecules, secretion of pro-inflammatory cytokines and chemokines, and a decrease in the expression of tight junction molecules. Together, these changes collectively create an environment that promotes the recruitment of circulating leukocytes across the BBB (209-211).

Inflammation within the CNS parenchymal microvasculature leads to upregulation of P/E-selectin on the BBB endothelium. Once upregulated, P/E-selectin interaction with P-selectin glycoprotein ligand 1 (PSGL-1) on T cells enables T-cell rolling (212-214). Subsequently, T cells require G protein-couple receptor (GPCR) signaling to firmly arrest on the BBB, this process is known involve chemokines such as CCL20 although other contributors could be at play (215). The adhesion process involves interactions between adhesion molecules (I-CAM, V-CAM) on the endothelium and their respective ligands (lymphocyte function associate antigen 1 [LFA-1], very late antigen 4 [VLA-4]) on activated T cells, allowing T cells to firmly attach to the luminal surface of the BBB endothelium irrespective of antigen specificity (208, 216-218). Once arrested, T cells begin to search for sites permissive to initiate diapedesis across the BBB. Once T cells have successfully crossed the BBB, they enter the subarachnoid space or perivascular space where

their next obstacle is the glia limitans (219). Upon successfully navigating the glia limitans with the aid of matrix metalloproteinases (MMPs), specifically MMP-2 and MMP-9, T cells gain access to the brain parenchyma where they can initiate their effector functions, contributing to the immune surveillance and potential modulation of neuroinflammatory responses within the CNS (220). Lastly, in-vitro models of the human BBB have identified type 1 T helper (Th1) cells to be especially efficient in breaching this barrier, highlighting a significant role in the immune response within the brain (221).

The BCSFB serves as another port of entry for T lymphocytes to the brain. The trafficking of T lymphocytes across the BCSFB involves similar molecules to those at the BBB, such as E and P-selectins, LFA-1 and VLA-4, I-CAM, and V-CAM. Moreover, many of these molecules are constitutively expressed by the epithelial cells of the choroid plexus, indicating that the BCSFB is a potentially permissible site for T lymphocytes even at homeostasis (152, 222, 223). The process begins with rolling and adhesion along the endothelium of choroid plexus fenestrated capillaries. Once adhered to the endothelium, T lymphocytes navigate toward sites of extravasation, following a chemokine gradient. After crossing the endothelium, they move through the choroid plexus stroma guided by chemokines and finally traverse the apical tight junctions of the choroid plexus epithelium to enter the CSF. While the mechanisms for trafficking across the BCSFB are not as well understood as the BBB, this additional barrier proves to be a viable entry point for T cells.

During neuro-inflammation, the leptomeningeal spaces are considered a checkpoint for activated effector T cells to enter the CNS (224). Specifically, activated T cells in the leptomeninges may adhere to the leptomeningeal space to actively infiltrate the brain parenchyma. Altogether, T cells in the CSF and resident myeloid cells in the choroid plexus could serve as potential targets for HIV, suggesting that the blood-CSF barrier is a critical and early gateway for viruses to invade the brain parenchyma.

Table 2 outlines essential mediators facilitating lymphocyte entry across CNS checkpoints, and how these are perturbed during HIV infection, providing a comprehensive overview of key components facilitating this process.

f) The Role of T cells in Neuroinflammation and Neurodegenerative Diseases

Growing evidence suggests that infiltrating and local T cells in the brain play a significant role in neuroinflammation, as well as in various age-related and neurodegenerative conditions. Firstly, aged individuals experience alterations to their memory T cell pool, with these cells increasingly adopting senescent or exhausted phenotypes (225, 226). The term “Inflammageing” denotes a chronic, low-grade inflammatory state characterized by increased levels of circulating IL-6 and TNF (227, 228). Initially thought to result from the accumulation of senescent cells, recent insights have demonstrated a central role for T cells in driving inflammageing (229-231). T cells contribute to inflammageing by continuously producing IFN-γ and TNF, which drive the activation of senescent programs in both local and distant cells (230). The breakdown of the BBB in aged individuals suggests that the influx of T cells into the brain parenchyma may increase with age and age associated neurodegenerative diseases.

Among the various models of neuroinflammation, multiple sclerosis (MS) stands out as a chronic, progressive inflammatory disorder that affects the brain and spinal cord. In MS, autoreactive myelin-specific Th1 and Th17 cells are key mediators of CNS pathology. Expression of IL-17 and IFN-γ within MS brain lesions highlights the involvement of Th17 cells in disrupting the BBB, facilitating the infiltration of the parenchyma, and promoting neuroinflammation through CD4 T cell recruitment (232). Other cell types including CCR7+ myeloid cells and CCR7- T cells were found within parenchymal MS lesions of the brain, suggestive of differentiation of central memory T cells upon restimulation (233).

Experimental autoimmune encephalomyelitis (EAE), a demyelinating disease of the CNS with clinical and pathological features similar to MS, is mediated by the migration of myelin-

specific T cells that are primed in the periphery and traffic to the CNS. Once inside the CNS, T cells are reactivated by antigen presenting cells (APCs) leading to neuroinflammation, demyelination and axonal damage (234). Phenotyping of infiltrating Th subsets in EAE demonstrate that Th1 cells are the dominant subset in the CNS and the constitutive depletion of CCR7+ CD4 T cells results in an impaired induction of EAE (235-237).

Alzheimer's disease (AD) is known to be mediated by microglia and astrocytes, but recent evidence suggests that T cells are also involved in the neuroinflammatory process. Namely, during AD, BBB integrity is compromised leading to increased T cell penetration to the brain parenchyma. T cell infiltration of the CNS results in neurotoxicity and neuronal cell death by Fas ligand-LFA-1-CD40 interactions (238). Furthermore, T cells can also promote neuroinflammation by engaging in crosstalk with microglial cells and secreting proinflammatory factors, such as IFN-γ within the CNS and IL-6, TNF-α and IL-1 within the periphery (239-241).

Other neuroinflammatory models have identified different determinants responsible for lymphocyte trafficking to the brain and associated neuroinflammation. For instance, mouse models of West Nile virus (WNV) infection have highlighted CCR5 as an antiviral and survival factor that regulates leukocyte trafficking to the infected brain (242). Similarly, models of neurotropic coronavirus infection demonstrate that activated CNS stromal cells secrete CCL19 and CCL21, which support recruitment and activation of antiviral CD8 T cells to protect against neuroinflammation (243). In models of brain injury, antigen experienced T cells secrete IFN-γ at the epithelium of the choroid plexus to promote entry of leukocytes (244). In summary, this growing body of evidence underscores the pivotal role of T cells in the pathogenesis of neuroinflammation and neurodegenerative diseases, revealing their involvement in both the initiation and propagation of inflammatory processes within the CNS across various conditions and models.

g) The role of T cells in HAND

There are a limited number of studies that have begun to unravel the role of T cells in HAND. In a rhesus model of acute T/F simian-human immunodeficiency virus (SHIV)-1157ipd3N4 intra-rectal/intra-vaginal infection (12 weeks post infection, wpi), Dr. Denise Hsu at the Walter Reed Army Institute of Research and colleagues identified a low-level $CD3^{+}CD4^{-}$ brain parenchyma infiltrate, with no difference in myeloid cell populations (245). In another rhesus study, SHIV-1157ipd3N4 intra-rectal/intra-vaginal infection resulted in active viral replication (spliced viral RNA) within CSF CD4 T cells as early as 4 weeks post infection (168). Furthermore, this model demonstrated that T cell infection levels were comparable between the CSF and peripheral blood. In 2018, Dr. J. Victor Garcia at the University of North Carolina at Chapel Hill and colleagues utilized a humanized mouse model of HIV infection to demonstrate that T cells can establish and maintain HIV infection within the brain in the complete absence of human myeloid cells (246). Lastly, in severe models of HAD, SIV+ memory CD4 T cells have been shown to infiltrate the neuroparenchyma adjacent to multi-nuclear giant cells (247). Together these non-human primate models and mouse models highlight the capacity of T lymphocytes to enter the CNS during SIV/HIV infection.

When T cell infiltrates have been identified within the CSF of humans, they have been associated with neurocognitive decline, warranting further investigation (248). Once CD4 T cells enter the CNS, it is hypothesized that they rapidly disseminate the virus to local perivascular macrophages and microglial cells (128). Because CD4 T cell populations in the CNS are infrequent compared to their myeloid counterparts, an alternative T cell reservoir could exist in the border CNS compartments (i.e. choroid plexus, skull bone marrow, etc.) which could maintain infection of the parenchyma (249). Further support of this hypothesis is illustrated by the identification of high levels of IP-10, a potent chemoattractant for Th1 cells, found in the CSF of PLWH (250).

4. HAND

a) HAND Overview

While ART and PrEP are effective at suppressing viral replication, HIV continues to affect millions of people globally. PLWH today continue to experience a variety of comorbidities including cardiovascular diseases, cancers, diabetes, chronic renal disease, and neurological disorders (251, 252). Neurological disorders in PLWH, historically referred to as HAND, result from atrophy to cognitive regions of the brain (e.g. prefrontal cortex [PFC]) and present as a spectrum of asymptomatic or symptomatic cognitive, motor, and behavioral deficiencies. Classifications for HAND were developed at a research conference in Frascati, Italy in 2006 (**Table 3**) (105). These classifications were developed to diagnose a spectrum of clinical conditions observed in HAND patients, ranging from mild cognitive impairment to severe dementia, typically categorized into three progressive stages:

1. **Asymptomatic Neurocognitive Impairment (ANI**): Individuals have impaired performance on neuropsychological tests but are independent in everyday functions.
2. **Mild Neurocognitive Disorder (MND**): Cognitive impairments become more apparent and begin to mildly interfere with everyday function, although individuals remain largely independent.
3. **HIV-associated Dementia (HAD):** This is the most severe form of HAND, where cognitive, behavioral, and motor impairments are significantly debilitating and there is an inability to complete tasks independently.

b) Risk factors of HAND

There have been limited prospective studies tracking the progression of cognitive deficiencies in PLWH, making it challenging to conclusively identify risk factors. Cross sectional and short-term prospective studies have identified several risk factors for HAND. These include

early immunosuppression (exemplified by nadir CD4 counts), age, hypercholesterolemia, increased plasma concentrations of TNF-α and MCP-1, and social determinants such as lower levels of education . A longitudinal study identified PLWH with detectable plasma HIV vRNA were more likely to develop white matter atrophy than their virally suppressed counterparts, suggesting that inadequate viral suppression (due to non-compliance or drug resistance) could underlie HAND progression (253).

As many of these risk factors are controlled by host genetics, there are a handful of emerging genetic risk factor candidates of HAND. There are three primary *APOE* alleles in humans: *APOE2*, *APOE3*, and *APOE4* each confer a different level of ND risk. Apolipoprotein E4 allele (*APOE4*) has emerged as a major risk factor for the development of dementia among all ethnic groups irrespective of gender (254, 255). The Hawaii Aging with HIV cohort study found that aged PLWH with an *APOE4* genotype are at a greater risk of developing dementia compared to younger PLWH (256, 257). Additionally, a neuroimaging study found that PLWH between the ages of 60 to 80 with an *APOE4* genotype experienced deficits in white matter network structure compared to non-carriers (258). Lastly, this subset of PLWH experiences greater cognitive deficits in tests measuring executive function, attention, and working memory compared to non-carriers (259).

A polymorphism in the TNF-α gene is also overexpressed in PLWH with dementia compared to those without. Additionally, a mutation the CCL2 allele is associated with a 4.5-fold higher risk of dementia outcomes in PLWH. Conversely, a meta-analysis revealed that the CCR5 Δ32 homozygous genotype (Δ32/ Δ32) could confer protection against HIV-1 acquisition, thereby contributing to a lower prevalence of HAND. In summary, these studies demonstrate that genes regulating APOε4, TNF-α and CCL2 as risk factors for HAND.

c) Neuronal and Immune Biomarkers of HAND

Various mediators of neuroinflammation and neuronal damage are observed in the CSF after HIV infection and currently serve as biomarkers for HAND disease progression. HIV-mediated CNS damage could occur soon after infection as neurofilament light chain (NFL) is found at high amounts in the CSF and has been associated with neuronal injury (260). Neopterin, a guanosine triphosphate metabolite, produced by macrophages increases in the CSF during HIV infection and is reflective of neurological disease progression (201, 261, 262). Quinolinic acid, a normal byproduct of the kynurenine pathway, is produced by activated macrophages and microglia (263). An excess of quinolinic acid in the CNS can lead to neuronal damage, induce apoptosis of astrocytes, and promote astrocyte production of various inflammatory mediators (264). Lastly, nitric oxide is a free radical that is released by CNS myeloid cells and is proposed to contribute to neuronal injury (265).

HIV can disseminate and create viral reservoirs throughout host tissues, including the brain where non-HIV target cells such as astrocytes are documented latent reservoirs of HIV (266). Despite ART, PLWH with suppressed peripheral viral loads continue to produce neuroinflammatory mediators, such as cytokines and chemokines. In the brain, HIV proteins transactivator of transcription (Tat) and gp120 have been associated with apoptosis of striatal neurons and have been found in the basal ganglia of PLWH with encephalitis (267-272).

d) Gaps in HAND

Although HAND still affects a large proportion of the HIV community, the neuropathogenesis still remains to be a puzzle with many pieces missing. The mechanisms leading to HAND are not fully understood but involve complex interactions between viral factors, immune activation, and inflammation, particularly in the CNS. This inflammation can lead to damage in neural circuits, critical for cognitive functions. Despite the widespread use of ART, which has dramatically reduced the prevalence of the most severe forms of HAND, milder forms

persist underscoring the need for research to develop therapeutic strategies to address these neurocognitive complications.

Here I will outline the major clinical gaps in HAND, focusing on research gaps in the milder forms of HAND and then identify gaps in animal models of HAND.

di) Diagnosis and Detection

There is currently a lack of sensitive and specific biomarkers for early and accurate detection of HAND. The current gold standard for HAND diagnosis relies on a complete neurocognitive battery assessment which tests the function of five key cognitive domains (attention-information processing, language, abstraction-executive, complex perceptual motor skills, memory (including learning and recall) simple motor skills or sensory perceptual skills) (101, 273). The neurocognitive battery assessment allows for classification of individuals into 3 groups of HAND – ANI, MND, or HAD (**Table 3**). Alternatively, mental status examinations are also utilized but lack the sensitivity and specificity needed for an accurate HAND diagnosis (274-276). Thus, there is a need for biomarker predictors of neurocognitive decline to accurately diagnose milder forms of HAND and importantly identify individuals at a higher risk of progressing to advanced cognitive decline (277). While we currently lack a definitive biomarker for categorizing disease progression, ongoing longitudinal and cross-sectional research within the AIDS Clinical Trials Group (ACTG) and other HIV patient cohorts demonstrate the potential of neuronal biomarkers, like NFL and the microtubule associate protein (Tau), as well as various immune biomarkers, to provide insights into the degree of disease advancement. These data are summarized in **Figure 1.**

Another obstacle is distinguishing a HAND diagnosis from other neurological diseases such as Alzheimer's. While Alzheimer's has been historically known as a disease primarily associated with Tau and amyloid beta proteins, it is becoming clearer that these proteins are also associated with HAND (278). Altogether these data emphasize the need to establish stronger

biomarker criteria for the diagnosis of HAND and classification among other neurological disorders.

Lastly, there is a limited number of diagnostic tools available for resource limited settings. In Third World countries it is not possible to perform neurocognitive battery assessments due to lack of trained professionals and limited access to healthcare in remote areas. A blood or CSF biomarker would allow professionals to obtain samples from local clinics to preform further evaluation at a local hospital.

dii) Understanding Pathogenesis

Another clinical gap is pinpointing the timing of **HIV entry to the CNS.** Studies of PLWH have demonstrated that HIV can breach the CNS compartment as early as the first 2 weeks (8 days presumed) post initial exposure (279). While this study detected viral RNA in the CSF during the initial eclipse phase and Fiebig I stage of HIV infection, it remains unclear whether the presence of the virus in the CSF is indicative of its entry into cognitive regions of the brain, such as the PFC and hippocampus (Hipp). The primary question in understanding acute viral entry to the brain centers on delineating **cellular carriers -** either monocyte or T cells, both identified as potential targets during the acute phase of infection.

The next question is, what is **the involvement of CNS gateways/barriers (described in Table 2) in HAND?** Is the entry of HIV into the brain occurring across the BBB or the BCSFB? As previously stated, the BBB is a highly selective barrier due to tight junctions formed between endothelial cells and astrocyte end feet. While the BBB is characterized as dysfunctional in the chronic phase of infection with identification of lesions and multinucleated giant cells (280), it remains to be determined if acute focal lesions are responsible for initial viral CNS dissemination, when peripheral viral loads are high. Following viral entry to the CNS during acute infection, mediators of inflammation and immune activation are rapidly induced within the CSF and brain parenchyma (279, 281, 282).

Clinically, untreated HIV-1 infection of leads to persistent inflammation, however it is still not known what **inflammatory processes occur to the CNS during primary infection?** Moreover, it is uncertain whether CNS immune activation alone is sufficient for the progression of HAND? While neuroinflammation appears to be the primary culprit of many neurological diseases, HIV-1 viral proteins have garnered attention for their potentially neurotoxic effect both in vitro and in vivo (196, 283-285). Ultimately, the question remains: which viral and/or immune mechanistic processes underlie the development of HIV associated damage to the CNS?

diii) Treatment

A big challenge in HAND is the establishment of **HIV reservoirs** in the CNS – where despite viral suppression with ART there are latently infected cells within the tissue that can serve as life-long reservoirs of virus. It remains to be determined if these reservoirs are established because of one entry event into the CNS or multiple entry events over the course of infection. While ART controls peripheral viral loads, there are some outstanding questions about the ability of ART to penetrate the CNS to prevent viral replication. More interestingly, potential egress of HIV-infected CD4 T cells from the CNS could in turn contribute to peripheral viral loads underscoring the importance of CNS viral suppression (7). As such, CNS penetrance effectiveness (CPE) scores of ART drugs, based on chemical properties, CSF concentrations, and effectiveness in suppressing CNS viral loads, have been assigned to more effectively target viral replication in CNS tissues – reviewed extensively elsewhere (286). In chapters III and IV, we utilized a standard 3-drug ART regimen used in the US that comprised of Tenofovir (Nucleoside/nucleotide reverse transcriptase inhibitor [NRTI]; low CPE), Emtricitabine (NRTI; moderate CPE) and Dolutegravir (Integrase Inhibitor; high CPE). In Third World countries, access to ART is mostly limited to generic ART regimens. Reports from WHO estimate that 87% of PLWH in Third World countries are treated with a combination of Lamivudine (NRTI; low/moderate CPE), which is easy to take and has low toxicity, and Tenofovir (287). The limited access of ART and low

CPE of ART used in Third World countries results in a disproportionate amount of PLWH that succumb to many chronic diseases, including HAND (288).

Microglia are potential targets of HIV infection within the CNS with a long half-life, as they have been found to not turnover without irradiation of the brain (289). These long-lived infected microglia among other cells composing the HIV reservoir within the CNS could contribute to long term neuroinflammation and neurodegeneration in HAND. Additionally, the CNS viral reservoir also impedes on the clinician's hope of utilizing full body irradiation to target all HIV reservoirs within the entire body. Furthermore, recent studies have identified that HIV can **independently replicate within the CNS despite suppression of systemic viral loads via ART** (138, 139). Novel ART regimens with better CNS penetrance may provide some long-term therapeutic benefit for HAND and can help suppress these long-term CNS reservoirs.

Another challenge is **CNS compartmentalization of virus**. This is when HIV-1 variants exist within the CNS that are genetically distinct from the blood (290-293). These compartmentalized viral clones create a formidable obstacle in eliminating viral populations within the CNS, requiring new approaches and cure strategies. Lastly, clinicians **mainly rely on biomarkers within blood** and CSF samples to gain insight into the pathological processes occurring within the brain. While many markers such as IP-10, NFL, and MCP-1 are associated with HAND progression, clinicians are still searching for a biomarker that can be used to evaluate the initial onset of disease and guide directed therapy for at risk-population groups (294-296). These clinical gaps underscore the need for robust animal models to study acute viral entry into the brain parenchyma especially within synapse dense regions of the brain responsible for cognition. An overview of HAND, Core diagnostic criterion are outlined in **Figure 1**. Putative supportive criterion encompassing neuronal and immune biomarkers to delineate the categories of HAND to improve diagnosis and detection of HAND are identified.

In summary, the clinical gaps identified underscore the need to understand mechanisms underlying pathogenesis of HAND which necessitate the use of primate models which recapitulate the disease process. These gaps encompass but are not limited to identifying acute cellular mediators of viral influx into the CNS and neuroinflammation and in mapping cellular players of chronic viral persistence and neuroinflammation.

e) Primate models to understand mechanisms

Since the discovery of HAND in 1986, monkey models were developed to study HIV-1 pathology within the brain (297, 298). As such, rhesus macaques were chosen to study HIV-1 pathology, as infection of macaques with SIV closely mimicked the kinetics and disease progression seen in humans (299). Early rhesus models developed to study HAND were models of accelerated CNS disease, reflecting the severe neuropathogenesis often observed in humans infected with HIV in the 1980s. These accelerated models commonly utilized SIVmac251 for infection paired with depletion of either CD4 or CD8 T cells. These animals develop a high incidence of encephalitis (50-100%) and experience a high rate of infected myeloid cells within the CNS, a common observation in postmortem brain tissue of AIDS patients. These early models were aimed at evaluating the pathological manifestations seen in AIDS patients and were successful at evaluating late-stage disease.

Over the past 40+ years the landscape of HAND has shifted substantially, while the frequency of disease among PLWH and animal models used to study the disease have remained largely the same. Most HAND animal models today still utilize pathogenic strains such as SIVmac251 and SIVmac239 in combination with CD4 or CD8 T cell depletion strategies to study HAND. Some newer animal models have emerged utilizing neurotropic strains of SIV that have been passaged in macaques for infectivity of local CNS populations, namely monocytes and macrophages, to accurately recapitulate late-stage disease. While these models have their purpose, newer animal models should focus on the current state of HAND, consistent with natural

disease progression and reservoir infection of the brain (**see Table 4**). Most importantly, these animal models **should be immune sufficient** as HIV-1 infection today with regular ART rarely results in progression to AIDS and encephalitis. Models utilizing SIVmac251 infection alone without T cell depletion are more likely to recapitulate salient aspects of HAND.

The rhesus macaque model plays a pivotal role in addressing key gaps in the study of CNS tissues, especially in the context of HAND disease progression (**see Figure 2**). Unlike human studies, which are often limited to post-mortem tissue analysis or CSF assessment, this animal model offers the significant advantage of examining all CNS tissues cross-sectionally at various critical controlled timepoints during infection. This comprehensive approach is crucial for evaluating not only distinct areas of the brain parenchyma but also the adjacent CNS border tissues, a component of the CNS that remains under-explored. My dissertation leverages the rhesus macaque model to probe three critical questions that aim to bridge these identified gaps as outlined below.

5. Statement of purpose

Global population data predicts that the number of people over the age of 60 will sharply rise in the next couple of decades, with estimations projecting this population to double by 2050. This sharp rise in aged individuals is expected to also introduce a greater burden of neurodegenerative diseases on the healthcare system, as age is the primary risk factor for neurodegeneration and subsequent neurocognitive impairment. One demographic at a much higher risk of developing age-related neurodegenerative diseases are PLWH. Despite considerable advancements in the treatment of PLWH, HAND continues to pose challenges. As detailed in previous sections, this is primarily due to a limited understanding of the mechanisms involved, particularly those concerning which immune cells are responsible for acute HIV infiltration of the CNS via the BBB and BCSFB, the role of immune cells in the CNS in activating neuroinflammatory pathways, and the chronic events driving both viral persistence and inflammatory processes. To begin to understand the role of CD4 T cells in HAND, we posited that answering fundamental questions conceptualized in **Figure 3** would be critical.

To address these knowledge gaps, we adopted the rhesus macaque model (*Macaca mulatta*), the gold-standard model of HIV pathogenesis, which offers two major advantages for studying HAND: firstly, it allows for the study of neocortical structures which are absent in mice; secondly, the model exhibits neuropathology similar to that observed in PLWH. This approach is aimed at gaining a deeper understanding of the inflammatory processes underlying acute and chronic neuroinflammation in HAND.

In Chapter II of my dissertation, we focus on a study using transmitted/founder (T/F), R5, T-cell tropic virus SHIV.CH505 – a virus uniformly dependent on CD4 for cellular entry. This study was designed to investigate the early stages of CNS viral seeding and associated neuroinflammatory gene signatures during the acute phase of infection. Although T cells in the humans and NHP CSF have been extensively studied, one of the critical areas lacking depth is

our understanding of T cell populations within the brain parenchyma. We utilized this T/F infection model to evaluate T cell gene signatures and SHIV induced transcriptional changes within synapse-dense regions of the brain in the setting of low to moderate plasma and CSF viral loads. Lastly, this chapter identifies evidence of increased CSF IP-10 paired with an increased frequency of Th1 cells infiltrating the pre-frontal cortex, alluding to an active role for T cells in neuroinflammation. This approach sets the groundwork for a deeper understanding of not only CD4 T cells but local immune populations such as microglia and monocytes in the brain parenchyma during homeostasis and their disruption during acute infection.

In Chapter III of my dissertation, we expanded on the foundation laid in Chapter II, this time employing a more pathogenic T-cell tropic strain, SIVmac251 to achieve peripheral viral loads typically observed during primary HIV infection. A cohort of infected animals received sub-optimal ART to recapitulate viral dynamics associated with HAND progression. Our objective was to evaluate HIV target T cell subsets within the brain parenchyma. Specifically, T lymphocyte subsets expressing CCR5/CD69 versus those expressing CCR7- during homeostasis and acute/chronic infection in the context of high plasma and CSF viral loads. This chapter addresses a critical gap in the field by delineating the cellular mediators of acute CNS viral infiltration and seeding, key events in establishing CNS infection and reservoirs. An additional focus of this chapter was in pinpointing the extent of CNS viral spread during both acute and chronic infection, particularly asking whether virus reaches brain regions responsible for cognitive functions, learning, and memory. Lastly, we deeply investigated CD45+ immune populations in the brain to gain a comprehensive understanding of the impact of HIV on the immune composition and T effector gene signatures induced during acute SIV infection.

In Chapter IV, we utilized a neurotropic virus, SIVCL757, passaged in non-human primates for tropism in myeloid cells, namely microglia and monocytes. The novelty of this study was the utilization of SIVCL757 to study the progression of neuroinflammation into the chronic phase of

infection as our study longitudinally evaluated peripheral blood and CSF with a cross sectional reading of the CNS tissues at 2 years post SIV infection in the setting of ART. Similar to Chapter II and III, this study continues to evaluate the T lymphocyte populations that comprise the rhesus macaque brain during homeostasis and disease with a specific focus on a CCR7+ CD4 memory subset. Here, we leveraged our accessibility of multiple CNS compartments, including understudied areas such as the dura mater and skull bone marrow, to extensively characterize the CCR7+ T cell populations found in the CNS. Our pivotal finding in this study was the observed decrease of CCR7+ CD4 T cells in the brain during SIV infection, alluding to a role of these cells in immune surveillance and an active response to chronic SIV infection.

Altogether, dissertation chapters II-IV make several key contributions to the field. Firstly, our research with primate models provides conclusive evidence that immunocompetent macaques infected with R5, T-cell tropic viruses serve as effective models for studying HIV CNS dissemination and acute/chronic neuroinflammatory pathways (addressing gaps in primate models outlined in Section 4e). Secondly, regarding immune composition, our data clearly illustrate the presence of distinct CD4 T cell subsets in all regions of the CNS contributing to our understanding of memory T cell subsets outlined in Section 3b. Finally, our studies reveal dysregulation in both the frequencies and subsets of CD4 T cells during chronic neuroinflammation contributing to gaps outlined in section 4dii. These findings described herein provide a foundation for future studies to investigate the mechanistic role of specific CD4 T cell subsets in the pathogenesis of HAND.

References

1. Anonymous. 1991. The HIV/AIDS epidemic: the first 10 years. MMWR Morb Mortal Wkly Rep 40:357.
2. Wilen CB, Tilton JC, Doms RW. 2012. HIV: cell binding and entry. Cold Spring Harb Perspect Med 2.
3. Simon V, Ho DD, Abdool Karim Q. 2006. HIV/AIDS epidemiology, pathogenesis, prevention, and treatment. Lancet 368:489-504.
4. Campbell JH, Hearps AC, Martin GE, Williams KC, Crowe SM. 2014. The importance of monocytes and macrophages in HIV pathogenesis, treatment, and cure. Aids 28:2175-87.
5. Wu L, KewalRamani VN. 2006. Dendritic-cell interactions with HIV: infection and viral dissemination. Nat Rev Immunol 6:859-68.
6. Aljawai Y, Richards MH, Seaton MS, Narasipura SD, Al-Harthi L. 2014. β-Catenin/TCF-4 signaling regulates susceptibility of macrophages and resistance of monocytes to HIV-1 productive infection. Curr HIV Res 12:164-73.
7. Lutgen V, Narasipura SD, Barbian HJ, Richards M, Wallace J, Razmpour R, Buzhdygan T, Ramirez SH, Prevedel L, Eugenin EA, Al-Harthi L. 2020. HIV infects astrocytes in vivo and egresses from the brain to the periphery. PLoS Pathog 16:e1008381.
8. Nyamweya S, Hegedus A, Jaye A, Rowland-Jones S, Flanagan KL, Macallan DC. 2013. Comparing HIV-1 and HIV-2 infection: Lessons for viral immunopathogenesis. Rev Med Virol 23:221-40.
9. Sharp PM, Hahn BH. 2011. Origins of HIV and the AIDS pandemic. Cold Spring Harb Perspect Med 1:a006841.
10. Keele BF, Giorgi EE, Salazar-Gonzalez JF, Decker JM, Pham KT, Salazar MG, Sun C, Grayson T, Wang S, Li H, Wei X, Jiang C, Kirchherr JL, Gao F, Anderson JA, Ping LH, Swanstrom R, Tomaras GD, Blattner WA, Goepfert PA, Kilby JM, Saag MS, Delwart EL, Busch MP, Cohen MS, Montefiori DC, Haynes BF, Gaschen B, Athreya GS, Lee HY, Wood N, Seoighe C, Perelson AS, Bhattacharya T, Korber BT, Hahn BH, Shaw GM. 2008. Identification and characterization of transmitted and early founder virus envelopes in primary HIV-1 infection. Proc Natl Acad Sci U S A 105:7552-7.
11. Salazar-Gonzalez JF, Salazar MG, Keele BF, Learn GH, Giorgi EE, Li H, Decker JM, Wang S, Baalwa J, Kraus MH, Parrish NF, Shaw KS, Guffey MB, Bar KJ, Davis KL, Ochsenbauer-Jambor C, Kappes JC, Saag MS, Cohen MS, Mulenga J, Derdeyn CA, Allen S, Hunter E, Markowitz M, Hraber P, Perelson AS, Bhattacharya T, Haynes BF, Korber BT, Hahn BH, Shaw GM. 2009. Genetic identity, biological phenotype, and evolutionary pathways of transmitted/founder viruses in acute and early HIV-1 infection. Journal of Experimental Medicine 206:1273-1289.
12. Li H, Bar KJ, Wang S, Decker JM, Chen Y, Sun C, Salazar-Gonzalez JF, Salazar MG, Learn GH, Morgan CJ, Schumacher JE, Hraber P, Giorgi EE, Bhattacharya T, Korber BT, Perelson AS, Eron JJ, Cohen MS, Hicks CB, Haynes BF, Markowitz M, Keele BF, Hahn BH, Shaw GM. 2010. High Multiplicity Infection by HIV-1 in Men Who Have Sex with Men. PLoS Pathog 6:e1000890.
13. Keele BF, Li H, Learn GH, Hraber P, Giorgi EE, Grayson T, Sun C, Chen Y, Yeh WW, Letvin NL, Mascola JR, Nabel GJ, Haynes BF, Bhattacharya T, Perelson AS, Korber BT, Hahn BH, Shaw GM. 2009. Low-dose rectal inoculation of rhesus macaques by SIVsmE660 or SIVmac251 recapitulates human mucosal infection by HIV-1. J Exp Med 206:1117-34.
14. Abrahams MR, Anderson JA, Giorgi EE, Seoighe C, Mlisana K, Ping LH, Athreya GS, Treurnicht FK, Keele BF, Wood N, Salazar-Gonzalez JF, Bhattacharya T, Chu H, Hoffman I, Galvin S, Mapanje C, Kazembe P, Thebus R, Fiscus S, Hide W, Cohen MS,

Karim SA, Haynes BF, Shaw GM, Hahn BH, Korber BT, Swanstrom R, Williamson C. 2009. Quantitating the multiplicity of infection with human immunodeficiency virus type 1 subtype C reveals a non-poisson distribution of transmitted variants. J Virol 83:3556-67.
15. Haaland RE, Hawkins PA, Salazar-Gonzalez J, Johnson A, Tichacek A, Karita E, Manigart O, Mulenga J, Keele BF, Shaw GM, Hahn BH, Allen SA, Derdeyn CA, Hunter E. 2009. Inflammatory genital infections mitigate a severe genetic bottleneck in heterosexual transmission of subtype A and C HIV-1. PLoS Pathog 5:e1000274.
16. AIDS GU. 2010. Global Report 2010.
17. Crum NF, Riffenburgh RH, Wegner S, Agan BK, Tasker SA, Spooner KM, Armstrong AW, Fraser S, Wallace MR. 2006. Comparisons of causes of death and mortality rates among HIV-infected persons: analysis of the pre-, early, and late HAART (highly active antiretroviral therapy) eras. J Acquir Immune Defic Syndr 41:194-200.
18. Di Carlo P, Immordino P, Mazzola G, Colletti P, Alongi I, Mineo M, Scognamillo M, Vitale F, Casuccio A. 2014. Determinants of HIV outpatient service utilization according to HIV parameters. J Int AIDS Soc 17:19611.
19. Hunt PW. 2014. HIV and aging: emerging research issues. Curr Opin HIV AIDS 9:302-8.
20. van Sighem AI, Gras LA, Reiss P, Brinkman K, de Wolf F. 2010. Life expectancy of recently diagnosed asymptomatic HIV-infected patients approaches that of uninfected individuals. Aids 24:1527-35.
21. Cohen MS, Chen YQ, McCauley M, Gamble T, Hosseinipour MC, Kumarasamy N, Hakim JG, Kumwenda J, Grinsztejn B, Pilotto JHS, Godbole SV, Mehendale S, Chariyalertsak S, Santos BR, Mayer KH, Hoffman IF, Eshleman SH, Piwowar-Manning E, Wang L, Makhema J, Mills LA, de Bruyn G, Sanne I, Eron J, Gallant J, Havlir D, Swindells S, Ribaudo H, Elharrar V, Burns D, Taha TE, Nielsen-Saines K, Celentano D, Essex M, Fleming TR. 2011. Prevention of HIV-1 Infection with Early Antiretroviral Therapy. New England Journal of Medicine 365:493-505.
22. Fauci AS, Lane HC. 2020. Four Decades of HIV/AIDS — Much Accomplished, Much to Do. New England Journal of Medicine 383:1-4.
23. Kim JH, Excler JL, Michael NL. 2015. Lessons from the RV144 Thai phase III HIV-1 vaccine trial and the search for correlates of protection. Annu Rev Med 66:423-37.
24. Burton DR, Desrosiers RC, Doms RW, Koff WC, Kwong PD, Moore JP, Nabel GJ, Sodroski J, Wilson IA, Wyatt RT. 2004. HIV vaccine design and the neutralizing antibody problem. Nature Immunology 5:233-236.
25. Fiebig EW, Wright DJ, Rawal BD, Garrett PE, Schumacher RT, Peddada L, Heldebrant C, Smith R, Conrad A, Kleinman SH, Busch MP. 2003. Dynamics of HIV viremia and antibody seroconversion in plasma donors: implications for diagnosis and staging of primary HIV infection. Aids 17:1871-9.
26. Weiss HA, Dickson KE, Agot K, Hankins CA. 2010. Male circumcision for HIV prevention: current research and programmatic issues. Aids 24 Suppl 4:S61-9.
27. Emau P, Jiang Y, Agy MB, Tian B, Bekele G, Tsai CC. 2006. Post-exposure prophylaxis for SIV revisited: animal model for HIV prevention. AIDS Res Ther 3:29.
28. Lee HY, Giorgi EE, Keele BF, Gaschen B, Athreya GS, Salazar-Gonzalez JF, Pham KT, Goepfert PA, Kilby JM, Saag MS, Delwart EL, Busch MP, Hahn BH, Shaw GM, Korber BT, Bhattacharya T, Perelson AS. 2009. Modeling sequence evolution in acute HIV-1 infection. J Theor Biol 261:341-60.
29. Anonymous. 2001. Diagnosis of Primary HIV-1 Infection. Annals of Internal Medicine 134:25-29.
30. Hecht FM, Busch MP, Rawal B, Webb M, Rosenberg E, Swanson M, Chesney M, Anderson J, Levy J, Kahn JO. 2002. Use of laboratory tests and clinical symptoms for identification of primary HIV infection. Aids 16:1119-29.

31. Robb ML, Eller LA, Kibuuka H, Rono K, Maganga L, Nitayaphan S, Kroon E, Sawe FK, Sinei S, Sriplienchan S, Jagodzinski LL, Malia J, Manak M, de Souza MS, Tovanabutra S, Sanders-Buell E, Rolland M, Dorsey-Spitz J, Eller MA, Milazzo M, Li Q, Lewandowski A, Wu H, Swann E, O'Connell RJ, Peel S, Dawson P, Kim JH, Michael NL. 2016. Prospective Study of Acute HIV-1 Infection in Adults in East Africa and Thailand. New England Journal of Medicine 374:2120-2130.
32. Brenchley JM, Schacker TW, Ruff LE, Price DA, Taylor JH, Beilman GJ, Nguyen PL, Khoruts A, Larson M, Haase AT, Douek DC. 2004. CD4+ T cell depletion during all stages of HIV disease occurs predominantly in the gastrointestinal tract. J Exp Med 200:749-59.
33. Mehandru S, Poles MA, Tenner-Racz K, Horowitz A, Hurley A, Hogan C, Boden D, Racz P, Markowitz M. 2004. Primary HIV-1 infection is associated with preferential depletion of CD4+ T lymphocytes from effector sites in the gastrointestinal tract. J Exp Med 200:761-70.
34. Stacey AR, Norris PJ, Qin L, Haygreen EA, Taylor E, Heitman J, Lebedeva M, DeCamp A, Li D, Grove D, Self SG, Borrow P. 2009. Induction of a Striking Systemic Cytokine Cascade prior to Peak Viremia in Acute Human Immunodeficiency Virus Type 1 Infection, in Contrast to More Modest and Delayed Responses in Acute Hepatitis B and C Virus Infections. Journal of Virology 83:3719-3733.
35. Kramer HB, Lavender KJ, Qin L, Stacey AR, Liu MK, di Gleria K, Simmons A, Gasper-Smith N, Haynes BF, McMichael AJ, Borrow P, Kessler BM. 2010. Elevation of intact and proteolytic fragments of acute phase proteins constitutes the earliest systemic antiviral response in HIV-1 infection. PLoS Pathog 6:e1000893.
36. Diebold SS, Kaisho T, Hemmi H, Akira S, Reis e Sousa C. 2004. Innate Antiviral Responses by Means of TLR7-Mediated Recognition of Single-Stranded RNA. Science 303:1529-1531.
37. Heil F, Hemmi H, Hochrein H, Ampenberger F, Kirschning C, Akira S, Lipford G, Wagner H, Bauer S. 2004. Species-specific recognition of single-stranded RNA via toll-like receptor 7 and 8. Science 303:1526-9.
38. Beignon A-S, McKenna K, Skoberne M, Manches O, DaSilva I, Kavanagh DG, Larsson M, Gorelick RJ, Lifson JD, Bhardwaj N. 2005. Endocytosis of HIV-1 activates plasmacytoid dendritic cells via Toll-like receptor– viral RNA interactions. The Journal of Clinical Investigation 115:3265-3275.
39. Thibault S, Fromentin R, Tardif MR, Tremblay MJ. 2009. TLR2 and TLR4 triggering exerts contrasting effects with regard to HIV-1 infection of human dendritic cells and subsequent virus transfer to CD4+T cells. Retrovirology 6:42.
40. Martinelli E, Cicala C, Van Ryk D, Goode DJ, Macleod K, Arthos J, Fauci AS. 2007. HIV-1 gp120 inhibits TLR9-mediated activation and IFN-α secretion in plasmacytoid dendritic cells. Proceedings of the National Academy of Sciences 104:3396-3401.
41. Borrow P, Bhardwaj N. 2008. Innate immune responses in primary HIV-1 infection. Curr Opin HIV AIDS 3:36-44.
42. Gasper-Smith N, Crossman DM, Whitesides JF, Mensali N, Ottinger JS, Plonk SG, Moody MA, Ferrari G, Weinhold KJ, Miller SE, Reich CF, 3rd, Qin L, Self SG, Shaw GM, Denny TN, Jones LE, Pisetsky DS, Haynes BF. 2008. Induction of plasma (TRAIL), TNFR-2, Fas ligand, and plasma microparticles after human immunodeficiency virus type 1 (HIV-1) transmission: implications for HIV-1 vaccine design. J Virol 82:7700-10.
43. Biron CA. 1999. Initial and innate responses to viral infections--pattern setting in immunity or disease. Curr Opin Microbiol 2:374-81.
44. Alter G, Teigen N, Ahern R, Streeck H, Meier A, Rosenberg ES, Altfeld M. 2007. Evolution of Innate and Adaptive Effector Cell Functions during Acute HIV-1 Infection. The Journal of Infectious Diseases 195:1452-1460.

45. Alter G, Martin MP, Teigen N, Carr WH, Suscovich TJ, Schneidewind A, Streeck H, Waring M, Meier A, Brander C, Lifson JD, Allen TM, Carrington M, Altfeld M. 2007. Differential natural killer cell-mediated inhibition of HIV-1 replication based on distinct KIR/HLA subtypes. J Exp Med 204:3027-36.
46. Martin MP, Gao X, Lee J-H, Nelson GW, Detels R, Goedert JJ, Buchbinder S, Hoots K, Vlahov D, Trowsdale J, Wilson M, O'Brien SJ, Carrington M. 2002. Epistatic interaction between KIR3DS1 and HLA-B delays the progression to AIDS. Nature Genetics 31:429-434.
47. Martin MP, Qi Y, Gao X, Yamada E, Martin JN, Pereyra F, Colombo S, Brown EE, Shupert WL, Phair J, Goedert JJ, Buchbinder S, Kirk GD, Telenti A, Connors M, O'Brien SJ, Walker BD, Parham P, Deeks SG, McVicar DW, Carrington M. 2007. Innate partnership of HLA-B and KIR3DL1 subtypes against HIV-1. Nature Genetics 39:733-740.
48. Tomaras GD, Yates NL, Liu P, Qin L, Fouda GG, Chavez LL, Decamp AC, Parks RJ, Ashley VC, Lucas JT, Cohen M, Eron J, Hicks CB, Liao HX, Self SG, Landucci G, Forthal DN, Weinhold KJ, Keele BF, Hahn BH, Greenberg ML, Morris L, Karim SS, Blattner WA, Montefiori DC, Shaw GM, Perelson AS, Haynes BF. 2008. Initial B-cell responses to transmitted human immunodeficiency virus type 1: virion-binding immunoglobulin M (IgM) and IgG antibodies followed by plasma anti-gp41 antibodies with ineffective control of initial viremia. J Virol 82:12449-63.
49. Wei X, Decker JM, Wang S, Hui H, Kappes JC, Wu X, Salazar-Gonzalez JF, Salazar MG, Kilby JM, Saag MS, Komarova NL, Nowak MA, Hahn BH, Kwong PD, Shaw GM. 2003. Antibody neutralization and escape by HIV-1. Nature 422:307-12.
50. Kamimura D, Bevan MJ. 2007. Naive CD8+ T cells differentiate into protective memory-like cells after IL-2 anti IL-2 complex treatment in vivo. J Exp Med 204:1803-12.
51. Kaufmann DE, Bailey PM, Sidney J, Wagner B, Norris PJ, Johnston MN, Cosimi LA, Addo MM, Lichterfeld M, Altfeld M, Frahm N, Brander C, Sette A, Walker BD, Rosenberg ES. 2004. Comprehensive analysis of human immunodeficiency virus type 1-specific CD4 responses reveals marked immunodominance of gag and nef and the presence of broadly recognized peptides. J Virol 78:4463-77.
52. Walker B, McMichael A. 2012. The T-cell response to HIV. Cold Spring Harb Perspect Med 2.
53. Lane HC, Depper JM, Greene WC, Whalen G, Waldmann TA, Fauci AS. 1985. Qualitative analysis of immune function in patients with the acquired immunodeficiency syndrome. Evidence for a selective defect in soluble antigen recognition. N Engl J Med 313:79-84.
54. Pitcher CJ, Quittner C, Peterson DM, Connors M, Koup RA, Maino VC, Picker LJ. 1999. HIV-1-specific CD4+ T cells are detectable in most individuals with active HIV-1 infection, but decline with prolonged viral suppression. Nat Med 5:518-25.
55. Rosenberg ES, Altfeld M, Poon SH, Phillips MN, Wilkes BM, Eldridge RL, Robbins GK, D'Aquila RT, Goulder PJ, Walker BD. 2000. Immune control of HIV-1 after early treatment of acute infection. Nature 407:523-6.
56. Lusso P. 2006. HIV and the chemokine system: 10 years later. The EMBO Journal 25:447-456.
57. Wan YY. 2010. Multi-tasking of helper T cells. Immunology 130:166-71.
58. Klatt NR, Brenchley JM. 2010. Th17 cell dynamics in HIV infection. Curr Opin HIV AIDS 5:135-40.
59. Sempere JM, Soriano V, Benito JM. 2007. T regulatory cells and HIV infection. AIDS Rev 9:54-60.

60. Hladik F, Sakchalathorn P, Ballweber L, Lentz G, Fialkow M, Eschenbach D, McElrath MJ. 2007. Initial events in establishing vaginal entry and infection by human immunodeficiency virus type-1. Immunity 26:257-70.
61. Boggiano C, Littman DR. 2007. HIV's vagina travelogue. Immunity 26:145-7.
62. Lackner AA, Veazey RS. 2007. Current concepts in AIDS pathogenesis: insights from the SIV/macaque model. Annu Rev Med 58:461-76.
63. Mattapallil JJ, Douek DC, Hill B, Nishimura Y, Martin M, Roederer M. 2005. Massive infection and loss of memory CD4+ T cells in multiple tissues during acute SIV infection. Nature 434:1093-7.
64. Douek DC, Roederer M, Koup RA. 2009. Emerging concepts in the immunopathogenesis of AIDS. Annu Rev Med 60:471-84.
65. Veazey RS, DeMaria M, Chalifoux LV, Shvetz DE, Pauley DR, Knight HL, Rosenzweig M, Johnson RP, Desrosiers RC, Lackner AA. 1998. Gastrointestinal Tract as a Major Site of CD4⁺ T Cell Depletion and Viral Replication in SIV Infection. Science 280:427-431.
66. Zhang Z, Schuler T, Zupancic M, Wietgrefe S, Staskus KA, Reimann KA, Reinhart TA, Rogan M, Cavert W, Miller CJ, Veazey RS, Notermans D, Little S, Danner SA, Richman DD, Havlir D, Wong J, Jordan HL, Schacker TW, Racz P, Tenner-Racz K, Letvin NL, Wolinsky S, Haase AT. 1999. Sexual transmission and propagation of SIV and HIV in resting and activated CD4+ T cells. Science 286:1353-7.
67. Zhang ZQ, Wietgrefe SW, Li Q, Shore MD, Duan L, Reilly C, Lifson JD, Haase AT. 2004. Roles of substrate availability and infection of resting and activated CD4+ T cells in transmission and acute simian immunodeficiency virus infection. Proc Natl Acad Sci U S A 101:5640-5.
68. Li Q, Duan L, Estes JD, Ma ZM, Rourke T, Wang Y, Reilly C, Carlis J, Miller CJ, Haase AT. 2005. Peak SIV replication in resting memory CD4+ T cells depletes gut lamina propria CD4+ T cells. Nature 434:1148-52.
69. Arthos J, Cicala C, Martinelli E, Macleod K, Van Ryk D, Wei D, Xiao Z, Veenstra TD, Conrad TP, Lempicki RA, McLaughlin S, Pascuccio M, Gopaul R, McNally J, Cruz CC, Censoplano N, Chung E, Reitano KN, Kottilil S, Goode DJ, Fauci AS. 2008. HIV-1 envelope protein binds to and signals through integrin alpha4beta7, the gut mucosal homing receptor for peripheral T cells. Nat Immunol 9:301-9.
70. Kader M, Wang X, Piatak M, Lifson J, Roederer M, Veazey R, Mattapallil JJ. 2009. Alpha4(+)beta7(hi)CD4(+) memory T cells harbor most Th-17 cells and are preferentially infected during acute SIV infection. Mucosal Immunol 2:439-49.
71. Chun TW, Engel D, Berrey MM, Shea T, Corey L, Fauci AS. 1998. Early establishment of a pool of latently infected, resting CD4(+) T cells during primary HIV-1 infection. Proc Natl Acad Sci U S A 95:8869-73.
72. Richman DD, Margolis DM, Delaney M, Greene WC, Hazuda D, Pomerantz RJ. 2009. The challenge of finding a cure for HIV infection. Science 323:1304-7.
73. Douek DC, Brenchley JM, Betts MR, Ambrozak DR, Hill BJ, Okamoto Y, Casazza JP, Kuruppu J, Kunstman K, Wolinsky S, Grossman Z, Dybul M, Oxenius A, Price DA, Connors M, Koup RA. 2002. HIV preferentially infects HIV-specific CD4+ T cells. Nature 417:95-8.
74. Plata F, Autran B, Martins LP, Wain-Hobson S, Raphaël M, Mayaud C, Denis M, Guillon JM, Debré P. 1987. AIDS virus-specific cytotoxic T lymphocytes in lung disorders. Nature 328:348-51.
75. Walker BD, Chakrabarti S, Moss B, Paradis TJ, Flynn T, Durno AG, Blumberg RS, Kaplan JC, Hirsch MS, Schooley RT. 1987. HIV-specific cytotoxic T lymphocytes in seropositive individuals. Nature 328:345-8.

76. Nixon DF, Townsend AR, Elvin JG, Rizza CR, Gallwey J, McMichael AJ. 1988. HIV-1 gag-specific cytotoxic T lymphocytes defined with recombinant vaccinia virus and synthetic peptides. Nature 336:484-7.
77. Lichterfeld M, Yu XG, Cohen D, Addo MM, Malenfant J, Perkins B, Pae E, Johnston MN, Strick D, Allen TM, Rosenberg ES, Korber B, Walker BD, Altfeld M. 2004. HIV-1 Nef is preferentially recognized by CD8 T cells in primary HIV-1 infection despite a relatively high degree of genetic diversity. Aids 18:1383-92.
78. Schmitz JE, Kuroda MJ, Santra S, Sasseville VG, Simon MA, Lifton MA, Racz P, Tenner-Racz K, Dalesandro M, Scallon BJ, Ghrayeb J, Forman MA, Montefiori DC, Rieber EP, Letvin NL, Reimann KA. 1999. Control of viremia in simian immunodeficiency virus infection by CD8+ lymphocytes. Science 283:857-60.
79. Pereyra F, Jia X, McLaren PJ, Telenti A, de Bakker PI, Walker BD, Ripke S, Brumme CJ, Pulit SL, Carrington M, Kadie CM, Carlson JM, Heckerman D, Graham RR, Plenge RM, Deeks SG, Gianniny L, Crawford G, Sullivan J, Gonzalez E, Davies L, Camargo A, Moore JM, Beattie N, Gupta S, Crenshaw A, Burtt NP, Guiducci C, Gupta N, Gao X, Qi Y, Yuki Y, Piechocka-Trocha A, Cutrell E, Rosenberg R, Moss KL, Lemay P, O'Leary J, Schaefer T, Verma P, Toth I, Block B, Baker B, Rothchild A, Lian J, Proudfoot J, Alvino DM, Vine S, Addo MM, Allen TM, et al. 2010. The major genetic determinants of HIV-1 control affect HLA class I peptide presentation. Science 330:1551-7.
80. Deeks SG, Tracy R, Douek DC. 2013. Systemic effects of inflammation on health during chronic HIV infection. Immunity 39:633-45.
81. Desquilbet L, Jacobson LP, Fried LP, Phair JP, Jamieson BD, Holloway M, Margolick JB, Study ftMAC. 2007. HIV-1 Infection Is Associated With an Earlier Occurrence of a Phenotype Related to Frailty. The Journals of Gerontology: Series A 62:1279-1286.
82. Siliciano JD, Kajdas J, Finzi D, Quinn TC, Chadwick K, Margolick JB, Kovacs C, Gange SJ, Siliciano RF. 2003. Long-term follow-up studies confirm the stability of the latent reservoir for HIV-1 in resting CD4+ T cells. Nat Med 9:727-8.
83. Hunt PW, Brenchley J, Sinclair E, McCune JM, Roland M, Page-Shafer K, Hsue P, Emu B, Krone M, Lampiris H, Douek D, Martin JN, Deeks SG. 2008. Relationship between T cell activation and CD4+ T cell count in HIV-seropositive individuals with undetectable plasma HIV RNA levels in the absence of therapy. J Infect Dis 197:126-33.
84. Hatano H, Jain V, Hunt PW, Lee TH, Sinclair E, Do TD, Hoh R, Martin JN, McCune JM, Hecht F, Busch MP, Deeks SG. 2013. Cell-based measures of viral persistence are associated with immune activation and programmed cell death protein 1 (PD-1)-expressing CD4+ T cells. J Infect Dis 208:50-6.
85. Srinivasula S, Lempicki RA, Adelsberger JW, Huang CY, Roark J, Lee PI, Rupert A, Stevens R, Sereti I, Lane HC, Di Mascio M, Kovacs JA. 2011. Differential effects of HIV viral load and CD4 count on proliferation of naive and memory CD4 and CD8 T lymphocytes. Blood 118:262-70.
86. Deeks SG, Kitchen CM, Liu L, Guo H, Gascon R, Narváez AB, Hunt P, Martin JN, Kahn JO, Levy J, McGrath MS, Hecht FM. 2004. Immune activation set point during early HIV infection predicts subsequent CD4+ T-cell changes independent of viral load. Blood 104:942-7.
87. Valdez H, Lederman MM. 1997. Cytokines and cytokine therapies in HIV infection. AIDS Clin Rev:187-228.
88. Appay V, Sauce D. 2008. Immune activation and inflammation in HIV-1 infection: causes and consequences. J Pathol 214:231-41.
89. Younes S-A, Yassine-Diab B, Dumont AR, Boulassel M-R, Grossman Z, Routy J-P, Sékaly R-P. 2003. HIV-1 Viremia Prevents the Establishment of Interleukin 2–producing HIV-specific Memory CD4+ T Cells Endowed with Proliferative Capacity. Journal of Experimental Medicine 198:1909-1922.

90. Harari A, Vallelian F, Pantaleo G. 2004. Phenotypic heterogeneity of antigen-specific CD4 T cells under different conditions of antigen persistence and antigen load. European Journal of Immunology 34:3525-3533.
91. Wendel BS, Fu Y, He C, Hernandez SM, Qu M, Zhang Z, Jiang Y, Han X, Xu J, Ding H, Jiang N, Shang H. 2020. Rapid HIV Progression Is Associated with Extensive Ongoing Somatic Hypermutation. J Immunol 205:587-594.
92. Wiley CA, Schrier RD, Nelson JA, Lampert PW, Oldstone MB. 1986. Cellular localization of human immunodeficiency virus infection within the brains of acquired immune deficiency syndrome patients. Proc Natl Acad Sci U S A 83:7089-93.
93. Navia BA, Price RW. 1987. The acquired immunodeficiency syndrome dementia complex as the presenting or sole manifestation of human immunodeficiency virus infection. Arch Neurol 44:65-9.
94. Robertson KR, Smurzynski M, Parsons TD, Wu K, Bosch RJ, Wu J, McArthur JC, Collier AC, Evans SR, Ellis RJ. 2007. The prevalence and incidence of neurocognitive impairment in the HAART era. Aids 21:1915-21.
95. Harezlak J, Buchthal S, Taylor M, Schifitto G, Zhong J, Daar E, Alger J, Singer E, Campbell T, Yiannoutsos C, Cohen R, Navia B. 2011. Persistence of HIV-associated cognitive impairment, inflammation, and neuronal injury in era of highly active antiretroviral treatment. Aids 25:625-33.
96. Farooqui T, Farooqui AA. 2009. Aging: An important factor for the pathogenesis of neurodegenerative diseases. Mechanisms of Ageing and Development 130:203-215.
97. Mekker A, Tchang VS, Haeberli L, Oxenius A, Trkola A, Karrer U. 2012. Immune senescence: relative contributions of age and cytomegalovirus infection. PLoS Pathog 8:e1002850.
98. McCutchan JA, Marquie-Beck JA, Fitzsimons CA, Letendre SL, Ellis RJ, Heaton RK, Wolfson T, Rosario D, Alexander TJ, Marra C, Ances BM, Grant I. 2012. Role of obesity, metabolic variables, and diabetes in HIV-associated neurocognitive disorder. Neurology 78:485-92.
99. Heaton RK, Clifford DB, Franklin DR, Jr., Woods SP, Ake C, Vaida F, Ellis RJ, Letendre SL, Marcotte TD, Atkinson JH, Rivera-Mindt M, Vigil OR, Taylor MJ, Collier AC, Marra CM, Gelman BB, McArthur JC, Morgello S, Simpson DM, McCutchan JA, Abramson I, Gamst A, Fennema-Notestine C, Jernigan TL, Wong J, Grant I. 2010. HIV-associated neurocognitive disorders persist in the era of potent antiretroviral therapy: CHARTER Study. Neurology 75:2087-96.
100. Chow FC. 2014. HIV infection, vascular disease, and stroke. Semin Neurol 34:35-46.
101. Woods SP, Moore DJ, Weber E, Grant I. 2009. Cognitive neuropsychology of HIV-associated neurocognitive disorders. Neuropsychol Rev 19:152-68.
102. Dore GJ, McDonald A, Li Y, Kaldor JM, Brew BJ. 2003. Marked improvement in survival following AIDS dementia complex in the era of highly active antiretroviral therapy. Aids 17:1539-45.
103. Nightingale S, Winston A, Letendre S, Michael BD, McArthur JC, Khoo S, Solomon T. 2014. Controversies in HIV-associated neurocognitive disorders. Lancet Neurol 13:1139-1151.
104. Heaton RK, Franklin DR, Ellis RJ, McCutchan JA, Letendre SL, Leblanc S, Corkran SH, Duarte NA, Clifford DB, Woods SP, Collier AC, Marra CM, Morgello S, Mindt MR, Taylor MJ, Marcotte TD, Atkinson JH, Wolfson T, Gelman BB, McArthur JC, Simpson DM, Abramson I, Gamst A, Fennema-Notestine C, Jernigan TL, Wong J, Grant I. 2011. HIV-associated neurocognitive disorders before and during the era of combination antiretroviral therapy: differences in rates, nature, and predictors. J Neurovirol 17:3-16.
105. Antinori A, Arendt G, Becker JT, Brew BJ, Byrd DA, Cherner M, Clifford DB, Cinque P, Epstein LG, Goodkin K, Gisslen M, Grant I, Heaton RK, Joseph J, Marder K, Marra CM,

McArthur JC, Nunn M, Price RW, Pulliam L, Robertson KR, Sacktor N, Valcour V, Wojna VE. 2007. Updated research nosology for HIV-associated neurocognitive disorders. Neurology 69:1789-99.
106. Navia BA, Jordan BD, Price RW. 1986. The AIDS dementia complex: I. Clinical features. Ann Neurol 19:517-24.
107. Ambrosius B, Gold R, Chan A, Faissner S. 2019. Antineuroinflammatory drugs in HIV-associated neurocognitive disorders as potential therapy. Neurol Neuroimmunol Neuroinflamm 6:e551.
108. Aylward EH, Henderer JD, McArthur JC, Brettschneider PD, Harris GJ, Barta PE, Pearlson GD. 1993. Reduced basal ganglia volume in HIV-1-associated dementia: results from quantitative neuroimaging. Neurology 43:2099-104.
109. Berger JR, Arendt G. 2000. HIV dementia: the role of the basal ganglia and dopaminergic systems. J Psychopharmacol 14:214-21.
110. Pérez-Cerdá F, Sánchez-Gómez MV, Matute C. 2015. Pío del Río Hortega and the discovery of the oligodendrocytes. Frontiers in Neuroanatomy 9.
111. Ginhoux F, Greter M, Leboeuf M, Nandi S, See P, Gokhan S, Mehler MF, Conway SJ, Ng LG, Stanley ER, Samokhvalov IM, Merad M. 2010. Fate Mapping Analysis Reveals That Adult Microglia Derive from Primitive Macrophages. Science 330:841-845.
112. Hoeffel G, Ginhoux F. 2015. Ontogeny of Tissue-Resident Macrophages. Frontiers in Immunology 6.
113. Ginhoux F, Guilliams M. 2016. Tissue-Resident Macrophage Ontogeny and Homeostasis. Immunity 44:439-449.
114. Lawson LJ, Perry VH, Gordon S. 1992. Turnover of resident microglia in the normal adult mouse brain. Neuroscience 48:405-415.
115. Ajami B, Bennett JL, Krieger C, Tetzlaff W, Rossi FMV. 2007. Local self-renewal can sustain CNS microglia maintenance and function throughout adult life. Nature Neuroscience 10:1538-1543.
116. Hashimoto D, Chow A, Noizat C, Teo P, Beasley MB, Leboeuf M, Becker CD, See P, Price J, Lucas D, Greter M, Mortha A, Boyer SW, Forsberg EC, Tanaka M, van Rooijen N, García-Sastre A, Stanley ER, Ginhoux F, Frenette PS, Merad M. 2013. Tissue-resident macrophages self-maintain locally throughout adult life with minimal contribution from circulating monocytes. Immunity 38:792-804.
117. Sheng J, Ruedl C, Karjalainen K. 2015. Most Tissue-Resident Macrophages Except Microglia Are Derived from Fetal Hematopoietic Stem Cells. Immunity 43:382-93.
118. Réu P, Khosravi A, Bernard S, Mold JE, Salehpour M, Alkass K, Perl S, Tisdale J, Possnert G, Druid H, Frisén J. 2017. The Lifespan and Turnover of Microglia in the Human Brain. Cell Rep 20:779-784.
119. Nimmerjahn A, Kirchhoff F, Helmchen F. 2005. Resting Microglial Cells Are Highly Dynamic Surveillants of Brain Parenchyma in Vivo. Science 308:1314-1318.
120. Tremblay M-È, Lowery RL, Majewska AK. 2010. Microglial Interactions with Synapses Are Modulated by Visual Experience. PLOS Biology 8:e1000527.
121. Wake H, Moorhouse AJ, Jinno S, Kohsaka S, Nabekura J. 2009. Resting Microglia Directly Monitor the Functional State of Synapses In Vivo and Determine the Fate of Ischemic Terminals. The Journal of Neuroscience 29:3974-3980.
122. Frost JL, Schafer DP. 2016. Microglia: Architects of the Developing Nervous System. Trends Cell Biol 26:587-597.
123. Colonna M, Butovsky O. 2017. Microglia Function in the Central Nervous System During Health and Neurodegeneration. Annual Review of Immunology 35:441-468.
124. Zhang Y, Chen K, Sloan SA, Bennett ML, Scholze AR, O'Keeffe S, Phatnani HP, Guarnieri P, Caneda C, Ruderisch N, Deng S, Liddelow SA, Zhang C, Daneman R, Maniatis T, Barres BA, Wu JQ. 2014. An RNA-Sequencing Transcriptome and Splicing

Database of Glia, Neurons, and Vascular Cells of the Cerebral Cortex. The Journal of Neuroscience 34:11929-11947.
125. Hong S, Beja-Glasser VF, Nfonoyim BM, Frouin A, Li S, Ramakrishnan S, Merry KM, Shi Q, Rosenthal A, Barres BA, Lemere CA, Selkoe DJ, Stevens B. 2016. Complement and microglia mediate early synapse loss in Alzheimer mouse models. Science 352:712-716.
126. Schafer DP, Stevens B. 2015. Microglia Function in Central Nervous System Development and Plasticity. Cold Spring Harb Perspect Biol 7:a020545.
127. Veenstra M, León-Rivera R, Li M, Gama L, Clements JE, Berman JW. 2017. Mechanisms of CNS Viral Seeding by HIV(+) CD14(+) CD16(+) Monocytes: Establishment and Reseeding of Viral Reservoirs Contributing to HIV-Associated Neurocognitive Disorders. mBio 8.
128. Hellmuth J, Valcour V, Spudich S. 2015. CNS reservoirs for HIV: implications for eradication. J Virus Erad 1:67-71.
129. Williams DW, Veenstra M, Gaskill PJ, Morgello S, Calderon TM, Berman JW. 2014. Monocytes mediate HIV neuropathogenesis: mechanisms that contribute to HIV associated neurocognitive disorders. Curr HIV Res 12:85-96.
130. Godai K, Takahashi K, Kashiwagi Y, Liu CH, Yi H, Liu S, Dong C, Lubarsky DA, Hao S. 2019. Ryanodine Receptor to Mitochondrial Reactive Oxygen Species Pathway Plays an Important Role in Chronic Human Immunodeficiency Virus gp120MN-Induced Neuropathic Pain in Rats. Anesth Analg 129:276-286.
131. Nicolini A, Ajmone-Cat MA, Bernardo A, Levi G, Minghetti L. 2001. Human immunodeficiency virus type-1 Tat protein induces nuclear factor (NF)-κB activation and oxidative stress in microglial cultures by independent mechanisms. Journal of Neurochemistry 79:713-716.
132. Solleiro-Villavicencio H, Rivas-Arancibia S. 2018. Effect of Chronic Oxidative Stress on Neuroinflammatory Response Mediated by CD4+T Cells in Neurodegenerative Diseases. Frontiers in Cellular Neuroscience 12.
133. Clements JE, Babas T, Mankowski JL, Suryanarayana K, Piatak M, Jr., Tarwater PM, Lifson JD, Zink MC. 2002. The central nervous system as a reservoir for simian immunodeficiency virus (SIV): steady-state levels of SIV DNA in brain from acute through asymptomatic infection. J Infect Dis 186:905-13.
134. Barber SA, Gama L, Dudaronek JM, Voelker T, Tarwater PM, Clements JE. 2006. Mechanism for the establishment of transcriptional HIV latency in the brain in a simian immunodeficiency virus-macaque model. J Infect Dis 193:963-70.
135. Zink MC, Brice AK, Kelly KM, Queen SE, Gama L, Li M, Adams RJ, Bartizal C, Varrone J, Rabi SA, Graham DR, Tarwater PM, Mankowski JL, Clements JE. 2010. Simian immunodeficiency virus-infected macaques treated with highly active antiretroviral therapy have reduced central nervous system viral replication and inflammation but persistence of viral DNA. J Infect Dis 202:161-70.
136. Churchill MJ, Gorry PR, Cowley D, Lal L, Sonza S, Purcell DFJ, Thompson KA, Gabuzda D, McArthur JC, Pardo CA, Wesselingh SL. 2006. Use of laser capture microdissection to detect integrated HIV-1 DNA in macrophages and astrocytes from autopsy brain tissues. Journal of NeuroVirology 12:146-152.
137. Avalos CR, Price SL, Forsyth ER, Pin JN, Shirk EN, Bullock BT, Queen SE, Li M, Gellerup D, O'Connor SL, Zink MC, Mankowski JL, Gama L, Clements JE. 2016. Quantitation of Productively Infected Monocytes and Macrophages of Simian Immunodeficiency Virus-Infected Macaques. Journal of Virology 90:5643-5656.
138. Canestri A, Lescure FX, Jaureguiberry S, Moulignier A, Amiel C, Marcelin AG, Peytavin G, Tubiana R, Pialoux G, Katlama C. 2010. Discordance between cerebral spinal fluid and plasma HIV replication in patients with neurological symptoms who are receiving suppressive antiretroviral therapy. Clin Infect Dis 50:773-8.

139. Peluso MJ, Ferretti F, Peterson J, Lee E, Fuchs D, Boschini A, Gisslén M, Angoff N, Price RW, Cinque P, Spudich S. 2012. Cerebrospinal fluid HIV escape associated with progressive neurologic dysfunction in patients on antiretroviral therapy with well controlled plasma viral load. Aids 26:1765-74.
140. An SF, Groves M, Gray F, Scaravilli F. 1999. Early entry and widespread cellular involvement of HIV-1 DNA in brains of HIV-1 positive asymptomatic individuals. J Neuropathol Exp Neurol 58:1156-62.
141. Thompson KA, Cherry CL, Bell JE, McLean CA. 2011. Brain cell reservoirs of latent virus in presymptomatic HIV-infected individuals. Am J Pathol 179:1623-9.
142. Sakka L, Coll G, Chazal J. 2011. Anatomy and physiology of cerebrospinal fluid. Eur Ann Otorhinolaryngol Head Neck Dis 128:309-16.
143. Damkier HH, Brown PD, Praetorius J. 2013. Cerebrospinal fluid secretion by the choroid plexus. Physiol Rev 93:1847-92.
144. Plog BA, Nedergaard M. 2018. The Glymphatic System in Central Nervous System Health and Disease: Past, Present, and Future. Annu Rev Pathol 13:379-394.
145. Telano LN, Baker S. 2024. Physiology, Cerebral Spinal Fluid, StatPearls. StatPearls Publishing Copyright © 2024, StatPearls Publishing LLC., Treasure Island (FL) ineligible companies. Disclosure: Stephen Baker declares no relevant financial relationships with ineligible companies.
146. Spector R, Robert Snodgrass S, Johanson CE. 2015. A balanced view of the cerebrospinal fluid composition and functions: Focus on adult humans. Exp Neurol 273:57-68.
147. Simon MJ, Iliff JJ. 2016. Regulation of cerebrospinal fluid (CSF) flow in neurodegenerative, neurovascular and neuroinflammatory disease. Biochim Biophys Acta 1862:442-51.
148. Attier-Zmudka J, Sérot J-M, Valluy J, Saffarini M, Macaret A-S, Diouf M, Dao S, Douadi Y, Malinowski KP, Balédent O. 2019. Decreased Cerebrospinal Fluid Flow Is Associated With Cognitive Deficit in Elderly Patients. Frontiers in Aging Neuroscience 11.
149. McBride JA, Striker R. 2017. Imbalance in the game of T cells: What can the CD4/CD8 T-cell ratio tell us about HIV and health? PLoS Pathog 13:e1006624.
150. Svenningsson A, Hansson GK, Andersen O, Andersson R, Patarroyo M, Stemme S. 1993. Adhesion molecule expression on cerebrospinal fluid T lymphocytes: evidence for common recruitment mechanisms in multiple sclerosis, aseptic meningitis, and normal controls. Ann Neurol 34:155-61.
151. Sallusto F, Lenig D, Förster R, Lipp M, Lanzavecchia A. 1999. Two subsets of memory T lymphocytes with distinct homing potentials and effector functions. Nature 401:708-712.
152. Kivisäkk P, Mahad DJ, Callahan MK, Trebst C, Tucky B, Wei T, Wu L, Baekkevold ES, Lassmann H, Staugaitis SM, Campbell JJ, Ransohoff RM. 2003. Human cerebrospinal fluid central memory CD4+ T cells: evidence for trafficking through choroid plexus and meninges via P-selectin. Proc Natl Acad Sci U S A 100:8389-94.
153. Gate D, Saligrama N, Leventhal O, Yang AC, Unger MS, Middeldorp J, Chen K, Lehallier B, Channappa D, De Los Santos MB, McBride A, Pluvinage J, Elahi F, Tam GK-Y, Kim Y, Greicius M, Wagner AD, Aigner L, Galasko DR, Davis MM, Wyss-Coray T. 2020. Clonally expanded CD8 T cells patrol the cerebrospinal fluid in Alzheimer's disease. Nature 577:399-404.
154. Trebst C, Sørensen TL, Kivisäkk P, Cathcart MK, Hesselgesser J, Horuk R, Sellebjerg F, Lassmann H, Ransohoff RM. 2001. CCR1+/CCR5+ mononuclear phagocytes accumulate in the central nervous system of patients with multiple sclerosis. Am J Pathol 159:1701-10.

155. Patil T, Garg RK, Jain A, Goel MM, Malhotra HS, Verma R, Singh GP, Sharma PK. 2015. Serum and CSF cytokines and matrix metalloproteinases in spinal tuberculosis. Inflamm Res 64:97-106.
156. Capogna E, Watne LO, Sørensen Ø, Guichelaar CJ, Idland AV, Halaas NB, Blennow K, Zetterberg H, Walhovd KB, Fjell AM, Vidal-Piñeiro D. 2023. Associations of neuroinflammatory IL-6 and IL-8 with brain atrophy, memory decline, and core AD biomarkers - in cognitively unimpaired older adults. Brain Behav Immun 113:56-65.
157. Derecki NC, Cardani AN, Yang CH, Quinnies KM, Crihfield A, Lynch KR, Kipnis J. 2010. Regulation of learning and memory by meningeal immunity: a key role for IL-4. J Exp Med 207:1067-80.
158. Brombacher TM, Nono JK, De Gouveia KS, Makena N, Darby M, Womersley J, Tamgue O, Brombacher F. 2017. IL-13-Mediated Regulation of Learning and Memory. J Immunol 198:2681-2688.
159. Li S, olde Heuvel F, Rehman R, Aousji O, Froehlich A, Li Z, Jark R, Zhang W, Conquest A, Woelfle S, Schoen M, O´Meara CC, Reinhardt RL, Voehringer D, Kassubek J, Ludolph A, Huber-Lang M, Knöll B, Morganti-Kossmann MC, Brockmann MM, Boeckers T, Roselli F. 2023. Interleukin-13 and its receptor are synaptic proteins involved in plasticity and neuroprotection. Nature Communications 14:200.
160. Maharaj AS, Walshe TE, Saint-Geniez M, Venkatesha S, Maldonado AE, Himes NC, Matharu KS, Karumanchi SA, D'Amore PA. 2008. VEGF and TGF-beta are required for the maintenance of the choroid plexus and ependyma. J Exp Med 205:491-501.
161. Serot JM, Béné MC, Foliguet B, Faure GC. 2000. Monocyte-derived IL-10-secreting dendritic cells in choroid plexus epithelium. J Neuroimmunol 105:115-9.
162. Hasegawa-Ishii S, Shimada A, Inaba M, Li M, Shi M, Kawamura N, Takei S, Chiba Y, Hosokawa M, Ikehara S. 2013. Selective localization of bone marrow-derived ramified cells in the brain adjacent to the attachments of choroid plexus. Brain Behav Immun 29:82-97.
163. Tan QC, Xing XW, Zhang JT, He MW, Ma YB, Wu L, Wang X, Wang HF, Yu SY. 2023. Correlation between blood glucose and cerebrospinal fluid glucose levels in patients with differences in glucose metabolism. Front Neurol 14:1103026.
164. LeVine SM. 2016. Albumin and multiple sclerosis. BMC Neurol 16:47.
165. Simonsen CS, Flemmen H, Lauritzen T, Berg-Hansen P, Moen SM, Celius EG. 2020. The diagnostic value of IgG index versus oligoclonal bands in cerebrospinal fluid of patients with multiple sclerosis. Mult Scler J Exp Transl Clin 6:2055217319901291.
166. Suzuki K, Zaunders J, Gates TM, Levert A, Butterly S, Liu Z, Ishida T, Palmer S, Rae CD, Jugé L, Cysique LA, Brew BJ. 2022. Elevation of cell-associated HIV-1 transcripts in CSF CD4+ T cells, despite effective antiretroviral therapy, is linked to brain injury. Proceedings of the National Academy of Sciences 119:e2210584119.
167. Lustig G, Cele S, Karim F, Derache A, Ngoepe A, Khan K, Gosnell BI, Moosa MS, Ntshuba N, Marais S, Jeena PM, Govender K, Adamson J, Kløverpris H, Gupta RK, Harrichandparsad R, Patel VB, Sigal A. 2021. T cell derived HIV-1 is present in the CSF in the face of suppressive antiretroviral therapy. PLoS Pathog 17:e1009871.
168. Sharma V, Creegan M, Tokarev A, Hsu D, Slike BM, Sacdalan C, Chan P, Spudich S, Ananworanich J, Eller MA, Krebs SJ, Vasan S, Bolton DL, the RS, Teams RSS. 2021. Cerebrospinal fluid CD4+ T cell infection in humans and macaques during acute HIV-1 and SHIV infection. PLOS Pathogens 17:e1010105.
169. Farhadian SF, Lindenbaum O, Zhao J, Corley MJ, Im Y, Walsh H, Vecchio A, Garcia-Milian R, Chiarella J, Chintanaphol M, Calvi R, Wang G, Ndhlovu LC, Yoon J, Trotta D, Ma S, Kluger Y, Spudich S. 2022. HIV viral transcription and immune perturbations in the CNS of people with HIV despite ART. JCI Insight 7.

170. Ganesh A, Lemongello D, Lee E, Peterson J, McLaughlin BE, Ferre AL, Gillespie GM, Fuchs D, Deeks SG, Hunt PW, Price RW, Spudich SS, Shacklett BL. 2016. Immune Activation and HIV-Specific CD8(+) T Cells in Cerebrospinal Fluid of HIV Controllers and Noncontrollers. AIDS Res Hum Retroviruses 32:791-800.
171. Kessing CF, Spudich S, Valcour V, Cartwright P, Chalermchai T, Fletcher JLK, Takata H, Nichols C, Josey BJ, Slike B, Krebs SJ, Sailsuta N, Lerdlum S, Jagodzinski L, Tipsuk S, Suttichom D, Rattanamanee S, Zetterberg H, Hellmuth J, Phanuphak N, Robb ML, Michael NL, Ananworanich J, Trautmann L. 2017. High Number of Activated CD8+ T Cells Targeting HIV Antigens Are Present in Cerebrospinal Fluid in Acute HIV Infection. Journal of acquired immune deficiency syndromes (1999) 75:108-117.
172. Sadagopal S, Lorey SL, Barnett L, Basham R, Lebo L, Erdem H, Haman K, Avison M, Waddell K, Haas DW, Kalams SA. 2008. Enhancement of human immunodeficiency virus (HIV)-specific CD8+ T cells in cerebrospinal fluid compared to those in blood among antiretroviral therapy-naive HIV-positive subjects. J Virol 82:10418-28.
173. Gisslen M, Keating SM, Spudich S, Arechiga V, Stephenson S, Zetterberg H, Di Germanio C, Blennow K, Fuchs D, Hagberg L, Norris PJ, Peterson J, Shacklett BL, Yiannoutsos CT, Price RW. 2021. Compartmentalization of cerebrospinal fluid inflammation across the spectrum of untreated HIV-1 infection, central nervous system injury and viral suppression. PLoS One 16:e0250987.
174. Williams DW, Byrd D, Rubin LH, Anastos K, Morgello S, Berman JW. 2014. CCR2 on CD14(+)CD16(+) monocytes is a biomarker of HIV-associated neurocognitive disorders. Neurol Neuroimmunol Neuroinflamm 1:e36.
175. Pulliam L, Gascon R, Stubblebine M, McGuire D, McGrath MS. 1997. Unique monocyte subset in patients with AIDS dementia. Lancet 349:692-5.
176. Imp BM, Rubin LH, Tien PC, Plankey MW, Golub ET, French AL, Valcour VG. 2017. Monocyte Activation Is Associated With Worse Cognitive Performance in HIV-Infected Women With Virologic Suppression. J Infect Dis 215:114-121.
177. Veenhuis RT, Abreu CM, Shirk EN, Gama L, Clements JE. 2021. HIV replication and latency in monocytes and macrophages. Semin Immunol 51:101472.
178. Muñoz-Nevárez LA, Imp BM, Eller MA, Kiweewa F, Maswai J, Polyak C, Olwenyi OA, Allen IE, Rono E, Milanini B, Kibuuka H, Ake JA, Eller LA, Valcour VG. 2020. Monocyte activation, HIV, and cognitive performance in East Africa. J Neurovirol 26:52-59.
179. Abdulle S, Mellgren A, Brew BJ, Cinque P, Hagberg L, Price RW, Rosengren L, Gisslén M. 2007. CSF neurofilament protein (NFL) -- a marker of active HIV-related neurodegeneration. J Neurol 254:1026-32.
180. Jessen Krut J, Mellberg T, Price RW, Hagberg L, Fuchs D, Rosengren L, Nilsson S, Zetterberg H, Gisslén M. 2014. Biomarker evidence of axonal injury in neuroasymptomatic HIV-1 patients. PLoS One 9:e88591.
181. Ellis RJ, Chenna A, Petropoulos CJ, Lie Y, Curanovic D, Crescini M, Winslow J, Sundermann E, Tang B, Letendre SL. 2022. Higher cerebrospinal fluid biomarkers of neuronal injury in HIV-associated neurocognitive impairment. J Neurovirol 28:438-445.
182. Pulliam L, Sun B, Mustapic M, Chawla S, Kapogiannis D. 2019. Plasma neuronal exosomes serve as biomarkers of cognitive impairment in HIV infection and Alzheimer's disease. J Neurovirol 25:702-709.
183. Molero-Luis M, Casas-Alba D, Orellana G, Ormazabal A, Sierra C, Oliva C, Valls A, Velasco J, Launes C, Cuadras D, Pérez-Dueñas B, Jordan I, Cambra FJ, Ortigoza-Escobar JD, Muñoz-Almagro C, Garcia-Cazorla A, Armangué T, Artuch R. 2020. Cerebrospinal fluid neopterin as a biomarker of neuroinflammatory diseases. Scientific Reports 10:18291.
184. Ghisoni K, Martins Rde P, Barbeito L, Latini A. 2015. Neopterin as a potential cytoprotective brain molecule. J Psychiatr Res 71:134-9.

185. Halford J, Shen S, Itamura K, Levine J, Chong AC, Czerwieniec G, Glenn TC, Hovda DA, Vespa P, Bullock R, Dietrich WD, Mondello S, Loo JA, Wanner IB. 2017. New astroglial injury-defined biomarkers for neurotrauma assessment. J Cereb Blood Flow Metab 37:3278-3299.
186. Ajami B, Bennett JL, Krieger C, McNagny KM, Rossi FMV. 2011. Infiltrating monocytes trigger EAE progression, but do not contribute to the resident microglia pool. Nature Neuroscience 14:1142-1149.
187. Ransohoff RM. 2011. Microglia and monocytes: 'tis plain the twain meet in the brain. Nature Neuroscience 14:1098-1100.
188. Nevalainen T, Autio A, Hurme M. 2022. Composition of the infiltrating immune cells in the brain of healthy individuals: effect of aging. Immunity & Ageing 19:45.
189. Wakim LM, Woodward-Davis A, Bevan MJ. 2010. Memory T cells persisting within the brain after local infection show functional adaptations to their tissue of residence. Proceedings of the National Academy of Sciences 107:17872-17879.
190. Smolders J, Heutinck KM, Fransen NL, Remmerswaal EBM, Hombrink P, Ten Berge IJM, van Lier RAW, Huitinga I, Hamann J. 2018. Tissue-resident memory T cells populate the human brain. Nature communications 9:4593-4593.
191. Zlotnik A, Yoshie O. 2000. Chemokines: a new classification system and their role in immunity. Immunity 12:121-7.
192. Christensen JE, Simonsen S, Fenger C, Sørensen MR, Moos T, Christensen JP, Finsen B, Thomsen AR. 2009. Fulminant lymphocytic choriomeningitis virus-induced inflammation of the CNS involves a cytokine-chemokine-cytokine-chemokine cascade. J Immunol 182:1079-87.
193. Lane TE, Asensio VC, Yu N, Paoletti AD, Campbell IL, Buchmeier MJ. 1998. Dynamic regulation of alpha- and beta-chemokine expression in the central nervous system during mouse hepatitis virus-induced demyelinating disease. J Immunol 160:970-8.
194. So EY, Kim BS. 2009. Theiler's virus infection induces TLR3-dependent upregulation of TLR2 critical for proinflammatory cytokine production. Glia 57:1216-26.
195. Aravalli RN, Hu S, Rowen TN, Palmquist JM, Lokensgard JR. 2005. Cutting edge: TLR2-mediated proinflammatory cytokine and chemokine production by microglial cells in response to herpes simplex virus. J Immunol 175:4189-93.
196. van Marle G, Henry S, Todoruk T, Sullivan A, Silva C, Rourke SB, Holden J, McArthur JC, Gill MJ, Power C. 2004. Human immunodeficiency virus type 1 Nef protein mediates neural cell death: a neurotoxic role for IP-10. Virology 329:302-318.
197. Klein RS, Lin E, Zhang B, Luster AD, Tollett J, Samuel MA, Engle M, Diamond MS. 2005. Neuronal CXCL10 directs CD8+ T-cell recruitment and control of West Nile virus encephalitis. J Virol 79:11457-66.
198. Vergote D, Butler GS, Ooms M, Cox JH, Silva C, Hollenberg MD, Jhamandas JH, Overall CM, Power C. 2006. Proteolytic processing of SDF-1α reveals a change in receptor specificity mediating HIV-associated neurodegeneration. Proceedings of the National Academy of Sciences 103:19182-19187.
199. Asensio VC, Campbell IL. 1999. Chemokines in the CNS: plurifunctional mediators in diverse states. Trends in Neurosciences 22:504-512.
200. Sasseville VG, Smith MM, Mackay CR, Pauley DR, Mansfield KG, Ringler DJ, Lackner AA. 1996. Chemokine expression in simian immunodeficiency virus-induced AIDS encephalitis. Am J Pathol 149:1459-67.
201. Cinque P, Brew BJ, Gisslen M, Hagberg L, Price RW. 2007. Cerebrospinal fluid markers in central nervous system HIV infection and AIDS dementia complex. Handb Clin Neurol 85:261-300.

202. Kelder W, McArthur JC, Nance-Sproson T, McClernon D, Griffin DE. 1998. Beta-chemokines MCP-1 and RANTES are selectively increased in cerebrospinal fluid of patients with human immunodeficiency virus-associated dementia. Ann Neurol 44:831-5.
203. Alt C, Laschinger M, Engelhardt B. 2002. Functional expression of the lymphoid chemokines CCL19 (ELC) and CCL 21 (SLC) at the blood-brain barrier suggests their involvement in G-protein-dependent lymphocyte recruitment into the central nervous system during experimental autoimmune encephalomyelitis. Eur J Immunol 32:2133-44.
204. Reboldi A, Coisne C, Baumjohann D, Benvenuto F, Bottinelli D, Lira S, Uccelli A, Lanzavecchia A, Engelhardt B, Sallusto F. 2009. C-C chemokine receptor 6–regulated entry of TH-17 cells into the CNS through the choroid plexus is required for the initiation of EAE. Nature Immunology 10:514-523.
205. Krumbholz M, Theil D, Cepok S, Hemmer B, Kivisäkk P, Ransohoff RM, Hofbauer M, Farina C, Derfuss T, Hartle C, Newcombe J, Hohlfeld R, Meinl E. 2005. Chemokines in multiple sclerosis: CXCL12 and CXCL13 up-regulation is differentially linked to CNS immune cell recruitment. Brain 129:200-211.
206. Krumbholz M, Theil D, Steinmeyer F, Cepok S, Hemmer B, Hofbauer M, Farina C, Derfuss T, Junker A, Arzberger T, Sinicina I, Hartle C, Newcombe J, Hohlfeld R, Meinl E. 2007. CCL19 is constitutively expressed in the CNS, up-regulated in neuroinflammation, active and also inactive multiple sclerosis lesions. J Neuroimmunol 190:72-9.
207. Engelhardt B, Ransohoff RM. 2005. The ins and outs of T-lymphocyte trafficking to the CNS: anatomical sites and molecular mechanisms. Trends Immunol 26:485-95.
208. Marchetti L, Engelhardt B. 2020. Immune cell trafficking across the blood-brain barrier in the absence and presence of neuroinflammation. Vasc Biol 2:H1-h18.
209. Engelhardt B, Ransohoff RM. 2012. Capture, crawl, cross: the T cell code to breach the blood-brain barriers. Trends Immunol 33:579-89.
210. Daneman R, Prat A. 2015. The blood-brain barrier. Cold Spring Harb Perspect Biol 7:a020412.
211. Liebner S, Dijkhuizen RM, Reiss Y, Plate KH, Agalliu D, Constantin G. 2018. Functional morphology of the blood-brain barrier in health and disease. Acta Neuropathol 135:311-336.
212. Kerfoot SM, Norman MU, Lapointe BM, Bonder CS, Zbytnuik L, Kubes P. 2006. Reevaluation of P-selectin and alpha 4 integrin as targets for the treatment of experimental autoimmune encephalomyelitis. J Immunol 176:6225-34.
213. Battistini L, Piccio L, Rossi B, Bach S, Galgani S, Gasperini C, Ottoboni L, Ciabini D, Caramia MD, Bernardi G, Laudanna C, Scarpini E, McEver RP, Butcher EC, Borsellino G, Constantin G. 2003. CD8+ T cells from patients with acute multiple sclerosis display selective increase of adhesiveness in brain venules: a critical role for P-selectin glycoprotein ligand-1. Blood 101:4775-82.
214. Sathiyanadan K, Coisne C, Enzmann G, Deutsch U, Engelhardt B. 2014. PSGL-1 and E/P-selectins are essential for T-cell rolling in inflamed CNS microvessels but dispensable for initiation of EAE. European Journal of Immunology 44:2287-2294.
215. Piccio L, Rossi B, Scarpini E, Laudanna C, Giagulli C, Issekutz AC, Vestweber D, Butcher EC, Constantin G. 2002. Molecular Mechanisms Involved in Lymphocyte Recruitment in Inflamed Brain Microvessels: Critical Roles for P-Selectin Glycoprotein Ligand-1 and Heterotrimeric Gi-Linked Receptors1. The Journal of Immunology 168:1940-1949.
216. Steiner O, Coisne C, Cecchelli R, Boscacci R, Deutsch U, Engelhardt B, Lyck R. 2010. Differential roles for endothelial ICAM-1, ICAM-2, and VCAM-1 in shear-resistant T cell arrest, polarization, and directed crawling on blood-brain barrier endothelium. J Immunol 185:4846-55.

217. Man S, Tucky B, Bagheri N, Li X, Kochar R, Ransohoff RM. 2009. alpha4 Integrin/FN-CS1 mediated leukocyte adhesion to brain microvascular endothelial cells under flow conditions. J Neuroimmunol 210:92-9.
218. Laschinger M, Engelhardt B. 2000. Interaction of alpha4-integrin with VCAM-1 is involved in adhesion of encephalitogenic T cell blasts to brain endothelium but not in their transendothelial migration in vitro. J Neuroimmunol 102:32-43.
219. Owens T, Bechmann I, Engelhardt B. 2008. Perivascular spaces and the two steps to neuroinflammation. J Neuropathol Exp Neurol 67:1113-21.
220. Agrawal S, Anderson P, Durbeej M, van Rooijen N, Ivars F, Opdenakker G, Sorokin LM. 2006. Dystroglycan is selectively cleaved at the parenchymal basement membrane at sites of leukocyte extravasation in experimental autoimmune encephalomyelitis. J Exp Med 203:1007-19.
221. Nishihara H, Soldati S, Mossu A, Rosito M, Rudolph H, Muller WA, Latorre D, Sallusto F, Sospedra M, Martin R, Ishikawa H, Tenenbaum T, Schroten H, Gosselet F, Engelhardt B. 2020. Human CD4+ T cell subsets differ in their abilities to cross endothelial and epithelial brain barriers in vitro. Fluids and Barriers of the CNS 17:3.
222. Carrithers MD, Visintin I, Viret C, Janeway CS, Jr. 2002. Role of genetic background in P selectin-dependent immune surveillance of the central nervous system. J Neuroimmunol 129:51-7.
223. Wolburg K, Gerhardt H, Schulz M, Wolburg H, Engelhardt B. 1999. Ultrastructural localization of adhesion molecules in the healthy. Cell and Tissue Research 296:259-269.
224. Schläger C, Körner H, Krueger M, Vidoli S, Haberl M, Mielke D, Brylla E, Issekutz T, Cabañas C, Nelson PJ, Ziemssen T, Rohde V, Bechmann I, Lodygin D, Odoardi F, Flügel A. 2016. Effector T-cell trafficking between the leptomeninges and the cerebrospinal fluid. Nature 530:349-353.
225. Elyahu Y, Hekselman I, Eizenberg-Magar I, Berner O, Strominger I, Schiller M, Mittal K, Nemirovsky A, Eremenko E, Vital A, Simonovsky E, Chalifa-Caspi V, Friedman N, Yeger-Lotem E, Monsonego A. 2019. Aging promotes reorganization of the CD4 T cell landscape toward extreme regulatory and effector phenotypes. Science Advances 5:eaaw8330.
226. Akbar AN, Henson SM. 2011. Are senescence and exhaustion intertwined or unrelated processes that compromise immunity? Nature Reviews Immunology 11:289-295.
227. Franceschi C, Campisi J. 2014. Chronic inflammation (inflammaging) and its potential contribution to age-associated diseases. J Gerontol A Biol Sci Med Sci 69 Suppl 1:S4-9.
228. Ferrucci L, Fabbri E. 2018. Inflammageing: chronic inflammation in ageing, cardiovascular disease, and frailty. Nat Rev Cardiol 15:505-522.
229. Mogilenko DA, Shpynov O, Andhey PS, Arthur L, Swain A, Esaulova E, Brioschi S, Shchukina I, Kerndl M, Bambouskova M, Yao Z, Laha A, Zaitsev K, Burdess S, Gillfilan S, Stewart SA, Colonna M, Artyomov MN. 2021. Comprehensive Profiling of an Aging Immune System Reveals Clonal GZMK(+) CD8(+) T Cells as Conserved Hallmark of Inflammaging. Immunity 54:99-115.e12.
230. Desdín-Micó G, Soto-Heredero G, Aranda JF, Oller J, Carrasco E, Gabandé-Rodríguez E, Blanco EM, Alfranca A, Cussó L, Desco M, Ibañez B, Gortazar AR, Fernández-Marcos P, Navarro MN, Hernaez B, Alcamí A, Baixauli F, Mittelbrunn M. 2020. T cells with dysfunctional mitochondria induce multimorbidity and premature senescence. Science 368:1371-1376.
231. Bharath LP, Agrawal M, McCambridge G, Nicholas DA, Hasturk H, Liu J, Jiang K, Liu R, Guo Z, Deeney J, Apovian CM, Snyder-Cappione J, Hawk GS, Fleeman RM, Pihl RMF, Thompson K, Belkina AC, Cui L, Proctor EA, Kern PA, Nikolajczyk BS. 2020. Metformin

Enhances Autophagy and Normalizes Mitochondrial Function to Alleviate Aging-Associated Inflammation. Cell Metab 32:44-55.e6.
232. Kebir H, Kreymborg K, Ifergan I, Dodelet-Devillers A, Cayrol R, Bernard M, Giuliani F, Arbour N, Becher B, Prat A. 2007. Human TH17 lymphocytes promote blood-brain barrier disruption and central nervous system inflammation. Nature Medicine 13:1173-1175.
233. Kivisäkk P, Mahad DJ, Callahan MK, Sikora K, Trebst C, Tucky B, Wujek J, Ravid R, Staugaitis SM, Lassmann H, Ransohoff RM. 2004. Expression of CCR7 in multiple sclerosis: implications for CNS immunity. Ann Neurol 55:627-38.
234. Fletcher JM, Lalor SJ, Sweeney CM, Tubridy N, Mills KH. 2010. T cells in multiple sclerosis and experimental autoimmune encephalomyelitis. Clin Exp Immunol 162:1-11.
235. Ando DG, Clayton J, Kono D, Urban JL, Sercarz EE. 1989. Encephalitogenic T cells in the B10.PL model of experimental allergic encephalomyelitis (EAE) are of the Th-1 lymphokine subtype. Cellular Immunology 124:132-143.
236. Voskuhl RR, Martin R, Bergman C, Dalal M, Ruddle NH, McFarland HF. 1993. T helper 1 (Th1) functional phenotype of human myelin basic protein-specific T lymphocytes. Autoimmunity 15:137-43.
237. Belikan P, Bühler U, Wolf C, Pramanik GK, Gollan R, Zipp F, Siffrin V. 2018. CCR7 on CD4(+) T Cells Plays a Crucial Role in the Induction of Experimental Autoimmune Encephalomyelitis. J Immunol 200:2554-2562.
238. Giuliani F, Goodyer CG, Antel JP, Yong VW. 2003. Vulnerability of human neurons to T cell-mediated cytotoxicity. J Immunol 171:368-79.
239. Schetters STT, Gomez-Nicola D, Garcia-Vallejo JJ, Van Kooyk Y. 2017. Neuroinflammation: Microglia and T Cells Get Ready to Tango. Front Immunol 8:1905.
240. Town T, Tan J, Flavell RA, Mullan M. 2005. T-cells in alzheimer's disease. NeuroMolecular Medicine 7:255-264.
241. Mietelska-Porowska A, Wojda U. 2017. T Lymphocytes and Inflammatory Mediators in the Interplay between Brain and Blood in Alzheimer's Disease: Potential Pools of New Biomarkers. J Immunol Res 2017:4626540.
242. Glass WG, Lim JK, Cholera R, Pletnev AG, Gao JL, Murphy PM. 2005. Chemokine receptor CCR5 promotes leukocyte trafficking to the brain and survival in West Nile virus infection. J Exp Med 202:1087-98.
243. Cupovic J, Onder L, Gil-Cruz C, Weiler E, Caviezel-Firner S, Perez-Shibayama C, Rülicke T, Bechmann I, Ludewig B. 2016. Central Nervous System Stromal Cells Control Local CD8(+) T Cell Responses during Virus-Induced Neuroinflammation. Immunity 44:622-633.
244. Kunis G, Baruch K, Rosenzweig N, Kertser A, Miller O, Berkutzki T, Schwartz M. 2013. IFN-γ-dependent activation of the brain's choroid plexus for CNS immune surveillance and repair. Brain 136:3427-40.
245. Hsu DC, Sunyakumthorn P, Wegner M, Schuetz A, Silsorn D, Estes JD, Deleage C, Tomusange K, Lakhashe SK, Ruprecht RM, Lombardini E, Im-Erbsin R, Kuncharin Y, Phuang-Ngern Y, Inthawong D, Chuenarom W, Burke R, Robb ML, Ndhlovu LC, Ananworanich J, Valcour V, O'Connell RJ, Spudich S, Michael NL, Vasan S. 2018. Central Nervous System Inflammation and Infection during Early, Nonaccelerated Simian-Human Immunodeficiency Virus Infection in Rhesus Macaques. J Virol 92.
246. Honeycutt JB, Liao B, Nixon CC, Cleary RA, Thayer WO, Birath SL, Swanson MD, Sheridan P, Zakharova O, Prince F, Kuruc J, Gay CL, Evans C, Eron JJ, Wahl A, Garcia JV. 2018. T cells establish and maintain CNS viral infection in HIV-infected humanized mice. J Clin Invest 128:2862-2876.
247. Lee CA, Beasley E, Sundar K, Smelkinson M, Vinton C, Deleage C, Matsuda K, Wu F, Estes JD, Lafont BAP, Brenchley JM, Hirsch VM. 2020. Simian Immunodeficiency Virus-

Infected Memory CD4⁺ T Cells Infiltrate to the Site of Infected Macrophages in the Neuroparenchyma of a Chronic Macaque Model of Neurological Complications of AIDS. mBio 11:e00602-20.
248. Grauer OM, Reichelt D, Grüneberg U, Lohmann H, Schneider-Hohendorf T, Schulte-Mecklenbeck A, Gross CC, Meuth SG, Wiendl H, Husstedt IW. 2015. Neurocognitive decline in HIV patients is associated with ongoing T-cell activation in the cerebrospinal fluid. Ann Clin Transl Neurol 2:906-19.
249. Zayyad Z, Spudich S. 2015. Neuropathogenesis of HIV: from initial neuroinvasion to HIV-associated neurocognitive disorder (HAND). Current HIV/AIDS reports 12:16-24.
250. Kolb SA, Sporer B, Lahrtz F, Koedel U, Pfister HW, Fontana A. 1999. Identification of a T cell chemotactic factor in the cerebrospinal fluid of HIV-1-infected individuals as interferon-gamma inducible protein 10. J Neuroimmunol 93:172-81.
251. Pourcher V, Gourmelen J, Bureau I, Bouee S. 2020. Comorbidities in people living with HIV: An epidemiologic and economic analysis using a claims database in France. PLoS One 15:e0243529.
252. Saloner R, Heaton RK, Campbell LM, Chen A, Franklin D, Jr., Ellis RJ, Collier AC, Marra C, Clifford DB, Gelman B, Sacktor N, Morgello S, McCutchan JA, Letendre S, Grant I, Fennema-Notestine C. 2019. Effects of comorbidity burden and age on brain integrity in HIV. Aids 33:1175-1185.
253. Nir TM, Jahanshad N, Ching CRK, Cohen RA, Harezlak J, Schifitto G, Lam HY, Hua X, Zhong J, Zhu T, Taylor MJ, Campbell TB, Daar ES, Singer EJ, Alger JR, Thompson PM, Navia BA, On behalf of the HIVNC. 2019. Progressive brain atrophy in chronically infected and treated HIV+ individuals. Journal of NeuroVirology 25:342-353.
254. Farrer LA, Cupples LA, Haines JL, Hyman B, Kukull WA, Mayeux R, Myers RH, Pericak-Vance MA, Risch N, van Duijn CM. 1997. Effects of age, sex, and ethnicity on the association between apolipoprotein E genotype and Alzheimer disease. A meta-analysis. APOE and Alzheimer Disease Meta Analysis Consortium. Jama 278:1349-56.
255. Sadigh-Eteghad S, Talebi M, Farhoudi M. 2012. Association of apolipoprotein E epsilon 4 allele with sporadic late onset Alzheimer`s disease. A meta-analysis. Neurosciences (Riyadh) 17:321-6.
256. Valcour V, Shikuma C, Shiramizu B, Watters M, Poff P, Selnes OA, Grove J, Liu Y, Abdul-Majid KB, Gartner S, Sacktor N. 2004. Age, apolipoprotein E4, and the risk of HIV dementia: the Hawaii Aging with HIV Cohort. J Neuroimmunol 157:197-202.
257. Kuhlmann I, Minihane AM, Huebbe P, Nebel A, Rimbach G. 2010. Apolipoprotein E genotype and hepatitis C, HIV and herpes simplex disease risk: a literature review. Lipids Health Dis 9:8.
258. Jahanshad N, Valcour VG, Nir TM, Kohannim O, Busovaca E, Nicolas K, Thompson PM. 2012. Disrupted brain networks in the aging HIV+ population. Brain Connect 2:335-44.
259. Chang L, Jiang C, Cunningham E, Buchthal S, Douet V, Andres M, Ernst T. 2014. Effects of APOE ε4, age, and HIV on glial metabolites and cognitive deficits. Neurology 82:2213-22.
260. Peluso MJ, Meyerhoff DJ, Price RW, Peterson J, Lee E, Young AC, Walter R, Fuchs D, Brew BJ, Cinque P, Robertson K, Hagberg L, Zetterberg H, Gisslén M, Spudich S. 2013. Cerebrospinal fluid and neuroimaging biomarker abnormalities suggest early neurological injury in a subset of individuals during primary HIV infection. J Infect Dis 207:1703-12.
261. Smith MO, Heyes MP, Lackner AA. 1995. Early intrathecal events in rhesus macaques (Macaca mulatta) infected with pathogenic or nonpathogenic molecular clones of simian immunodeficiency virus. Laboratory Investigation; a Journal of Technical Methods and Pathology 72:547-558.

262. Sönnerborg AB, von Stedingk L-V, Hansson L-O, Strannegård OO. 1989. Elevated neopterin and beta2-microglobulin levels in blood and cerebrospinal fluid occur early in HIV-1 infection. Aids 3:277-284.
263. Smith DG, Guillemin GJ, Pemberton L, Kerr S, Nath A, Smythe GA, Brew BJ. 2001. Quinolinic acid is produced by macrophages stimulated by platelet activating factor, Nef and Tat. Journal of neurovirology 7:56-60.
264. Guillemin GJ, Croitoru-Lamoury J, Dormont D, Armati PJ, Brew BJ. 2003. Quinolinic acid upregulates chemokine production and chemokine receptor expression in astrocytes. Glia 41:371-381.
265. Lane TE, Buchmeier MJ, Watry DD, Fox HS. 1996. Expression of inflammatory cytokines and inducible nitric oxide synthase in brains of SIV-infected rhesus monkeys: applications to HIV-induced central nervous system disease. Molecular Medicine 2:27-37.
266. Wahl A, Al-Harthi L. 2023. HIV infection of non-classical cells in the brain. Retrovirology 20:1.
267. Berger JR, Nath A. 1997. HIV dementia and the basal ganglia. Intervirology 40:122-31.
268. Jones M, Olafson K, Del Bigio MR, Peeling J, Nath A. 1998. Intraventricular injection of human immunodeficiency virus type 1 (HIV-1) tat protein causes inflammation, gliosis, apoptosis, and ventricular enlargement. J Neuropathol Exp Neurol 57:563-70.
269. Hayman M, Arbuthnott G, Harkiss G, Brace H, Filippi P, Philippon V, Thomson D, Vigne R, Wright A. 1993. Neurotoxicity of peptide analogues of the transactivating protein tat from Maedi-Visna virus and human immunodeficiency virus. Neuroscience 53:1-6.
270. Hofman FM, Dohadwala MM, Wright AD, Hinton DR, Walker SM. 1994. Exogenous tat protein activates central nervous system-derived endothelial cells. J Neuroimmunol 54:19-28.
271. Kruman, II, Nath A, Maragos WF, Chan SL, Jones M, Rangnekar VM, Jakel RJ, Mattson MP. 1999. Evidence that Par-4 participates in the pathogenesis of HIV encephalitis. Am J Pathol 155:39-46.
272. Nath A, Haughey NJ, Jones M, Anderson C, Bell JE, Geiger JD. 2000. Synergistic neurotoxicity by human immunodeficiency virus proteins Tat and gp120: protection by memantine. Ann Neurol 47:186-94.
273. Elbirt D, Mahlab-Guri K, Bezalel-Rosenberg S, Gill H, Attali M, Asher I. 2015. HIV-associated neurocognitive disorders (HAND). Isr Med Assoc J 17:54-9.
274. Haddow LJ, Floyd S, Copas A, Gilson RJC. 2013. A Systematic Review of the Screening Accuracy of the HIV Dementia Scale and International HIV Dementia Scale. PLOS ONE 8:e61826.
275. Sakamoto M, Marcotte TD, Umlauf A, Franklin DJ, Heaton RK, Ellis RJ, Letendre S, Alexander T, McCutchan JA, Morgan EE, Woods SP, Collier AC, Marra CM, Clifford DB, Gelman BB, McArthur JC, Morgello S, Simpson D, Grant I, Group C. 2013. Concurrent Classification Accuracy of the HIV Dementia Scale for HIV-Associated Neurocognitive Disorders in the CHARTER Cohort. JAIDS Journal of Acquired Immune Deficiency Syndromes 62:36-42.
276. Zipursky AR, Gogolishvili D, Rueda S, Brunetta J, Carvalhal A, McCombe JA, Gill MJ, Rachlis A, Rosenes R, Arbess G, Marcotte T, Rourke SB. 2013. Evaluation of brief screening tools for neurocognitive impairment in HIV/AIDS: a systematic review of the literature. Aids 27:2385-401.
277. Chan P, Brew BJ. 2014. HIV associated neurocognitive disorders in the modern antiviral treatment era: prevalence, characteristics, biomarkers, and effects of treatment. Curr HIV/AIDS Rep 11:317-24.

278. Peterson J, Gisslen M, Zetterberg H, Fuchs D, Shacklett BL, Hagberg L, Yiannoutsos CT, Spudich SS, Price RW. 2014. Cerebrospinal fluid (CSF) neuronal biomarkers across the spectrum of HIV infection: hierarchy of injury and detection. PLoS One 9:e116081.
279. Valcour V, Chalermchai T, Sailasuta N, Marovich M, Lerdlum S, Suttichom D, Suwanwela NC, Jagodzinski L, Michael N, Spudich S, van Griensven F, de Souza M, Kim J, Ananworanich J. 2012. Central nervous system viral invasion and inflammation during acute HIV infection. J Infect Dis 206:275-82.
280. Budka H, Costanzi G, Cristina S, Lechi A, Parravicini C, Trabattoni R, Vago L. 1987. Brain pathology induced by infection with the human immunodeficiency virus (HIV). A histological, immunocytochemical, and electron microscopical study of 100 autopsy cases. Acta Neuropathol 75:185-98.
281. Sailasuta N, Ross W, Ananworanich J, Chalermchai T, DeGruttola V, Lerdlum S, Pothisri M, Busovaca E, Ratto-Kim S, Jagodzinski L, Spudich S, Michael N, Kim JH, Valcour V, for the RVSpt. 2012. Change in Brain Magnetic Resonance Spectroscopy after Treatment during Acute HIV Infection. PLOS ONE 7:e49272.
282. Lentz MR, Kim WK, Kim H, Soulas C, Lee V, Venna N, Halpern EF, Rosenberg ES, Williams K, González RG. 2011. Alterations in brain metabolism during the first year of HIV infection. J Neurovirol 17:220-9.
283. King JE, Eugenin EA, Buckner CM, Berman JW. 2006. HIV tat and neurotoxicity. Microbes and Infection 8:1347-1357.
284. Sami Saribas A, Cicalese S, Ahooyi TM, Khalili K, Amini S, Sariyer IK. 2018. HIV-1 Nef is released in extracellular vesicles derived from astrocytes: evidence for Nef-mediated neurotoxicity. Cell Death & Disease 8:e2542-e2542.
285. Kanmogne GD, Kennedy RC, Grammas P. 2002. HIV-1 gp120 Proteins and gp160 Peptides Are Toxic to Brain Endothelial Cells and Neurons: Possible Pathway for HIV Entry into the Brain and HIV-Associated Dementia. Journal of Neuropathology & Experimental Neurology 61:992-1000.
286. Letendre S, Marquie-Beck J, Capparelli E, Best B, Clifford D, Collier AC, Gelman BB, McArthur JC, McCutchan JA, Morgello S, Simpson D, Grant I, Ellis RJ. 2008. Validation of the CNS Penetration-Effectiveness rank for quantifying antiretroviral penetration into the central nervous system. Arch Neurol 65:65-70.
287. WHO U, Avenir Health (ed). 2022. Antiretroviral medicines in low- and middle-income countries: forecasts of global and regional demand for 2020-2024. https://www.who.int/publications/i/item/9789240041264. Accessed
288. Howlett WP. 2019. Neurological disorders in HIV in Africa: a review. Afr Health Sci 19:1953-1977.
289. Ransohoff RM, Perry VH. 2009. Microglial Physiology: Unique Stimuli, Specialized Responses. Annual Review of Immunology 27:119-145.
290. Wong JK, Ignacio CC, Torriani F, Havlir D, Fitch NJ, Richman DD. 1997. In vivo compartmentalization of human immunodeficiency virus: evidence from the examination of pol sequences from autopsy tissues. J Virol 71:2059-71.
291. Sturdevant CB, Joseph SB, Schnell G, Price RW, Swanstrom R, Spudich S. 2015. Compartmentalized Replication of R5 T Cell-Tropic HIV-1 in the Central Nervous System Early in the Course of Infection. PLOS Pathogens 11:e1004720.
292. Ritola K, Robertson K, Fiscus SA, Hall C, Swanstrom R. 2005. Increased human immunodeficiency virus type 1 (HIV-1) env compartmentalization in the presence of HIV-1-associated dementia. J Virol 79:10830-4.
293. Pillai SK, Pond SL, Liu Y, Good BM, Strain MC, Ellis RJ, Letendre S, Smith DM, Günthard HF, Grant I, Marcotte TD, McCutchan JA, Richman DD, Wong JK. 2006. Genetic attributes of cerebrospinal fluid-derived HIV-1 env. Brain 129:1872-83.

294. Yuan L, Qiao L, Wei F, Yin J, Liu L, Ji Y, Smith D, Li N, Chen D. 2013. Cytokines in CSF correlate with HIV-associated neurocognitive disorders in the post-HAART era in China. J Neurovirol 19:144-9.
295. Gisslén M, Price RW, Andreasson U, Norgren N, Nilsson S, Hagberg L, Fuchs D, Spudich S, Blennow K, Zetterberg H. 2016. Plasma Concentration of the Neurofilament Light Protein (NFL) is a Biomarker of CNS Injury in HIV Infection: A Cross-Sectional Study. EBioMedicine 3:135-140.
296. Ragin AB, Wu Y, Storey P, Cohen BA, Edelman RR, Epstein LG. 2006. Monocyte chemoattractant protein-1 correlates with subcortical brain injury in HIV infection. Neurology 66:1255-7.
297. Lackner AA, Dandekar S, Gardner MB. 1991. Neurobiology of Simian and Feline Immunodeficiency Virus Infections. Brain Pathology 1:201-212.
298. Lackner AA, Smith MO, Munn RJ, Martfeld DJ, Gardner MB, Marx PA, Dandekar S. 1991. Localization of simian immunodeficiency virus in the central nervous system of rhesus monkeys. The American journal of pathology 139:609-621.
299. Gardner MB. 1990. SIV infection of macaques: a model for AIDS vaccine development. Dev Biol Stand 72:259-66.

Introduction Figures

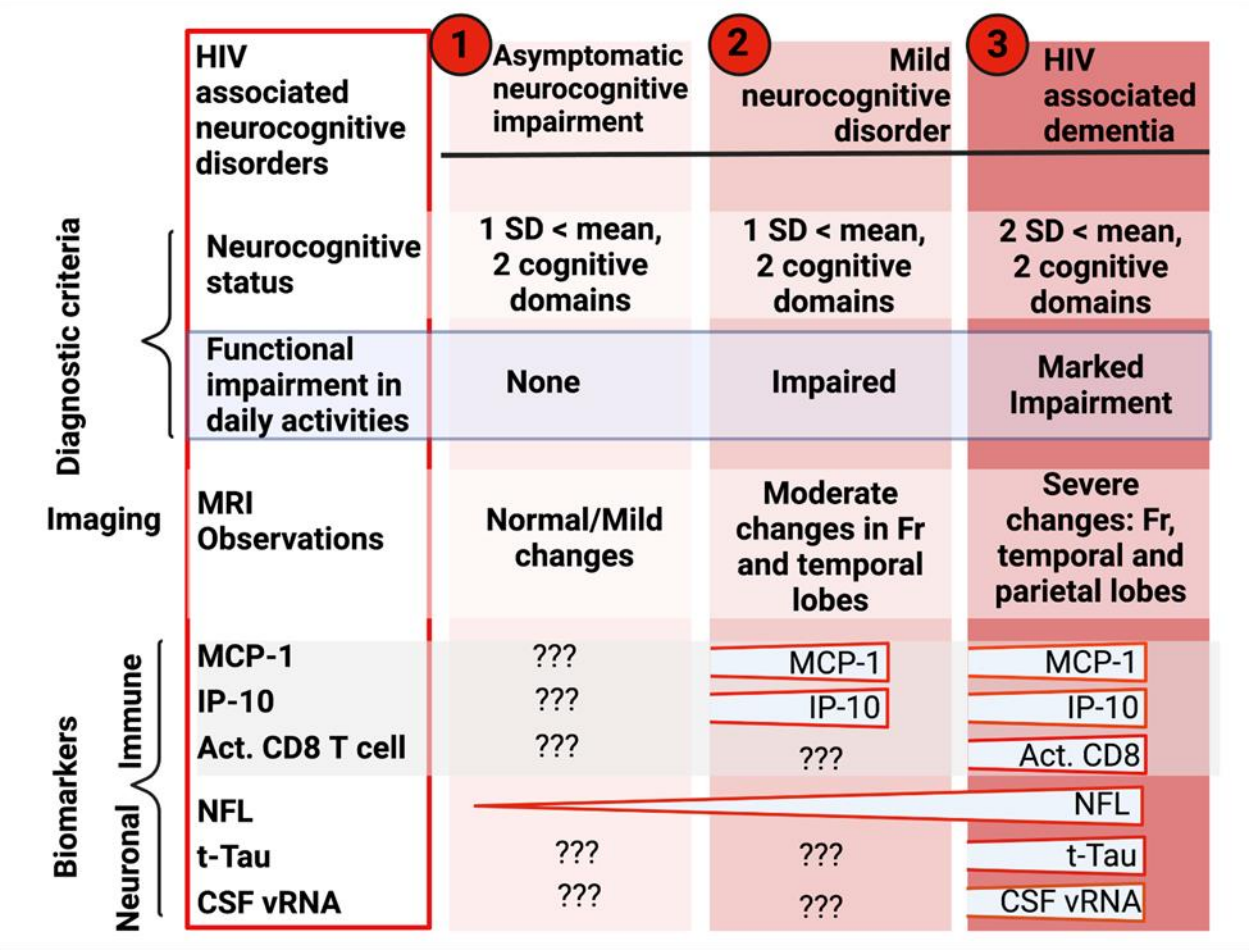

Figure 1. Diagnostic criteria and associated biomarkers of HAND. An overview of HAND, Core diagnostic criterion are outlined. Putative supportive criterion encompassing neuronal and immune biomarkers to delineate the categories of HAND to improve diagnosis and detection of HAND are identified.

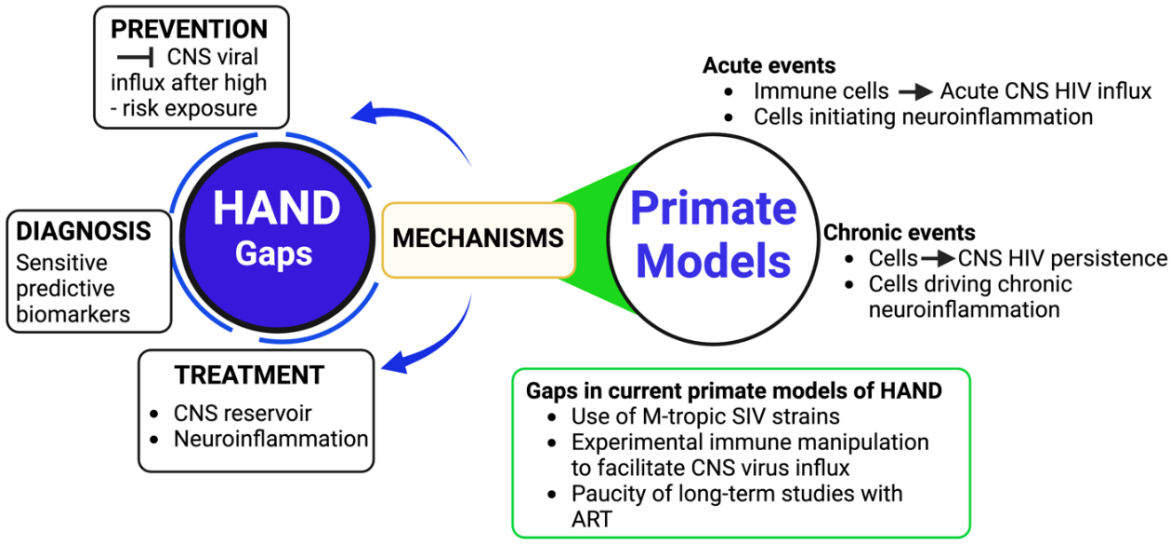

Figure 2. Understanding HIV-Associated Neurocognitive Disorders (HAND) Through Primate Models: A Flow Chart Overview. This flow chart delineates the process by which primate models contribute to bridging knowledge gaps in our understanding of HIV-Associated Neurocognitive Disorders (HAND). Starting from the identification of specific research gaps in HAND, the chart progresses through the utilization of primate models to address these gaps, and ultimately, how these models can inform future research and therapeutic strategies.

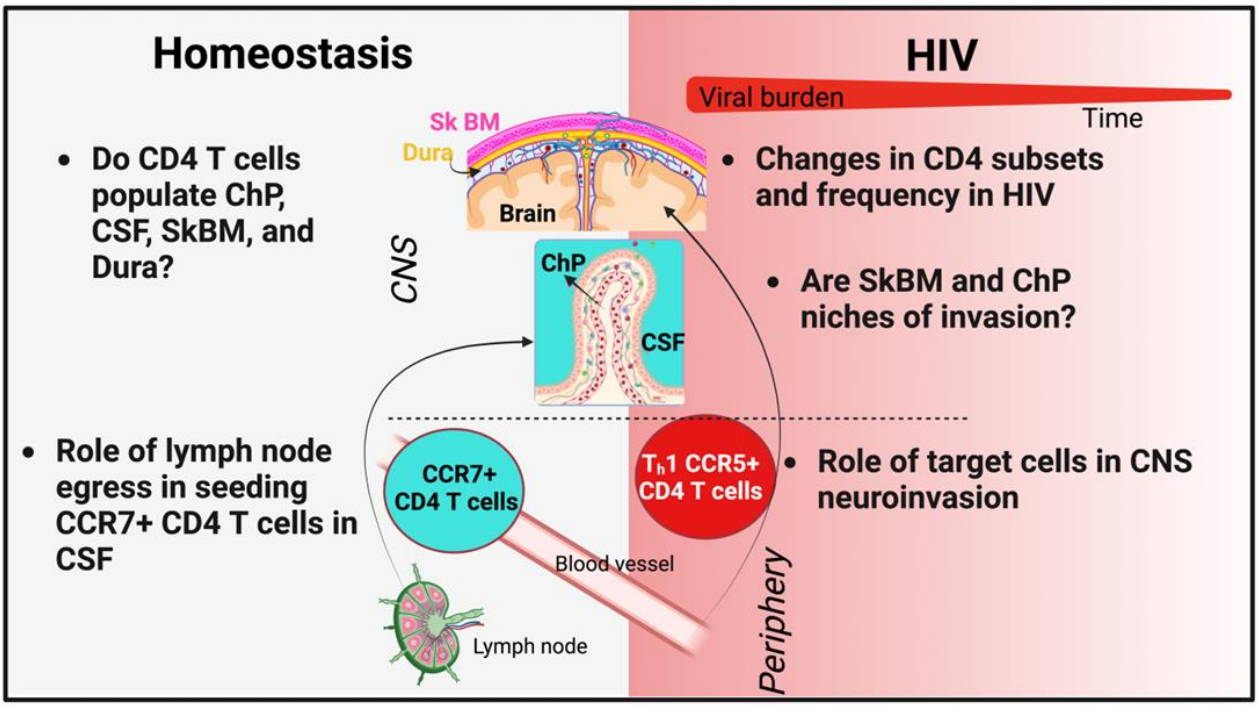

Figure 3. Graphic illustration highlighting pertinent questions related to T lymphocyte populations in the CNS during homeostasis and HIV infection.

Introduction Tables

		Blood / Blood plasma	Choroid plexus	Brain parenchyma	Source
Homeostasis	Cytokines	IL-6, IL-8, IL-4, IP-10	CCL20, VEGF, TGF-β, IL-10, CXCL12, IP-10	IL-13	(155-162)
	Glucose	Glucose	-	-	(163)
	Albumin	Albumin	-	-	(164)
	IgG	IgG	-	-	(165)
CNS Inflammation/ Injury/ HIV	CD4 T cells	CXCR3+ CCR5+ CD4+ T cells CD26+ CD4 T cells CD4 T cells Central memory CD4 T cells	-	-	(166-169)
	CD8 T cells	HIV-specific CD8+ CCR5+ T_{EM} cells Activated CD8 T cells IFN-γ+ CD8 T cells	-	-	(170-172)
	Monocytes	sCD14, Activated monocytes, CCR2	-	-	(173-178)
	HIV vRNA	HIV vRNA	-	-	(166)
	HIV vDNA	HIV vDNA	-	-	(166)
	Markers of neuronal injury	CCR2	-	NFL, tTau, exosomes	(174, 179-182)
	Markers of microglial activation	-	-	Neopterin	(173, 183, 184)
	Markers of astrocyte activation	-	-	S100β, GFAP, APOE, Neopterin	(173, 183-185)

Table 1. Overview of CSF composition and origins. Delineates various cytokines, lymphocyte populations, immune activation markers, glucose and albumin found within the CSF along with their origins (peripheral – blood plasma, CNS – choroid plexus, CNS – brain parenchyma) during homeostasis or CNS inflammation/injury/HIV.

Gateways to CNS entry	**1.** BBB → Brain parenchyma		**2.** Leptomeningeal Blood vessels	**3.** BCSF → CSF in Ventricular space	
	Vascular endothelium lining parenchyma	*Glia limitans*		*ChP endothelium*	*ChP epithelium*
Selectins	P-selectin E-selectin	-	-	P-selectin	P-selectin
HIV infection	P-selectin E-selectin	-	-	-	-
Integrins heterodimers	LFA-1 VLA-4	-	LFA-1 VLA-4	-	LFA-1 VLA-4
HIV infection	LFA-1 VLA-4	-	-	-	-
Adhesion molecules	ICAM-1 VCAM-1	-	-	PECAM-1	ICAM-1 VCAM-1
HIV infection	ICAM-1 VCAM-1	-	-	-	-
GPCR	-	-	-	-	-
HIV infection	-	-	-	-	-
Chemokines	CCL19 CCL21	-	CCL5	-	CCL19 CCL20
HIV infection	IP-10 MCP-1 CCL3 CCL4 CCL5	-	-	-	-
MMP	-	-	-	-	-
HIV infection	-	MMP2 MMP9	-	-	-

Table 2. Overview of Key Factors in Lymphocyte Trafficking Across CNS Barriers. Delineates the various selectins, integrins, adhesion molecules, GPCR, chemokines, and MMPs implicated in the trafficking of lymphocytes across the CNS's protective barriers. Column 1 describes players involved in crossing the BBB barrier. Column 2 describes players involved in crossing the leptomeningeal vessels. Column 3 describes players involved in crossing the BCSFB. Additional rows, highlight the factors implicated at homeostasis (white) and HIV infection (grey). (-) denotes unknown role in the corresponding process. ChP (Choroid Plexus)

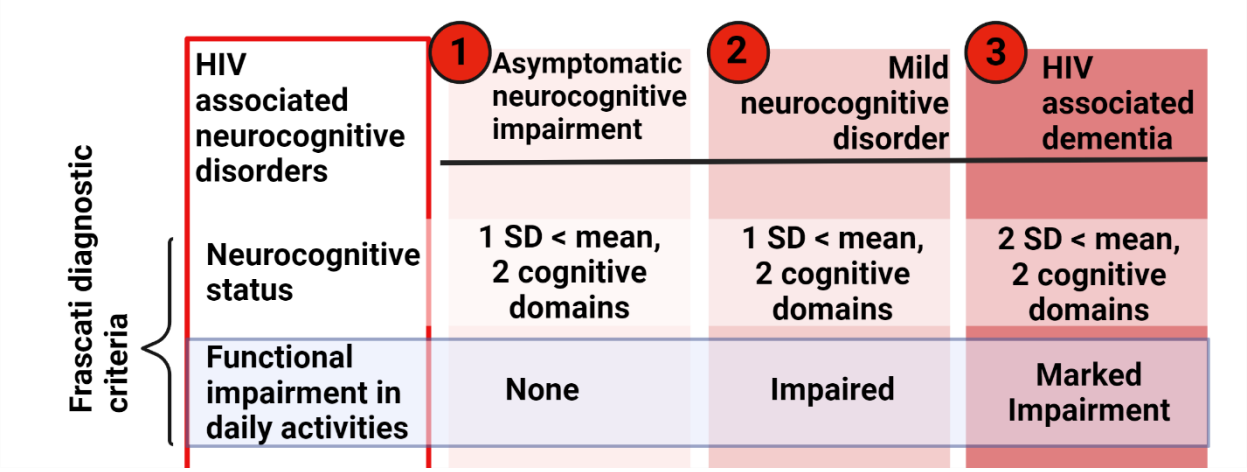

Table 3. Categories of HAND – Neurocognitive domains of the brain (at a minimum of 5) are assessed using a neuropsychological assessment. Functional status is typically self-reported, and no consensus measures exist for HAND criteria. SD- standard deviation.

	Cons	Pros	Degree of T cell infection	Degree of myeloid cell infection	Takeaway from each model
SIVCL757	►Does not efficiently replicate in PBMCs ►Does not accurately reflect moderate HAND ►Reflects compartmentalized virus in late stage viremia ►Low viremia ►Tough to detangle the contribution of CD4 T cells and myeloid cells on CNS seeding/neuroinflammation	► Efficiently replicates in MDMs ► High rate of SIVE ► Infects CD4 T cells to a moderate degree ► Early infection of the brain	+	+++	Can be utilized to study the contributions of CD4 T cells in late-stage disease where myeloid cells are primary targets of infection. Given the rate of CD4 depletion in this model is lower than that seen in SHIV or SIV mac251 infection, hypothetically these cells should be observed more easily within the CNS.
SHIV.CH505	►Moderate viremia ►SHIV env mutation may not accurately reflect natural infection	► Most transmitted /founder viruses replicate poorly in macrophages ► Great model to study T cell infectivity - high rate of replication in CD4 T cells ► Early infection of the brain	+++	-/+	The preferential infection of T cells in this model allows for the study of their unique contribution to the CNS during acute infection. However, the infection/depletion of these cells complicates the assessment of this population.
SIVmac251	►Composition of swarm varies after amplification in cell culture ►Infection of macrophages during acute infection ►Unregulated can lead to HIVE ►Tough to detangle the contribution of CD4 T cells and Myeloid cells on CNS seeding/neuroinflammation	► Primarily T cell tropic ► Macrophage infection during acute infection ► Infection mirrors human pathogenesis ► Early infection of the brain ► Well studied model	+++	+	Well established, highly pathogenic model to study the natural course of HIV infection and the neuroinflammatory contributions of both myeloid and T cells in the CNS. This model favors the infection of T cells relative of myeloid cells during acute infection

Table 4. Pros and Cons of using different SIV infection models to study moderate HAND.

Highlights the advantages and disadvantages of three different SIV viral strains that were utilized in this dissertation to investigate the role of T cells in HAND.

CHAPTER 2: Neuroinflammatory transcriptional programs induced in rhesus pre-frontal cortex white matter during acute SHIV infection

****Published in: Journal of Neuroinflammation, 2022 Oct 6; 19 (1):250. doi: 10.1186/s12974-022-02610-y. PMID: 36203187; PMCID: PMC9535930.*

Presented in dissertation as published with the one change. Co-first authors order is swapped, with Elizaldi presented first and Hawes second.

CHAPTER II

In Chapter II, we built upon a previous finding that demonstrated an influx of CD3+ T cells into the rhesus macaque brain parenchyma 12 weeks after infection with T/F SHIV-1157ipd3N4. This study also observed CD4-associated vRNA in the CSF by week 3 post infection (described on page 27). Our primary objective in Chapter II was to determine if infection with a CCR5 tropic T/F virus resulted in viral spread within the brain parenchyma. To evaluate this question, we employed twenty rhesus macaques that were previously vaccinated with a DNA-protein vaccine and were subsequently intravaginally infected with T/F SHIV.CH505, a highly potent SHIV variant. Post infection we observed that three animals were protected, while the others exhibited low to moderate viral loads in plasma and CSF (peaking at <100,000 copies). This cohort of vaccinated/infection challenged macaques provided a unique model to investigate the extent of acute viral neuroinvasion and neuroinflammation under conditions mimicking natural transmission. Following these initial observations, we intravenously infected the three protected animals to conduct a comprehensive analysis of transcriptional changes within the brain (four specific brain regions sampled) and phenotype isolated T cells from the PFC. Together, Chapter II sheds light on the acute dynamics of viral seeding in the CNS, amidst low-to-moderate viremia.

Neuroinflammatory transcriptional programs induced in rhesus pre-frontal cortex white matter during acute SHIV infection

Sonny R. Elizaldi[1,2#], Chase E. Hawes[1,2#], Danielle Beckman[3], Giovanne B. Diniz[3], Yashavanth Shaan Lakshmanappa[2], Sean Ott[3], Blythe P. Durbin-Johnson[4], Ashok R. Dinasarapu[5], Andrea Gompers[2], John H. Morrison[3,6], Smita S. Iyer[2,3,7]

Affiliations: [1]Graduate Group in Immunology, University of California, Davis, CA 95616, USA; [2]Center for Immunology and Infectious Diseases, University of California, Davis, CA 95616, USA;[3]California National Primate Research Center, University of California, Davis, CA 95616, USA; [4]Division of Biostatistics, School of Medicine, University of California, Davis, CA 95616, USA; [5]Department of Human Genetics, Emory University, Atlanta, GA; [6]Department of Neurology, School of Medicine, University of California, Davis, CA 95616, USA; [7]Department of Pathology, Microbiology, and Immunology, School of Veterinary Medicine, University of California, Davis, CA 95616, USA

#Both authors contributed equally.

Abstract

Background

Immunosurveillance of the central nervous system (CNS) is vital to resolve infection and injury. However, immune activation within the CNS in the setting of chronic viral infections, such as HIV-1, is strongly linked to progressive neurodegeneration and cognitive decline. Establishment of HIV-1 in the CNS early following infection underscores the need to delineate features of acute CNS immune activation, as these early inflammatory events may mediate neurodegenerative processes. Here, we focused on elucidating molecular programs of neuroinflammation in brain regions based on vulnerability to neuroAIDS and/or neurocognitive decline. To this end, we assessed transcriptional profiles within the subcortical white matter of the pre-frontal cortex (PFCw), as well as synapse dense regions from hippocampus, superior temporal cortex, and caudate nucleus, in rhesus macaques following infection with Simian/Human Immunodeficiency Virus (SHIV.C.CH505)

Methods

We performed RNA extraction and sequenced RNA isolated from 3 mm brain punches. Viral RNA was quantified in the brain and cerebrospinal fluid by RT-qPCR assays targeting SIV Gag. Neuroinflammation was assessed by flow cytometry and multiplex ELISA assays.

Results

RNA sequencing and flow cytometry data demonstrated immune surveillance of the rhesus CNS by innate and adaptive immune cells during homeostasis. Following SHIV infection, viral entry and integration within multiple brain regions demonstrated vulnerabilities of key cognitive and motor function brain regions to HIV-1 during the acute phase of infection. SHIV-induced transcriptional alterations were concentrated to the PFCw and STS with upregulation of gene expression pathways controlling innate and T-cell inflammatory responses. Within the PFCw,

gene modules regulating microglial activation and T cell differentiation were induced at 28 days post-SHIV infection, with evidence for stimulation of immune effector programs characteristic of neuroinflammation. Furthermore, enrichment of pathways regulating mitochondrial respiratory capacity, synapse assembly, and oxidative and endoplasmic reticulum stress were observed. These acute neuroinflammatory features were substantiated by increased influx of activated T cells into the CNS.

Conclusions

Our data show pervasive immune surveillance of the rhesus CNS at homeostasis and reveal perturbations of important immune, neuronal, and synaptic pathways within key anatomic regions controlling cognition and motor function during acute HIV infection. These findings provide a valuable framework to understand early molecular features of HIV associated neurodegeneration.

INTRODUCTION

The central nervous system (CNS) houses a complex array of innate and adaptive immune cells facilitating immunosurveillance during homeostasis [1,2,3]. Furthermore, the CNS is permissive to activated lymphocytes, expressing CNS homing receptors, via the blood–brain and blood–cerebrospinal fluid barriers during the effector phase of the immune response [4, 5]. These features underlie the immune response of neuroinflammation, which evolved to protect CNS tissues. Yet, when sustained, chronic neuroinflammation results in oxidative stress and cellular damage impairing synaptic and neuronal function which underlies the initiation and progression of neurodegeneration [6]. One demographic at a notably higher risk of developing age-related neurodegenerative diseases are people living with HIV (PLWH).

Following mucosal transmission, HIV initially replicates in gut-associated lymphoid tissue with subsequent systemic dissemination and rapid establishment of the viral reservoir in major organ systems, including the CNS. While neurons are not targets for HIV-1, entry of infected immune effectors (CD4 T cells and monocytes) via the barrier systems results in CNS viral dissemination during the acute phase of infection. Antiretroviral therapy (ART) is associated with cognitive improvements; however, 50% of PLWH on therapy remain symptomatic for a spectrum of cognitive impairments called HIV-associated neurocognitive disorders (HAND) [7,8,9,10]. A study of nine HIV + PLWH initiating ART within 4 months of acquisition showed evidence for compartmentalized HIV DNA within the cerebrospinal fluid (CSF), indicating establishment of the CNS reservoir early following infection [11]. Viral influx to the CSF was associated with inflammation as evidenced by the association between CSF HIV-1 RNA and CSF neopterin, a marker of inflammation and immune activation [12]. Several studies demonstrate white and gray matter frontal atrophy early following HIV infection [13,14,15], while neural injury within the striatum and decrease in size of the caudate nucleus are documented in chronic disease [16]. Thus, neuropathological analyses in PLWH demonstrate early CSF viral influx, CNS inflammation

and early structural alterations in the frontal cortex as key pathological components of HAND. However, molecular changes underlying acute neuroinflammation in the HIV-infected brain and disruption of cellular programs in the pre-frontal cortex and other regions linked to cognition and motor control remain understudied. Therefore, delineating molecular signatures characteristic of the acute HIV infected brain is important to gain deeper insights into pathways underlying progressive neurodegeneration. Furthermore, RNA sequencing approaches may provide greater resolution into biological processes and networks otherwise overlooked by cellular/tissue-based techniques.

To understand the molecular underpinnings of acute neuroinflammation, we performed RNA-sequencing of the pre-frontal cortex subcortical white matter (PFCw) in animals infected with SHIV.C.CH505 HIV-1 virus (SHIV), a CD4-tropic transmitted/founder (T/F) virus [17, 18]. In addition, three synapse-dense regions; hippocampus (HP), superior temporal sulcus (STS), and caudate nucleus (CN), were chosen based on their relevance to neurocognitive decline and/or known patterns of pathology in neuroAIDS [19,20,21]. Our approach revealed novel insights into HIV-1-induced transcriptional changes in the brain, and the data support three main conclusions: first, that there is pervasive immune surveillance of the rhesus CNS at homeostasis. Second, HIV-1 dissemination within the brain induces perturbations in key biological pathways regulating inflammation and antiviral signaling, oxidative and nitrosative stress, and endoplasmic reticulum (ER) stress. Third, pathways regulating T helper 1 inflammation and microglial activation are induced within the PFCw during acute HIV-1 infection. Our data provide an important framework to understand determinants of acute neuroinflammation and lay the foundation for identifying immune mechanisms underlying neuropathogenesis in HIV infection.

RESULTS AND DISCUSSION

Study design

To identify major transcriptional features of the brain during acute HIV infection, we reasoned that infecting young animals with a virus that recapitulates properties of T/F viruses would allow us to understand inflammatory consequences of acute HIV-1 dissemination to the CNS in the HIV susceptible demographic. To this end, we infected young adult rhesus macaques (5.2–5.6 [years.months], n = 3) intravenously with the R5 CD4 tropic SHIV.C. CH505 virus, a T/F virus with Env substitutions conferring strong engagement with rhesus CD4 resulting in high replication in vivo and consequent depletion of CCR5 + CD4 T cells in mucosal tissues. Furthermore, delayed development of autologous neutralizing antibodies 3–6 month post-infection assures acute viral dissemination [17, 18].

Animals were euthanized at week 4 post-SHIV infection to capture transcriptional perturbations induced by innate and adaptive immune responses to viral seeding in the CNS. At necropsy, the entire brain was excised en bloc, following saline perfusion, and regional punch biopsies were obtained from four major brain regions associated with cognition or motor behaviors. As white matter pathology is commonly observed in Human AIDS, we collected tissue from the subcortical white matter of the prefrontal cortex (PFCw), a region that contains multiple myelinated circuits linked to cognitive and motor functions, to evaluate transcriptional changes in white matter tissue. In addition, we collected samples of synapse-rich areas: the caudate nucleus, a region involved in motor control and typically afflicted in neurotropic HIV infection, in addition to the gray matter of the superior temporal sulcus (STS) and hippocampal formation (HP), which are linked to cognition and memory, respectively, and thus key regions for cognitive decline as seen in aging, AIDS, and Alzheimer's Disease (Fig. 1A, Additional file 1: Table S1). Brain regions were identified using anatomical maps in the macaque brain atlas [22]. In addition, four SHIV unexposed animals (3.6–6.6 [years.months]) were assessed to establish baseline transcriptome

profiles. Following bulk RNA extraction from 28 total samples (SHIV n = 12; SHIV unexposed n = 16), we performed 3'-tag RNA sequencing on extracted RNA (RNA-seq) from regional tissue punches and obtained gene expression levels, denoted as normalized read counts (NRC).

Molecular signatures of innate immune surveillance in the rhesus brain

To explore gene expression patterns during homeostasis, we systematically assessed transcriptional features across brain regions in SHIV unexposed animals. Comparison of NRCs demonstrated equivalent gene expression across brain regions (PFCw, 17,717; STS, 17,221; CN, 17,861; HP, 17,550). As illustrated, NRC range (0.139–10,000) and distribution (average 0.5% genes > 1000 NRC, 12.57% genes between 100 and 999.99 NRC, and 87% genes < 99.99 NRC) was comparable across regions (Additional file 1: Fig. S1, Additional file 2: Table S2).

T-distributed stochastic neighbor embedding (t-SNE) analysis of the brain transcriptome revealed regional specification, an observation consistent with topographical gene expression of primate brain transcriptomes [23] (Fig. 1B, Additional file 1: Fig. S2). To identify region-specific biological modules, we used weighted gene co-expression network analysis (WGCNA) and constructed gene co-expression networks [24, 25]. WGCNA of the four brain regions identified a total of 17 modules with 8 region-specific modules denoted by color (PFCw [MEgreen, MEbrown, MEmidnightblue, MEmagenta,], CN [MEpurple, MEred], STS [MEtan], HP [MEsalmon]) (Fig. 1C) demonstrating functional specification by region. Gene Ontology (GO) analysis of regional modules identified functions related to cognitive behavior, sensory processing, synapse formation, neuron projections, metabolic processes, and signaling pathways (Fig. 1D, Additional file 1: Fig. S3). Notably, the PFCw-specific MEgreen and MEbrown modules showed representation of immune functions including innate immune response, positive regulation of macrophage differentiation, antigen processing and presentation, positive regulation of interferon-alpha, cell activation, cellular response to dsRNA, B cell differentiation, negative regulation of NF-kB signaling, and inflammatory response. Enrichment for these terms was consistent with

microglia gene signatures in humans and macaques and their increased frequencies in white matter tissue [26, 27] (Fig. 1D). Overall, the data showed spatial regulation of functional processes across the rhesus brain with representation of immunological processes in the white matter.

We next investigated regional expression of genes regulating innate immune responses. While the microglia-specific marker, TMEM119, was not expressed likely due to lower sensitivity of bulk RNA-sequencing in capturing lower expressed transcripts [27], P2RY12, another microglia specific marker was expressed across all regions (Fig. 1E). Markers commonly associated with microglia and macrophages—CD68, CD14, integrin subunit alpha M (ITGAM [CD11b]), CX3CR1 (Fractalkine receptor with corresponding high expression of the ligand, CX3CL1 [Additional file 1: Fig. S4]), and CD163—were also expressed with no regional biases evident. Genes regulating antigen presentation—the major histocompatibility II (MHCII) genes, MAMU–DOB, MAMU–DRB1, MAMU–DRA were expressed across all brain regions. Correspondingly, CIITA, a co-activator regulating MHCII mRNA transcription, was also widely expressed. CD80, a costimulatory ligand for T-cell activation, and allograft inflammatory factor 1 (AIF1), upregulated by activated microglia and referred to as IBA1, were similarly expressed in all regions. CD86, another costimulatory molecule, was enriched in the CN (adjusted $p < 0.0000001$) relative to other synapse dense regions (STS, HP), while CD40 was expressed at low levels (< 1 NRC) across all sampled tissues (Fig. 1E).

Next, we assessed regional expression of genes regulating antiviral responses. The ubiquitously expressed interferon receptor genes (IFNAR1, IFNAR2, IFNGR1, IFNGR2), were found in all brain regions with minimal regional variation (Fig. 1F). Furthermore, genes encoding downstream signal transduction molecules (STAT1, STAT2, JAK1, JAK2, TYK2) were correspondingly expressed as were the interferon regulatory factors (IRF1–9), proteins regulating interferon production (Fig. 1F). We found the interferon-stimulated genes ISG15, MX1, MX2, OAS1–3 and OASL to be widely expressed in parallel with expression of pattern recognition

receptors (Fig. 1G), indicating the rhesus brain was poised to respond to viral infection. Expression of HIV restriction factors such as SAMHD1, BST2 (tetherin), TRIM5 (TRIM5α), and the apolipoprotein B mRNA editing enzyme catalytic subunit 3H (APOBEC3H) were also observed in all sampled regions suggesting these tissues may modulate HIV replication efficiency (Fig. 1G). Despite the regional variability in select genes (i.e., CD86), our data indicate that microglia, macrophage, and antiviral gene programs are comparably expressed across the rhesus brain at homeostasis.

T cell resident immune signatures within the rhesus brain

We next sought to determine regional expression of adaptive immune genes to understand immunosurveillance of the CNS during homeostasis. Global expression of the T cell chemokines CCL8, CCL24, CXCL12, and CX3CL1 was suggestive of T cell recruitment to both white matter regions, and across three distinct regions of telencephalon, CN, STS, and HP (Additional file 1: Fig. S4). Consistent with this hypothesis, we observed expression of canonical T-cell genes CD3E, CD4, and CD8A across all sampled regions (Fig. 2A). Since STAT proteins both regulate and precede cytokine-induced responses in antigen experienced CD4 T cells, we sought to determine if genes encoding these proteins were concomitantly expressed. STAT4, STAT6, and STAT3 which are pivotal for Th1, Th2, and Th17 CD4 helper programs, respectively, were broadly expressed. We also noted the IL-12 receptor components (IL-12Rβ1 and IL-12Rβ2) which transmit Th1 differentiation cues, to be expressed in all regions. CCR5, a Th1 chemokine receptor and HIV entry co-receptor, was expressed at low levels (average NRC = 0.09) primarily in the HP (Fig. 2A). In contrast, however, we did not detect expression of the canonical Th1 transcription factor, TBX21, and Th1 chemokine receptor, CXCR3.

Evaluation of Th2 associated genes showed expression of GATA-3 (a Th2 differentiation and neurogenesis factor) in all brain regions, except for one HP sample [28]. Furthermore, IL-4R transcripts were also expressed, while expression of the Th2 specific chemokine receptor CCR4

was mostly absent (Fig. 2A). The expression of Th17-related genes (RORC [RORγt], IL-23R, and CCR6) and Treg associated genes (FOXP3 and STAT5A) (Fig. 2A) was consistent with seeding of the healthy brain by microbiome specific T cells and T regulatory cells [3]. Assessment of cytolytic genes revealed that cytotoxic T cell and NK cell effector molecules (GZMB [granzyme B], PRF1 [perforin 1], and GNLY [granulysin]), which mediate clearance of virally infected cells, were expressed at low levels (NRC < 2). Genes regulating memory CD8 T cell differentiation (EOMES and RUNX3) were expressed in most regions, with the exception for EOMES which was absent in the CN. Cytokine receptors IL-7R and IL-15Rα, necessary for memory T-cell homeostasis, were expressed with significantly elevated levels of IL-15Rα in the CN (adjusted $p < 0.01$) relative to other synapse dense regions, such as the HP and STS. IL-2 receptor family proteins IL2Rγ, which serves as a subunit of the IL-7 and IL-15 receptors, and IL2Rα were also correspondingly expressed. Genes expressed by central memory T-cells (Tcms), CD28 and SELL (CD62L), were observed in all regions, but transcripts for CCR7, a chemokine receptor mediating T-cell trafficking to secondary lymphoid organs, was not detected in any samples. In addition to Tcm markers, signatures associated with tissue resident memory (Trm) T cells such as αE integrin (ITGAE [CD103]) were readily observed in all sampled regions. CD69, another Trm marker, was expressed in the PFCw, STS, and HP, but absent in the CN (Fig. 2A). The sphingosine 1 receptor, S1PR1, mediating T-cell egress was expressed in all three synapse dense regions and PFCw. In addition, we observed widespread expression of integrin beta 1 (ITGB1) across brain regions compared to integrin beta 7 (ITGB7), which is consistent with the role of α4β1 in regulating immune cell migration to the brain [29]. Together, these data support the prevalence of a heterogenous CNS T cell population composed of Th1, Th2, Th17 with Trm features in the rhesus brain, consistent with T cell profiles reported in healthy mouse and human brains [3, 30].

Next, to substantiate our gene expression data demonstrating surveillance of the rhesus brain by T cells, we performed flow cytometry analysis on CNS tissues from a comparable cohort

of SHIV unexposed rhesus macaques. To assess brain-resident lymphocytes, we performed saline perfusion and removed the meningeal layers prior to processing the brain samples. The perfused brain was subjected to collagenase digestion and mononuclear cells were enriched by percoll density gradient (Fig. 2B). Immune cell frequencies in the brain were compared to that in cerebrospinal fluid (CSF) and the CNS draining lymph nodes to delineate relative immune composition in these distinct CNS associated compartments. Consistent with observations in mice and humans, microglia (CD11b + CD45lo/int cells) constituted the predominant immune subset in the rhesus brain (Fig. 2C–E). Furthermore, T-cells were readily observed in the rhesus CNS with brain CD8 and CD4 T cells consisting of approximately 0.1% of total parenchymal cells (Fig. 2C–E).

After establishing CNS surveillance by CD4 and CD8 T cells by flow cytometry, we assessed regional expression of effector cytokine transcripts during homeostasis by RNA sequencing. The IL-1 family cytokines, IL-1β, IL-18, and IL-33 were expressed in all sampled regions (Fig. 2F). Other IL-1 family cytokines along with specific IL-2 common γ-chain cytokines, such as IL-2, IL-9, and IL-15, which regulate immune cell proliferation, were variably detected with relatively low expression levels (< 2 NRC) in the rhesus brain. IL-7, another IL-2 receptor γ-chain family cytokine, was exclusively expressed in the HP, while IL-5, an IL-2 receptor β-chain family cytokine was expressed in all regions. IL-6 and IL-19 family cytokines along with TNF-α, with the exception of one PFCw sample (Animal 44288 [TNF: 0.3 NRC]), were undetectable and expression of IL-12, IL-10, and IL-17 family cytokines was variable among samples. IL-12 family cytokines, IL-12β, a Th1 inducing cytokine was expressed in some samples from the PFCw, STS, and HP but was absent in CN. IL-23α subunit that supports Th17 differentiation, was expressed in most brain regions. IL-12 family cytokines (IL-12α and IL-27) were not expressed. IL-10 family cytokine expression was variable with IL-10 expressed in the HP and STS of two animals and IL-26 in the PFCw, STS, and HP of three animals (Fig. 2F). Except for IL-25, associated with Th2

responses and maintenance of blood brain barrier integrity [31], cytokines of the IL-17 family were not detected (Fig. 2F).

To substantiate homeostatic cytokine and chemokine RNA-seq data, we performed protein-based analysis of the CSF from 8 uninfected rhesus macaques utilizing the O-link platform [32] (Fig. 2G). The cytokine milieu within the CSF is a composite of mediators generated from three distinct compartments; cytokines produced by cells within the brain parenchyma and drained in CSF via the interstitial fluid; cytokines produced by choroid plexus epithelial cells, myeloid cells and T cells within the choroid plexus stroma; and plasma cytokines transported across the blood–CSF (BCSF) barrier [33]. Commensurate with gene expression data, we found the CSF was immunologically rich with expression of IL-1 family cytokines and their receptors (IL-18, IL-18R1); IL-2 common γ chain cytokine, IL-7; innate cytokines, IL-6, and IL-8 and IL-12β subunit. Among the CCL-chemokines, CCL2, produced by choroid plexus epithelial cells and stromal cells [34], was detected as were the CCR5 ligands, CCL3 and CCL4. The Th17 chemokine, CCL20 and the Th1 chemokines, CXCL10, CXCL11 and CX3CL1 were found in the CSF. In contrast to studies in mice, levels of IL-4 and IFN-γ were below the level of detection in macaque CSF (data not shown) [35]. Altogether, these data demonstrate a rich cellular and soluble immune landscape resulting from homeostatic immune surveillance in the rhesus CNS—both parenchymal and CSF compartments.

Changes in brain transcriptome following SHIV infection

After establishing molecular features of the adult macaque brain, we sought to delineate changes in the brain transcriptome during acute SHIV infection. To determine CNS viral dissemination, we first assessed CSF vRNA trajectories during acute viremia (Fig. 3A). Viral kinetics in cell-free CSF paralleled plasma viremia, with 2 log fold lower viral loads in the CSF compared to plasma (week 2 median viral loads/ml: plasma, 1.3 × 10^6; CSF, 19,000), with a strong correlation between these distinct compartments ($r = 0.96$, $p < 0.001$) (Fig. 3A). To formally

assess viral dissemination within the rhesus CNS, we performed a comprehensive assessment of vRNA and vDNA across several brain regions and CNS tissues obtained post-mortem. The data showed dissemination of SHIV (vRNA, expressed as copies/10^6 cell equivalent) to regions sampled for RNA sequencing analysis: the PFC white matter (4.1–240), HP (3.3–460), STS (4.3–240), and CN (2.5–16). Furthermore, we observed detectable vRNA in the PFC grey matter, Hypothalamus (Hypo), Cerebellum (Cere), Inferior Parietal (IP), Anterior Cingulate Cortex (ACC), Amygdala (Amy), and primary visual cortex (V1) of the brain, and the choroid plexus stroma (CP) indicating widespread dissemination of SHIV within the rhesus CNS (Fig. 3B). The presence of vRNA in the Dura mater (1200–24,000) and deep cervical nodes (7700–66,000) was consistent with CNS antigen clearance via the lymphatics. vRNA strongly correlated with pro-viral DNA levels ($r = 0.82$, $p < 0.001$), suggesting early seeding of viral reservoirs in major brain regions (Fig. 3B), consistent with reports that blocking T cell and monocyte extravasation via the blood–brain barrier significantly decreases vDNA in the frontal cortex in SIV infected rhesus macaques [29]. The stability of the CSF Glucose/Albumin ratio indicated that CNS viral entry was not associated with breakdown of the blood–brain or the BCSF barriers, suggesting immune cell recruitment to the CNS may mediate viral entry (Fig. 3B).

To identify principal features of the SHIV infected brain, we conducted WGCNA on all 28 brain samples from both infected and uninfected animals using log2 counts per million reads (Fig. 3C). We identified a total of 21 gene co-expression modules with 4 modules highly associated with SHIV infection: pink (393 genes), turquoise (1466 genes), and blue (1411 genes) within the STS, and royal blue (30 genes) in the PFCw and the STS. Figure 3D shows module eigengenes characterized by their expression patterns in different brain regions and the corresponding GO terms enriched in each module.

Genes within these 4 modules were enriched for GO terms corresponding to neuroinflammation, such as oxidative and nitrosative stress (e.g., microsomal glutathione S-

transferase 3 [MGST3], peroxiredoxin [PRDX3], and the mitochondrial citrate carrier, SLC25A43) (Additional file 1: Fig. S5). While we did not observe differential expression of genes regulating excitotoxicity, several genes regulating synaptic markers were differentially induced, e.g., the synaptobrevins (vesicle associated membrane protein [VAMP] 3, 8), synaptophysin, and dynamin 3; suggestive of early synaptic changes following SHIV infection (S5). Despite the low abundance of synapses in white matter tissues, alterations in synaptic gene pathways observed in the PFCw could be attributed to interstitial white matter neurons reported in both human and rhesus white matter tissue [36, 37]. Altogether, these data show viral entry and dissemination within the CNS, with corresponding upregulation of gene programs associated with neuroinflammation in the PFCw and STS.

Enrichment of inflammatory gene signatures in the PFC white matter following SHIV infection

To investigate gene expression changes resulting from CNS viral dissemination, we first applied t-SNE analysis to gene expression data from all samples, which revealed clustering of gene expression profiles between infected and control animals by brain region (Additional file 1: Fig. S6). Using DEG analysis to compare infected versus uninfected animals (criteria: $p < 0.01$ threshold for false discovery rate [FDR] and absolute value of log2 fold change ≥ 1), we found regional differences in SHIV-induced transcriptomic changes (STS: 884 DEGs; PFCw: 871 DEGs; CN: 203 DEGs; HP 92 DEGs) (Fig. 4A) with the STS and PFCw exhibiting the most distinctive transcriptional profiles following infection. Notably, differentially expressed genes in PFCw and STS were EGR2 and BHLHE40, transcription factors regulating IFN-γ production from CD4 T cells and microglia [38, 39] and ISM1 secreted by activated CD4 T cells [40]. COX7A2 and DGAT2 involved in oxidative phosphorylation and lipid metabolism, respectively, were also induced implicating these pathways in the acute neuroinflammatory response to SHIV infection [41, 42] (Fig. 4B, Additional File 1: Fig S5).

To gain insights into molecular programs induced following SHIV infection, we conducted pathway analyses for DEGs associated with SHIV infection in the PFCw and STS. Of the 526 uniquely regulated genes in the PFCw, pathways regulating oxidative phosphorylation, glutathione metabolism, and Systemic Lupus Erythematosus were enriched alongside processes encompassing T cell homeostasis, and IL-6 signaling. Within the STS, amino acid metabolism, antigen processing and presentation, and steroid biosynthesis pathways were most significantly upregulated after infection. The 286 DEGs that overlapped between the PFCw and STS represented pathways associated with Parkinson's Disease, the proteasome pathway, and steroid hormone biosynthesis (Fig. 4C). These data reveal perturbation in important immune, neuronal, synaptic, and metabolic pathways within key anatomic regions controlling cognition during acute SHIV infection.

Next, we sought to identify genes regulating inflammatory processes within the PFCw. To this end, we integrated expression analysis with inflammatory biological pathways utilizing gene set enrichment analysis (GSEA). GSEA revealed enrichment of genes regulating T cell differentiation (Fig. 4D); these included T cell chemotaxis (enrichment score [ES] = 0.65; top genes PIK3CD, STK39, PIK3CG, WNK1, CCR2 and CXCL16); T cell differentiation (ES = 0.5; top genes, RARα, IL23α, LEF1, GATA3, NLRP3, IRF1, BATF, and BCL-6), (ES = 0.5), and response to IL-6 (ES = 0.45; top genes, STAT3, RELA, SMAD4, CBL, IL6R, IL6ST, JAK1, ST3GAL6).

Several genes among those differentially expressed in the PFCw encoded for proteins regulating T cell and microglial activation. Among the most highly induced genes was the transcriptional regulator, EGR2, which has been implicated in neuronal plasticity in response to inflammation and Th1 CD4 T cell proliferation [38, 43]. Similarly, the IL-1β-induced transcription factor, BHLHE40, which negatively regulates IL-10 production and drives T cell mediated neuroinflammation was also upregulated in the PFCw following infection [39, 44]. ISM1, a gene

encoding the secreted protein Isthmin which regulates NK and Th17 CD4 T cell effector functions [40], was also induced (Fig. 4E).

Several genes related to chemokine and cytokine receptors showed elevated expression levels within the PFCw following SHIV infection. This included CXCR4, a chemokine receptor, which is elevated in neurodegenerative diseases and expressed by a variety of immune cells, including T cells, and activated microglia [45]. Cytokine receptor subunits IL-27Rα and IL-23Rα, expressed by activated immune cells were significantly induced in the PFCw after infection [46, 47]. Connective tissue growth factor/Nephroblastoma overexpressed gene family 1 (CCN1), an inducible extracellular matrix protein secreted by reactive astrocytes was upregulated in the PFCw [48]. The kinase, CAMK1, which regulates CCN1 expression and is induced in astrocytes following Zika infection [49], was also correspondingly elevated (Fig. 4E). This gene expression program indicated that astrocyte, microglial, and T cell activation programs were induced in the frontal cortex white matter following SHIV infection. In contrast to genes regulating immune cell activation, we also found that the orphan nuclear receptor and transcription factor NR4A1 (NUR77), an intrinsic negative regulator of microglial and T cell activation [50], was upregulated. Similarly, the immune checkpoint inhibitor, programmed cell death-2 (PDCD2) was also elevated in the PFCw. Intriguingly, expression of HLA-DP and CD86 were decreased, suggestive of a net diminution in expression or reduction in numbers of antigen presenting cells in the PFCw following infection (Fig. 4E).

Based on these transcriptional changes and SHIV dissemination within distinct brain regions, we hypothesized that activated T cells were actively recruited to the CNS during acute SHIV infection. To this end, we assessed immune composition of the CSF over the course of infection and found increased frequencies of CD4 and CD8 T cells expressing PD-1, a marker for TCR stimulation, indicative of CNS influx of activated T cells during acute infection. We observed a significant increase in CXCR3 + PD-1 + CD4 and CD8 T cells denoting potential recruitment of

antigen-specific cells (Fig. 4F), consistent with reports of CD8 T cell influx into the CSF during acute HIV-1 infection [51]. However, unlike the reported influx of Th17 in neuroinflammatory disease models, negligible expression of CCR6 was found on CSF CD4 T cells. This increase in CXCR3 + CD4 and CD8 T cells was consistent with induction of IP-10 in CSF following infection (Fig. 4G), and the relative higher levels of IP-10 in CSF compared to the systemic compartment, indicating CNS production of IP-10 both during homeostasis and infection. In line with the increase in Th1 inflammatory response in the CSF, we found evidence for a net increase in CXCR3 + CD4 and CD8 T cells in the PFC during acute SHIV infection (Fig. 4H). Together, these data demonstrate that viral dissemination together with Th1 CD4 T cell and CXCR3 + CD8 T cell infiltration within the CNS occur during acute stages of infection and correspond with the induction neuroinflammatory gene programs in the PFCw.

In addition to immune genes, we found that the primary astrocyte GABA/glycine transporter SLC6A11, within the neurotransmitter family, was upregulated in the SHIV infected PFCw relative to uninfected controls. While SLC6A11 is not altered in neurodegenerative diseases, a net increase in reactive astroglia could explain increased levels of this transporter [52] (Additional file 1: Fig. S7). SLC32A1, which mediates GABA/glycine uptake into synaptic vesicles was also upregulated. Correspondingly, we observed increased expression of the mesencephalic astrocyte-derived neurotrophic growth factor (MANF)—an ER stress inducible factor reported to rescue neuronal loss in several neurological disorders [53]. In addition, genes regulating RNA levels of ATP synthase and transport subunits were induced after SHIV infection suggestive of alterations in mitochondrial respiratory capacity and cholesterol synthesis. These observations suggest that molecular changes in synaptic functions and bioenergetic pathways in the brain can occur during the early stages of SHIV infection.

Rhesus macaque models have been informative in characterizing SIV associated neuroinflammatory processes, with models of neurotropic SIV infection showing increased

frequencies of memory CD4 T-cells, B-cells, and macrophages in the brain parenchyma of infected animals developing encephalitis versus animals without encephalitis [54]. Studies using SHIV have demonstrated early viral seeding of the CNS and CD4 T cell infiltration into the brain parenchyma using immunohistochemistry, suggesting that neuroinflammatory processes may be initiated during the early stages of infection [55]. Our findings add to this important body of work by demonstrating features of SHIV-induced transcriptional perturbations during the acute phase of infection within regions of the brain associated with cognition, memory, and motor control. Interestingly, the neocortical association regions STS and the prefrontal subcortical white matter appeared to be more vulnerable to virus-induced alterations than caudate and hippocampus, which mirrors their enhanced vulnerability to age-related changes. This may be attributed to the magnitude of inflammatory processes resultant from initial viral dissemination within the PFC and STS, as observed viral loads were not markedly higher in these regions. These data emphasize the need for deeper analysis into the composition and activation status of immune cells within spatially distinct regions of the brain following HIV infection to identify key cellular players in HIV associated neuroinflammation. In all, our findings demonstrate vulnerabilities within these key regions both to HIV-1 dissemination and neuroinflammation during the acute phase of infection.

While our reported observations are novel, our study has several limitations. First, we performed our analysis in young adult rhesus macaques in consideration of age range of populations vulnerable to primary HIV infection; therefore, whether the extent of neuroinflammatory shifts following HIV-1 infection differ across the age spectrum and during chronic HIV infection are important questions that were not addressed in this study. Second, given observed viral influx in both the white and synapse-rich areas of the PFC, transcriptional changes to gray matter areas within the PFC warrant consideration. Third, our extensive virological analysis demonstrated viral influx and evidence for integration within multiple brain regions, including the hypothalamus, amygdala, and cerebellum. Capturing molecular changes in these

regions and using single cell approaches to gain comprehensive insights into pathways disrupted within neuronal, glial, and immune cells during acute HIV infection is an important consideration for future studies. Finally, histopathological assessments of the PFC and STS, not performed herein, would provide important insights into whether observed transcriptional perturbations were associated with pathological sequalae during the acute HIV infection.

In summary, our transcriptomic data, flow cytometric analysis of immune cell populations and quantification of CNS cytokines reveal pervasive immune surveillance of the rhesus CNS at homeostasis. Comparison of transcriptional profiles between uninfected animals and SHIV infected animals revealed significant alterations to gene expression in the PFCw and STS after infection. These changes included differential expression of genes associated with IL-6 responses, oxidative stress, and T-cell differentiation, activation, and chemotaxis. Furthermore, we observed SHIV-associated alterations in genes regulating astrocyte homeostatic functions, synaptic functions, and bioenergetic pathways suggesting that neuroinflammatory processes may alter normal neuron and glial cell activity in the brain. These neuroinflammatory gene profiles were substantiated by flow cytometric analysis which showed influx of Th1 CD4 T and CXCR3 + CD8 T cells into the CNS of infected animals over the course of infection. Together the data demonstrate that neuroinflammatory changes to the CNS, within the first weeks following SHIV infection, drives early functional molecular changes in normal neuronal and glial cell populations. Overall, our data provide hitherto unappreciated insights into the impact of SHIV infection on molecular processes in the rhesus brain; the data will be a useful primer to understand molecular mechanisms that drive subsequent neurodegeneration.

METHODS

Rhesus Macaques

Seven colony bred Rhesus macaques (Macaca mulatta, 1 male, 6 females, age 3.6–6.6 [years.months]) housed at the California National Primate Research Center (CNPRC) in accordance with the American Association for Accreditation of Laboratory Animal Care guidelines were used for the study. All protocols used in the study were approved by the Institutional Animal Care and Use Committee at UC Davis. Animals in the SHIV infected group were previously immunized with Clade C DNA-prime/protein vaccine and were infected 20 weeks after final protein boost through the intravenous route with SHIV. C.CH505, as described previously[56]. Infected animals were euthanized at 4 week post-infection. Viral titers were assessed in the blood and cerebrospinal fluid (CSF) of SHIV infected animals on a weekly basis. For blood and CSF collections, animals were anesthetized with 10 mg/kg ketamine administered intramuscularly. EDTA-anticoagulated blood was collected via intravenous blood draws and CSF by cisterna magna puncture. SHIV unexposed control animals were selected from opportunistic aged-matched medical culls for unrelated non-neurological conditions and showed no history of neurological impairment (Additional file 1: Table S1).

SHIV.C.CH505 virus and preparation

SHIV.C. CH505 was selected as the virus recapitulates attributes of primary HIV-1 strains. Briefly, SHIV.C. CH505 is a T/F virus engineered to strongly bind rhesus CD4 T cells while retaining antigenicity and tier2 neutralization sensitivity of the ancestral HIV-1 C.CH505 [17]. Replication efficiencies of SHIV.C. CH505 are comparable to pathogenic SIV strains in vivo and result in depletion of CCR5 + CCR6 + CD4 T cells within mucosal tissues [18]. SHIV. C.CH505 virus stocks at 189 ng/mL propagated in primary activated rhesus CD4 T cells were provided by George Shaw and Nancy Miller (National Institute of Health) and stored in liquid nitrogen. On day of virus administration, stocks were thawed on ice water and diluted fourfold in RPMI 1640. 0.5 mL

of working inoculum was loaded into 1 mL Tuberculin syringes and stored on ice until animal challenge.

Brain tissue collection and RNA extraction

At necropsy, brains were perfused in-vivo via cardiac saline perfusion and removed from the cranial cavity en bloc. Four regions were chosen based on their relevance to neurocognitive decline and/or known patterns of pathology in neuroAIDS. We were also informed by our preliminary microscopic observations in SIV-infected rhesus monkeys (data not shown). Subcortical white matter associated with the dorsolateral pre-frontal cortex was chosen due to the age-related myelin pathology described for this region that drives cognitive decline in aged monkeys [57] as well as the occurrence of similar white matter pathology observed in neuroAIDS cases [13, 58, 59]. The hippocampal formation (HP) was chosen for its relevance to age-related cognitive decline and neurodegenerative disorders in general [19]. Superior temporal sulcus gray matter (STS) was chosen for similar relevance to cognitive function and the high degree of microscopic pathology seen in preliminary analyses of rhesus macaques following SIV infection (data not shown). Finally, the caudate nucleus (CN) was included due to the extensive pathology seen in this motor system structure in neuroAIDS [20]. Tissues for RNA-seq were collected as follows: PFCw—a scalpel was used to dissect the white matter of the medial and inferior frontal gyri, between Bregma + 16 and + 10 mm, corresponding predominantly to the white matter subjacent to the dorsolateral prefrontal cortex. Care was exercised to minimize the collection of gray matter; CN—a round punch (3 mm in diameter) was collected from the head of the caudate nucleus, between Bregma + 6 and 0 mm, with negligible involvement of the internal capsule; HP—3 mm round punch was collected between Bregma -14 to -20 mm and involved all major subdivisions of the dentate gyrus and hippocampus proper, as well as part of the adjacent subicular complex while excluding the entorhinal cortex; STS—at approximately the same level of the hippocampal formation biopsy, a 3 mm round punch was taken from the intermediate

portion of the superior temporal sulcus, involving both the dorsal and ventral banks. The punch was performed at an angle with respect to the surface of the block, allowing the experimenter to follow the progressively dorsal position of the STS in the rostrocaudal direction, which minimized the inadvertent collection of neighboring white matter. Tissue samples collected from the PFCw, STS, CN, and HP were stored in RLT buffer with ß-mercaptoethanol (BME), flash frozen, and stored at − 80 °C until RNA extraction. RNA was extracted from samples using a Qiagen RNeasy lipid tissue mini kit and sent to the UC Davis DNA Technologies and Expression Analysis Core for 3'-tag RNA sequencing.

Additional samples were collected from the deep cervical lymph nodes (dCLN), choroid plexus stroma (CP), dura mater (dura), prefrontal cortex gray matter (PFCg), hypothalamus (Hypo), cerebellum (Cere), inferior parietal (IP), anterior cingulate cortex (ACC), amygdala (Amy), and visual cortex (V1) of the brain and used exclusively for viral RNA and DNA quantification. Brain tissues from these regions were obtained as follows: PFCg—3 mm punches were obtained from both dorsal and ventral banks of the dorsolateral prefrontal cortex, along the principal sulcus, corresponding to Brodmann area 46; Hypo—a scalpel was used to isolate a block containing the anterior and tuberal divisions of the hypothalamus. The block was dorsally limited by the anterior commissure and laterally confined by the internal capsule; Cere—a scalpel was used to dissect a small sample of the lateral hemisphere of the posterior cerebellar lobe. The resulting sample consisted almost exclusively of cerebellar cortical matter; IP—a scalpel was used to isolate the gray matter on the surface of the inferior parietal lobule, corresponding to Brodmann area 7; ACC—3 mm punches were obtained from the gray matter of the supracallosal anterior cingulate gyrus, corresponding to Brodmann area 24; Amy—3 mm punches were collected from the basolateral complex and the medial and central nuclei of the amygdala; V1—3 mm punches were collected from Brodmann area 17, along the calcarine sulcus. Care was taken to minimize the

inadvertent collection of white matter; CP—choroid plexus samples were extracted from the temporal and occipital horns of the lateral ventricle.

3'-Tag RNA sequencing

RNA integrity and quality was confirmed using microcapillary electrophoresis on an Agilent Bioanalyzer. Libraries were sequenced using 3'tag-RNA-seq on an Illumina HiSeq 4000 platform as previously described [63.] with slight modifications. In brief, barcoded sequencing libraries were prepared each from 500 ng total RNA sample and libraries' fragment size distribution were verified using micro-capillary gel electrophoresis on a LabChip GX system (PerkinElmer, Waltham, MA). Libraries were quantified using a Qubit fluorometer (LifeTechnologies, Carlsbad, CA), and pooled into equimolar ratios. The library pool was Exonuclease VII (NEB, Ipswich, MA) treated, SPRI-bead purified with KapaPure beads (Kapa Biosystems/Roche, Basel, Switzerland), and quantified via qPCR with a Kapa Library Quant kit (Kapa Biosystems) on a QuantStudio 5 RT-PCR system (Applied Biosystems, Foster City, CA). Libraries were sequenced on a HiSeq 4000 sequencer (Illumina, San Diego, CA) with single-end 100 bp reads with 12 million raw reads per sample. The raw read data were filtered using HTStream (version 1.3.2) which included screening for contaminants (such as PhiX), removal of PCR duplicated reads, rRNA removal, quality-based trimming, and adapter trimming. STAR (version 2.7.9a) [61] was used to align the processed data to the rhesus genome (Mmul10). Custom R code was then used for read and alignment quality assessment as well as to collate counts into a single table for downstream analysis.

Differential gene expression analysis

Genes were excluded from differential gene expression analysis if they were expressed in less than 50% of samples for at least one brain region, lacked annotation, or were found to have duplicated gene symbols. Differential gene expression analysis was performed using the

limma-voom Bioconductor pipeline (limma version 3.44.3, edgeR version 3.30.3) in R. Analysis in limma used a model including effects for brain regions, SHIV infection, and their interactions. Estimates and standards errors were adjusted for within-animal correlations. Differentially expressed genes (DEGs) were defined as genes with p value < 0.01 and adjusted (False discovery rate correction) p values < 0.1 unless otherwise indicated. Gene ontology (GO) and KEGG pathway enrichment analysis was performed using ShinyGO v0.60 webserver [62].

Weighted gene correlation network analysis (WGCNA)

The weighted gene co-expression network analysis (WGCNA) was implemented using the WGCNA R package, version 1.69, in R version 4.0.1. WGCNA was performed using a signed network with a robust biweight midcorrelation. A soft-thresholding power of 27 was chosen for analysis of data from uninfected control animals and 23 for analysis of data from both uninfected control and SHIV exposed animals. Soft-thresholding power was set using the pickSoftThreshold function, to achieve a scale-free topology index greater than 0.85. Modules associated with a single brain region were identified by fitting a linear fixed effects model to each module eigengene. A module was defined as being associated with a single region if the eigengene was significantly higher in that region compared to all other regions, based on the region effect from the linear mixed effects model. Similarly, modules significantly associated with SHIV infection were defined as such if the module eigengene was significantly higher in SHIV infected samples compared to uninfected control samples for at least one brain region. The linear mixed effects model for both analyses utilized a fixed effect for brain region and a random effect for animals, and residual variance were allowed to vary by brain regions. For the analysis of samples from both uninfected control and SHIV exposed animals, SHIV infection was also incorporated as a fixed effect in the linear mixed effects model. Gene ontology (GO) enrichment analyses were conducted using Fisher's exact test as implemented in the Bioconductor package topGO. Results reported are for the biological process (BP) GO terms.

Inflammatory analytes

For measurement of inflammatory analytes, triton inactivated samples were shipped to Olink Proteomics at Stanford University. A 92-biomarker inflammation panel was run according to manufacturer's instructions. Protein levels are expressed as normalized protein expression (NPX) values, an arbitrary unit. Inflammatory analytes in CSF and plasma were analyzed using a proximity extension assay (O link, Proteomics) as described [63].

Flow Cytometry

Cell staining was performed as previously described [32]. Briefly, surface staining was performed with the following antibody panel (Additional file 1: Table S3) for 30 min at 4 °C. After washing with 1X phosphate buffered saline (PBS), cells were fixed and permeabilized using Cytofix/Cytoperm buffer set for 20 min at room temperature in the dark. Cells were washed twice with 1X FACS buffer and re-suspended in 200μL of FACS buffer. Fluorescence was measured using a BD FACSymphony cell analyzer with FACSDiva version 8.0.1 software (FLowJo LLC). Compensation, gating, and analysis were performed using FlowJo (versions 9 and 10). Reagents used for flow cytometry are listed in Additional file 1: Table S3.

Quantitative RT-PCR for viral RNA and DNA in the brain, CSF, and plasma

Plasma, CSF, and brain viral RNA and DNA were quantified using an established quantitative RT-PCR (qRT-PCR) assays from the AIDS and Cancer Virus Program, Leidos Biomedical Research Inc., Frederick National Laboratory by reported methods [64] described by Li et al. [17] In brief, quantification of plasma, CSF, and brain SHIV RNA and DNA were performed using real-time qRT-PCR and qPCR assays targeting a conserved region in SIV gag.

Serum biochemistry

Biochemistry analysis on serum samples was performed using Piccolo® BioChemistry Plus disks, that were run on the Piccolo® Xpress Chemistry Analyzer (Abbott), according to the manufacturer's instructions. Serum analytes that were assessed include albumin, alkaline phosphatase (ALP), amylase, aspartate aminotransferase (AST), C-reactive protein, calcium, creatinine, gamma glutamyl transferase (GGT), glucose, total protein, blood urea nitrogen (BUN), and uric acid.

CSF and serum IP-10

A Legendplex assay (BioLegend) was performed to evaluate cytokines in rhesus macaque sera and CSF. The assay was performed according to the manufacturer's instructions. Samples were acquired on a BD LSR Fortessa cell analyzer.

Statistics

Differentially expressed genes (DEGs) and corresponding p values were determined using linear mixed effects models taking into account brain region and/or SHIV infection effects. Benjamini–Hochberg False discovery rate adjusted p values were utilized to account for type I errors. DEGs were defined as $p < 0.01$ and $Log2FC > 1.5$ unless otherwise noted. Two-tailed Spearman correlation analyses were used for comparing vRNA versus vDNA copy numbers and plasma versus CSF vRNA levels. Fisher's exact test was used to identify significantly enriched GO terms within gene sets. Wilcoxon signed ranked test was used for longitudinal comparison of CSF T cell frequencies in SHIV infected animals.

REFERENCES

1. Mrdjen, D., et al., *High-Dimensional Single-Cell Mapping of Central Nervous System Immune Cells Reveals Distinct Myeloid Subsets in Health, Aging, and Disease.* Immunity, 2018. **48**(3): p. 599.

2. Korin, B., et al., *High-dimensional, single-cell characterization of the brain's immune compartment.* Nat Neurosci, 2017. **20**(9): p. 1300-1309.

3. Pasciuto, E., et al., *Microglia Require CD4 T Cells to Complete the Fetal-to-Adult Transition.* Cell, 2020. **182**(3): p. 625-640 e24.

4. Carrithers, M.D., et al., *Role of genetic background in P selectin-dependent immune surveillance of the central nervous system.* J Neuroimmunol, 2002. **129**(1-2): p. 51-7.

5. Kivisakk, P., et al., *Human cerebrospinal fluid central memory CD4+ T cells: evidence for trafficking through choroid plexus and meninges via P-selectin.* Proc Natl Acad Sci U S A, 2003. **100**(14): p. 8389-94.

6. Ransohoff, R.M., *How neuroinflammation contributes to neurodegeneration.* Science, 2016. **353**(6301): p. 777-83.

7. Saloner, R. and L.A. Cysique, *HIV-Associated Neurocognitive Disorders: A Global Perspective.* J Int Neuropsychol Soc, 2017. **23**(9-10): p. 860-869.

8. Gott, C., et al., *Cognitive change trajectories in virally suppressed HIV-infected individuals indicate high prevalence of disease activity.* PLoS One, 2017. **12**(3): p. e0171887.

9. Cardenas, V.A., et al., *Evidence for ongoing brain injury in human immunodeficiency virus-positive patients treated with antiretroviral therapy.* J Neurovirol, 2009. **15**(4): p. 324-33.

10. Price, R.W., et al., *Evolving character of chronic central nervous system HIV infection.* Semin Neurol, 2014. **34**(1): p. 7-13.

11. Oliveira, M.F., et al., *Early Antiretroviral Therapy Is Associated with Lower HIV DNA Molecular Diversity and Lower Inflammation in Cerebrospinal Fluid but Does Not Prevent the Establishment of Compartmentalized HIV DNA Populations.* PLoS Pathog, 2017. **13**(1): p. e1006112.

12. Dahl, V., et al., *Low levels of HIV-1 RNA detected in the cerebrospinal fluid after up to 10 years of suppressive therapy are associated with local immune activation.* AIDS, 2014. **28**(15): p. 2251-8.

13. Ragin, A.B., et al., *Brain alterations within the first 100 days of HIV infection.* Ann Clin Transl Neurol, 2015. **2**(1): p. 12-21.

14. Kieburtz, K., et al., *Cognitive performance and regional brain volume in human immunodeficiency virus type 1 infection.* Arch Neurol, 1996. **53**(2): p. 155-8.

15. Israel, S.M., et al., *Different roles of frontal versus striatal atrophy in HIV-associated neurocognitive disorders.* Hum Brain Mapp, 2019. **40**(10): p. 3010-3026.

16. Grahn, J.A., J.A. Parkinson, and A.M. Owen, *The cognitive functions of the caudate nucleus.* Prog Neurobiol, 2008. **86**(3): p. 141-55.

17. Li, H., et al., *Envelope residue 375 substitutions in simian-human immunodeficiency viruses enhance CD4 binding and replication in rhesus macaques.* Proceedings of the National Academy of Sciences of the United States of America, 2016. **113**(24): p. E3413-E3422.

18. Bar, K.J., et al., *Simian-Human Immunodeficiency Virus SHIV.CH505 Infection of Rhesus Macaques Results in Persistent Viral Replication and Induces Intestinal Immunopathology.* J Virol, 2019. **93**(18).

19. Morrison JH, Baxter MG. The ageing cortical synapse: hallmarks and implications for cognitive decline. Nature Rev Neurosci, 2012,13(4):240-50.

20. Albright AV, Soldan SS, Gonzales-Scarano F. Pathogenesis of human immunodeficiency virus-induced neurological disease. J Neurovirol. 2003;9(2):222-7.

21. Navia BA, Cho E-S,Petito CK, Price RW. The AIDS dementia complex: II. Neuropathology. Ann Neurol. 1986; 19(6):525-35. https://doi.org/10.1002/ana.410190603.

22. Kadharbatcha Saleem, N.L., *A Combined MRI and Histology Atlas of the Rhesus Monkey Brain in Stereotaxic Coordinates*. 2nd ed. 2012.

23. Yin, S., et al., *Transcriptomic and open chromatin atlas of high-resolution anatomical regions in the rhesus macaque brain.* Nat Commun, 2020. **11**(1): p. 474.

24. Stuart, J.M., et al., *A gene-coexpression network for global discovery of conserved genetic modules.* Science, 2003. **302**(5643): p. 249-55.

25. Langfelder, P. and S. Horvath, *Eigengene networks for studying the relationships between co-expression modules.* BMC Systems Biology, 2007. **1**(1): p. 54.

26. Mittelbronn, M., et al., *Local distribution of microglia in the normal adult human central nervous system differs by up to one order of magnitude.* Acta Neuropathol, 2001. **101**(3): p. 249-55.

27. Dubbelaar, M.L., et al., *Transcriptional profiling of macaque microglia reveals an evolutionary preserved gene expression program.* Brain Behav Immun Health, 2021. **15**: p. 100265.

28. Zhao, G.Y., et al., *Expression of the transcription factor GATA3 in the postnatal mouse central nervous system.* Neurosci Res, 2008. **61**(4): p. 420-8.

29. Campbell, J.H., et al., *Anti-alpha4 antibody treatment blocks virus traffic to the brain and gut early, and stabilizes CNS injury late in infection.* PLoS Pathog, 2014. **10**(12): p. e1004533.

30. Smolders, J., et al., *Tissue-resident memory T cells populate the human brain.* Nat Commun, 2018. **9**(1): p. 4593.

31. Sonobe, Y., et al., *Interleukin-25 expressed by brain capillary endothelial cells maintains blood-brain barrier function in a protein kinase Cepsilon-dependent manner.* J Biol Chem, 2009. **284**(46): p. 31834-42.

32. Verma, A., et al., *Monoclonal antibodies protect aged rhesus macaques from SARS-CoV-2-induced immune activation and neuroinflammation.* Cell Rep, 2021. **37**(5): p. 109942.

33. Schwerk, C., et al., *The choroid plexus-a multi-role player during infectious diseases of the CNS.* Front Cell Neurosci, 2015. **9**: p. 80.

34. Shimada, A. and S. Hasegawa-Ishii, *Increased cytokine expression in the choroid plexus stroma and epithelium in response to endotoxin-induced systemic inflammation in mice.* Toxicol Rep, 2021. **8**: p. 520-528.

35. Baruch, K., et al., *CNS-specific immunity at the choroid plexus shifts toward destructive Th2 inflammation in brain aging.* Proc Natl Acad Sci U S A, 2013. **110**(6): p. 2264-9.

36. Sedmak, G. and M. Judas, *White Matter Interstitial Neurons in the Adult Human Brain: 3% of Cortical Neurons in Quest for Recognition.* Cells, 2021. **10**(1).

37. Kostovic, I. and P. Rakic, *Cytology and time of origin of interstitial neurons in the white matter in infant and adult human and monkey telencephalon.* J Neurocytol, 1980. **9**(2): p. 219-42.

38. Dai, R., et al., *EGR2 is elevated and positively regulates inflammatory IFNgamma production in lupus CD4(+) T cells.* BMC Immunol, 2020. **21**(1): p. 41.

39. Lin, C.C., et al., *IL-1-induced Bhlhe40 identifies pathogenic T helper cells in a model of autoimmune neuroinflammation.* J Exp Med, 2016. **213**(2): p. 251-71.

40. Valle-Rios, R., et al., *Isthmin 1 is a secreted protein expressed in skin, mucosal tissues, and NK, NKT, and th17 cells.* J Interferon Cytokine Res, 2014. **34**(10): p. 795-801.

41. Ghosh, S., et al., *Bioenergetic regulation of microglia.* Glia, 2018. **66**(6): p. 1200-1212.

42. Durocher, M., et al., *Inflammatory, regulatory, and autophagy co-expression modules and hub genes underlie the peripheral immune response to human intracerebral hemorrhage.* J Neuroinflammation, 2019. **16**(1): p. 56.

43. Mengozzi, M., et al., *Erythropoietin-induced changes in brain gene expression reveal induction of synaptic plasticity genes in experimental stroke.* Proc Natl Acad Sci U S A, 2012. **109**(24): p. 9617-22.

44. Lin, C.C., et al., *Bhlhe40 controls cytokine production by T cells and is essential for pathogenicity in autoimmune neuroinflammation.* Nat Commun, 2014. **5**: p. 3551.

45. Bonham, L.W., et al., *CXCR4 involvement in neurodegenerative diseases.* Transl Psychiatry, 2018. **8**(1): p. 73.

46. Li, J., et al., *IL-27 subunits and its receptor (WSX-1) mRNAs are markedly up-regulated in inflammatory cells in the CNS during experimental autoimmune encephalomyelitis.* J Neurol Sci, 2005. **232**(1-2): p. 3-9.

47. Nitsch, L., et al., *CNS-Specific Synthesis of Interleukin 23 Induces a Progressive Cerebellar Ataxia and the Accumulation of Both T and B Cells in the Brain: Characterization of a Novel Transgenic Mouse Model.* Mol Neurobiol, 2019. **56**(12): p. 7977-7993.

48. Yan, L. and B. Chaqour, *Cysteine-rich protein 61 (CCN1) and connective tissue growth factor (CCN2) at the crosshairs of ocular neovascular and fibrovascular disease therapy.* J Cell Commun Signal, 2013. **7**(4): p. 253-63.

49. Sun, J., et al., *Zika virus promotes CCN1 expression via the CaMKIIalpha-CREB pathway in astrocytes.* Virulence, 2020. **11**(1): p. 113-131.

50. Rothe, T., et al., *The Nuclear Receptor Nr4a1 Acts as a Microglia Rheostat and Serves as a Therapeutic Target in Autoimmune-Driven Central Nervous System Inflammation.* J Immunol, 2017. **198**(10): p. 3878-3885.

51. Kessing, C.F., et al., *High Number of Activated CD8+ T Cells Targeting HIV Antigens Are Present in Cerebrospinal Fluid in Acute HIV Infection.* J Acquir Immune Defic Syndr, 2017. **75**(1): p. 108-117.

52. Boisvert, M.M., et al., *The Aging Astrocyte Transcriptome from Multiple Regions of the Mouse Brain.* Cell Rep, 2018. **22**(1): p. 269-285.

53. Xu, S., et al., *Mesencephalic astrocyte-derived neurotrophic factor (MANF) protects against Abeta toxicity via attenuating Abeta-induced endoplasmic reticulum stress.* J Neuroinflammation, 2019. **16**(1): p. 35.

54. Lee, C.A., et al., *Simian Immunodeficiency Virus-Infected Memory CD4(+) T Cells Infiltrate to the Site of Infected Macrophages in the Neuroparenchyma of a Chronic Macaque Model of Neurological Complications of AIDS.* mBio, 2020. **11**(2).

55. Hsu, D.C., et al., *Central Nervous System Inflammation and Infection during Early, Nonaccelerated Simian-Human Immunodeficiency Virus Infection in Rhesus Macaques.* J Virol, 2018. **92**(11).

56. Verma, A., et al., *Impact of Th1 CD4 Follicular Helper T Cell Skewing on Antibody Responses to an HIV-1 Vaccine in Rhesus Macaques.* J Virol, 2020. **94**(6).

57. Peters, A. and C. Sethares, *Aging and the myelinated fibers in prefrontal cortex and corpus callosum of the monkey.* J Comp Neurol, 2002. **442**(3): p. 277-91.

58. McMurtray, A., et al., *Cortical atrophy and white matter hyperintensities in HIV: the Hawaii Aging with HIV Cohort Study.* J Stroke Cerebrovasc Dis, 2008. **17**(4): p. 212-7.

59. Cohen, R.A., T.R. Seider, and B. Navia, *HIV effects on age-associated neurocognitive dysfunction: premature cognitive aging or neurodegenerative disease?* Alzheimers Res Ther, 2015. **7**(1): p. 37.

60. Bowen L, von Biela VR, McCormick SD, Regish AM, Water SC, Durbin-Johnson B, Britton M, Settles ML, Donnelly DS, Laske SM, Carey MP, Brown RJ, Zimmerman CE, Cooke S. Transcriptomics response to elevated water temperatures in adult migrating Yukon River Chinook salmon (Oncorhynchus tshawytscha). Conserv Physiol. 2020;8(1):coaa084. https//doi.org/10.1093/conphys/coaa084

61. Dobin, A., et al., *STAR: ultrafast universal RNA-seq aligner.* Bioinformatics, 2012. **29**(1): p. 15-21.

62. Ge, S.X., D. Jung, and R. Yao, *ShinyGO: a graphical gene-set enrichment tool for animals and plants.* Bioinformatics, 2019. **36**(8): p. 2628-2629.

63. Assarsson, E., et al., *Homogenous 96-plex PEA immunoassay exhibiting high sensitivity, specificity, and excellent scalability.* PLoS One, 2014. **9**(4): p. e95192.

64. Hansen, S.G., et al., *Immune clearance of highly pathogenic SIV infection.* Nature, 2013. **502**(7469): p. 100-104.

FIGURES

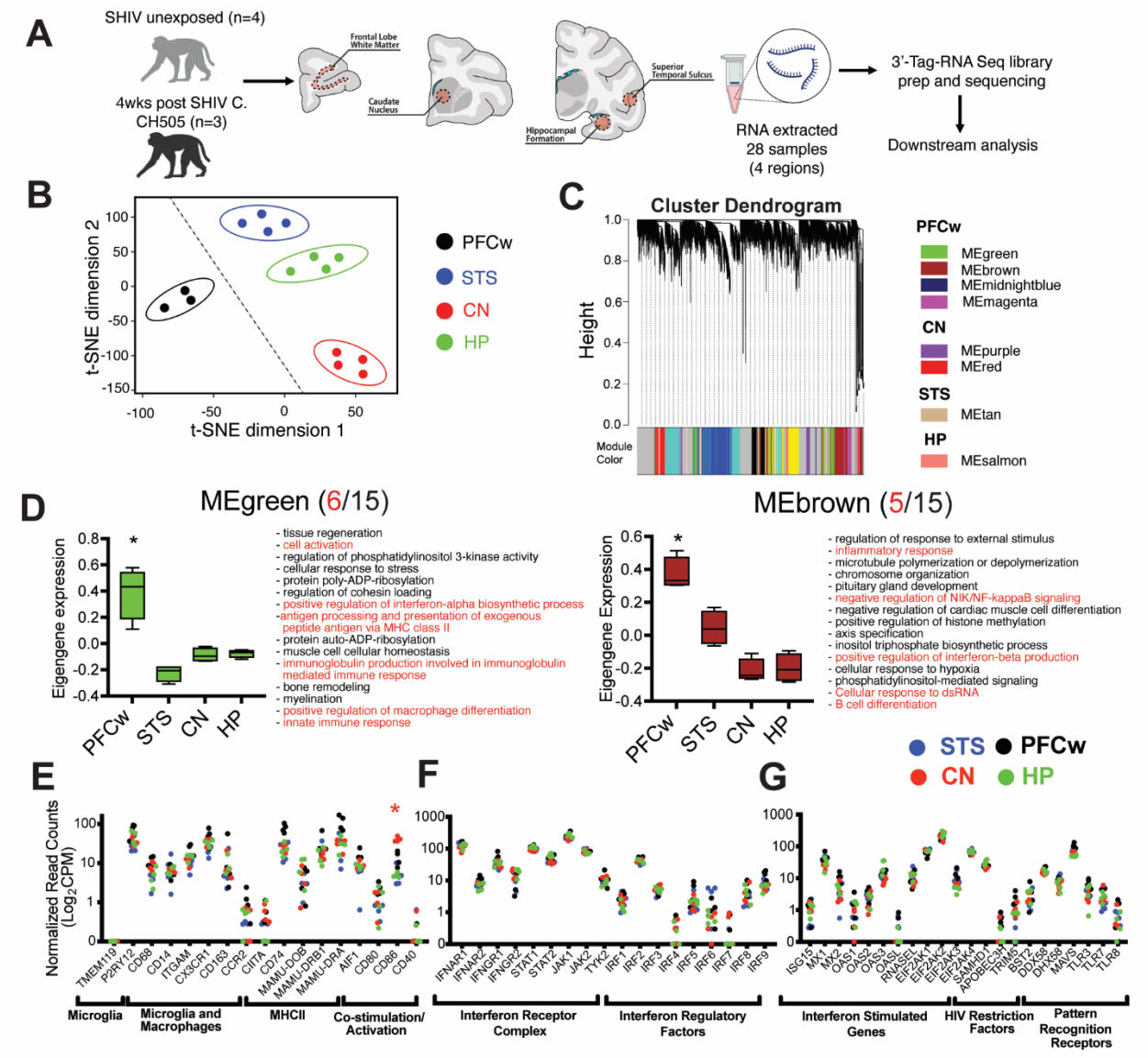

Fig. 1 Molecular signatures of innate immune surveillance in the brain of uninfected rhesus macaques. (A) Study schematic: rhesus macaques were infected with SHIV. C.CH505 intravenously (n = 3; 3 females; ages 5.2–5.6 [years.months]) and euthanized at 4 week post-infection. Uninfected animals from opportunistic medical culls (n = 4; 1 male, 3 females; ages 3.6–6.5 [years.months]) were used as controls. 3 mm brain punches were collected from the subcortical white matter of the prefrontal cortex (PFCw) between Bregma + 16 and + 10 mm, the caudate nucleus (CN) between Bregma + 6 and 0 mm, and the superior temporal sulcus (STS)

and hippocampus (HP) between Bregma − 14 and − 20 mm. Total RNA was extracted from bulk tissue samples and 3'-tag RNA-seq was performed. **(B)** t-Stochastic neighborhood embedding (t-SNE) clustering of gene expression profiles from uninfected control animals. Outlier sample (Animal 43661, pre-frontal cortex white matter control) is removed from the plot. **(C)** Cluster dendrogram of gene co-expression modules, indicated by color (Left), and region-specific modules (Right) generated from weighted gene co-expression network analysis of tissue-specific gene expression profiles from uninfected animals. **(D)** Regional eigengene expression and corresponding top fifteen most significantly enriched ($p < 0.01$ by Fisher's exact test) biological processes GO terms within MEgreen (Left) and MEbrown (Right) modules. Red text indicates terms related to immunological processes. Regional expression levels of genes associated with macrophages/microglia **(E)** and anti-viral responses **(F, G)** in uninfected animals expressed in Log2 counts per million (CPM). **(B)** Circles indicate 95% confidence intervals. Dotted line indicates separation of white matter and gray matter sample clusters. **(D)** Box plots indicate quartiles. *P < 0.05 by linear mixed effects models (region effect). E * adjusted $p < 0.01$ and Log2 fold change (FC) > 1.5 relative other synapse dense regions (STS, CN, and/ or HP). Asterisk color corresponds to a region (CN [red]) for which a gene is differentially regulated relative to other synapse dense regions. **(E–G)** Datapoints indicate samples from a single brain region and animal.

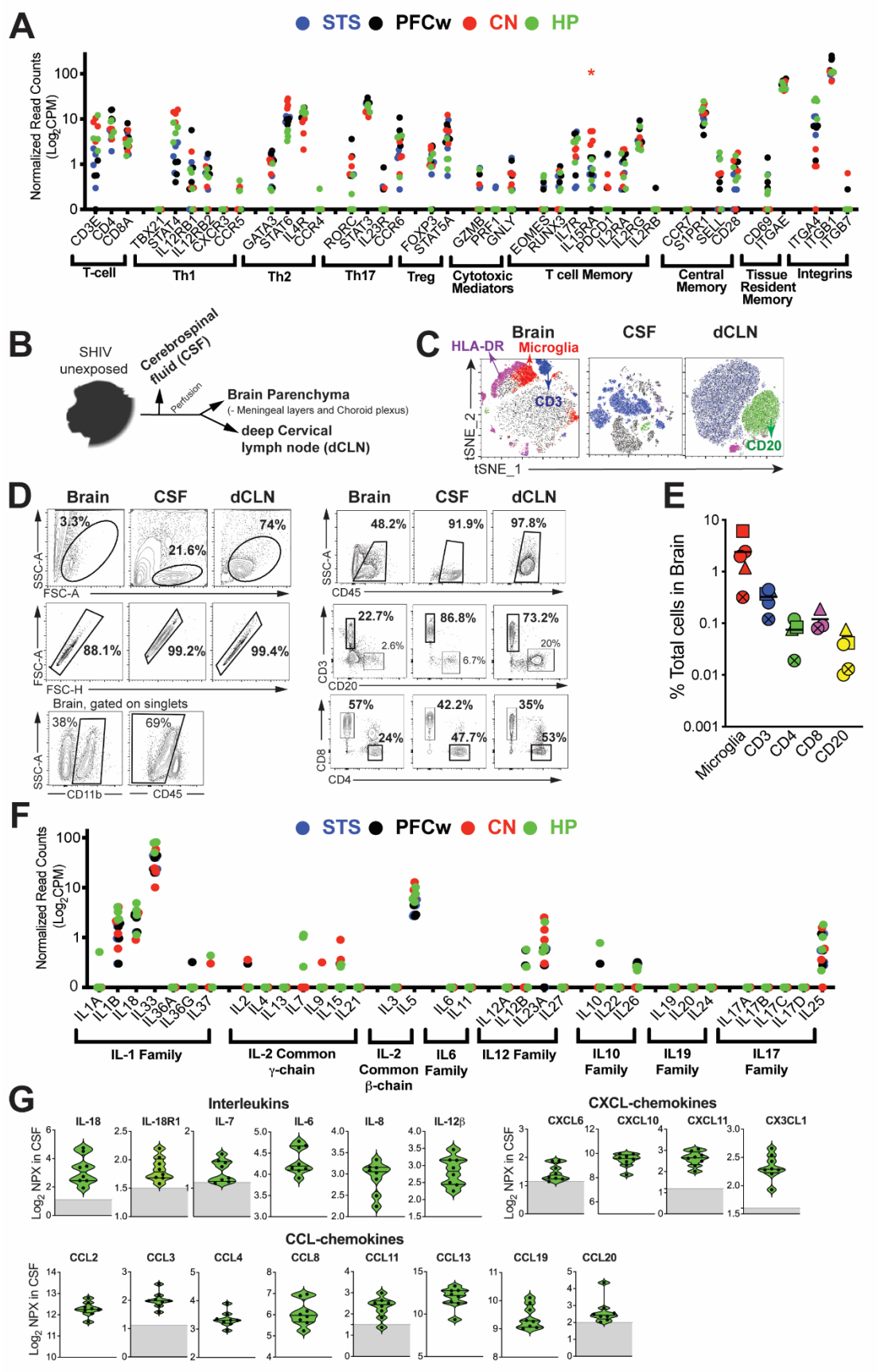
A
STS PFCw CN HP
Normalized Read Counts (Log2 CPM)
CD3E CD4 CD8A
TBX21 STAT4 IL12RB1 IL12RB2 CXCR3 CCR5
GATA3 STAT6 IL4R CCR4
RORC STAT3 IL23R CCR6
FOXP3 STAT5A
GZMB PRF1 GNLY
EOMES RUNX3 IL7R IL15RA PDCD1 IL2RA IL2RG IL2RB
CCR7 S1PR1 SELL CD28
CD69 ITGAE
ITGA4 ITGB1 ITGB7
T-cell
Th1
Th2
Th17
Treg
Cytotoxic Mediators
T cell Memory
Central Memory
Tissue Resident Memory
Integrins
B
SHIV unexposed
Cerebrospinal fluid (CSF)
Perfusion
Brain Parenchyma
(- Meningeal layers and Choroid plexus)
deep Cervical lymph node (dCLN)
C
Brain
CSF
dCLN
HLA-DR
Microglia
CD3
CD20
tSNE_2
tSNE_1
D
Brain
CSF
dCLN
3.3%
21.6%
74%
SSC-A
FSC-A
88.1%
99.2%
99.4%
FSC-H
Brain, gated on singlets
38%
69%
CD11b
CD45
48.2%
91.9%
97.8%
CD45
22.7%
2.6%
86.8%
6.7%
73.2%
20%
CD3
CD20
57%
24%
42.2%
47.7%
35%
53%
CD8
CD4
E
% Total cells in Brain
Microglia
CD3
CD4
CD8
CD20
F
STS PFCw CN HP
Normalized Read Counts (Log2 CPM)
IL1A IL1B IL18 IL33 IL36A IL36G IL37
IL2 IL4 IL13 IL7 IL9 IL15 IL21
IL3 IL5
IL6 IL11
IL12A IL12B IL23A IL27
IL10 IL22 IL26
IL19 IL20 IL24
IL17A IL17B IL17C IL17D IL25
IL-1 Family
IL-2 Common γ-chain
IL-2 Common β-chain
IL6 Family
IL12 Family
IL10 Family
IL19 Family
IL17 Family
G
Interleukins
IL-18
IL-18R1
IL-7
IL-6
IL-8
IL-12β
CXCL-chemokines
CXCL6
CXCL10
CXCL11
CX3CL1
Log2 NPX in CSF
CCL-chemokines
CCL2
CCL3
CCL4
CCL8
CCL11
CCL13
CCL19
CCL20

Fig. 2 T cell resident immune signatures within the rhesus brain at homeostasis. (A) Regional expression of genes associated with T-cell populations in uninfected animals. Brackets indicate corresponding T-cell subsets associated with genes. **(B)** Sampling schematic indicating collection of cerebrospinal fluid (CSF), total brain parenchyma and deep cervical lymph node (dCLN) from a comparable group of uninfected rhesus macaques (ages 6 years [two animals], 11 years [one animal], and 16 years [one animal]; one male, three females) for flow cytometric analysis **(C–E) (C)** t-SNE plots clustering of immune cell populations in the brain (left), CSF (middle), and dCLN (right) by phenotype. **(D)** Gating strategy for microglia (CD11b+CD45lo/int) (Left) and CD4/CD8 T cells (Right) in the brain, CSF, and dCLN. **(E)** Frequency of microglia and lymphocyte populations among total cells in rhesus macaque brain tissue. **(F)** Regional expression of cytokine genes in uninfected animals. Brackets indicate cytokine families. **(G)** Quantification of interleukin, CXCL-chemokines, and CCL-chemokines levels (expressed in Log2 Normalized Protein Expression [Log2NPX]) in the CSF of a cohort of uninfected animals (age 21–22 years; 8 females) [32]. **(A, F)** Data points indicate samples derived from brain region (indicated by color) and animal. *Adjusted $p < 0.01$ relative other synapse dense regions (STS, CN, and/or HP). Asterisk color corresponds to a region (CN [red]) for which a gene is differentially regulated relative to other synapse dense regions. Data points indicate individual animals **(E, G)** with symbols indicating specific animals **(E)** Bars in violin plots indicate quartiles and gray bars indicate limits of detection.

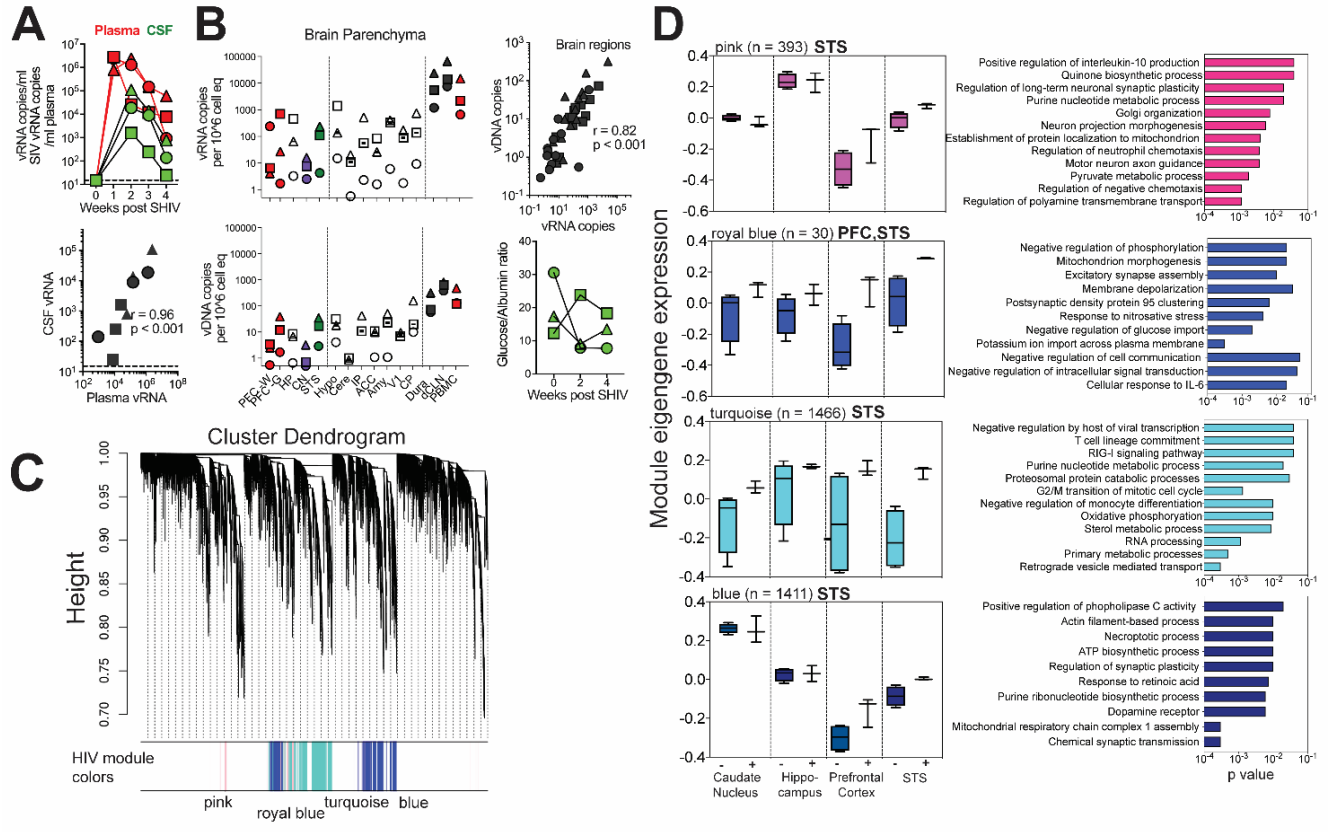

Fig. 3 Changes in brain transcriptome following SHIV dissemination in the CNS. (A) Kinetics of plasma (red) and CSF (green) viral loads following intravenous infection with. SHIV.C.CH505. CSF vRNA correlates with Plasma vRNA ($r = 0.96$, $p < 0.001$; two-tailed Spearman correlation). **(B)** vRNA and vDNA copies in various brain regions, dura mater, deep cervical lymph nodes, and PBMCs. Correlation of vDNA with vRNA from all brain regions sampled ($r = 0.82$, $p < 0.001$; two-tailed Spearman correlation). Bottom graph shows ratio of CSF glucose and albumin (in mg/dL) during acute viremia. **(C)** Cluster dendrogram showing modules of significantly co-expressed genes associated with SHIV infection indicated by color (pink [393 genes] royal blue [30 genes], turquoise [1466 genes], blue [1411 genes]). **(D)** Expression levels of module eigengene based on SHIV infection status (+ infected, −uninfected) in the pre-frontal cortex white matter (PFCw), superior temporal sulcus (STS), caudate nucleus, and hippocampus (Left). Significantly enriched biological process gene ontology (GO) terms in SHIV-specific gene co-expression modules

(Right). **(D)** Box plots indicate quartiles. P values determined by Fisher's exact test. **(A, B)** Symbols indicate individual animals. **(A)** Data points in correlation plot indicate samples collected from individual animals (referenced by shape) and collection timepoint (weeks 1–4). **(B)** Data points in correlation plot indicate samples collected from individual animals and tissues (Brain regions, Dura mater, deep cervical lymph nodes, and PBMCs).

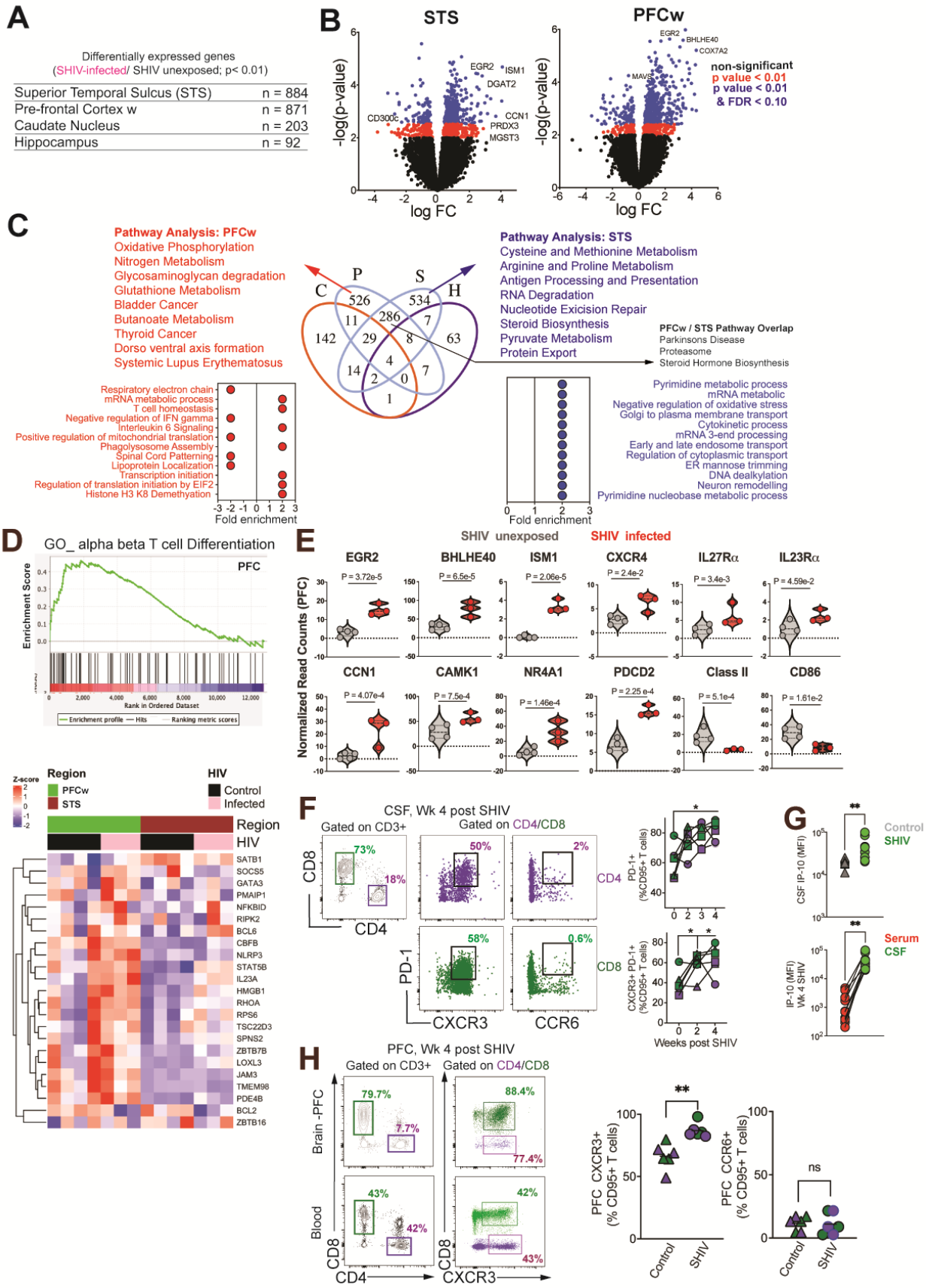
A
Differentially expressed genes
(SHIV-infected/ SHIV unexposed; p< 0.01)
Superior Temporal Sulcus (STS) n = 884
Pre-frontal Cortex w n = 871
Caudate Nucleus n = 203
Hippocampus n = 92
B
STS
PFCw
-log(p-value)
log FC
EGR2
ISM1
DGAT2
CD300C
CCN1
PRDX3
MGST3
BHLHE40
COX7A2
MAVS
non-significant
p value < 0.01
p value < 0.01
& FDR < 0.10
C
Pathway Analysis: PFCw
Oxidative Phosphorylation
Nitrogen Metabolism
Glycosaminoglycan degradation
Glutathione Metabolism
Bladder Cancer
Butanoate Metabolism
Thyroid Cancer
Dorso ventral axis formation
Systemic Lupus Erythematosus
Respiratory electron chain
mRNA metabolic process
T cell homeostasis
Negative regulation of IFN gamma
Interleukin 6 Signaling
Positive regulation of mitochondrial translation
Phagolysosome Assembly
Spinal Cord Patterning
Lipoprotein Localization
Transcription initiation
Regulation of translation initiation by EIF2
Histone H3 K8 Demethylation
Fold enrichment
P
S
C
H
526
534
11
286
7
142
29
8
63
14
4
7
2
0
1
Pathway Analysis: STS
Cysteine and Methionine Metabolism
Arginine and Proline Metabolism
Antigen Processing and Presentation
RNA Degradation
Nucleotide Excision Repair
Steroid Biosynthesis
Pyruvate Metabolism
Protein Export
PFCw / STS Pathway Overlap
Parkinsons Disease
Proteasome
Steroid Hormone Biosynthesis
Pyrimidine metabolic process
mRNA metabolic
Negative regulation of oxidative stress
Golgi to plasma membrane transport
Cytokinetic process
mRNA 3-end processing
Early and late endosome transport
Regulation of cytoplasmic transport
ER mannose trimming
DNA dealkylation
Neuron remodelling
Pyrimidine nucleobase metabolic process
Fold enrichment
D
GO_ alpha beta T cell Differentiation
PFC
Enrichment Score
Rank in Ordered Dataset
Enrichment profile
Hits
Ranking metric scores
Z-score
Region
PFCw
STS
HIV
Control
Infected
Region
HIV
SATB1
SOCS5
GATA3
PMAIP1
NFKBID
RIPK2
BCL6
CBFB
NLRP3
STAT5B
IL23A
HMGB1
RHOA
RPS6
TSC22D3
SPNS2
ZBTB7B
LOXL3
JAM3
TMEM98
PDE4B
BCL2
ZBTB16
E
SHIV unexposed
SHIV infected
Normalized Read Counts (PFC)
EGR2
P = 3.72e-5
BHLHE40
P = 6.5e-5
ISM1
P = 2.06e-5
CXCR4
P = 2.4e-2
IL27Rα
P = 3.4e-3
IL23Rα
P = 4.59e-2
CCN1
P = 4.07e-4
CAMK1
P = 7.5e-4
NR4A1
P = 1.46e-4
PDCD2
P = 2.25 e-4
Class II
P = 5.1e-4
CD86
P = 1.61e-2
F
CSF, Wk 4 post SHIV
Gated on CD3+
Gated on CD4/CD8
CD8
CD4
73%
18%
50%
2%
58%
0.6%
PD-1
CXCR3
CCR6
PD-1+ (%CD95+ T cells)
CXCR3+ PD-1+ (%CD95+ T cells)
Weeks post SHIV
G
CSF IP-10 (MFI)
Control
SHIV
IP-10 (MFI) Wk 4 SHIV
Serum
CSF
H
PFC, Wk 4 post SHIV
Gated on CD3+
Gated on CD4/CD8
Brain -PFC
Blood
79.7%
7.7%
88.4%
77.4%
43%
42%
42%
43%
PFC CXCR3+ (% CD95+ T cells)
PFC CCR6+ (% CD95+ T cells)
Control
SHIV
ns

Fig. 4 SHIV-induced alterations of genes regulating inflammatory pathways in the PFC white matter. Differential gene expression analysis between SHIV infected and unexposed animals. (A) Number of differentially expressed genes (DEGs) (adjusted $p < 0.01$) with respect to SHIV infection status identified in the STS, PFC white matter (w), CN, and HP. **(B)** Volcano plots displaying Log fold change (FC) and significance (-log p value) of genes expressed in the STS (Left) and PFCw (Right) after SHIV infection. Colors indicate significant thresholds of genes (p value < 0.01 and False discovery rate (FDR) adjusted p value < 0.10 [blue]; p value < 0.01 [red]; non-significant [black]). **(C)** Venn diagram indicating the number of overlapping DEGs from SHIV infected versus uninfected comparisons in the PFCw (P), STS (S), CN (C), and HP (H) (Center). GSEA–KEGG pathway analysis of DEGs exclusive to the PFCw (Left, Red), STS (Right, blue), or shared between the PFCw and STS (Right, gray). Plots indicate fold change by GSEA–GP–BP pathway enrichment between SHIV infected and uninfected animals in the PFCw (Left, Red) and STS (Right, Blue). **(D)** Gene set enrichment analysis of transcripts related to alpha beta T cell differentiation GO:0046632 from PFCw DEG profiles (Top) and heatmap showing expression levels of corresponding genes in the PFCw (green) and STS (red) of SHIV infected (pink) and uninfected (black) animals (Bottom). **(E)** Expression level of DEGs regulating inflammatory processes, immune cell functions, and synaptic functions in the PFCw of SHIV infected (red) and uninfected (gray) animals. **(F)** Gating for activated CD4 T-cells (top) and CD8 T cells (bottom) and frequency of PD1 +, PD1+ CXCR3+, PD1+ CCR6+ CD4 T-cells in the CSF of SHIV infected and uninfected animals over the course of infection. **(G)** IP-10 levels in CSF and serum expressed as Median Fluorescence Intensity (MFI) run using Legend plex assay in controls and SHIV infected animals (n = 7 animals infected with SHIV.C.CH505 intravaginally and n = 3 intravenously). **(H)** Gating for activated T cells isolated from the PFC, frequency of CXCR3 + CD4 and CD8 T cells in controls versus SHIV infected animals. Symbols indicate individual animals. **(A, B, F–H)** P values for gene expression data derived from linear mixed effects model. **(F, H)** *P < 0.05 by Wilcoxon sign ranked test. **(G)** **P < 0.01 by Mann–Whitney test

Supplementary Tables

Animal ID	Sample ID	SHIV Exposed	Sex	Age (years.months)	Med cull	Code	Brain tissue	Tissue weight (mg)	A260/A280	A260/A230	Total RNA conc (ug)
43361	SI61	No	M	6.6	Right leg lameness	SI61S-1	Superior Temporal Sulcus	74.0	2.06	2.24	25.74
						SI61H-2	Hippocampus	114.2	2.08	2.27	39.16
						SI61C-3	Caudate Nucleus	91.6	2.09	2.22	33.06
						SI61P-4	PFC A46 (w)	53.5	2.07	2.27	22.96
45821	SI21	No	F	3.6	Arthritis	SI21S-5	Superior Temporal Sulcus	124.8	2.10	2.30	53.59
						SI21H-6	Hippocampus	50.5	2.10	2.25	31.2
						SI21C-7	Caudate Nucleus	65.6	2.11	2.28	34.23
						SI21P-8	PFC A46 (w)	39.5	2.10	2.07	15.3
44003	SI03	No	F	5.11	Arthritis	SI03S-9	Superior Temporal Sulcus	84.2	2.10	2.31	50.42
						SI03H-10	Hippocampus	76.7	2.09	1.86	30.45
						SI03C-11	Caudate Nucleus	90.1	2.09	1.96	32.4
						SI03P-12	PFC A46 (w)	72.3	2.05	2.13	16.8
44288	SI88	No	F	5.9	Diarrhea	SI88S-13	Superior Temporal Sulcus	104.2	2.07	2.27	33.58
						SI88H-14	Hippocampus	83.9	2.07	2.28	29.11
						SI88C-15	Caudate Nucleus	104.5	2.08	2.25	31.01
						SI88P-16	PFC A46 (w)	69.8	2.06	2.15	9.89
44164	SI64	Yes	F	5.5	Euthanasia 4 weeks post SHIV	SI64S-17	Superior Temporal Sulcus	40.2	2.05	2.12	19.8
						SI64H-18	Hippocampus	50.4	2.07	2.20	27.57
						SI64C-19	Caudate Nucleus	35.9	2.06	1.89	20.32
						SI64P-20	PFC A46 (w)	26.7	2.07	2.22	14.45
44104	SI04	Yes	F	5.2	Euthanasia 4 weeks post SHIV	SI04S-21	Superior Temporal Sulcus	52.3	2.08	2.30	29.22
						SI04H-22	Hippocampus	43.3	2.06	2.29	21.26
						SI04C-23	Caudate Nucleus	47.2	2.07	2.37	21.64
						SI04P-24	PFC A46 (w)	17.0	2.08	2.18	9.6
44032	SI25	Yes	F	5.6	Euthanasia 4 weeks post SHIV	SI32S-25	Superior Temporal Sulcus	46.5	2.07	2.24	21.56
						SI32H-26	Hippocampus	54.3	2.06	2.20	23.57
						SI32C-27	Caudate Nucleus	40.6	2.08	2.22	19.22
						SI32P-28	PFC A46 (w)	43.5	2.06	2.21	20.06

Table S1 Animal/Sample Data. Animal information—Animal ID, Sex, Age, SHIV infection status, and medical cull rationale. Sample Information—Sample ID, Sample Code, Tissue identity, Tissue weight (mg), purified RNA absorbance ratios (A260/A280 and A260/A230), and sample RNA yield.

Reagent	Flurochrome	Clone	Catalog no.	Source
PD-1	PE-Cy7	EH12.2H7	329918	Biolegend
CD3	AF700	SP34-2	557917	BD Biosciences
CD4	BV650	L200	563737	BD Biosciences
CD8	BV510	SK1	563919	BD Biosciences
CD20	BV421	2H7	302328	Biolegend
CD95	BUV 737	DX2	564710	BD Bioscience
Live/Dead	APC-Cy7		L34976	Life Technologies
CXCR3	APC	IC6	550967	BD Biosciences
CD45	AF-488	HI30	557803	BD Biosciences
CD11b	BV-510	ICRF44	563088	Thermofisher
HLA-DR	BV-785	L243	307642	Biolegend
CCR6	PE-Dazzle	G034e3	353430	Biolegend
Cytofix/cytoperm			51-2090KZ	BD Biosciences

Table S3. Reagents used for flow cytometric analysis.

Supplementary Figures

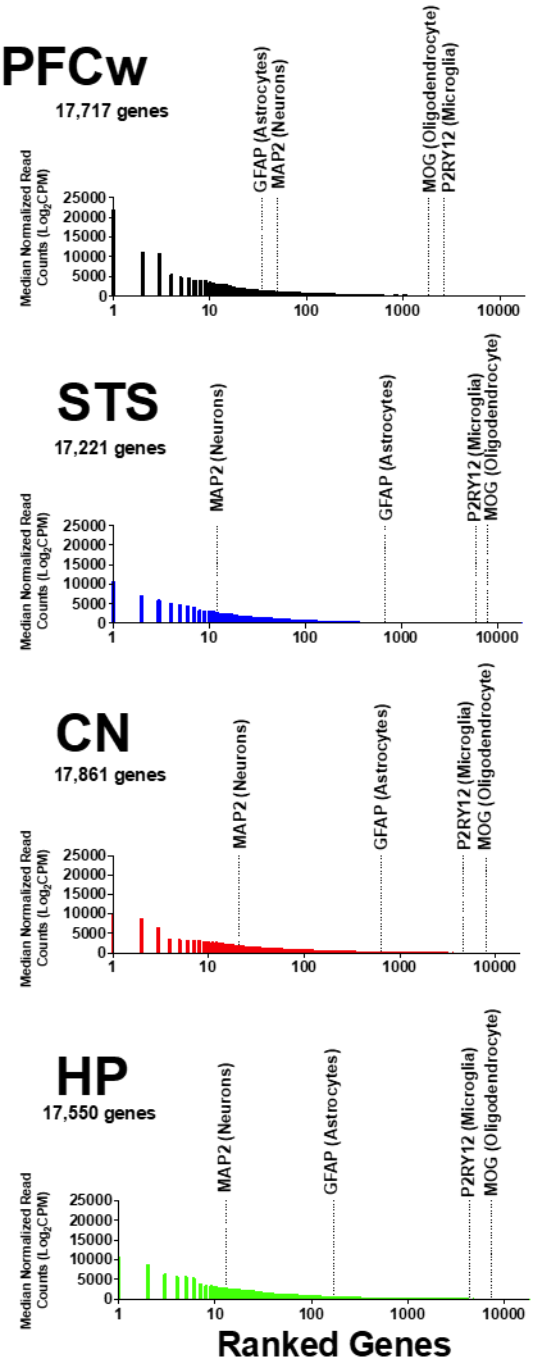

Fig S1. Ranked genes by median normalized read counts in units of Log2 counts per million (Log2CPM) in the subcortical white matter of the pre-frontal cortex (PFCw), and gray matter of the superior temporal sulcus (STS), caudate nucleus (CN), and hippocampus (HP) of uninfected animals. Dotted lines indicate location of marker genes

associated with neurons (MAP2), astrocytes (GFAP), microglia (P2RY12), and oligodendrocytes (MOG) within ranked distribution.

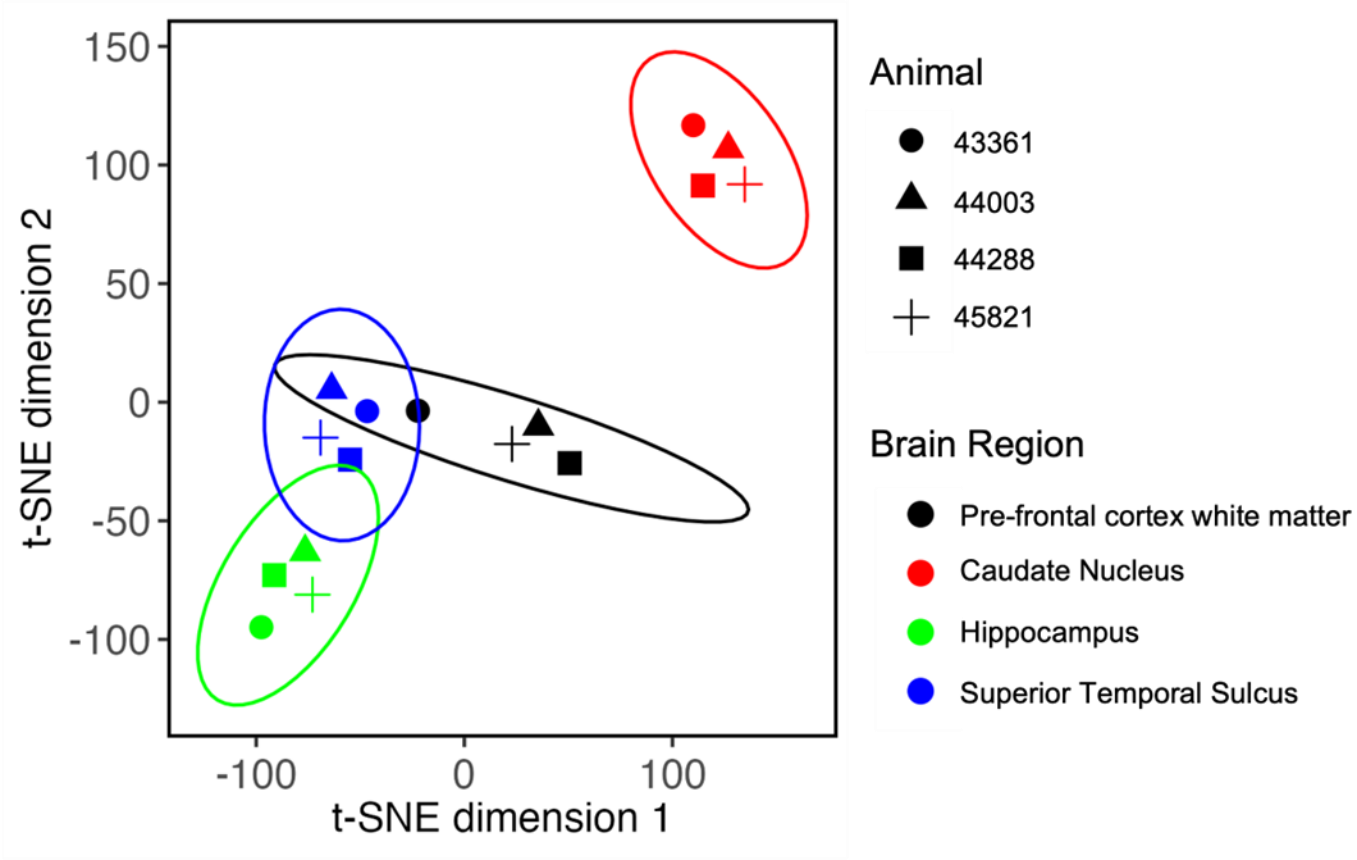

Fig. S2. T-stochastic neighborhood embedding analysis (t-SNE) of gene expression profiles from the pre-frontal cortex white matter (black), superior temporal sulcus (blue), caudate nucleus (red), and hippocampus (green) of uninfected animals. Outlier sample [Animal 43661 pre-frontal cortex white matter] is included. Symbols represent individual animals. Circles indicate 95% confidence intervals.

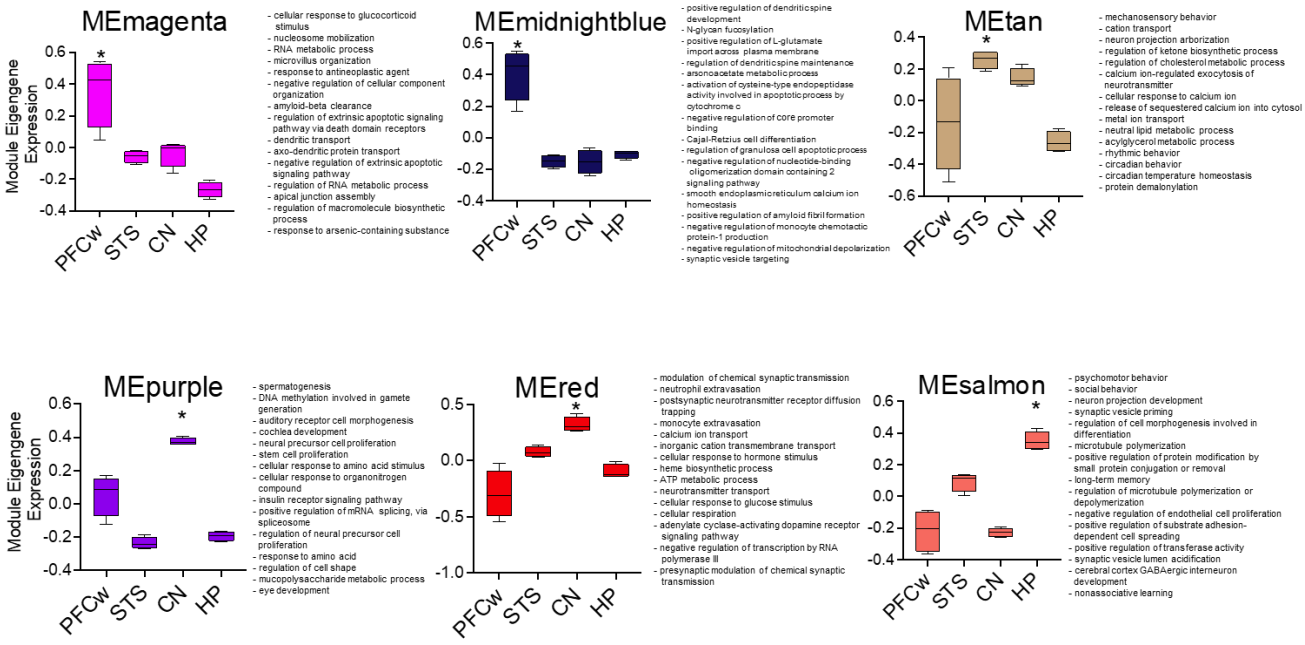

Fig. S3. Regional eigengene expression and corresponding top fifteen most significantly enriched ($p < 0.01$ by Fisher's exact test) biological processes GO terms within region specific modules (PFCw-specific [MEmagenta, MEmidnightblue], STS-specific [MEtan], CN-specific [MEpurple, MEred], HP-specific [MEsalmon]) determined by weighted gene co-expression network analysis from uninfected animals. *$p < 0.05$ by linear mixed effects model (region effect). Boxplots represent quartiles.

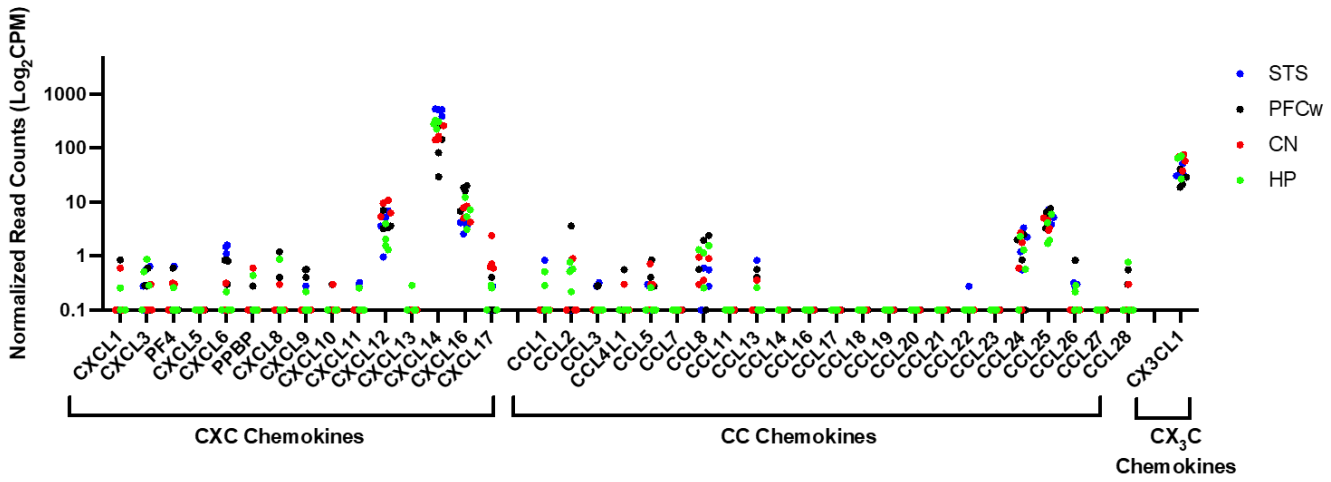

Fig. S4. Normalized read counts of genes encoding for chemokines in the STS (blue), PFCw (black), CN (red), and HP (green) of uninfected animals. Expression levels are displayed in normalized read counts in units of Log2 counts per million (Log2CPM). Brackets indicate structural chemokine classes.

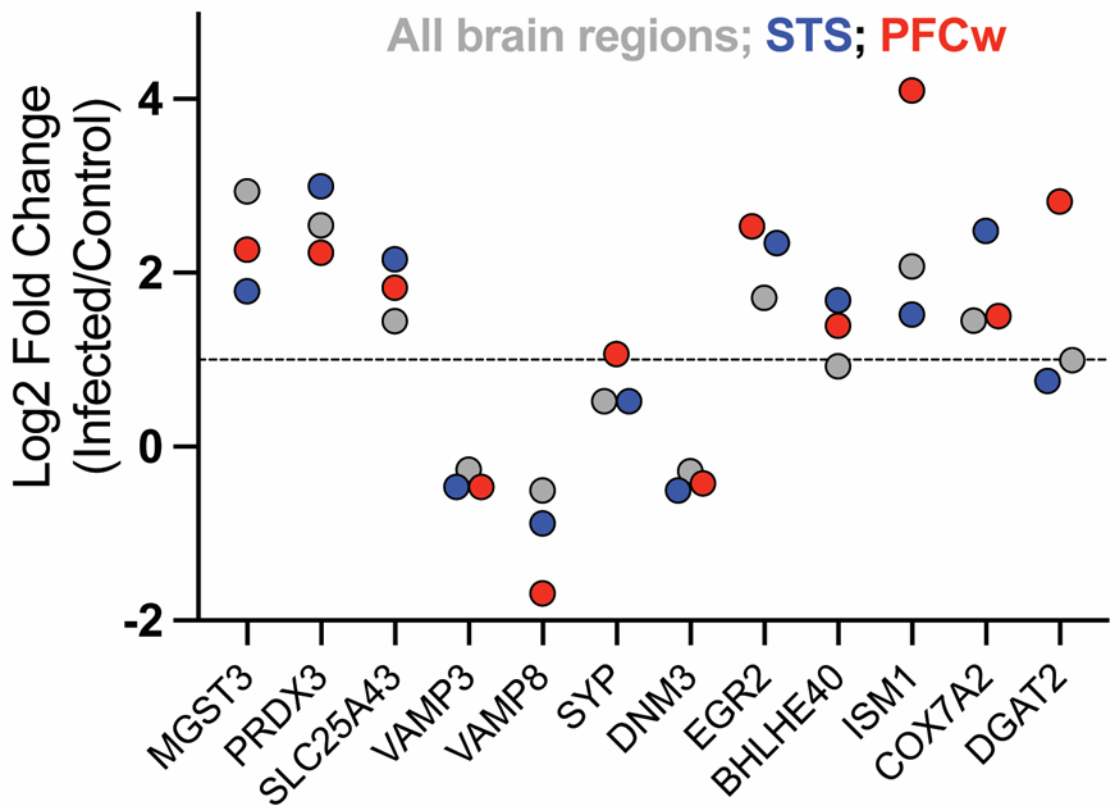

Fig. S5. Log2 Fold change of genes regulating inflammatory processes and synaptic functions between SHIV infected and uninfected animals in all brain regions (gray), STS (blue), and PFCw (red). Dotted line indicates a fold change of 1.

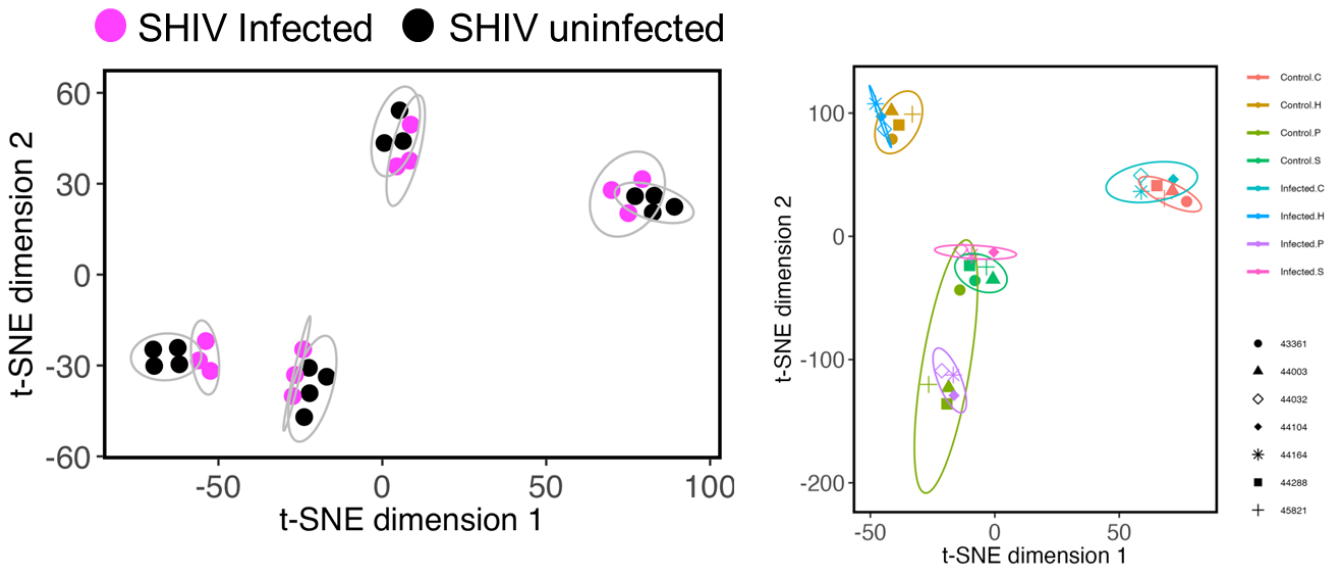

Fig. S6. T-stochastic neighborhood embedding (t-SNE) analysis of gene expression profiles from SHIV infected and uninfected animals. (Left) t-SNE plot indicates clustering of gene expression profiles by region and SHIV infection status (SHIV infected [pink], uninfected [black]) with removal of outlier sample [Animal 43661 Pre-frontal cortex white matter]. (Right) t-SNE plot shows all samples including the outlier with data points indicating regions (pre-frontal cortex white matter (P), superior temporal sulcus [S], caudate nucleus [C], hippocampus [H]) and infection status (color) and individual animals (symbols). Circles indicate 95% confidence intervals.

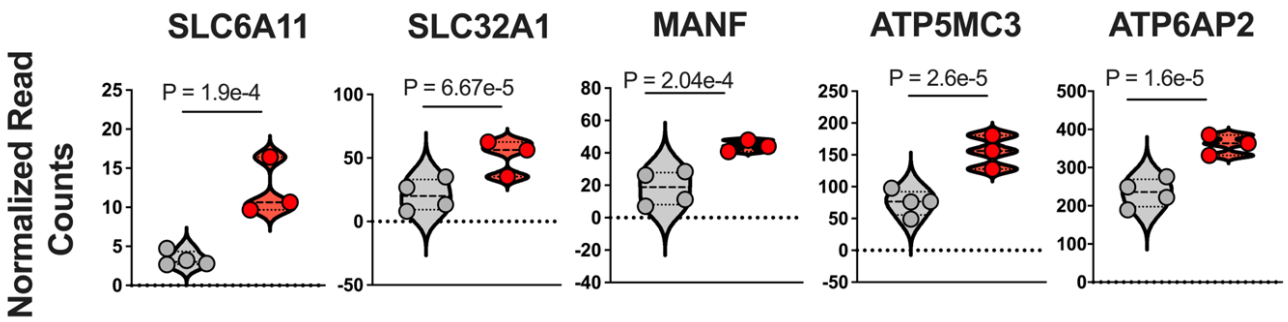

Fig. S7 Expression levels of genes (expressed as normalized read counts in units of Log2 Counts per million [CPM]) related to synaptic functions, endoplasmic reticulum stress, and ATP synthase subunits in the PFCw of SHIV infected (red) and uninfected (gray) animals. Violin plots indicate quartiles. P values determined by linear mixed effects model.

CHAPTER 3: Deep Analysis of CD4 T cells in the Rhesus CNS during SIV infection

****Published in: PLOS Pathogens. 2023 Dec 7;19(12):e1011844. Doi:10.1371/journal.ppat.1011844. PMID: 38060615; PMCID: PMC10729971*

Presented in dissertation as published.

CHAPTER III

Building upon our knowledge gained using SHIV.CH505 in Chapter II, we next aimed to rigorously evaluate the distribution of CCR5+ CD4+ HIV target cells within the brain and key peripheral tissues, including the skull bone marrow, to understand the broader landscape of potential viral reservoirs. This effort was designed to improve upon the limitations encountered in Chapter II, where the use of bulk transcriptomics resulted in difficulties determining differences between individual cells at the population level. Most importantly, we faced difficulties identifying and phenotyping rare T lymphocytes populations within the brain parenchyma. To address this, we utilized single-cell RNA sequencing to analyze highly purified CD45+ cells extracted from the brain parenchyma, both under normal conditions and during acute SIVmac251 infection. This advanced approach allowed us to delve into the specific transcriptional profiles of CD4 T cells in the brain, a level of detail previously unexplored within the rhesus CNS. Additionally, we investigated the degree of CD4 depletion in the brain across both acute and chronic phases of infection, particularly under sub-optimal antiretroviral therapy (ART) in the context of a highly virulent infection, with peak plasma viral loads surpassing 10^6 copies. This comprehensive analysis aimed to shed light on: (a) the dynamics of CD4 T cells within the CNS, (b) their susceptibility to depletion during HIV infection, and (c) the potential consequence of their depletion on CNS health and function. In summary, this chapter offers insights into the fate of CD4 T cells in the CNS during acute HIV infection, providing information about cellular distribution, transcriptional activity, and the overarching consequences of viral invasion and immune response within the brain and adjacent CNS tissue niches.

Deep analysis of CD4 T cells in the Rhesus CNS during SIV infection

Sonny R Elizaldi[1], Anil Verma[2], Zhong-Min Ma[3], Sean Ott[3], Dhivyaa Rajasundaram[4], Chase Hawes[1], Yashavanth Shaan Lakshmanappa[2], Mackenzie L. Cottrell[5], Angela D. M. Kashuba[5], Zandrea Ambrose[6], Jeffrey D. Lifson[7], John H. Morrison[3,8], Smita S. Iyer[2,3,9]

[1]Graduate Group in Immunology, UC Davis, CA, USA; [2]Department of Pathology, School of Medicine, University of Pittsburgh, PA, USA; [3]California National Primate Research Center, UC Davis, CA, USA; [4]Department of Pediatrics, School of Medicine, University of Pittsburgh, PA,USA; [5]Eshelman School of Pharmacy, University of North Carolina, Chapel Hill, NC, USA; [6]Department of Microbiology and Molecular Genetics, School of Medicine, University of Pittsburgh, PA, USA; [7]AIDS and Cancer Virus Program, Frederick National Laboratory, Frederick, MD, USA; [8]Department of Neurology, School of Medicine, UC Davis, CA,USA; [9]Department of Pathology, Microbiology, and Immunology, School of Veterinary Medicine, UC Davis, CA,USA

ABSTRACT

Virologic suppression with antiretroviral therapy (ART) has significantly improved health outcomes for people living with HIV, yet challenges related to chronic inflammation in the central nervous system (CNS)—known as Neuro-HIV- persist. As primary targets for HIV-1 with the ability to survey and populate the CNS and interact with myeloid cells to co-ordinate neuroinflammation, CD4 T cells are pivotal in Neuro-HIV. Despite their importance, our understanding of CD4 T cell distribution in virus-targeted CNS tissues, their response to infection, and potential recovery following initiation of ART remain limited. To address these gaps, we studied ten SIVmac251-infected rhesus macaques using an ART regimen simulating suboptimal adherence. We evaluated four macaques during the acute phase pre-ART and six during the chronic phase. Our data revealed that HIV target CCR5+ CD4 T cells inhabit both the brain parenchyma and adjacent CNS tissues, encompassing choroid plexus stroma, dura mater, and the skull bone marrow. Aligning with the known susceptibility of CCR5+ CD4 T cells to viral infection and their presence within the CNS, high levels of viral RNA were detected in the brain parenchyma and its border tissues during acute SIV infection. Single-cell RNA sequencing of CD45+ cells from the brain revealed colocalization of viral transcripts within CD4 clusters and significant activation of antiviral molecules and specific effector programs within T cells, indicating CNS CD4 T cell engagement during infection. Acute infection led to marked imbalance in the CNS CD4/CD8 ratio which persisted into the chronic phase. These observations underscore the functional involvement of CD4 T cells within the CNS during SIV infection, enhancing our understanding of their role in establishing CNS viral presence. Our findings offer insights for potential T cell-focused interventions while underscoring the challenges in eradicating HIV from the CNS, particularly in the context of sub-optimal ART.

AUTHOR SUMMARY

Antiretroviral therapy (ART) has improved health outcomes of people living with HIV. However, there are still challenges, especially in the central nervous system (CNS), where ongoing inflammation can lead to neurological disorders. Our study focused on understanding the role of CD4 T cells in the brain during HIV infection and sub-optimal treatment adherence. We used a model with SIV-infected rhesus monkeys to study the AIDS virus in the brain and surrounding tissues. We discovered that a subset of CD4 T cells, which are vulnerable to HIV, are present throughout the CNS. During the early stages of infection, we noticed high levels of the virus in both the brain and nearby tissues. By examining these CD4 T cells at a single-cell level, we found that they actively respond to the virus by initiating specific antiviral effector functions to fight it. Overall, our study helps us understand the role of CD4 T cells within the CNS during both acute and chronic HIV infection. This knowledge could help us develop new ways to target the virus in the CNS and devise treatments for complications related to Neuro-HIV.

INTRODUCTION

Improved access to early and sustained antiretroviral therapy (ART) has significantly enhanced the life expectancy of people living with HIV (PLWH). Studies show that immediate ART initiation upon diagnosis is the most effective approach to achieving positive long-term health outcomes (1-4). However, often, ART is not initiated until well after clinical symptoms have become evident (5, 6). Delay in treatment initiation leads to systemic viral dissemination and a decline in CD4 T cell counts, which puts PLWH at a higher risk of developing chronic inflammatory disorders that can affect multiple organ systems, particularly the brain (7, 8). Indeed, the severity of cognitive impairment at the time of ART initiation is the strongest predictor of persistent neurocognitive deficits despite long-term ART, underscoring the significance of early-stage viral spread and neuroinflammation in the disease process and indicating that substantial neurological damage is inflicted early following infection (9-12). As the population of PLWH continues to age, gaining a deeper understanding of the immune factors that drive acute neuroinflammation and contribute to persistent chronic neuroinflammation during ART become increasingly vital.

Originally identified as the AIDS dementia complex, HIV-associated neurocognitive disorders (HAND) or Neuro-HIV encompass a range of neurologic complications varying from mild to severe cognitive and motor impairments (13-15). While severe forms of Neuro-HIV are less prevalent today, HIV infection continues to impact the brain, leading to HAND or HIV-associated brain injury (HABI) (16). It is hypothesized that early HIV entry into the central nervous system (CNS) causes lasting effects on the brain, termed legacy HABI, even with suppressive ART. Additionally, as the infection progresses, active HABI contributes to a gradual cognitive decline. The role of immune activation in driving neuroinflammation in Neuro-HIV is crucial, but the specific cellular mediators responsible for both neuroinflammation and viral persistence in the CNS during chronic infection, as well as immune activation prior to ART initiation, are not yet fully understood.

The historical identification of multinucleated giant cells in brain parenchyma and encephalitic lesions, along with the association of HIV-1 with brain parenchymal macrophages in AIDS patients, brought focus to brain-resident myeloid cells as crucial drivers of viral persistence and neuroinflammation (17, 18). Observations of CNS compartmentalized viral variants, assessed by viral genomic sequencing within the cerebrospinal fluid (CSF) showed ability to mediate infection of cells with lower levels of CD4, and longer half-lives post-acute infection. These data indicated that long-lived cells such as brain-resident macrophages and microglia gradually replace CD4 T cells as the primary source of the virus in the CNS during the chronic phases of infection (19, 20). To reproduce these outcomes, studies in non-human primate models utilized macrophage tropic viral clones that do not depend on high CD4 receptor expression for entry. Additionally, accelerated experimental models intended to increase the frequency, severity, and kinetics of CNS disease in NHP employed CD8 depletion strategies in combination with R5-T cell tropic viruses to induce an immunosuppressive state, leading to the frequent, early development of classic encephalitis lesions typically observed in end-stage Neuro-HIV (21-25). These accelerated models have contributed to our understanding of how HIV establishes itself in the brain during early infection and quickly multiplies within the CNS during profound immune dysfunction. However, it is essential to note that they do not offer insights into CNS dissemination during most natural transmissions.

To understand the neuroinflammatory triggers leading to neurodegeneration in the modern ART era, it is crucial to leverage our enhanced understanding of CNS immune surveillance to explore viral dissemination in multiple immune-rich niches of the CNS during both acute infection and suppressive ART. To achieve our research objectives, we utilized two macaque cohorts. The first cohort consisted of macaques acutely infected with SIVmac251, and they received no ART. The second cohort was infected with SIVmac251 and assessed up to week 42 post infection. We initiated ART at week 3 and therapy was periodically interrupted to simulate

suboptimal adherence, referred to as deferred non-adherent ART regimen. We aimed to characterize the viral-immune interactions involved in establishment and persistence of SIV infection in the CNS. Our findings support three major conclusions. Firstly, we observed that antigen-experienced CD4 T cells present within the brain parenchyma, choroid plexus stroma, dura mater, skull bone marrow, and CSF exhibit a distinctive profile expressing either CCR5 or CCR7. During acute infection, we observed high tissue viral loads within the frontal and temporal lobes, as well as in border tissues, including the lymphoid niche of the skull bone marrow. Associated CD4 T cell depletion within these compartments was suggestive of ongoing CD4 T cell infection in the CNS which was not rescued following suppressive ART. Notably, the relative distribution of CCR5 and CCR7 subsets remained stable throughout this process. Secondly, we found that during ART, CSF viral RNA (vRNA) was below the limit of detection (<15 vRNA copies/ml CSF) despite persistent low vRNA levels in the brain, underscoring the intricate nature of viral control in the CNS. Thirdly, we document a previously unknown potential HIV reservoir in the skull bone marrow. Together, our studies provide insights into the interplay between viral dissemination, CNS T lymphocytes, and neuroinflammation, critical to inform the development of targeted approaches to mitigate progressive neurodegeneration in the context of modern ART.

RESULTS

Study Design

To understand HIV-1 CNS involvement during both the acute and chronic phases of infection, we conducted studies using two macaque cohorts. We employed CCR5-tropic SIVmac251 to replicate acute and chronic HIV-1 effects on the CNS during natural transmission. The first cohort, known as the Acute 251 cohort, comprised four macaques assessed at week 3 pi (SIV, w3). The second cohort, referred to as the Chronic 251 cohort (n = 6), was followed for a duration of up to 42 weeks post-infection (pi). Throughout the study, we collected plasma and CSF samples to capture viral and immune kinetics in both the systemic and the CNS compartments. Four uninfected age-matched animals served as controls. At necropsy, tissues were collected following trans-cardiac saline perfusion to ensure that the assessment of immune cells in the CNS compartment reflected CNS tissues without contributions from vasculature contents. Detailed information about the animals can be found in S1 Table. Gating strategy for identifying T cells in control and SIV CNS tissues is outlined in S1 and S2 Figs.

To capture early-stage dynamics in the CNS prior to ART initiation, we utilized the Acute 251 cohort (Fig 1A). In this study, we applied both flow cytometry analysis of CNS immune cells and single-cell RNA sequencing on CD45+ cells extracted from the brain. This comprehensive approach allowed us to gain deeper insights into the acute neuroinflammatory programs initiated in CNS CD4 T cells during this critical stage. We collected post-mortem punch biopsies of the brain parenchyma, immediately after the brain was excised, for viral quantification. The remainder of the right hemisphere was collected in media and processed immediately post-harvest to extract single cell suspensions for flow cytometry analysis.

In the Chronic 251 cohort, our objective was to induce cycles of viral suppression and rebound throughout the course of infection, resembling scenarios of intermittent poor adherence

to medication or drug resistance, as observed in real-life chronic HIV infections. To achieve this, we employed a 3-drug ART regimen comprising of nucleoside/nucleotide reverse transcriptase inhibitors (NRTIs) Emtricitabine (FTC), tenofovir disoproxil fumarate (TDF) and the integrase inhibitor Dolutegravir (DTG), which was initiated at week 3 post-SIV inoculation, after peak viremia. In clinical studies, FTC and DTG attain therapeutic concentrations within the CNS (26, 27), while TFV's limited CSF diffusion, estimated at only 5%, leads to lower CNS penetration effectiveness scores (28, 29). As CSF escape is an indicator of resistance, longitudinal assessment of paired plasma and CSF viral loads was performed.

Treatment interruption commenced when CSF viral (v) RNA levels fell below 100 copies/mL at two consecutive time points, with corresponding plasma viral loads below 10,000 copies/mL (ATI: weeks 9–10 post-infection). An exception to this protocol was animal 38359, where ATI was initiated at week 9 when CSF vRNA was 120 copies/mL, a deviation prompted by a decline in plasma viral loads (**S2 Table**).

Subsequently, ART was re-initiated when CSF vRNA exceeded 1000 copies/mL at a single time point. These repeated cycles of treatment interruption and initiation continued throughout the chronic phase of infection. Two-to-four weeks prior to necropsy, all SIV-infected animals received ART, and levels of antiretroviral drugs in the plasma, CSF, prefrontal cortex (PFC), and colon were quantified.

CNS viral dissemination and neuroinflammation linked to decline in CSF CCR5+ CD4 T cells.

In line with observations in humans (30, 31), we identified that the non-inflamed CSF allows entry of CD4 T cells, typified by an antigen-experienced CD28+ CD95+ phenotype. Notably, we identified the presence of a distinct CCR5+CCR7- subset, comprising approximately 34% (median) of antigen-experienced CD4 T cells in the CSF (range: 15-46%) in contrast to only

4% observed in blood and lymph nodes (**Figure 1B)**. The CCR5+ CCR7- subset of CD8 T cells exhibited higher prevalence in the blood (median 26%). Interestingly, like their CD4 counterparts, these frequencies were even more elevated in the CSF (median 76%, **S3A Fig**). On the other hand, CCR5- CCR7+CD4 T cells were most prevalent in the blood, constituting 73% (range: 61–82%), whereas they accounted for 58% in the CSF (range: 43–75%).

Based on the presence in the CSF of CCR5+ CCR7- CD4 T cells, consistent with ongoing immune surveillance, we posited that rapid influx of infected CD4 T cells into the CSF following systemic viral replication would lead to acute CNS viral dissemination. Complete blood counts with differential quantitation revealed an expected decrease in CD4 T cell counts in 5/6 animals (4-fold decline at week 4 relative to week 0, $p < 0.05$) with no significant change in total lymphocyte counts during acute infection (**S3B–S3D Fig**). During the initial week post-infection, the median levels of CSF vRNA were approximately 15,000 copies. By the second week, CSF vRNA reached a peak of 1.2x10^6 copies before gradually declining to 4.4x10^5 copies by the third week. These observed patterns closely paralleled viral kinetics in plasma, albeit at lower levels (**Fig 1C–1D**).

Measurement of levels of interleukin 8, monocyte chemotactic protein (MCP-1) and interferon protein 10 (IP-10) demonstrated significant induction of MCP-1 and IP-10 in plasma, peaking at week 1 and gradually declining afterward, while remaining significantly higher than baseline levels at week 3 (**Figs 1E and S4**). In contrast to plasma levels, CSF MCP-1 concentrations did not change significantly, and CSF IP-10 levels displayed a distinct pattern, continuously increasing over time (**Fig 1F**). At week 2, CSF IP-10 levels showed a strong correlation with plasma IP-10 levels, indicating that either CSF IP-10 was influenced by systemic induction, or that intrathecal IP-10 production occurred at a similar level as systemic IP-10 induction (**Fig 1G**).

Despite high viral loads, CD28+ CD95+ cells constituted the majority of CD4 T cells in the CSF during acute infection (**Fig 1H**). At week 3, a notable decrease in the proportion of T cells in

the CSF was observed (**Fig 1I**), driven by a sharp decline in CD4 T cell frequencies during weeks 2 and 3 (**Fig 1J**). Remarkably, although IP-10, which promotes Th1 cell ingress, was elevated, the proportion of CCR5+ CD4 T cells in the CSF declined. However, the CCR5+ CD8 T cell and CCR7+ CD4 T cell subsets remained relatively stable, suggesting the decline was specific to viral replication in target cells within the CSF (**S5 Fig**). As a result, a significant decrease in CD4:CD8 ratio in both CSF and blood ensued (**Fig 1K**).

Quantifying Gag-specific CD8 T cells using the CM9 tetramer in A*01 animals (n = 2) unveiled the presence of antigen-specific CD8 T cells infiltrating the CSF (**Fig 1L**). These cells prominently displayed CD69 expression, signifying activation. Correspondingly, analysis of CD69+ CD8 T cell frequencies demonstrated inverse association with CSF vRNA levels. Furthermore, an increase in CD28- effector memory CD8 T cells in the CSF was observed, indicative of active CD8 T cell surveillance of the CNS during acute SIV infection (**Fig 1M**).

Viral suppression following ART initiation at week 3 led to significant CD4 T cell rebound both in systemic and CSF compartments (both $p < 0.05$) with expected reconstitution of CCR5+ CD4 T cells (**Fig 1N–1O**). The decrease in CD4 T cells during viral replication and rebound following viral suppression supports local viral replication as a contributor to CSF viral loads. This interpretation is supported by evidence in macaques and humans of CD4-cell associated spliced vRNA within CSF indicative of active CD4 infection (32). Since our studies did not assess cell-associated CSF virus, however, we cannot rule out the potential contribution of virions transiting to the CSF from other sites of origin to total CSF vRNA levels.

Assessment of CSF albumin, total protein, and glucose levels indicated that the blood-brain barrier (BBB) maintained its functional integrity despite ongoing viral replication and neuroinflammatory response (S6 Fig).

CCR5+ CD4 T_h1 cells populate brain parenchyma.

Prior to delving into the effects of infection on brain T cell responses, we elucidated the distribution of CD4 T cells within the non-inflamed CNS of SIV-uninfected macaques. The tissues we analyzed included the brain parenchyma and its border-associated compartments, such as the choroid plexus stroma (ChP). The ChP plays a crucial role as the interface between the circulation and the CSF. Given its immune composition, the ChP was gently extracted from the frontal horn and the body of the lateral ventricle, using clean forceps, with care taken to avoid disruption of surrounding tissue. The extracted ChP was subjected to visual inspection to verify absence of contamination from the surrounding parenchyma and was subsequently pooled together. Additionally, we studied the dura mater (dura), which represents the outermost meningeal layer and supports the meningeal lymphatics. Another important compartment we examined was the skull bone marrow (Sk BM), allowing us to assess the lymphoid niche of the calvaria (33-35). To complement our investigation, we also included the draining lymph nodes of the brain, the deep cervical lymph nodes (dCLN) and the ileum as a non-CNS tissue.

As demonstrated in **Fig 2A**, flow cytometry analysis of single cell suspensions obtained from CNS tissues of SIV-unexposed control macaques, following saline perfusion, revealed clear identification of distinct CD4 and CD8 T cell subsets. Notably, there was a predominance of CD8 T cells over CD4 T cells in the brain, with a CD8:CD4 ratio of 2.8 (**Fig 2B**). To delineate CD4 T cell helper profiles in the CNS, we examined the brain, Sk BM, and spleen for expression patterns of CCR5 in the context of CCR6, a marker for Th17 cells and CXCR3, the canonical Th1 marker. Our analysis revealed that CD4 T cells in the brain expressed minimal amounts of CCR6 but were predominantly CXCR3+, consistent with CXCR3-mediated ingress of T cells to the CNS. Among CXCR3+ CD4 Th1 cells, the expression of CCR5 was found to be approximately 47% in the brain, 40% in SkBM, and 14% in the spleen. This indicates that a significant proportion of Th1 cells in the brain and SkBM could potentially be susceptible to R5-tropic infection through CCR5-

mediated mechanisms (**Figs 2C and S7A–S7B**). The evaluation of integrin heterodimers α4β7 and α4β1 revealed relatively higher α4β1 expression. In a Boolean analysis that considered CCR5 co-expression, the predominant subset consisted of α4β1+ CCR5+ cells, indicating that Th1 cells in the CNS concurrently expressed both α4β1 and CCR5. A comparable expression pattern was also noted in the spleen, as illustrated in **Fig 2D**.

The distinct patterns observed in the CSF for CCR5 and CCR7 were similarly observed within the brain parenchyma and other CNS tissues (**Fig 2E**). However, the frequencies of CCR7+ CD4 T cells were lower in the brain, and on average in the Dura, compared to the CSF (**Fig 2F**). Furthermore, when we examined the polyfunctionality of CD4 T cells, specifically their ability to produce cytokines TNF-α, IFN-γ, and IL-2 after stimulation with PMA/ionomycin, we observed robust cytokine production in brain CD4 CD95+ T cells, like their counterparts in the spleen (**Fig 2G**). Notably, there were some distinctions; splenic CD4 T cells exhibited a higher propensity to produce IL-2, leading to increased frequencies of IL-2 single-positive and IL-2/TNF-α co-producing cells. Conversely, the brain showed significant prevalence of IFN-γ single-positive cells, aligning with the phenotypic data underscoring functionality of Th1 cells in the brain, akin to their counterparts in lymphoid tissues (**Fig 2H**).

CD4 T cells depleted in CNS tissues during acute SIV infection.

Next, we studied the Acute cohort (**Fig 3A**) and investigated the impact on CD4 T cells in different CNS compartments during the acute phase of infection. Our analysis of all examined CNS tissues revealed a notable decrease in the relative proportion of CD4 T cells, accompanied by a corresponding increase in CD8 T cells compared to uninfected control animals (**Fig 3B**).

During acute SIV infection, the brain and border tissues (Dura and Sk BM) displayed distinct phenotypic distributions of CCR5+ and CCR7+ CD4 T cell populations, similar to the distribution seen in the non-inflamed brain during homeostasis. Notably, the CCR5+ CD4 T cell

subset exhibited higher expression levels of CD69, PD-1, and CXCR3, indicating an activated and effector-like phenotype, while the CCR7+ CD4 T cells showed a quiescent phenotype, suggestive of a more resting state (**S7C–S7D Fig**). In the CNS tissues, both CCR5 and CCR7 subsets of CD4 T cells were present at varying frequencies. The brain predominantly had CCR5+ CD4 T cells, whereas the spinal cord and Sk BM showed enrichment of CCR7+ CD4 T cells, resembling the distribution observed in bone marrow of long bones and lymphoid tissues (**Fig 3C–3D**).

During acute SIV infection, the brain and border tissues (dura and Sk BM) displayed distinct phenotypic distributions of CCR5+ and CCR7+ CD4 T cell populations, similar to the distribution seen in the non-inflamed brain during homeostasis. Notably, the CCR5+ CD4 T cell subset exhibited higher expression levels of CD69, PD-1, and CXCR3, indicating an activated and effector-like phenotype, while the CCR7+ CD4 T cells showed a quiescent phenotype, suggestive of a more resting state (**S5E-F**). In the CNS tissues, both CCR5 and CCR7 subsets of CD4 T cells were present at varying frequencies. The brain predominantly had CCR5 CD4 T cells, whereas the spinal cord and Sk BM showed enrichment of CCR7 CD4 T cells, resembling the distribution observed in bone marrow of long bones and lymphoid tissues (**Figure 3C**).

To investigate the relationship between CCR5 and CCR7 expression during acute SIV infection, we examined the relative co-expression of two markers—PD-1, which indicates TCR stimulation, and CD69, a marker for acute activation and tissue residency. By analyzing t-SNE plots gated on CD4 CD95 T cells expressing a combination of either CCR5, CCR7, CD69, PD-1, we found that the majority of PD-1 and CD69 expression occurred within the CCR5-expressing CD4 T cells (**Fig 3E**). Relative distribution of these subsets demonstrated that cells co-expressing CCR5 CD69 and PD-1, as well as CCR5 and CD69, were most abundant in the brain and comparable to frequencies in dura (**Fig 3F–3G**), relative to other compartments. Conversely, cells expressing CCR7 but neither of the other three markers (CCR7 single positive, SP) were

significantly higher in the lymphoid tissues, as expected, relative to the brain. Altogether, the data show distinct compartmentalization of CCR5+ and CCR7+ CD4 T cells and reveal that despite CD4 T cell depletion within the brain parenchyma, both CCR5 and CCR7 subsets co-exist during acute infection.

T Cell clusters within SIV-Infected Brain.

To gain deeper insights into the inflammatory programs induced in T cells within the brain following SIV infection, we conducted single-cell transcriptomic profiling of CD45+ cells extracted from the brain of the Acute cohort. This analysis included 4 samples from acute SIV-infected macaques and 2 uninfected controls (**Fig 4A**). For the uninfected control samples, we observed a median of 115,884 mean reads per cell, with a median of 29,278 total genes detected. The SIV-infected brain samples exhibited 107,659 reads per cell and 29,541 identified genes. Following cluster analysis of the SIV-infected brain samples, we identified six distinct immune clusters. Interestingly, all clusters except for the dendritic cell (DC) cluster were shared with control samples reflecting differential DC dynamics induced by SIV infection (**Fig 4B**).

To characterize these cell clusters further, we analyzed highly expressed genes within clusters across all animals. In the CD8 TCM cluster, we observed significantly higher expression of key transcription factors, such as ID2 (1.5-fold relative to TEM in both control and SIV) and JUNB (2.2-fold relative to TEM in control, 1.9-fold relative to TEM in SIV). Additionally, we observed higher expression of essential regulators of T cell signaling, like THEMIS (2.5-fold relative to TEM in control, 1.7-fold relative to TEM in SIV) and BTG1, a regulator of quiescence (1.9-fold relative to TEM in control, 1.8-fold relative to TEM in SIV), among others (**Figs 4C and S8A**). Conversely, the CD8 TEM cluster exhibited the expression of transcription regulators linked to effector differentiation, specifically IKZF2 and ZEB2, both exhibiting an approximate two-fold increase in control samples. Intriguingly, in both control and SIV conditions, over 50% of cells in both CD8 TEM and TCM clusters expressed CD69, highlighting the presence of a diverse

spectrum of differentiation states within these clusters. Furthermore, in control samples, we observed an enrichment of IL7R in the CD8 TCM cluster, while this enrichment was absent in the SIV samples, signifying transcriptional changes in response to infection.

The CD4 TCM cluster displayed expression of canonical TCM genes CD28 and IL7R, while the monocyte/macrophage cluster showed FC receptor and Class II gene expression. The NK cell cluster was marked by expression of killer cell lectin-like receptor (KLR) genes (36). Notably, the DC cluster was unique to the SIV condition and showed distinct expression of the canonical myeloid transcription factor IRF8, as well as genes regulating antigen presentation, including CD74 (37).

Next, we aimed to identify viral transcripts within individual cells and assess their correlation with CD4 T cell immune clusters. To quantify viral transcripts, we developed a custom reference by integrating the SIV isolate SIVmac251.RD.tf5 (SIVmac251) data with the *M. mulatta* (Mmul_10) genome files. Once our tailored reference was successfully established, it served as the basis for the count matrix, which included viral transcripts, facilitating subsequent analyses. Within SIV-infected brain and spleen samples, we observed a spectrum of SIV RNA transcript expression levels, whereas in the control samples, no expression was detected, confirming the validity of our approach (**S8B**). Following the application of a threshold for expression above 1, we observed majority of vRNA-positive cells were concentrated within the CD4 and monocyte clusters in both the brain and spleen with some evidence for background signal in myeloid and CD8 T cell clusters (**S8B–S8C**). Therefore, we subsequently merged CD4 and monocyte clusters. The combined UMAP, with overlayed SIVmac251 reference sequence, highlighted mapped reads associated with CD4 T cell clusters (total number of vRNA+ cells >1 = 11) and, to a certain extent, monocyte/macrophage clusters (total number of vRNA+ cells = 1) in the brain (**Fig 4D–4E**). Examination of splenic CD45+ cells exhibited SIV RNA co-localization with CD4 T cells (total number of vRNA+ cells = 4). The inset displays the percentage of SIV transcripts expressed in

vRNA+ CD4 T cells in both the brain and spleen. Microscopic analysis of the prefrontal cortex (PFC) using RNAscope confirmed our PCR data, revealing the co-localization of viral RNA (vRNA) with CD3+ cells in the CNS parenchyma (**Fig 4F**).

T Cell Effector Molecular Programs Induced within the SIV-Infected Brain

Upon comparing each immune cluster between SIV-infected brain samples and controls (**S9 Fig**) and focusing on genes differentially up or downregulated with adjusted p values of < 0.05, we noted the induction of a transcriptional program regulated by interferons, viral infection, and pattern recognition receptors across all clusters (**Fig 5A**). The observed transcriptional program encompassed several key components, such as interferon alpha inducible protein 27 (IFI27, up 8.8-fold, CD4 TCM; 6.4-fold, CD8 TCM; 7.8-fold, CD8 TEM; 13.7-fold, Mono/Mac; 21-fold, NK), IFI16 (5.1-fold, CD4 TCM; 3.4-fold CD8 TCM; 4.4-fold, CD8 TEM; 8.5-fold, Mono/Mac; 9.7-fold, NK); interferon stimulated genes which induce transcription of antiviral factors—ISG15 (2.8-fold CD4 TCM; 2.1-fold CD8 TCM; 2.6-fold, CD8 TEM; 3.6-fold, Mono/Mac; 4.2-fold, NK) and ISG20 (1.6-fold, Mono/Mac (39). Also induced were the MX Dynamin like GTPases 1 and 2 (MX1 (1.8-fold, CD4 TCM; 1.4-fold, CD8 TCM; 3.3-fold, Mono/Mac; 2.3-fold, NK), MX2 (2.4-fold, Mono/Mac; 1.5-fold, NK). Notably, within the monocyte/macrophage cluster the cytidine deaminase targeting primate lentiviruses, apolipoprotein B mRNA editing enzyme catalytic subunit 3A (APOBEC3A), was induced 3-fold (41).

The pattern of antiviral gene expression in brain parenchymal CD4 T cells closely resembled that observed for CD4 and monocyte/macrophage clusters in the spleen, suggesting that CD4 T cells in both compartments exhibited similar biological responses to viral infection (**Fig 5B**). Within CD4 TCM cluster, genes representing pathways regulating antiviral response, cytolytic function, defense response, metabolism were highly induced (**Fig 5C**). Among genes significantly downregulated in the CD4 T cell clusters within the SIV-infected brain and spleen, we observed the following changes: the S-adenosylmethionine sensor, BMT2, exhibited

substantial reductions, with a remarkable 22-fold decrease in the brain and an even more pronounced 25-fold decrease in the spleen. The aryl hydrocarbon receptor (AHR) was also downregulated (1.6-fold in the brain and 2.9-fold in the spleen), along with the RNA binding protein RBPMS (3.2-fold in the brain and 1.8-fold in the spleen). Moreover, the anti-inflammatory adenosine receptor ADORA2b (12-fold in the brain and 13-fold in the spleen) and the glucocorticoid receptor NR3C1 (1.7-fold in the brain and 1.6-fold in the spleen) were decreased. Notably, the downregulation of IL7R (1.6-fold) and CD4 (1.4-fold) in brain CD4 T cells indicated T cell activation (**Fig 5D**).

Based on induction of genes related to T cell activation and differentiation (CCL5, LAG3, ZEB2) and cytolytic function (GZMM, NKG7), and downregulation of IL7R in the TCM cluster during SIV, we hypothesized that the observed changes in gene expression patterns reflected a spectrum of T cell differentiation states. To test this hypothesis, we utilized an unbiased pseudotime approach where we identified four distinct lineages (**S10 Fig**), each characterized by unique gene expression profiles. Lineage 4 predominantly consisted of CD8 TEM, while Lineages 1 and 3 distinguished themselves through the expression of genes indicative of the transition from TCM to TEM states (**Figs 5E and S10B–S10C**). Along this trajectory was induction of genes associated with cell cycle progression (TK1, MKI67, EIF1, S100A10, S100A4), immune cell activation and differentiation (ZEB2, KLF2, CD52) (42), cytotoxic function (PFN1, GZMB, GZMH, NKG7, and CST7) (43). Modest upregulation of genes from the ribosomal family, involved in regulating translation was also observed. In contrast, canonical TCM genes, such as IL7R and LTB, were downregulated in this lineage, suggesting a distinct pattern of gene expression associated with the differentiation process induced by SIV infection. **Fig 5F** illustrates gene expression changes across pseudotime in T cells from control and SIV brain. Notably, increasing expression of ZEB2 aligns with infection induced effector T cell differentiation Conversely, the decline in LTB expression is linked to SIV indicative of T cell activation, while lower GzmB

expression in control T cells aligns with induction of cytolytic programs following SIV infection. Collectively, the data revealed induction of an antiviral transcriptional program across all immune clusters, underscoring the robustness of the immune response; each cluster exhibited unique inflammatory pathways tailored to complement the specialized antiviral functions of individual immune subsets.

vRNA in brain regions controlling cognitive function and within CNS border tissues.

The sc RNA seq and flow cytometry data demonstrating co-existence of activated CCR5+ CCR7- CD4 T cells alongside quiescent CCR7+ CCR5- CD4 T cells in the Acute cohort raised possibilities regarding their potential roles in viral replication. To delve into this hypothesis, we quantified cell-associated vRNA and vDNA levels within specific CNS tissues (**Fig 6A**). We collected post-mortem punch biopsies (~30 mg) from specific regions of interest, including both white (w) and gray (g) matter regions of the PFC and temporal lobe, such as the superior temporal sulcus (STS). Additionally, we assessed other CNS regions, including the hippocampus (Hp), pituitary (Pit), a circumventricular organ, as well as the border tissues (ChP, dura, Sk BM). The data revealed high levels of vRNA within the brain parenchyma, with a median of 0.16x10^5 vRNA copies per 10^6 cells (**Fig 6B**). The viral loads in the border tissues were also high, with the ChP exhibiting a median of 5x10^5 vRNA copies, the Dura 5x10^6 vRNA copies, and the SkBM with 0.6x10^5 vRNA copies, indicating widespread viral dissemination throughout the CNS.

Assessment of vDNA across these regions showed a median of 135 vDNA copies/106 total cell equivalents observed in the frontal and temporal lobes (**Fig 6C**). Viral DNA was prominently observed in border tissues, with the Dura showing the highest levels at 11,000 copies/106 total cell equivalents. The elevated viral burden in the dura aligns with its role in draining antigens from the CNS. The computation of the vRNA/vDNA ratio indicated active viral expression across all regions within CNS. Particularly noteworthy was the observation of higher ratios in white matter regions, known to harbor T cells (44) (**Figure 6C**). This observation aligns

with imaging studies in PLWH, which have demonstrated widespread and rapid loss in white matter volume during the early stages of infection, while loss in gray matter is more defined and localized to specific regions of the parenchyma, such as the caudate nucleus (45, 46). Collectively, the combination of phenotypic data, sc analysis, RNAscope, and viral load analysis indicates that the CNS is permissive to R5-T cell tropic viruses.

Assessment of T cell phenotype furthermore revealed a significant increase in the relative proportion of the CD28- effector memory subset within both CD4 and CD8 T cells in the brain parenchyma during acute SIV (**Fig 6E–6F**). However, when expressed as a percentage of CD3, a contrasting trend emerged: a decrease in CD28- CD95+ CD4 T cells alongside an increase in CD28- CD95+ CD8 T cells was evident, implying potential CD4 depletion coupled with CD8 T cell infiltration (**Fig 6G**). This observation aligns with trend for inverse association between CCR5+ CD4 T cell frequencies in CNS and concurrent plasma viral load and substantial expression of α4 integrin and PD-1 on CD28- CD95+ CD8 T cells, indicating influx of antigen-stimulated/specific CD8 T cell to the brain parenchyma (**Fig 6H**).

Decrease in vRNA in Brain during Antiretroviral Therapy.

To complement our data characterizing the establishment of CNS infection over the first 3 weeks of infection in the Acute cohort, we turned to the Chronic cohort, in which we initiated ART at week 3 pi (**Fig 7A**). The time taken to achieve viral suppression in the CNS (defined as CSF vRNA copies at or below 15) varied between 3 to 7 weeks (**Fig 7B**). During this period, transient on-ART increases in the CSF vRNA level occurred between 5 and 7 weeks in some animals, except for one animal, 38889 (Mamu A*01). Remarkably, 38889 demonstrated notable CSF viral suppression even without ART suggestive of SIV-specific CD8 T cell mediated viral control in the CSF in this animal, an observation supported by CSF influx of Gag-CM9 CD8 T cells as shown in **Fig 1L**.

In all animals, there was an initial rapid decay of CSF viremia up to week 6, which closely mirrored the decay of plasma viral loads during ART. Subsequent suppressive periods showed shorter intervals, consistent with lower initial CSF viral loads (median 5,150 vRNA copies/mL) and rapid decay kinetics. Once cycles of ART withdrawal were initiated, plasma and CSF vRNA rebound was observed for all animals, except for 38889, which achieved suppression of CSF vRNA (but not plasma vRNA) while off ART.

To assess evidence of viral expression in the setting of short-term ART suppression of viral replication, we implemented a strategy where all animals were on ART for a period of 2–4 weeks before necropsy. This intervention led to significant reduction of CSF vRNA levels to < 15 copies/mL. We also evaluated the penetration of antiretroviral drugs (ARVs) into CSF. For this purpose, we quantified ARV levels in both plasma and CSF samples obtained at the time of necropsy. To gain a deeper understanding of ARV metabolism and intracellular levels of active metabolites, we investigated the presence of di and tri-phosphorylated forms of TFV/FTC within tissues. The timing of sample collection was carefully coordinated to measure trough levels in plasma and CSF. Specifically, samples were obtained 9–12 hours after the last ART dosage and were immediately processed to preserve sample integrity. To examine tissue-specific effects, post-mortem punch biopsies were collected from the PFC and colon, weighed, and flash-frozen for subsequent analysis.

All three ARVs were measured, and the active metabolites of the NRTIs were quantified in colonic (a site of peripheral viral replication) and PFC (a cognitive area of the brain affected in chronic HIV) tissue. Consistent with previous studies, FTC exhibited the highest penetration, with CSF levels similar to those observed in plasma (median ng/mL; plasma: 20.8; CSF: 12.5) (**Fig 7C**). DTG was also found above the lower limit of quantification (LLOQ) in CSF for all animals (median ng/mL; plasma: 329; CSF: 4.2, $p<0.05$). On the other hand, TFV showed detectable levels in the CSF of only 2 out of 5 animals (median ng/mL; plasma: 58.8; CSF: 1.2, $p<0.05$). We

investigated the penetration of ARVs into brain tissue and observed that all ARVs were able to penetrate the brain, with levels of TFV, FTC, and DTG above the LLOQ (**Fig 7D**). However, it's important to note that these levels were at least 10-fold lower compared to those observed in colonic tissue. Importantly, we observed the accumulation of TFV di-phosphate (DP) in the PFC, indicating the penetration of ARVs into the CNS (**Fig 7E**).

Measurement of CSF viral loads demonstrated that vRNA levels were low to below threshold of detection. In the gray matter of the PFC, measurable vRNA levels were observed in only 2 out of 6 animals, while all animals tested negative in the white matter of the PFC (**Fig 7F**). Interestingly, in the temporal lobe, there was a higher likelihood of focal viral expression, with most animals showing vRNA in the STS and Hp. Within the border tissues, detectable vRNA in the dura and Sk BM was found in all animals; however, vRNA in ChP in most animals was not measurable, in line with concurrent absence of vRNA in CSF. Evidence of viral infection was observed with vDNA demonstrable across the brain parenchyma in all animals (**Fig 7G**). These collective findings strongly support the conclusion that lymphotropic viruses establish viral reservoirs in the CNS. Having observed the active induction of IP-10 during acute viral infection within the CNS, we further explored its potential as a biomarker for ongoing viral replication during the chronic phase. Despite viral suppression, we observed a trend for higher IP-10 levels in CSF relative to baseline and concurrent plasma levels at week 7. The lack of a consistent pattern in CSF IP10 during ART and interruption periods diminishes its reliability as a potential CSF biomarker for viral control and rebound during chronic infection (**S11 Fig**).

Persistent CD4 depletion in CNS during chronic infection

The presence of vRNA in the brain parenchyma and associated border tissues during suboptimal ART led us to hypothesize that CD4 T cells would remain depleted in the CNS during chronic infection. To explore this, we assessed CD4 T cell frequencies in various CNS compartments, including blood, brain, choroid plexus, CSF, dura, Sk BM, and dCLN (**Fig 8A–8B**).

Our analysis confirmed our hypothesis, revealing a significant reduction in CD4 T cell frequencies compared to uninfected control animals (**Fig 8C**).

In humanized mice, HIV infection leads decrease in CD4 T cell counts and an increase in CD8 T cell counts in the brain. However, after the initiation of ART treatment, CD4 T cell levels in the brain return to normal, a contrast to current observations in macaques. This disparity may be attributed to several factors, such as the multiple rounds of ATI and the relatively brief duration of ART in macaques. Furthermore, CD4 T cell levels are reported as percentages herein, a metric influenced by both CD4+ and CD8+ T cell counts.

To further investigate the changes within CD4 T cell subsets during acute and chronic infection in the brain parenchyma, we focused on Th1 cells expressing α4β1 and CCR5, and compared them to distribution observed in the spleen. The proportion of CXCR3+CCR5+ CD4 T cells remained constant with infection, while there was a relative decline in these cells in the spleen during the acute phase. Meanwhile, both α4β1+ CD4 Th1 and α4β1+ CCR5+ Th1 cells were significantly reduced during acute infection in both the brain and spleen (**Fig 8D**).

During the chronic phase, subsets expressing either CCR5 or CCR7 were still observed (**Fig 8E**). t-SNE plots of CD4 CD95 T cells expressing CCR5/CCR7/CD69/PD-1 demonstrated a distribution pattern similar to that observed during acute infection (**Fig 8F–8G**). Notably, cells expressing PD-1 but not CCR7, CD69, or CCR5 (PD-1 single positive (SP) were present at higher frequencies during the chronic phase (**Fig 8H**). This increase in the relative frequencies of the PD-1 SP subset was also observed in the dCLN. Furthermore, while PD-1+ CD69+ CD4 T cells were not significantly higher in the brain during the chronic phase, their frequencies were elevated in the dura and dCLN. Additionally, an increase in the CCR7+ PD-1+ CD4 T cell subset was noted in the dura and dCLN. Overall, the data show that there is an increase in CD4 T cells expressing PD-1 within the brain parenchyma and CNS during the chronic phase of infection, even with

suppressive ART. This increase indicates ongoing antigen-mediated T cell stimulation in CNS, likely due to relatively short period of ART for 2–4 weeks prior to necropsy.

DISCUSSION

A deeper understanding of immune mechanisms driving viral establishment, persistence, and neuroinflammation holds the potential to improve the quality of life for those living with HIV by addressing neurological complications and cognitive impairments early and effectively. Our findings provide significant insights into the immune environment within the brain parenchyma during both acute and chronic HIV infection. Specifically, we have identified distinct subsets of activated CCR5+ CD4 T cells and resting CCR7+ CD4 T cells. This discovery, coupled with our existing knowledge of these cell subsets derived from lymphoid and mucosal tissues (49-52), strongly supports the hypothesis that the immune milieu in the brain facilitates both active viral replication and the persistence of viral reservoirs during R5-T cell tropic infections. Notably, our single-cell, phenotypic, and functional analyses demonstrate striking parallels between CD4 T cells in the brain parenchyma and those within the spleen during acute SIV infection. Beyond the brain parenchyma, our research sheds light on the immune composition of brain border tissues, uncovering HIV target CCR5+ CD4 T cells in the choroid plexus, dura, and skull bone marrow. The presence of vRNA and vDNA in these areas, along with their interconnectedness, holds significant implications. These findings indicate that CSF viral loads can provide more comprehensive insights than previously appreciated. They may not only reflect viral activity in the brain parenchyma and blood but also indicate viral presence in the choroid plexus and skull bone marrow. Equally notable is the existence of a lymphoid niche composed of CCR7+ CD4 T cells expressing IL-7R in the CNS. This finding is important as homeostatic proliferation of these cells could contribute to the longevity of virally infected cells within the CNS. In summary, our work not only sheds light on the intricate CD4 T cell landscape within the CNS but also highlights the active responses of T cells in the brain to SIV infection.

In addition to CD4 T cells, our single-cell analysis of CD45+ cells from the brain demonstrates the presence of distinct CD8 TCM and TEM clusters during acute SIV infection.

While we did not identify a definitive resident memory (TRM) cluster (53) the expression of CD69 transcripts within TEM and CD69 surface expression strongly suggests the co-existence of effector and resident CD8 T cells within the rhesus brain parenchyma. Furthermore, CD69 alone, in the absence of CD103, is shown to be sufficient in identifying TRM in non-CNS tissues (54). This indicates that T cells in the brain exhibit a spectrum of differentiation states and respond rapidly to SIV infection in the CNS. Notably, we observed the upregulation of the canonical pathogen-specific effector chemokine, CCL5, in the CD8 TEM cluster. Additionally, the presence of Ki-67, a marker for cellular proliferation, and increase in CD28-effector memory CD8 T cells in the brain is consistent with active recruitment of SIV-specific CD8 T cell effectors to the brain parenchyma during acute infection (55, 56). Our single-cell analysis of the CD4 T cell cluster in the brain also uncovered crucial details into the immune response during acute SIV infection. We observed a significant downregulation of key genes, such as IL7R and CD4, indicating strong T cell activation. Additionally, the expression of important anti-inflammatory receptors, including ADORA2B (receptor for extracellular adenosine) and the glucocorticoid receptor NR3C1, was also reduced. Conversely, we also noted the activation of antiviral IFN genes, signifying the active engagement of CD4 T cells within the brain. Importantly, this antiviral gene expression pattern closely paralleled what was observed in CD4 clusters within the spleen, indicating a shared antigen-specific and bystander response pattern across infected tissues. Exploring clonal heterogeneity of T cell subsets will yield deeper insights into immune response dynamics within the CNS during infection.

Although we did not measure cell-associated vRNA in CD4 T cells in the CSF in our studies, we infer the contribution of productive CD4 infection to CSF viral burdens. This inference is supported by the fact that R5-T cell tropic viruses, such as SIVmac251, require high levels of CD4 to enter cells. Previous research has also shown rapid viral decay following ART initiation, which aligns with our observations, consistent with replication in short-lived T cell effectors (47)

(57). Recent studies have shown spliced cell-associated viral RNA in CSF CD4 T cells during the acute stages of HIV-1 infection and weeks 2, 4, and 8 in SHIV-infected macaques, supporting active viral transcription within CSF CD4 T cells (32). Studies in PLWH during suppressive ART further support this model (32, 58). Utilizing the T cell activation marker CD26 to distinguish HIV virions derived from CD4 T cells versus macrophages, Lustig et al. report T cell-derived virus in the CSF, even in individuals experiencing CSF escape - controlled viral replication in periphery evidence by plasma viral loads below the limit of detection in presence of concurrent CSF viral loads (58). Although compartmentalized virus in the CSF has been attributed to viral replication in brain-resident myeloid cells (20), compartmentalized replication of R5-T cell tropic T/F virus in ART-naive PLWH has also been observed (57). Altogether these data support the importance of CD4 T cells in contributing to acute stage CNS viral burden and neuroinflammation, setting the stage for legacy effects.

The presence of HIV target CCR5+ CD4 Th1 cells in immune-rich compartments within the CNS beyond the CSF highlights their potential role in supporting viral replication. Notably, higher levels of vRNA within the dura, compared to the parenchyma, might be attributed to transitory cells draining from the brain and subarachnoid space through dural lymphatic vessels, although the possibility of resident cells in this compartment cannot be ruled out (33, 59). Another intriguing site is the choroid plexus stroma, positioned at the interface of peripheral blood and CSF, known to harbor macrophages and dendritic cells. The presence of CCR5+ CD4 T cells and vRNA in this tissue underscores its importance in terms of inflammation and viral evolution. Of particular significance is the potential establishment of reservoirs in the skull bone marrow niche of the CNS, which has access to the dura and brain, especially in the context of inflammation (60, 61). Based on the mobilization of the myeloid niche from the skull bone marrow to the brain during inflammation (60), investigating whether a similar phenomenon occurs for T cells could yield valuable insights into their migration and role in seeding the brain with virally reactivated CD4 T

cells. Furthermore, the homeostatic proliferation of CCR7+ CD4 T cells and clonal expansion within the marrow may contribute to reservoir maintenance, potentially enabling the transit of cell-free or cell-associated virus to border tissues of the brain and the CSF. Assessing viral sequences in sorted CCR5+ and CCR7+ subsets across CNS compartments and in peripheral subsets during acute and chronic infection under suppressive ART will provide deeper insights into their respective roles in promoting viral replication and persistence.

The strategic positioning of CXCR3+ CCR5+ CD4 T cells within the CNS—including the brain parenchyma, CSF, choroid plexus stroma, dura, and skull bone marrow—highlights their significance not only in neuroinflammation but also in sustaining CNS viral presence. In support of this concept, consistent elevation of CSF IP-10 levels compared to plasma throughout infection signifies a CNS environment primed for CXCR3-IP-10 mediated T cell ingress. This implies that the CNS remains receptive to CCR5+ CD4 T cell infiltration, potentially perpetuating viral presence. Equally pivotal is data showing that despite CD4 T cell depletion during infection, frequencies of CCR5 and CCR7 within the CNS remain relatively stable. This stability prompts consideration that underlying mechanisms sustain a pool of CCR5+ CD4 T cells within the CNS. The presence of CCR5+ CD4 T within the skull bone marrow, coupled with activation of the skull bone marrow niche during neuroinflammation, indicates possible conduit for cell-free or cell-associated viral migration from the skull bone marrow to the brain (61). By investigating dynamics of viral sequences across different CNS compartments, future studies may uncover insights into CNS viral evolution and the role of CCR5+ CD4 T cells in driving this process.

Once inside the brain, T cell engagement with brain-resident innate immune cells can trigger immune activation. Indeed, the consideration of brain resident microglia and macrophages is paramount in understanding the full extent of viral dissemination and neuroinflammation within the CNS. As major immune cells expressing CD4 and CCR5, albeit at lower levels than CD4+ T cells, they become crucial targets for viral infection in the CNS (57, 62). High responsiveness of

microglia to IFN-γ, a classic CD4+ Th1 cell cytokine, can activate them, leading to the release of free radicals and inflammatory mediators like TNF-α and IL-1β, ultimately contributing to neuronal death (63-65). This ensuing inflammation, particularly the induction of IP-10, could then trigger waves of Th1 CD4 T and CD8 T cell influx, further intensifying immune activation. Such a continuous cycle of viral replication and immune activation could contribute to viral persistence within the CNS. Conducting proof-of-principle studies to investigate these mechanisms and delineating the role of immune trafficking across distinct CNS compartments is of import as they hold the potential to significantly advance our understanding of the cells involved in acute and chronic neuroinflammation, as well as viral persistence within the CNS.

While our findings significantly contribute to our understanding of CD4 T cell responses in the CNS following acute and chronic SIV infection, it is crucial to acknowledge limitations in our study. First, our primary focus on modeling sub-optimal ART adherence inherently restricts the applicability of our findings, particularly regarding CNS viral persistence and immune activation, to fully suppressed settings. Second, our study did not evaluate SIV-specific T cell responses or the differential distribution of SIV-specific CD8 T cells across various brain regions, encompassing white and gray matter, and border tissues or frontal and temporal regions of the brain. These unexplored aspects undoubtedly hold important implications for virological control in distinct regions of the brain parenchyma and CNS. Lastly, exploration of viral sequences in CSF compared to plasma temporally, and across distinct CNS compartments during acute and chronic infection is important. This is an aspect that has not been addressed but holds significant potential to yield crucial insights into the virological and immunological determinants of viral persistence and control within the CNS.

In conclusion, our findings provide insights into viral replication and immune responses within the CNS. They have important implications for understanding disease progression, viral persistence, and the challenges in eradicating the virus from the CNS.

FIGURES

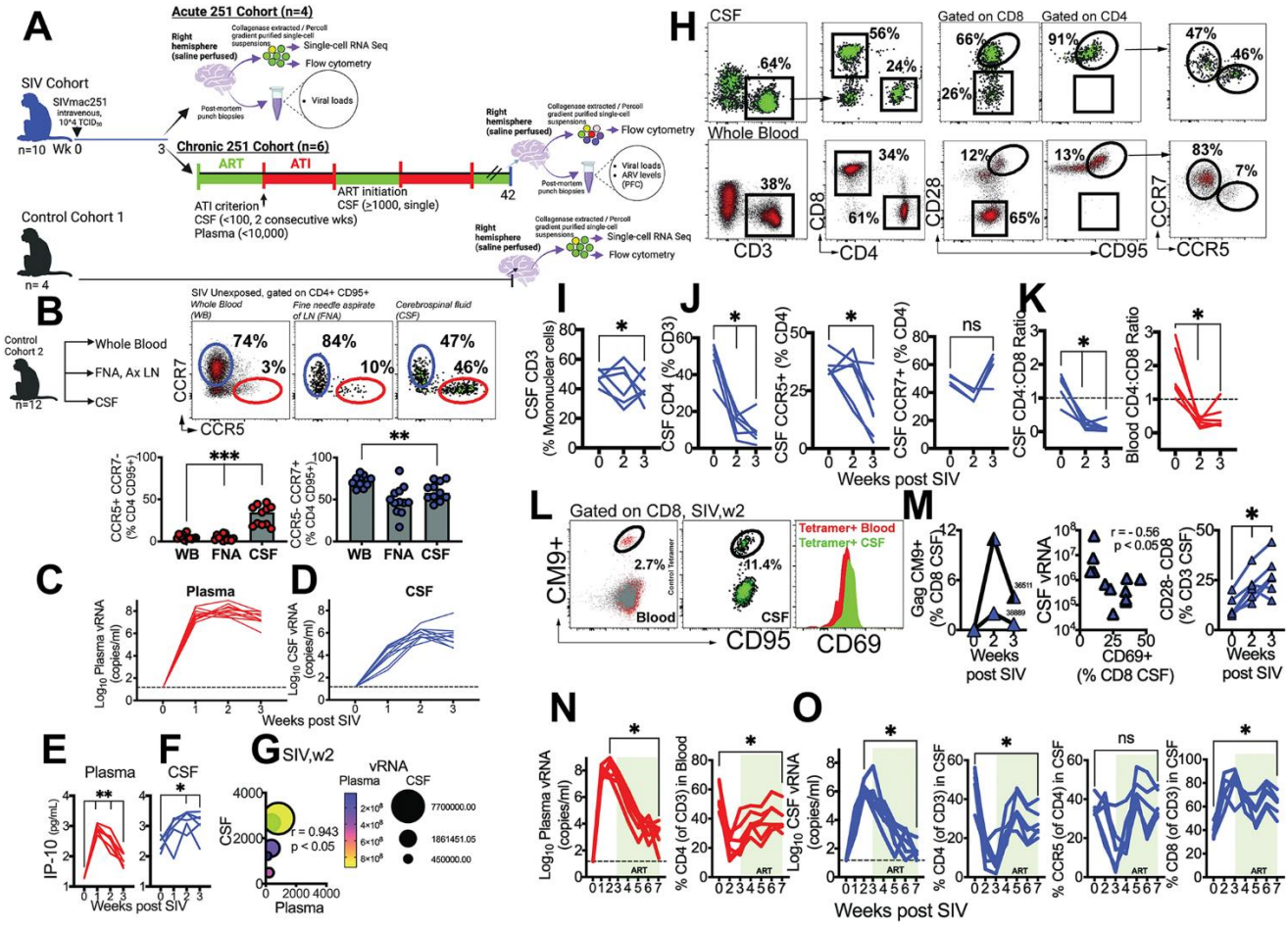

Fig 1. CNS viral dissemination and neuroinflammation linked to decline in CSF CCR5+ CD4 T cells.

Study design showing **(A)** SIV (Acute 251 (n = 4) and Chronic 251(n = 6) cohorts and Control 1 cohort (n = 4). **(B)** Flow cytometry plots illustrate discrete distribution patterns of CCR5 and CCR7 on CD4+ CD95+ cells in blood, lymph node fine needle aspirate (FNA), and CSF. Bar graphs show frequencies of CD4 subsets across compartments. Animals from Control Cohort 2 assessed (n = 12). Kinetics of viral RNA (copies/mL) measured by RT-qPCR in **(C)** plasma and **(D)** CSF following SIVmac251 infection (n = 10, both acute and chronic 251 cohorts assessed). Horizontal dashed line indicates limit of detection (15 vRNA copies/ml). Concentrations of IP-10 (pg/mL)

measured in **(E)** plasma and **(F)** CSF by Legend Plex flow-cytometry based bead assay. **(G)** Bubble plot shows correlation of CSF and plasma IP-10 at week 2 post SIVmac251, Spearman correlation, two-tailed p value shown. Bubble size denotes CSF viral load, and bubble color plasma viral load (n = 6, chronic 251 cohort assessed). **(H)** Flow cytometry plot illustrates CD4+ CD95+ T cells express CCR5 and CCR7 in CSF. **(I)** Kinetics of CSF T cells during acute SIV. **(J)** Kinetics of CD4 T cells in CSF; graphs show % CD4 T cells, %CCR5+ CD4 T cells and % CCR7+ CD4 T cells in CSF. **(K)** CD4:CD8 Ratio in CSF and Blood (n = 6, chronic 251 cohort assessed). **(L)** Flow plot shows Gag CM9+ CD8 T cells in blood and CSF (in A*01 animal 36511). CM9+ CD8 T cells in CSF express CD69. **(M)** Kinetics of CM9+ CD8 T cells in CSF (n = 2 A*01s in chronic cohort). Correlation plot shows CD69+ CD8 T cell frequencies in CSF at weeks 2 and 3 inversely associate with CSF vRNA. Spearman correlation, two-tailed p value shown. Kinetics of CD28- CD8 CSF T cells (% CD3) shown (n = 6, chronic 251 cohort assessed). **(N)** Plasma viral loads during ART (week 3–7), CD4 T cell rebound following viral suppression. **(O)** shows CSF vRNA during ART and CD4 T cell rebound and reconstitution of CCR5+ CD4 T (n = 6, chronic 251 cohort assessed). Significant differences by two tailed Wilcoxon matched-pairs signed rank test, ***, p< 0.01; **, 0< 0.01 in B. Significant differences by one tailed Mann Whitney test, *, p< 0.05 in E and F. Significant differences by one-tailed Wilcoxon matched-pairs signed rank test, *, p< 0.05 in I-O.

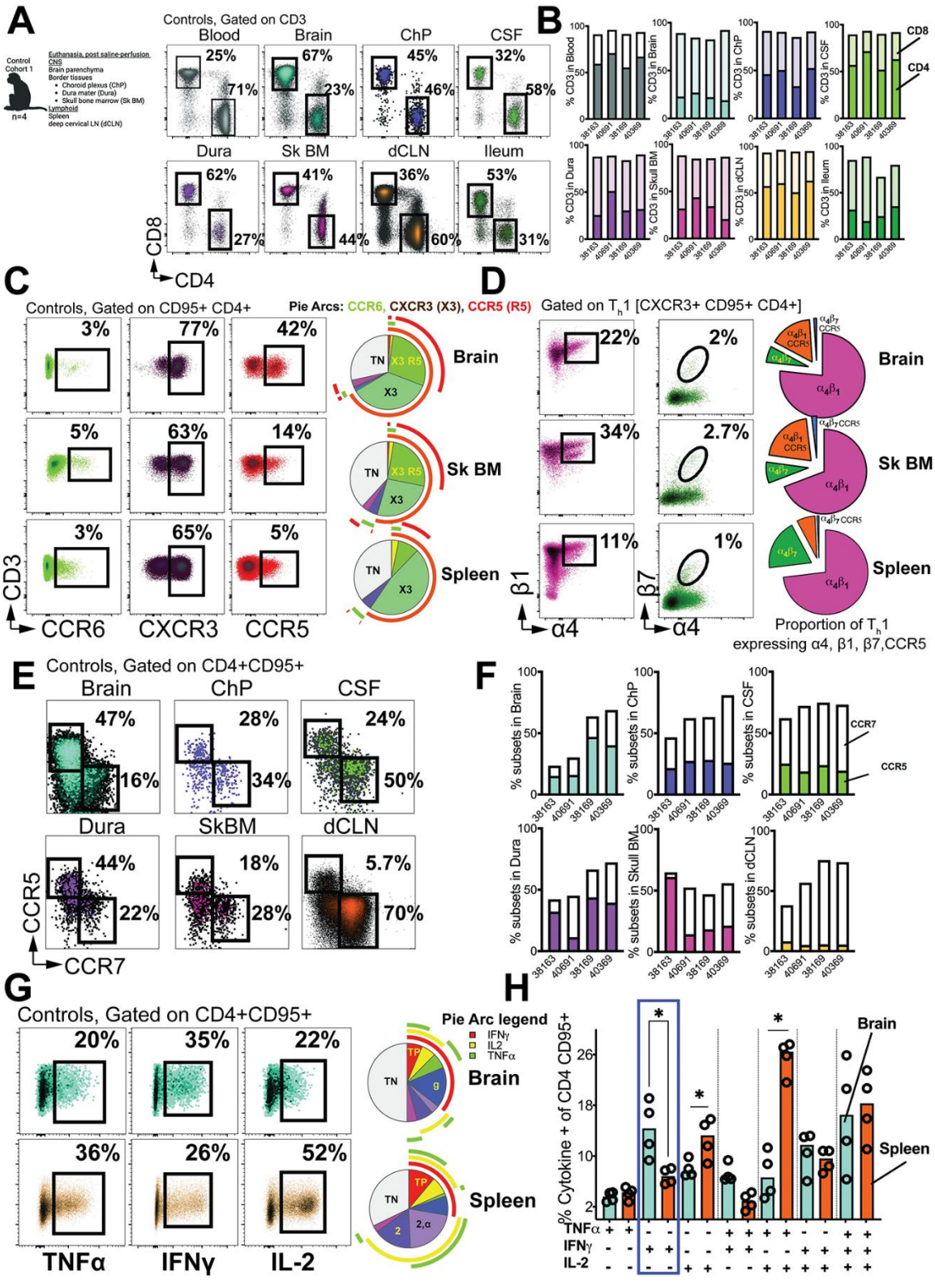
A
Controls, Gated on CD3
Blood
Brain
ChP
CSF
Dura
Sk BM
dCLN
Ileum
CD8
CD4
B
% CD3 in Blood
% CD3 in Brain
% CD3 in ChP
% CD3 in CSF
% CD3 in Dura
% CD3 in Skull BM
% CD3 in dCLN
% CD3 in Ileum
CD8
CD4
C
Controls, Gated on CD95+ CD4+
Pie Arcs: CCR6, CXCR3 (X3), CCR5 (R5)
Brain
Sk BM
Spleen
CD3
CCR6
CXCR3
CCR5
D
Gated on Th1 [CXCR3+ CD95+ CD4+]
Brain
Sk BM
Spleen
β1
α4
β7
α4
Proportion of Th1 expressing α4, β1, β7,CCR5
E
Controls, Gated on CD4+CD95+
Brain
ChP
CSF
Dura
SkBM
dCLN
CCR5
CCR7
F
% subsets in Brain
% subsets in ChP
% subsets in CSF
% subsets in Dura
% subsets in Skull BM
% subsets in dCLN
CCR7
CCR5
G
Controls, Gated on CD4+CD95+
TNFα
IFNγ
IL-2
Pie Arc legend
IFNγ
IL2
TNFα
Brain
Spleen
H
% Cytokine + of CD4 CD95+
Brain
Spleen
TNFα
IFNγ
IL-2

Fig 2. CCR5+ CD4 Th1 cells populate brain parenchyma.

(A) Flow cytometry plots illustrate frequencies of CD4 and CD8 T cells in blood, CNS tissues, dCLN, and ileum in controls. **(B)** Contingency plots show % CD4 (solid) and % CD8 (transparent) in each of the control cohort 1 animals (n = 4) assessed. **(C)** Surface expression of CCR6, CXCR3, and CCR5 on CD95+ CD4 T cells. Pie chart shows preponderance of CXCR3+ CCR5+ (X3 R5) subset in brain relative to spleen. **(D)** Flow plots and pie chart illustrate expression of α4β1, α4β7, and CCR5 on CD4 Th1 cells. **(E)** CCR5 / CCR7 distinction in CNS. **(F)** Contingency plots show % CCR5 (solid) and % CCR7 frequencies (transparent) in each of the control cohort 1 animals (n = 4) assessed. **(G)** Flow plots show cytokine production following 3-hour stimulation with PMA/Ionomycin in controls (n = 4). **(H)** Pie Chart and bar graph show proportion of cytokine producing cells across brain (n = 4) and spleen. (n = 4) Significant differences by one tailed Mann Whitney test, *, $p < 0.05$ in H.

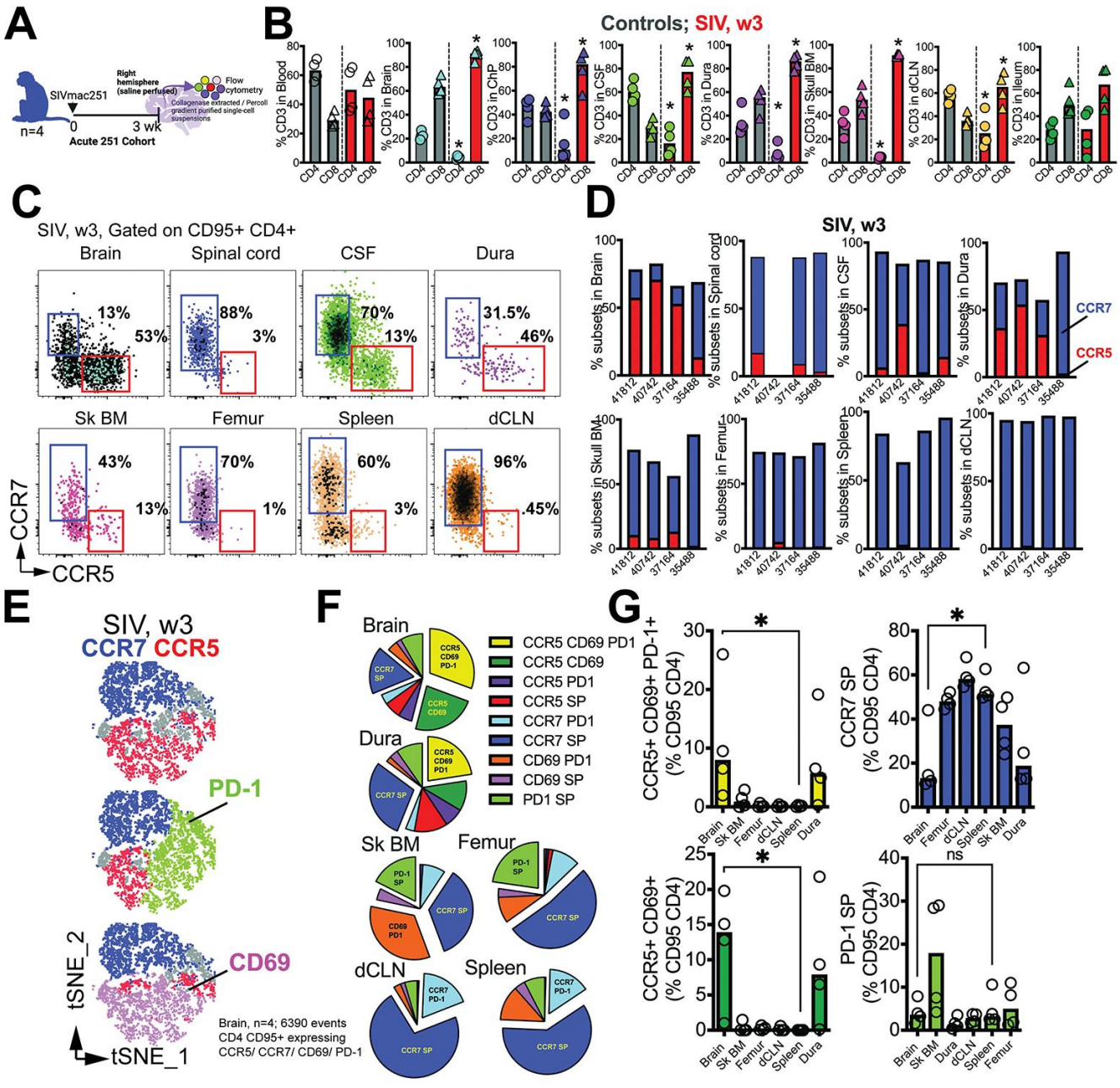

Fig 3. CD4 T cells depleted in CNS tissues during acute SIV infection.

(A) Acute 251 cohort (n = 4) assessed. **(B)** Bar graphs show T cell frequencies in blood, CNS tissues, dCLN, and ileum in control and SIV infected (week 3 pi) macaques**. (C)** Flow plots and **(D)** contingency plots show CCR5+ / CCR7+ CD4 T cell subset frequencies at 3 weeks post SIV (n = 4). **(E)** t-SNE plots gated on CD4+CD95+ cells in Brain expressing CCR7/CCR5/PD-1/CD69 (n = 4 samples, 6390 events). **(F)** Pie chart demonstrating proportion of CD4 T cells

expressing combination of markers (CCR7/CCR5/PD-1/CD69). **(G)** shows distribution of specific subsets across tissues. Significant differences by one tailed Mann Whitney test, *, p< 0.05 in A and F. Schematics were generated using BioRender.

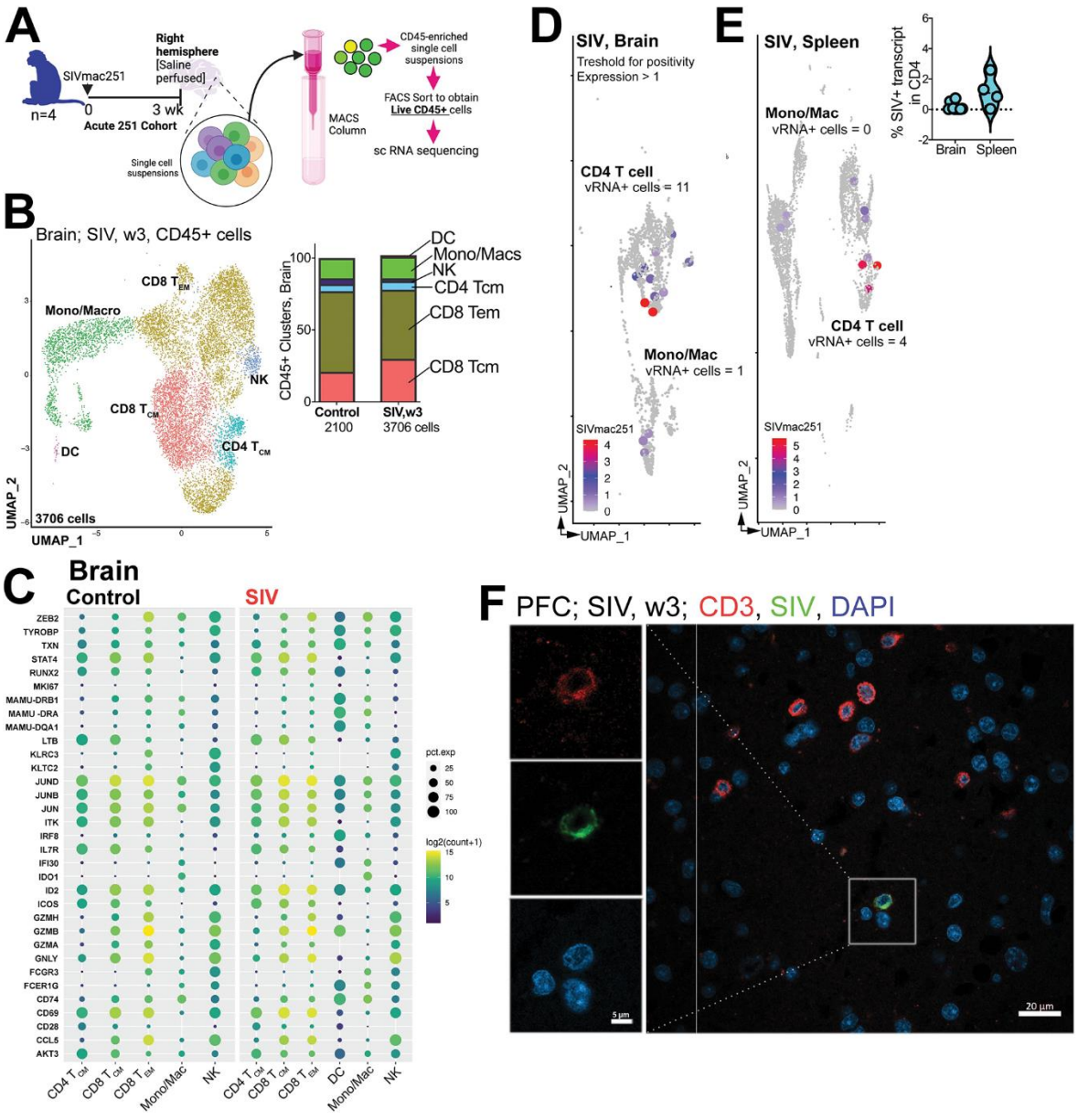

Figure 4. T Cell clusters within SIV-Infected Brain. (A) Schematic of single cell profiling of CD45+ cells in brain (n = 4 Acute 251 cohort, n = 2 Control cohort 1). Sequence alignment to

M.mulatta (Mmul_10) reference using 10X Genomics protocol (CellRanger V.6.0) was performed. The generated cell-by-gene count matrix was used for downstream analysis using the Seurat based integrative analysis workflow. The filtered count matrix (percentage of mitochondrial reads <10, and gene expressed in more than 10 cells) was log-normalized, with top variable genes used for graph-based cell clustering with a resolution of 0.5 and visualized using Uniform Manifold Approximation and Projection (UMAP). **(B)** UMAP of scRNA-seq transcriptional profiles from brain shows 6 clusters. Cell clusters are color-coded based on cell types. Cluster identity was assigned by a combination of approaches—cluster-specific differentially expressed genes, expert knowledge, canonical list of marker genes, and automated annotations using immune reference atlas through SingleR. Inset shows cell proportions in each cluster by experimental group. **(C)** Dot plot of select marker gene expression. Dot size represents proportion of cells expressing gene and color designates expression level. To quantify viral transcripts, we designed a custom reference using CellRanger mkref pipeline. We integrated FASTA and GTF files of SIVmac251 into M. mulatta (Mmul_10) genome references. This tailored reference facilitated downstream analysis by including viral transcripts in the count matrix. UMAP of SIV RNA expression in cell clusters (SIV RNA+ cell size increased for clarity) in **(D)** brain and **(E)** spleen. Number of cells from each cluster positive for vRNA provided. After filtering cells expressing SIV transcript above a threshold 1, %SIV+ for CD4 T cells was determined by dividing the count of the SIV transcript by the total gene count (inset). **(F)** shows SIV RNA in parenchyma and perivascular regions of the brain using ISH with probe against SIV RNA. SIV RNA+ (green) CD3+ T cells (red) with nucleus (DAPI, blue) in PFC; box (CD3+ SIV+ cell).

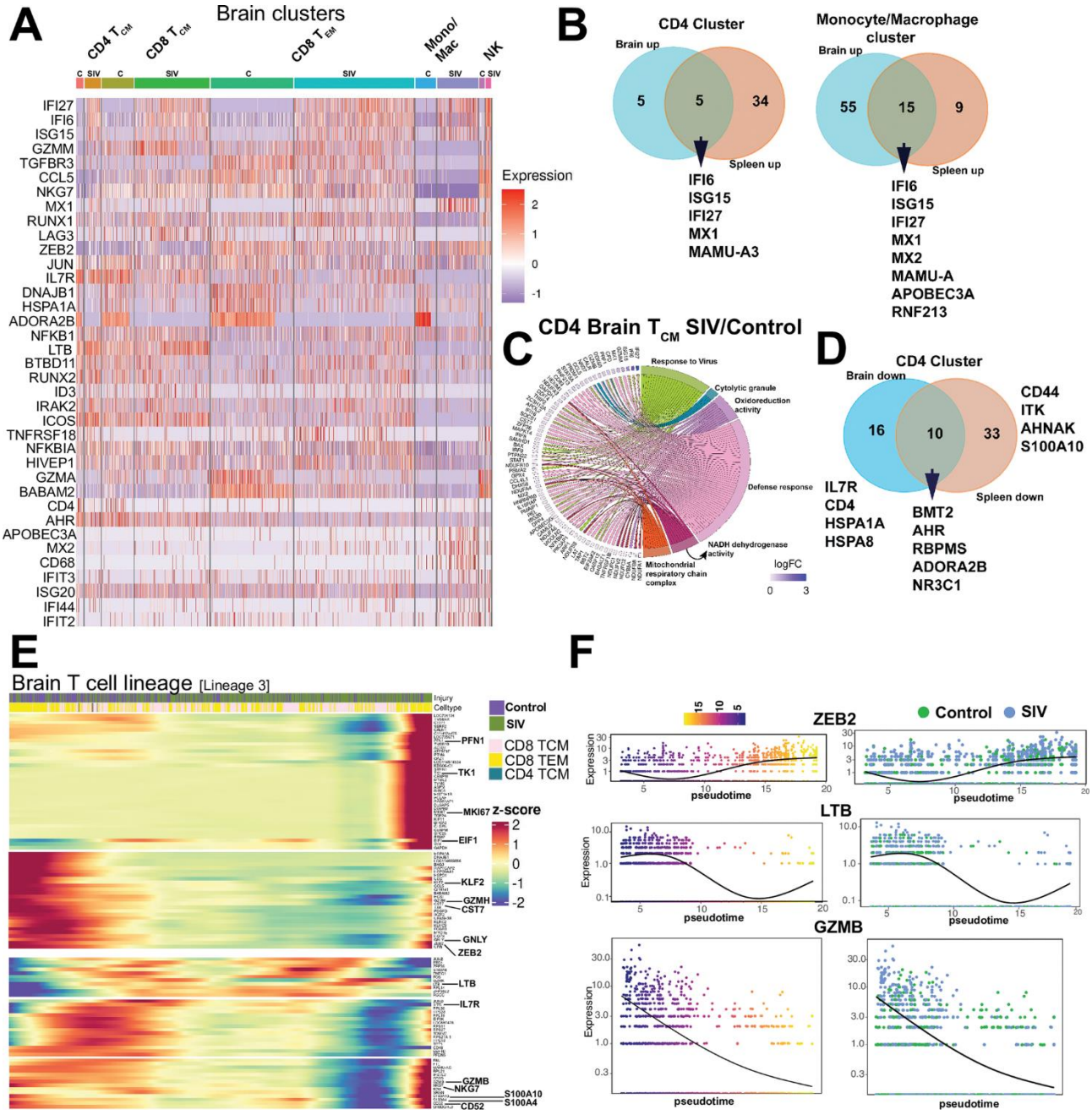

Figure 5. T Cell Effector Molecular Programs Induced within the SIV-Infected Brain. Differential gene expression (DGE) analysis of the immune clusters across conditions was performed using functions from Seurat; selection threshold of (adjusted p-value < 0.05, |log2 FC| > 0.25) based on Benjamini-Hochberg correction. **(A)** Heat map of DGE genes in controls **(C)** versus SIV for each immune cluster. **(B)** Venn diagram shows shared interferon stimulated genes

upregulated post SIV across brain and spleen CD4 T cell and monocyte/macrophage immune clusters. **(C)** Chord plot show pathways and corresponding genes enriched in SIV versus control CD4 TCM cell cluster in brain. **(D)** Venn diagram shows shared genes downregulated post SIV in brain and spleen CD4 T cell clusters. We used the monocle3 based workflow to estimate lineage differentiation between the cell populations based on the experimental conditions. We extracted the subsets of identified cell types from our integrated Seurat object and further inferred the trajectory graphs. Using the defined root node (TCM), we chose lineages based on the shortest path connecting the root node and the leaf node. After establishing different lineages, we implemented a differential gene test to find genes that changed as a function of pseudotime based on a combination of Moran's statistic and q-value and visualized using heatmaps and individual gene trajectory plots. **(E)** Heatmap (Lineage 3) shows changes in gene expression in lineage comprising of T cells. Along this trajectory was induction of genes associated with cell cycle progression (TK1, MKI67, EIF1, S100A10, S100A4), immune cell activation and differentiation (ZEB2, KLF2, CD52) [41], cytotoxic function (PFN1, GZMB, GZMH, NKG7, and CST7). Canonical TCM genes, such as IL7R and LTB, were downregulated in this lineage. **(F)** shows expression levels genes of select genes from heat map (ZEB2, LTB, GZMB) along pseudo-time as a function of infection.

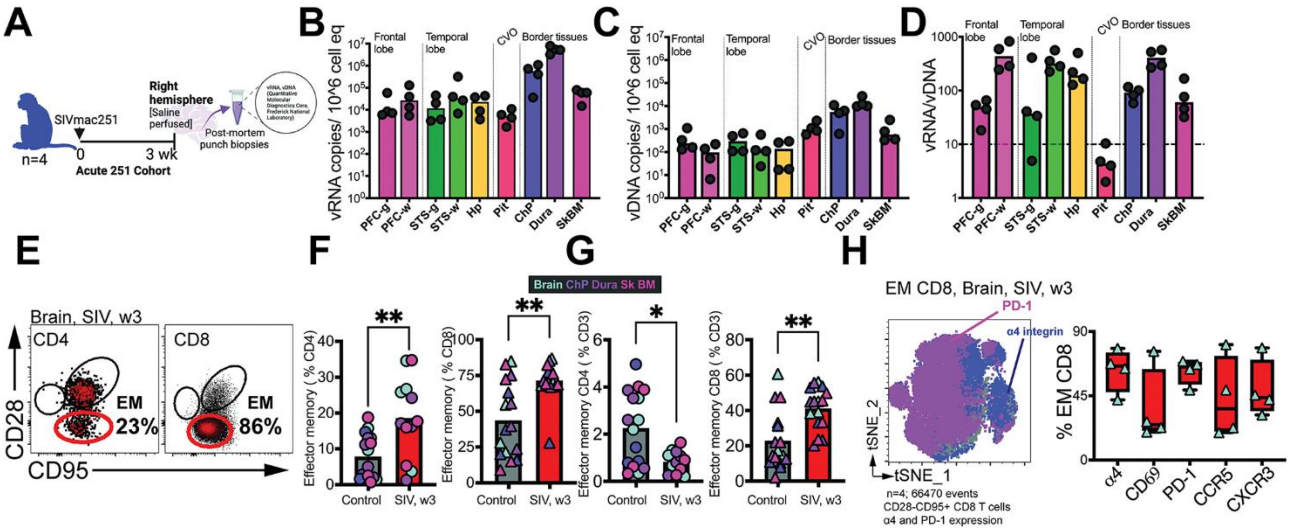

Figure 6. vRNA in brain regions controlling cognitive function and within CNS border tissues. **(A)** Acute 251 cohort (n = 4) assessed. **(B)** SIV vRNA **(C)** SIV vDNA (copies/10^6 cells) in brain regions specified (RT-qPCR on post-mortem punch biopsies from specified regions. **(D)** shows vRNA/vDNA ratio. **(E)** Flow plot of CD4 and CD8 T cells in brain parenchyma during SIV shows identification CD28- CD95+ effector memory (EM) cells **(F)** increase in % EM CD4 and CD8 T cells during acute SIV in CNS tissues specified. **(G)** shows decrease in EM CD4 (% CD3) and increase in EM CD8 (% CD3) T cells during acute SIV in CNS tissues specified. **(H)** t-SNE plots gated on EM CD8 T cells in Brain (n = 4 samples, 66470 events) overlayed with PD1 and α4 integrin expression. Box and whisker plots show expression of specific markers in EM CD8 T cells in brain. Significant differences by two-tailed Mann Whitney test, **p< 0.01, * p< 0.05 in F-G.

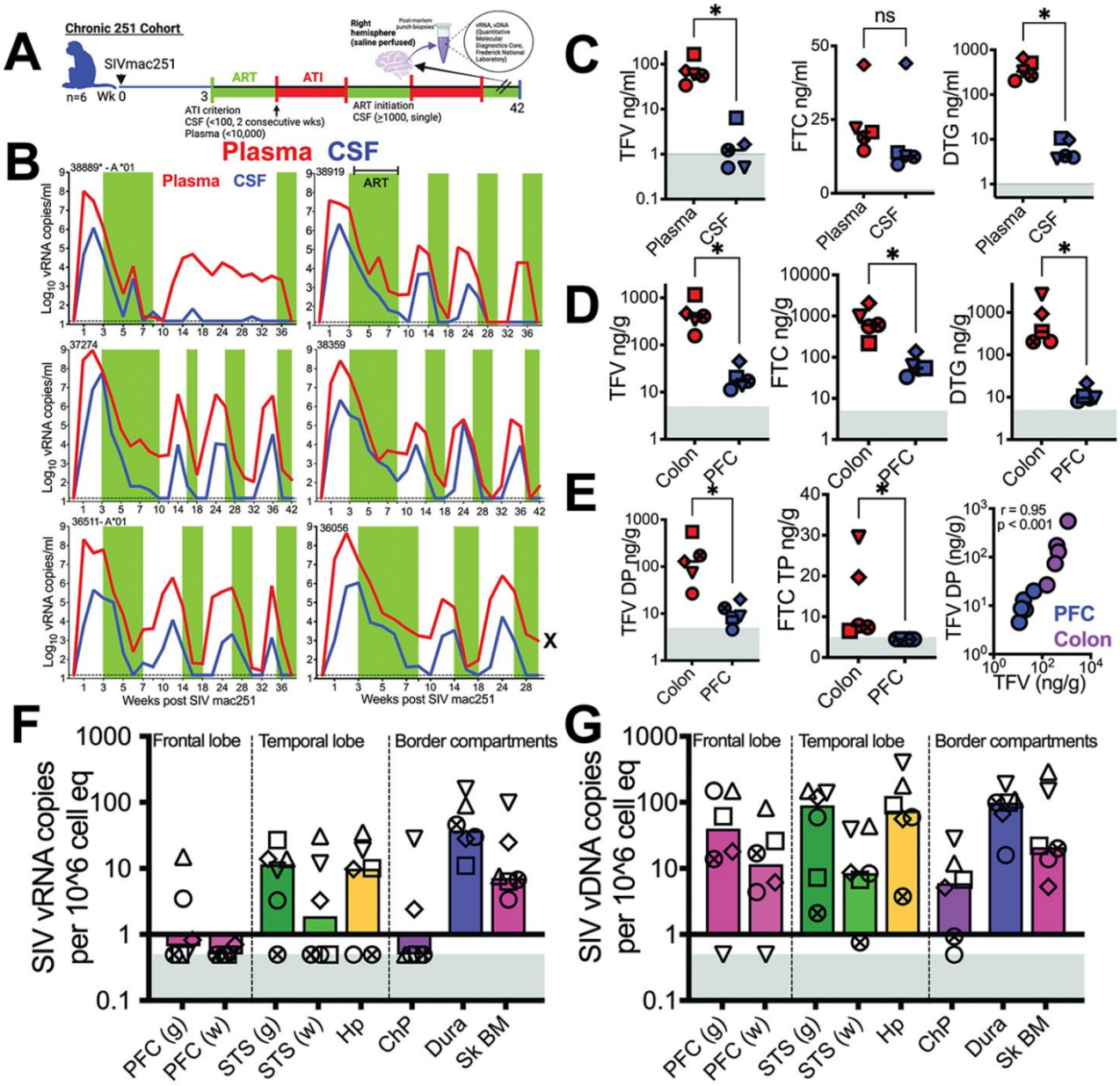

Figure 7. Decrease in vRNA in brain during Antiretroviral Therapy. (A) Chronic 251 cohort (n = 6) assessed. **(B)** Kinetics of plasma (red lines) and CSF (blue lines) viral suppression and rebound (vRNA copies/mL fluid, measured by RT-qPCR) over the course of ART initiation and interruption. Green bars indicate periods of ART with FTC, TDF, and DTG. Horizontal dashed line indicates limit of detection (15 vRNA copies/ml). **(C)** Concentration of ARVs (ng/mL) in plasma and CSF quantified by LC-MS. **(D)** Concentration of ARVs (ng/mg) in PFC and colonic tissue. **(E)** shows active phosphorylated forms of TFV and FTC. Spearman correlation, two-tailed p value

shown. Sampling was performed 2–4 weeks post ART initiation with last ARV dose administered 9–12 hours prior to necropsy, FTC = emtricitabine, TDF = tenofovir disoproxil fumarate, DTG = dolutegravir, Gray shaded area represents lower limit of quantification of assay. **(F)** SIV vRNA **(G)** SIV vDNA (copies/10^6 cells) in brain region (RT-qPCR on post-mortem punch biopsies from specified regions. Gray shaded area represents viral loads below threshold of detection. Significant differences by two tailed Wilcoxon matched-pairs signed rank test, * p< 0.05 in C-E.

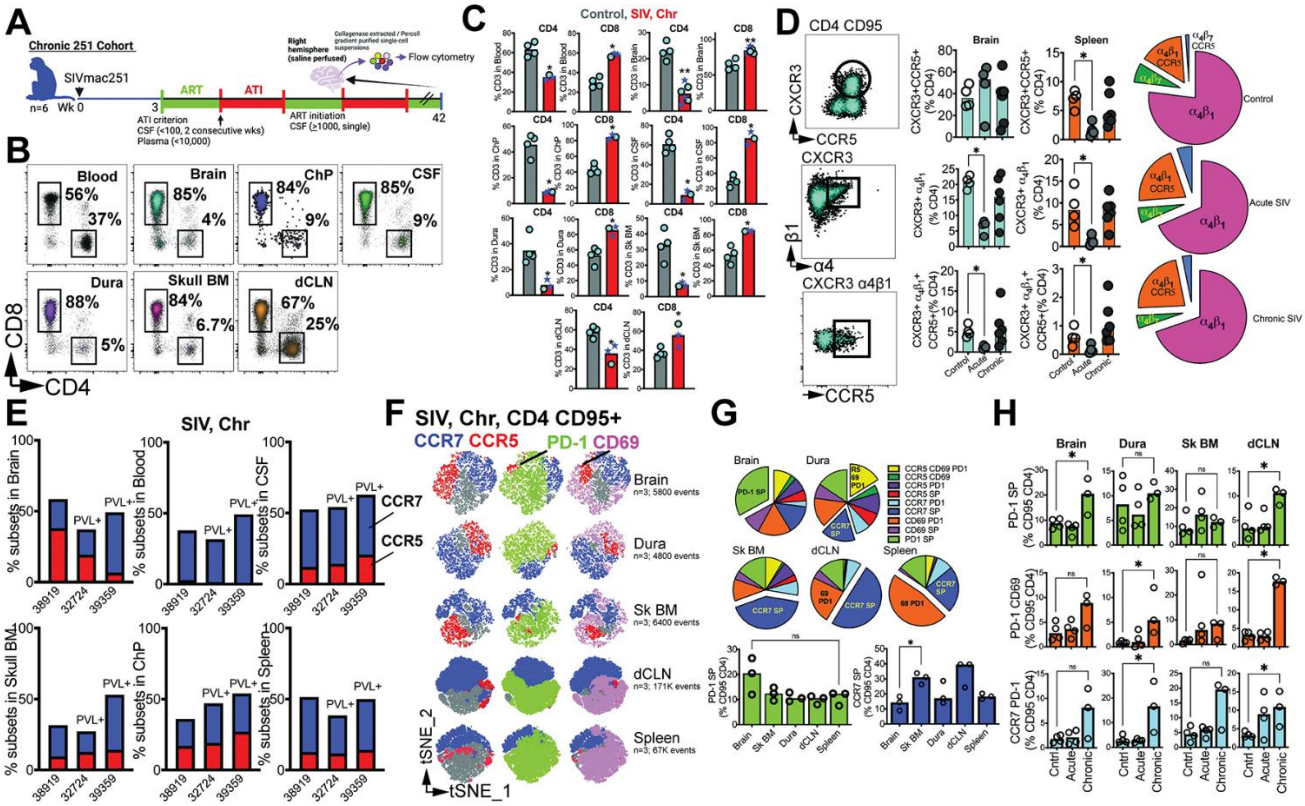

Figure 8. Persistent CD4 depletion in CNS during chronic infection. (A) Chronic 251 cohort assessed; flow cytometry analysis performed on 4/6 animals. **(B)** Flow cytometry plots illustrate frequencies of CD4 and CD8 T cells in blood, CNS tissues, and dCLN. **(C)** Bar graphs show T cell frequencies across blood, CNS tissues, and dCLN in control and Chronic SIV infected macaques (n = 4, plasma viral RNA+ shown in star symbols). **(D)** flow plots (top to bottom) show CD4 CD95 cells co-expressing CXCR3 and CCR5; Th1 cells expressing α4β1, and α4β1 Th1 cells expressing CCR5. Bar graphs show frequencies in brain and spleen and pie charts illustrate

relative proportion of subsets in brain (n = 4). **(E)** Contingency plots show distribution of CCR5 / CCR7 CD4 T cells in chronic SIV infection (n = 3 based on criterion of CD4 events > 100 in all CNS tissues). **(F)** t-SNE plots gated on CD4+CD95+ cells expressing CCR7/CCR5/PD-1/CD69 (n = 3). **(G)** pie chart demonstrates proportion of CD4 T cells expressing combination of markers (CCR7/CCR5/PD-1/CD69). **(H)** shows distribution of specific subsets. Significant differences by one tailed Mann Whitney test, *, $p < 0.05$.

Data and materials availability

RNA-seq dataset is accessible at **GSE221815**.

Materials and Methods.

Ethics statement.

All animals were bred and housed at the California National Primate Research Center (CNPRC) in accordance with the American Association for Accreditation of Laboratory Animal Care (AAALAC) guidelines. All studies were approved by the University of California, Davis Institutional Animal Care and Use Committee (IACUC).

Rhesus macaques.

For Acute 251 studies, four (1 male and 3 females, 11–17 years) colony-bred Indian origin rhesus macaques (*Macaca mulatta*) were utilized. For the Chronic 251 study, six adult (1 male and 5 females) Indian origin rhesus macaques (*Macaca mulatta*) were utilized. At study initiation, animals were 11.2–17.4 years of age with a median weight of 10.5 kg. Four rhesus macaques served as controls (12–16 years, 1 male and 3 females). All animals were SIV negative (SIV-), simian T-cell leukemia virus negative (STLV-), and simian retrovirus negative (SRV-); and had no history of dietary, pharmacological, or surgical manipulation (***S1 Table***).

SIVmac251 infection.

Rhesus macaques were infected intravenously with (104 TCID50) SIVmac251 (2017 stock from CNPRC at 2.5 x 10^4 TCID50/mL, grown in rhesus peripheral blood mononuclear cells). Prior to inoculation, the virus was reconstituted in plain RPMI (virus stock: RPMI ratio 4:1) in total injection volume of 500 μl.

Antiretroviral therapy.

We formulated a triple-ART regimen described by Del Prete et al. [66] containing the nucleo(s/t)ide reverse transcriptase inhibitors emtricitabine (FTC) and tenofovir disoproxil

fumarate (TDF) [from Gilead] with the integrase strand transfer inhibitor dolutegravir (DTG) [from GSK].

Viral RNA Quantification.

Quantification of plasma, CSF, and tissue viral RNA and viral DNA were performed essentially as previously described (67) with assays performed in the Quantitative Molecular Diagnostics Core of the AIDS and Cancer Virus Program at Leidos Biomedical Research Inc., Frederick National Laboratory.

ARV measurement.

ARV concentrations in plasma, CSF, and tissue samples were quantified by LC/MS in the Clinical Pharmacology and Analytical Chemistry Core, UNC Center for AIDS Research as previously described (68).

Specimen collection and processing.

Cerebrospinal fluid, blood, and lymph node fine needle aspirates were sampled and processed as described previously (69, 70). For isolation of single cell suspensions from CNS compartments; tissues were mechanically dissociated and digested in DMEM with 0.25% trypsin and 5 units per mL of DNase I for 45 minutes at 37^{o}C. Digested tissues were homogenized using a pipette controller and 10mL serological pipette. The homogenized tissue was subsequently filtered through a metallic strainer followed by a 180μm nylon strainer and 100μm SMART strainer. Cells were washed in media and spun down at 1200 rpm for 10 minutes. Mononuclear cells were collected using a 21% and 75% Percoll gradient. Post gradient enrichment, cells were washed, counted, and up to 2x10^6 million cells were stained with panel of fluorophore conjugated antibodies or cryopreserved for future analysis.

Flow Cytometry.

Whole blood, CSF, and fine needle lymph node aspirates (FNA) were freshly stained and acquired on the same day following collection. Mononuclear cells obtained from necropsy tissues were either freshly stained and acquired the same day or stained following cryopreservation. For cryopreserved cells, samples were thawed in ice baths and diluted in complete media. Cells were then washed and incubated in complete media with 2 units/mL of DNAse I for 15 minutes at 37^{o}C. Cells were washed with complete media and counted prior to staining. Whole blood samples were treated with BD FACS Lysing Solution (BD Bioscience) for 10 minutes and washed with 1X FACS buffer (phosphate buffered saline with 1.5mM sodium azide, 2% fetal bovine serum, 10mM EDTA) prior to surface staining. Antibodies for surface staining were prepared in Brilliant Stain Buffer Plus (BD Biosciences) and incubated with cells at 4^{o}C for 30 minutes and washed twice with FACS buffer. Sample acquisition and fluorescence measurements were performed on a BD Bioscience FACSymphony utilizing FACSDiva software (Version: 8. 0.1). Sample compensation, population gating, and analysis was performed using FlowJo (Version 10.8.1)

Legendplex assay.

This assay (BioLegend, USA) was conducted following the manufacturer's instructions to assess cytokine levels in plasma and CSF. Briefly, IP-10 (CXCL10, A6, cat# 740335), IL-8 (B7, cat#740344) and MCP-1(B9, cat#740345) multiplex beads were sonicated for two minutes in a sonicator bath (Thermo Fisher, USA). These multiplex beads were then appropriately diluted in assay buffer and added to a V-bottomed plate. Plasma samples were diluted 2-fold in dilution buffer, while CSF samples were used without further dilution. Both sample types were added to the V-bottomed plate containing multiplex beads and left to incubate overnight at 4°C on a microplate shaker at 150rpm. The next day, the plate was washed twice with washing buffer and 25µl of detection antibody was added to each well followed by washing and incubation for 1 hour on a microplate shaker at room temperature (RT). Then, 25µl of SA-PE was added into each well

directly and incubated for 30 min at RT. The plate was washed twice and resuspended in 200µL of wash buffer. The samples were acquired on a BD LSR Fortessa (BD Biosciences, USA) cell analyzer, with 900 events collected from each sample for analysis. The concentration (pg/mL) of IP-10 (CXCL10), IL-8, and MCP-1 was determined by extrapolating the values from the standard curve.

Cerebrospinal Fluid and Serum Biochemistries.

Animal CSF and serum chemistries were quantified using a Piccolo Xpress Chemistry Analyzer (Abbott) with Piccolo BioChemistry Plus disks in accordance with manufacturer's instructions. Chemistry panel analytes included albumin, glucose, and total protein.

Intracellular cytokine staining assay.

The polyfunctionality of CD4 T cells was assessed using intracellular cytokine staining (ICS). Brain and spleen cells were stimulated with 1X Cell Stimulation Cocktail (PMA and ionomycin) (eBioscience, USA) along with R10 media in the presence of 0.2µg CD28/49d co-stimulatory antibodies (BD) per test. Unstimulated controls were treated with volume-controlled DMSO (Sigma-Aldrich). Cells were incubated in 5% CO_2 at 37°C and after 1 hour of stimulation, protein transport inhibitors 2µl/mL GolgiPlug (Brefeldin A) and 1.3µl/mL GolgiStop (Monensin) (BD, Biosciences, USA) was added to tubes and further incubated for 3 hours at 37°C, 5% CO_2. Following stimulation, cells were stained for ICS surface markers CD3, CD4, CD8, and CD95. Subsequently, the cells were fixed using cytofix/cytoperm for 10 min at 4°C, then permeabilized with 1X Perm wash buffer (BD, Biosciences, USA), and stained with intracellular markers TNF-α,

IFN-γ, and IL-2 for 45 min. Finally, cells were washed and acquired on the same day using a BD FACSymphony flow cytometer.

Cell Preparation for Sequencing Studies.

Cryopreserved mononuclear cells from rhesus brain were thawed at room temperature, placed in fresh complete media (For splenic cells: RPMI supplemented with 10% HI-FBS, 1% L-glutamine, 1% penicillin-streptomycin; For brain tissue derived cells: DMEM supplemented with 10% HI-FBS, 1% L-glutamine, 1% penicillin-streptomycin) and treated with 2 units/mL of DNase I (Roche Diagnostics) for 15 minutes at 37^{o}C. Cells were washed in complete media and CD45+ cells isolated using CD45 magnetic bead separation for non-human primates (Miltenyi Biotec CD45 Microbeads non-human primate) in accordance with the manufacturer's protocol. Enriched CD45+ cells were stained for CD45 and a live dead marker for subsequent flow cytometric sorting. Live CD45+ cells were characterized and quantified on a BD FACSymphony cell analyzer and sorted utilizing a FACS Aria and suspended in RPMI for single cell RNA sequencing studies.

Single Cell RNA sequencing.

Sample barcoding, assembly of gel-beads in emulsion (GEM), GEM reverse transcription, cDNA amplification and cleanup, and library construction were performed according to the Chromium Next GEM single cell 3' v3.1 protocol from 10X Genomics. Sequencing was performed by SeqMatic LLC on a NovaSeq 6000 platform using S4 200 flow cells with paired end reads ran in four replicates with an average of 111,000 reads per cell. Sample demultiplexing, generation of FASTQ files, sequence alignment, gene counting, and sample aggregation were performed using the Cellranger pipeline version 7.1.0. Samples that passed data quality control steps (removal of samples with low quality reads, low frequency of mapped reads, low number of reads per cell, high mtRNA signature), were used for subsequent analyses. Sequenced reads were

aligned to the Mmul_10 genome reference for Rhesus macaque, and raw count matrices were generated which were used as the input to the Seurat integrated analysis pipeline (Seurat V4.3.0). Quality control was done at the gene and cell level accounting for the median number of genes, and mitochondrial gene percentage using quality control plots.

Bioinformatics.

To process the sequencing data, we performed sequence alignment to the reference genome of *M.mulatta* (Mmul_10) using the 10X Genomics protocol (CellRanger V.6.0). The generated cell-by-gene count matrix was used for downstream analysis using the Seurat based integrative analysis workflow. The filtered count matrix (percentage of mitochondrial reads <10, and gene expressed in more than 10 cells) was log-normalized, and the top variable genes were used to perform the graph-based cell clustering with a resolution of 0.5 and visualized using Uniform Manifold Approximation and Projection (UMAP). Cluster identity was assigned by a combination of approaches which includes identifying cluster-specific differentially expressed genes, expert knowledge, canonical list of marker genes, and automated annotations using immune reference atlas through SingleR. Differential gene expression (DEG) analysis of the different cell-types across conditions was performed using the functions from Seurat and were selected at a threshold of (adjusted P-value < 0.05, |log2 FC| > 0.25) based on Benjamini-Hochberg correction. Gene-set enrichment analysis, and functional annotation was implemented through clusterProfiler 4.0, and visualized using custom scripts. All downstream data analysis was performed using R v4.2.0. We used the monocle3 based workflow to estimate lineage differentiation between the cell population based on the experimental conditions. We extracted the subsets of the identified celltypes from our integrated Seurat object and further inferred the trajectory graphs. Using the defined root node (T_{CM}), we selected lineages based on the shortest path that connects the root node and the leaf node. After establishing the different lineages, we implemented a differential gene test to find genes that change as a function of pseudotime based

on a combination of Moran's statistic and q-value and visualized using heatmaps and individual gene trajectory plots. To count the viral transcripts in the data, we built a custom reference using the CellRanger mkref pipeline. We downloaded the FASTA and created the GTF files of Simian immunodeficiency virus isolate SIVmac251.RD.tf5 (SIVmac251) and added it to the reference genome files of *M.mulatta* (Mmul_10). The customized reference was successfully created, and the generated count matrix which includes the viral transcript was used in all steps of further downstream analysis. All downstream data analysis was performed using R v4.2.0. Venn diagrams were created utilizing http://bioinformatics.psb.ugent.be/webtools/Venn/

In situ hybridization (ISH) and CD3 immuno-fluorescence.

In situ hybridization (ISH) and CD3 immuno-fluorescence were carried out following a modified version of the manufacturer's protocol (Document Number 322452-USM, 322360-USM, and UM323100, ACD) for RNAscope® ISH built on our previously established work (71). The procedure involved several steps using the RNAscope 2.5 HD brown Detection Kit and RNAscope® Multiplex Fluorescent Reagent Kit (ACD). Initially, four-micron deparaffinized paraffin sections underwent pretreatment with 1X Target Retrieval Buffer at 100°C for 15 minutes, followed by RNAscope Protease Plus at 40°C for 30 minutes before hybridization with probes at 40°C for 2 hours. Subsequent signal amplification steps were conducted after hybridization. Detection of the signal was achieved using a DAB solution for 10 minutes or TSA Vivid fluorophore 5 (Cat# 323271, ACD) for 10 minutes at room temperature. For slides subjected to RNAsope alone, hematoxylin counterstaining was performed, followed by dehydration, cover slipping, and visualization under bright-field microscopy using a Zeiss Imager Z1 (Carl Zeiss). In cases where RNAscope was combined with CD3 immuno-fluorescence, slides underwent an additional IHC staining process following RNAscope ISH. This involved an overnight incubation at 4°C with Rat polyclonal anti-CD3 (Abcam) at a 1:100 dilution. Detection of CD3 cells was facilitated by using Alexa Fluor 568 goat anti-rat IgG (Invitrogen). After DAPI staining, slides were cover-slipped with

ProLong Gold anti-fade mounting agent (Invitrogen). In each ISH run, probe RNAscope Probe - SIVmac239 (Cat# 405661) was accompanied by probes for dihydrodipicolinate reductase (dapB) or RNAscope 3-plex negative control probe. Tissues from SIV-uninfected animals were also hybridized with the SIV probes to serve as negative controls. To ensure the quality and consistency of the ISH assay, RNAscope® Probe - Mau-Ppib and RNAscope 3-plex positive control probe were employed as positive controls for RNA quality. Visualizations were carried out using appropriate filters, and images were captured with a Zeiss LSM800 confocal microscope and Zeiss Imager Z2 (Carl Zeiss).

Statistical Analyses.

Wilcoxon signed rank test were used for paired analyses (i.e., longitudinal and within group comparisons). Mann-Whitney U-test were used for unpaired comparison between animal cohorts/treatment groups. Test were performed in GraphPad Prism (Version 9.5.1) with significance values denoted as follows: * $p < 0.05$, ** $p < 0.01$, *** $p < 0.001$, **** $p < 0.0001$.

Supporting Information

S1 Table. Non-human primate cohort (Acute and Chronic 251 studies)

Group	Animal ID	Sex	Age (years. months) at Nx.	Weight (kg) at Nx.	Site	Virus ($1x10^4$ $TCID_{50}$)	IgG antibody* control (25mg/kg)	ART Regimen
Acute 251 Cohort (n=4)	41812	F	11.02	7.30	CNPRC	SIVmac251	Anti-desipramine	-
	40742	M	12.04	12.00	CNPRC	SIVmac251	Anti-desipramine	-
	37164	F	16.01	10.83	CNPRC	SIVmac251	Anti-desipramine	-
	35488	F	17.04	10.48	CNPRC	SIVmac251	Anti-desipramine	-
Chronic 251 Cohort (n=6)	38889[&]	F	14.06	11.31	CNPRC	SIVmac251	-	FTC/TDF/DTG
	38919	F	14.06	8.63	CNPRC	SIVmac251	-	FTC/TDF/DTG
	36056	F	18.06	9.96	CNPRC	SIVmac251	-	FTC/TDF/DTG
	37274	F	16.06	8.67	CNPRC	SIVmac251	-	FTC/TDF/DTG
	39359	M	14.04	13.36	CNPRC	SIVmac251	-	FTC/TDF/DTG
	36511[&]	F	17.06	10.34	CNPRC	SIVmac251	-	FTC/TDF/DTG
Control Cohort 1 (n=4)	38163	F	15.07	7.48	CNPRC	-	-	-
	40691	M	12.07	12.18	CNPRC	-	-	-
	38691	F	14.10	13.56	CNPRC	-	-	-
	40499	F	12.11	9.79	CNPRC	-	-	-
Control Cohort 2 (n=12)	47161	M	3.05	6.21	CNPRC	-	-	-
	45781	M	5.05	6.1	CNPRC	-	-	-
	46235	M	4.06	10.58	CNPRC	-	-	-
	46551	M	4.04	7.34	CNPRC	-	-	-
	46548	M	4.04	6.28	CNPRC	-	-	-
	47081	M	3.06	4.3	CNPRC	-	-	-
	45721	F	5.06	9.76	CNPRC	-	-	-
	47154	M	3.05	4.87	CNPRC	-	-	-

	46410	M	4.05	7.76	CNPRC	-	-	-
	46354	M	4.06	8.39	CNPRC	-	-	-
	47466	M	3.04	5.15	CNPRC	-	-	-
	47387	F	3.04	5.05	CNPRC	-	-	-

SIV: Simian Immunodeficiency Virus; ART: Anti-Retroviral Therapy; FTC: Emtricitabine; TDF: Tenofovir disoproxil fumarate; DTG: Dolutegravir; CNPRC: California National Primate Research Center

*****Antibody treatments were administered at 1 week prior to SIV infection and every subsequent 10-day interval at doses of 25mg/kg intravenously (neat) over the course of the study.

&, Mamu A*01^{+}

S2 Table. Plasma and CSF vRNA in Chronic 251 cohort.

	38889*	38919	36056	37274	38359	36511*
Wk1						
Wk 2						
Wk 3	Initiate	Initiate	Initiate	Initiate	Initiate	Initiate
Wk 4						
Wk 5						
Wk 6						
Wk 7						
Wk 8						Interrupt
Wk 9	Interrupt	Interrupt	Interrupt		Interrupt	Interrupt
Wk 10				Interrupt		
Wk 14		Initiate	Initiate		Initiate	Initiate
Wk 16				Initiate		
Wk 18		Interrupt	Interrupt		Interrupt	Interrupt
				Interrupt		
Wk 26		Initiate	Initiate	Initiate	Initiate	
						Initiate
			Emergency Nx			
Wk 30		Interrupt		Interrupt	Interrupt	Interrupt
Wk 35						Initiate
Wk 37	Initiate	Initiate		Initiate	Initiate	Initiate

Plasma viral load

Time pi	38889*	38919	36056	37274	38359	36511*
Wk1	100,000,000	38,000,000	19,000,000	270,000,000	17,000,000	210,000,000
Wk 2	31,000,000	26,000,000	460,000,000	920,000,000	260,000,000	40,000,000
Wk 3	1,200,000	14,000,000	16,000,000	91,000,000	37,000,000	61,000,000
Wk 4	14,000	110,000	960,000	3,000,000	1,700,000	350,000
Wk 5	400	5,000	28,000	63,000	38,000	22,000
Wk 6	12,000	41,000	13,000	8,100	1,400	250
Wk 7	25	650	4,400	18,000	4,800	3,700
Wk 8	N/A	N/A	N/A	N/A	N/A	N/A
Wk 9	25	400	1,800	4,300	3,800	4,200
Wk 10	15	430	1,400	2,400	3,200	300,000
Wk 14	30,000	58,000	55,000	4,500,000	42,000	65,000
Wk 16	49,000	180	40	66,000	290	65
Wk 18	13,000	Below 23	90	250	60	60
Wk 26	9,000	3,000	410,000	1,000,000	11,000	590,000
Wk 30	4,500	15		180	Below 15	36
Wk 36	2,100	20,000		3,700,000	90,000	1,000
Wk 40	15	15		470	15	15
Wk 42				140	65	

CSF viral load

Time pi	38889*	38919	36056	37274	38359	36511*
Wk1	48,000	82,000	970	14,000	63,000	6,400
Wk 2	1,200,000	2,200,000	680,000	7,700,000	2,200,000	450,000
Wk 3	44,000	140,000	1,100,000	60,000,000	360,000	170,000
Wk 4	830	11,000	9,100	42,000	200,000	100,000
Wk 5	25	1200	5,700	2600	5200	220
Wk 6	2,500	360	2,200	65	1,300	<15
Wk 7	Below 15	65	40	65	650	65
Wk 8	N/A	N/A	N/A	N/A	N/A	N/A
Wk 9	Below 45	45	Below 45	Below 41	120	41
Wk 10	Below 15	15	below 15	15	430	360
Wk 14	Below 15	5,500	3,500	10,000		400
Wk 16	65	Below 15	Below 29	65	Below 15	Below 15
Wk 18	Below 15	Below 15	Below 15	Below 15	Below 15	15
Wk 26	Below 15	320	970	9,700	2,600	2,100
Wk 30	25	Below 15		Below 15	Below 15	Below 15
Wk 36	Below 15			35,000	8,600	15
Wk 40	15	15		Below 15	15	15
Wk 42				15	15	

* denote Mamu A*01 animals

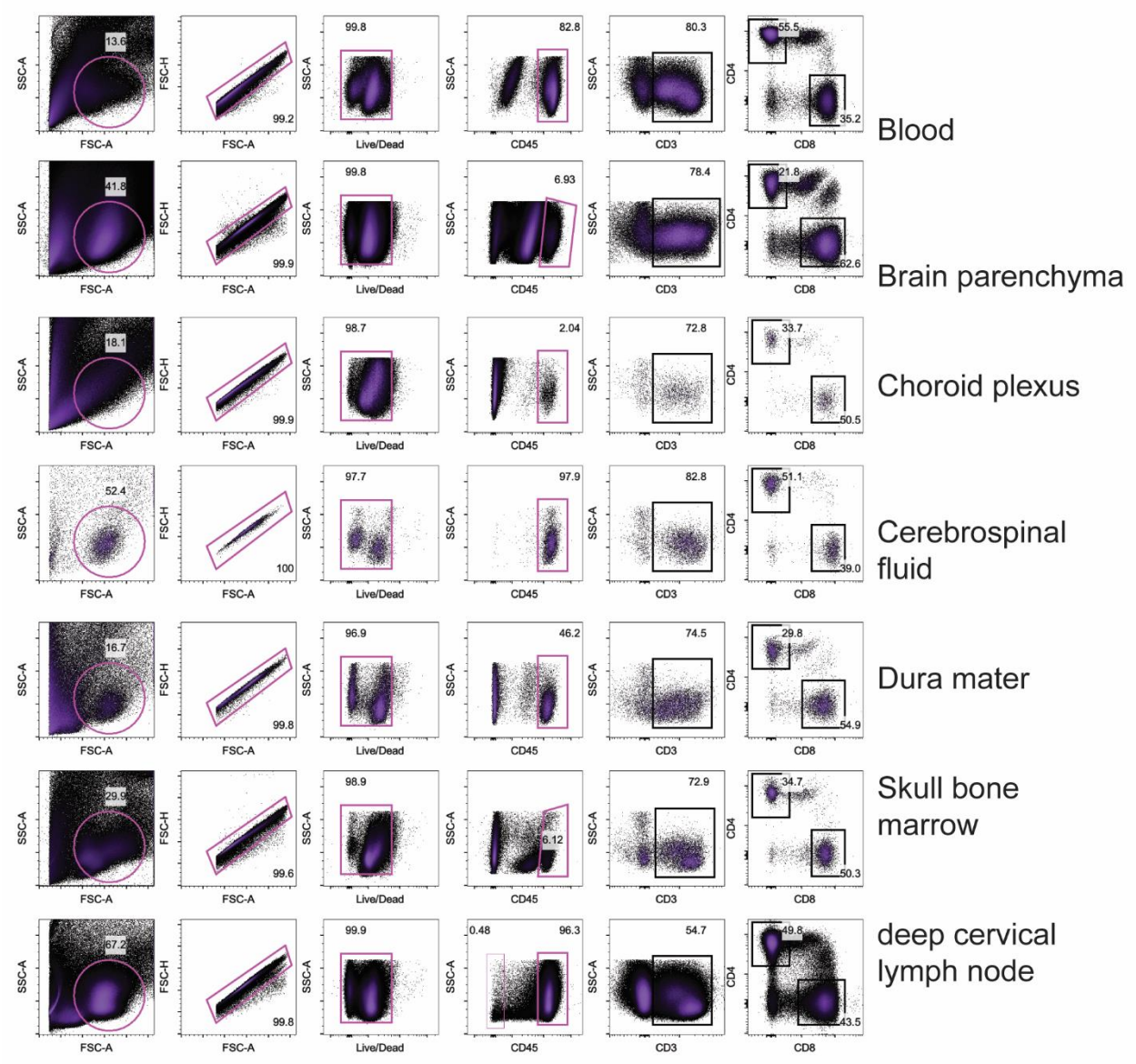

S1 Figure. Gating strategy for CNS tissues in SIV unexposed controls.

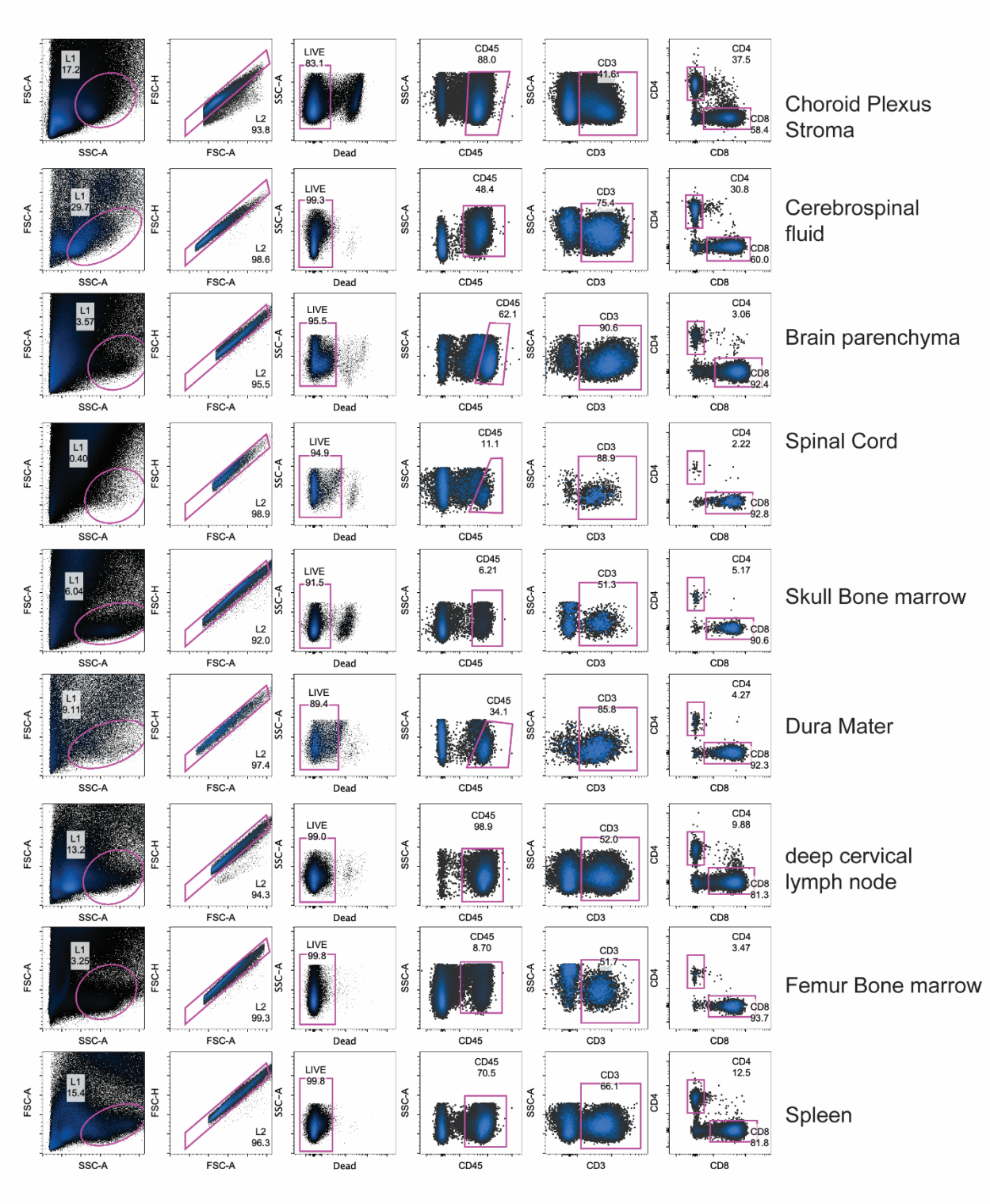

S2 Figure. Gating strategy for CNS tissues in Acute SIV infection.

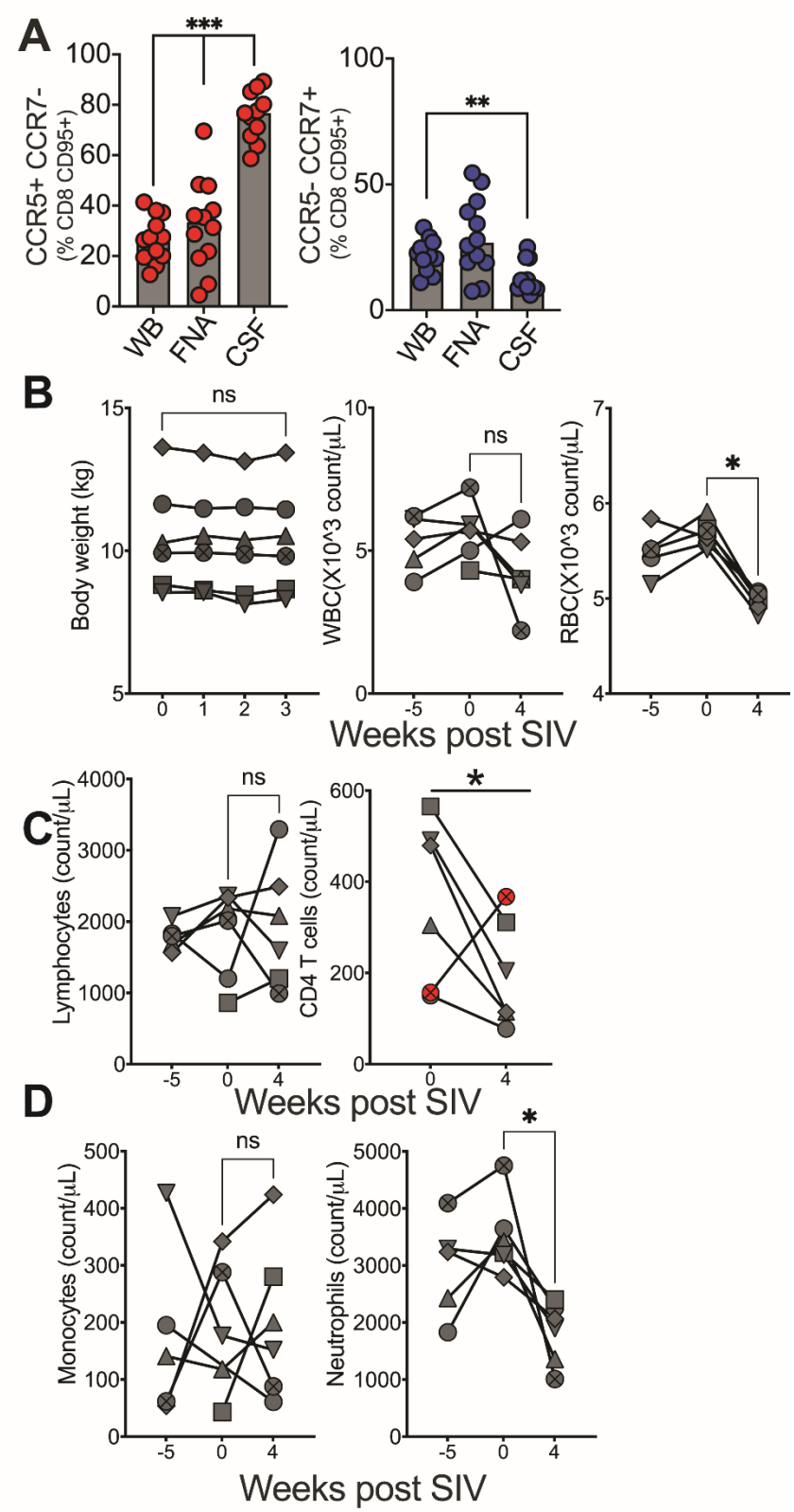
A
CCR5+ CCR7- (% CD8 CD95+)
CCR5- CCR7+ (% CD8 CD95+)
***
**
WB
FNA
CSF
B
Body weight (kg)
WBC(X10^3 count/µL)
RBC(X10^3 count/µL)
ns
*
Weeks post SIV
C
Lymphocytes (count/µL)
CD4 T cells (count/µL)
D
Monocytes (count/µL)
Neutrophils (count/µL)

S3 Figure. CCR5/CCR7 dichotomy during homeostasis/Blood counts during acute SIVmac251 infection. (A) Bar graphs illustrate discrete distribution patterns of CCR5 and CCR7 on CD8+ CD95+ cells in blood, lymph node FNA, and CSF in Control cohort 2 (n = 12). **(B)** Kinetics of body weight, white blood counts (WBC), red blood counts (RBC). **(C)** Kinetics of lymphocyte, CD4 T cells, monocyte, and neutrophil counts during first 4 weeks of SIVmac251 infection in Chronic 251 cohort (n = 6). Significant differences by Wilcoxon matched-pairs signed rank test, *, p< 0.05 **, 0< 0.01, ***, p< 0.01. For CD4 T cell counts, p value corresponds to 5/6 animals in gray.

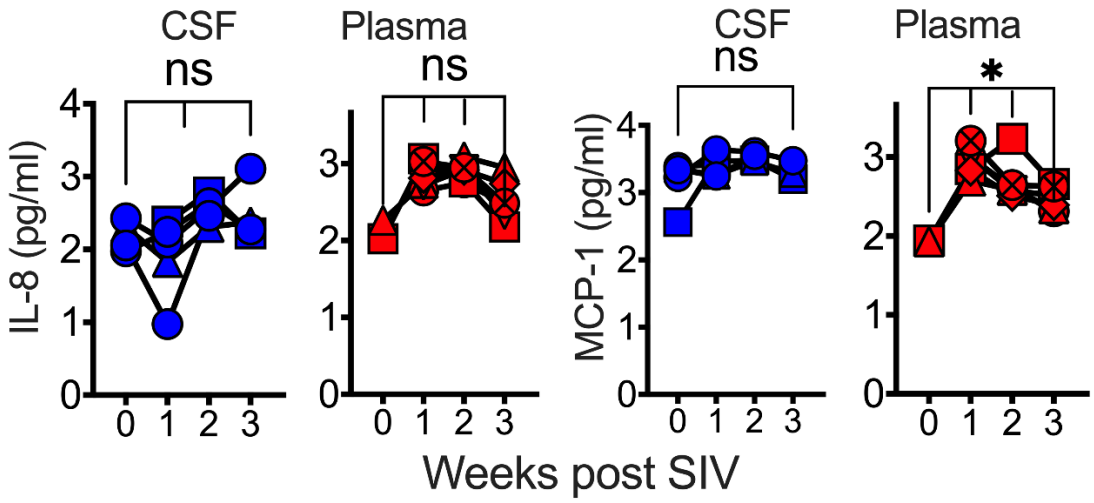

S4 Figure. Plasma and CSF cytokines during acute SIVmac251 infection. Kinetics of IL-8 and MCP-1 measured by Legend plex assay during first 3 weeks of SIVmac251 infection in Chronic 251 cohort (n = 6). Significant differences by Mann Whitney test *, p< 0.05.

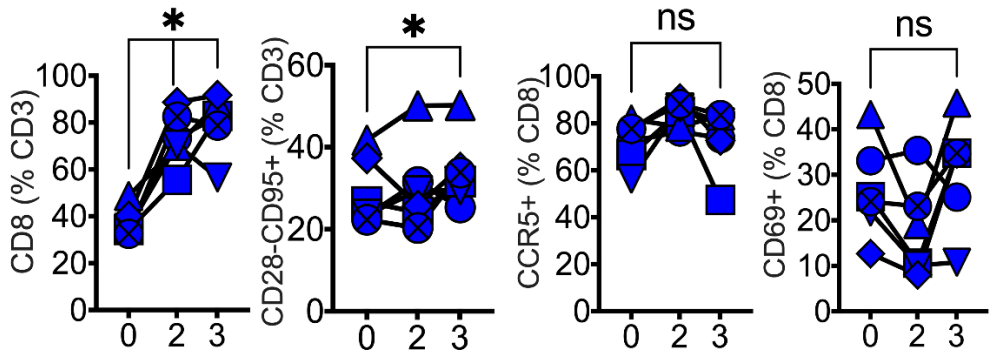

S5 Figure. CSF CCR5+ CD8 T cell frequencies do not decrease during acute SIV infection.

Shows % CD8 T cells, % CD28- CD95+ CD8 T cells, %CCR5+ CD8 T cells, and % CD69+ CD8 T cells in CSF in Chronic 251 cohort (n = 6). Significant differences by one-tailed Wilcoxon matched-pairs signed rank test, *, p< 0.05.

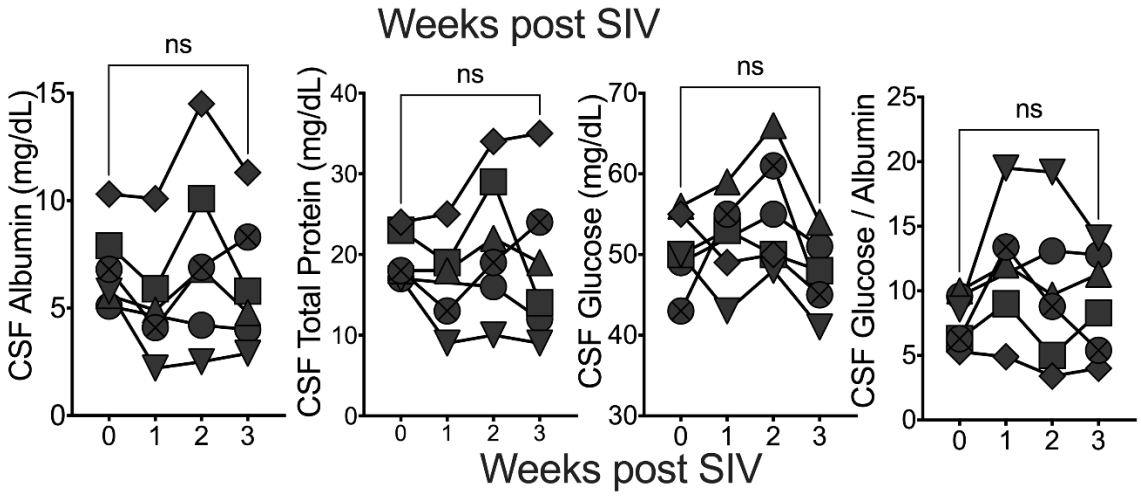

S6 Figure. CSF parameters during acute SIVmac251 infection. CSF albumin, protein, glucose, and glucose/albumin ratio during first 3 weeks of SIVmac251 infection in Chronic 251 cohort (n = 6).

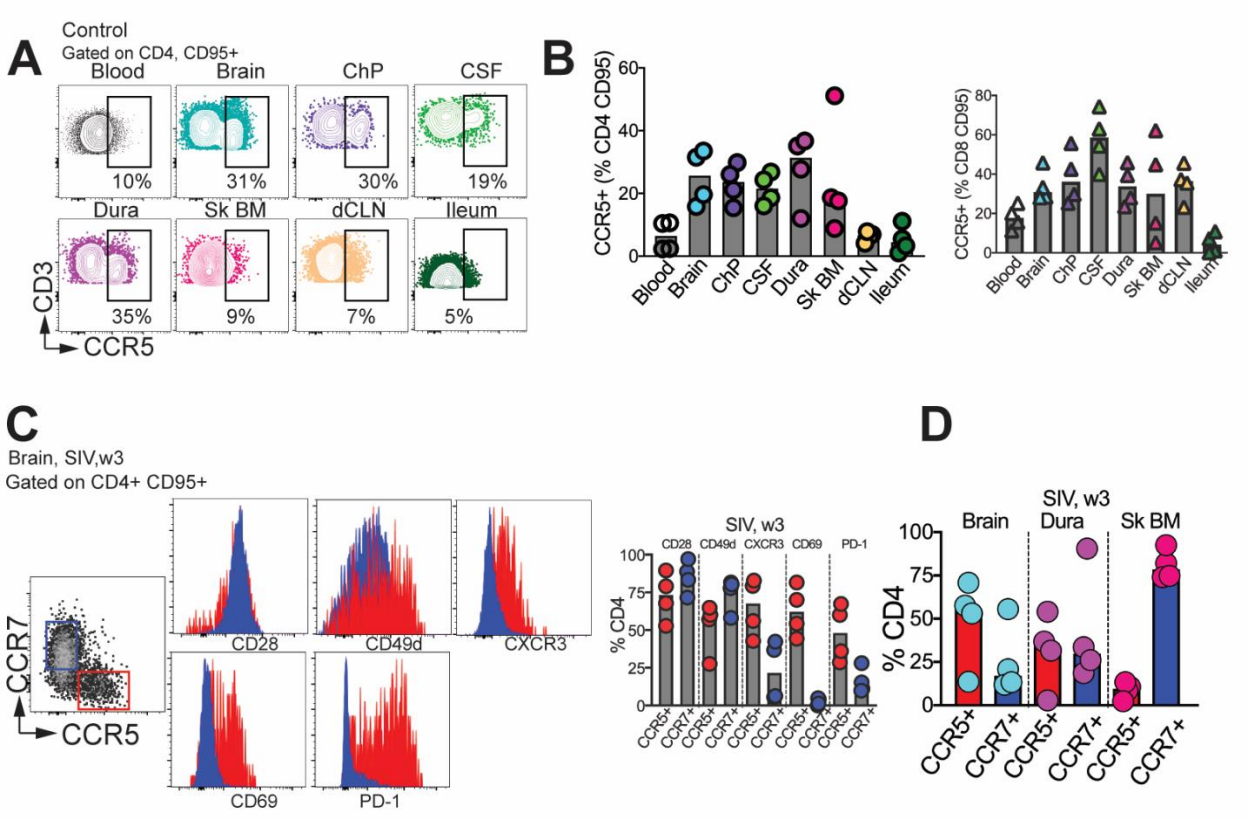

S7 Figure. CCR5+ CD4 T cells populate parenchymal and border CNS tissues.

(A) Flow plots and **(B)** bar graphs show CCR5 expression on CD4+CD95+ T cells in controls, second bar graph shows CCR5 CD8 frequencies. Control 1 cohort (n = 4) assessed. **(C)** shows phenotype of CCR5+ CCR7- versus CCR7+CCR5- cells. **(D)** bar graph of CCR5 /CCR7+ CD4 T cell subset frequencies in brain, dura, and skull bone marrow at 3 weeks post SIV. Acute 251 (n = 4) cohort assessed.

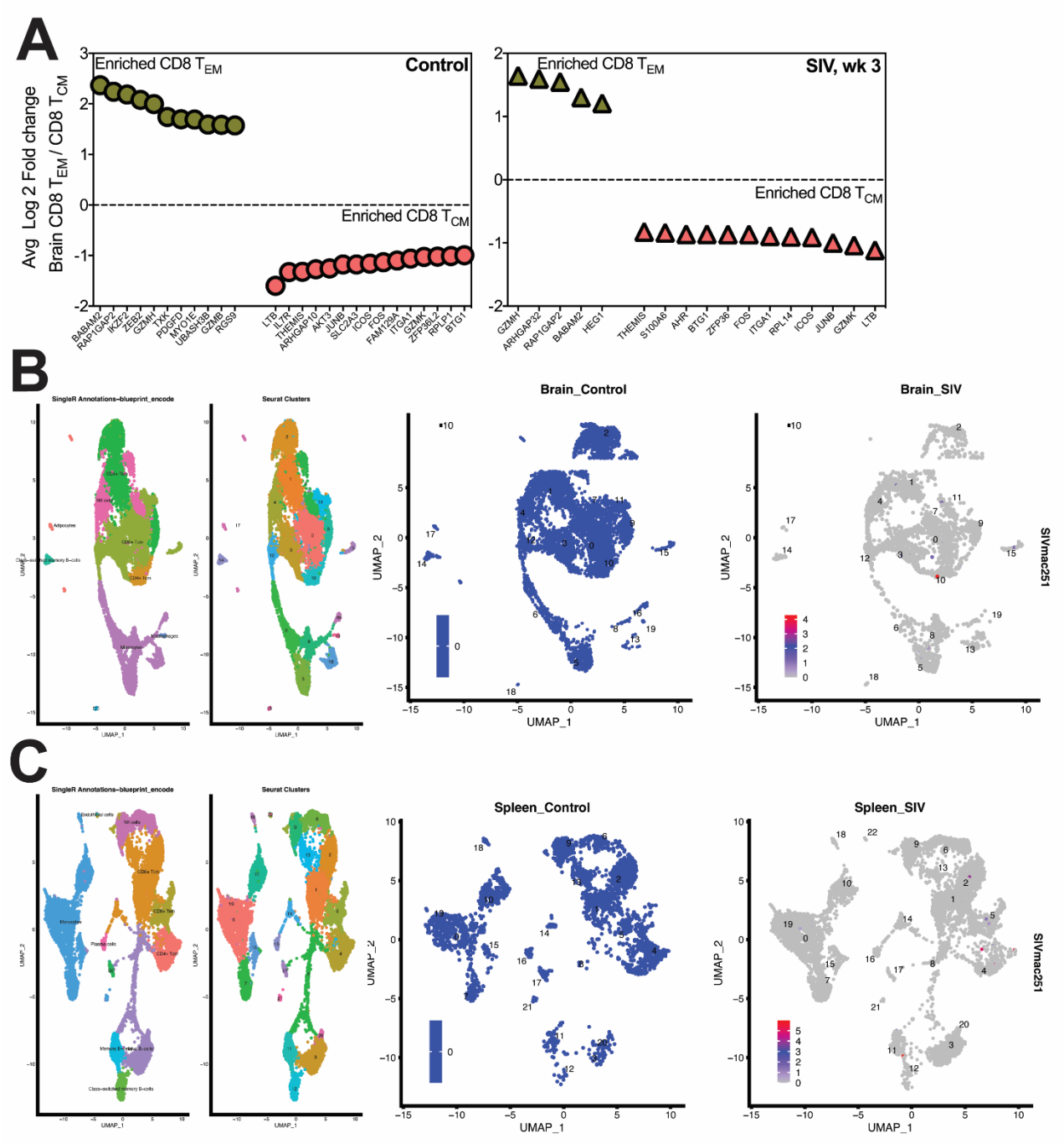

S8 Fig. SIVRNA localizes with immune clusters in brain and spleen. (A) Genes enriched in TEM and TCM clusters in control and SIV brain (p.adj < 0.05). **(B)** UMAP of immune clusters in brain and vRNA expression in clusters in control and SIV. **(C)** UMAP of immune clusters in spleen and vRNA expression in clusters in control and SIV. Acute 251 (n = 4) cohort assessed.

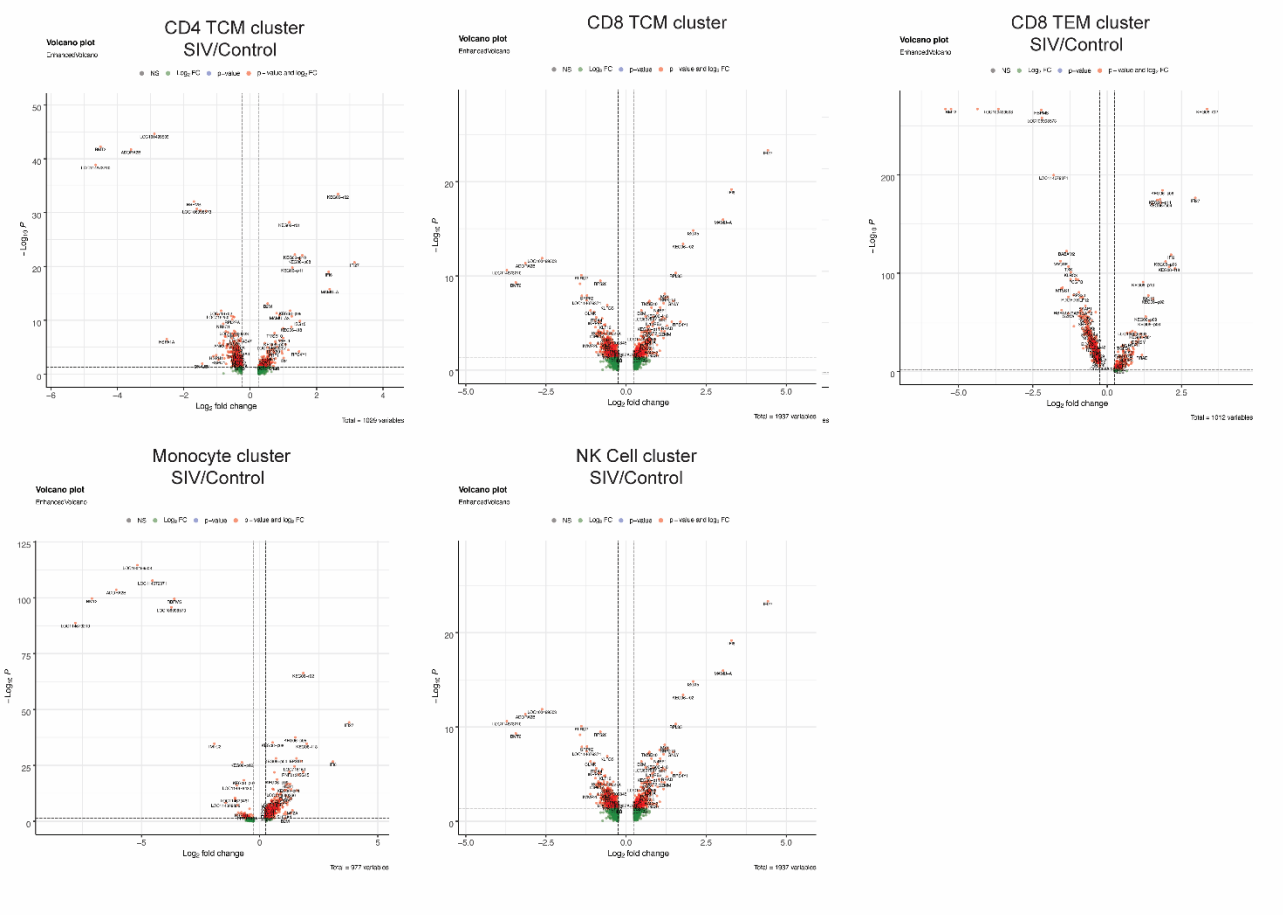

S9. Fig Volcano plots of DEG in SIV brain. Volcano plots of immune clusters show genes up and downregulated in SIV relative to controls. Genes meeting padj and fold-change cut-off are denoted in red. Acute 251 (n = 4) cohort assessed.

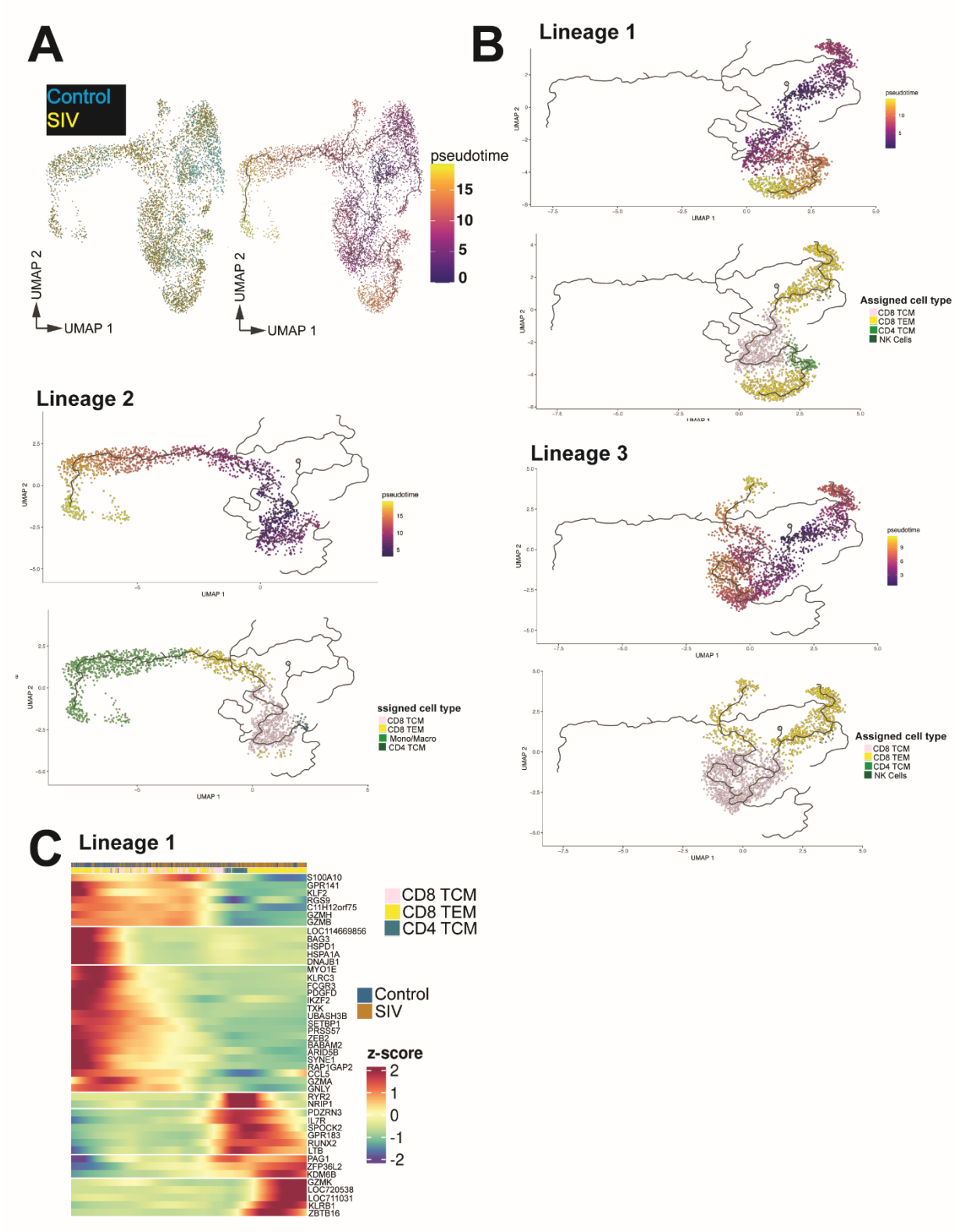
A
Control
SIV
UMAP 2
UMAP 1
pseudotime
15
10
5
0
B
Lineage 1
pseudotime
Assigned cell type
CD8 TCM
CD8 TEM
CD4 TCM
NK Cells
Lineage 2
pseudotime
ssigned cell type
CD8 TCM
CD8 TEM
Mono/Macro
CD4 TCM
Lineage 3
pseudotime
Assigned cell type
CD8 TCM
CD8 TEM
CD4 TCM
NK Cells
C
Lineage 1
S100A10
GPR141
KLF2
RGS9
C11H12orf75
GZMH
GZMB
LOC114669856
BAG3
HSPD1
HSPA1A
DNAJB1
MYO1E
KLRC3
FCGR3
PDGFD
IKZF2
TXK
UBASH3B
SETBP1
PRSS57
ZEB2
BABAM2
ARHDSB
SYNE1
RAP1GAP2
CCL5
GZMA
GNLY
RYR2
NRIP1
PDZRN3
IL7R
SPOCK2
GPR183
RUNX2
LTB
PAG1
ZFP36L2
KDM6B
GZMK
LOC720538
LOC711031
KLRB1
ZBTB16
CD8 TCM
CD8 TEM
CD4 TCM
Control
SIV
z-score
2
1
0
-1
-2

S10. Fig. Pseudotime plots of Control and SIV brain. (A) UMAP. **(B)** pseudotime trajectory comprising of distinct immune clusters shows Lineages 1–3. Lineage 4 comprised only of CD8 TEM. **(C)** shows heat map comprising of T cell clusters from Lineage 1. Acute 251 (n = 4) cohort assessed.

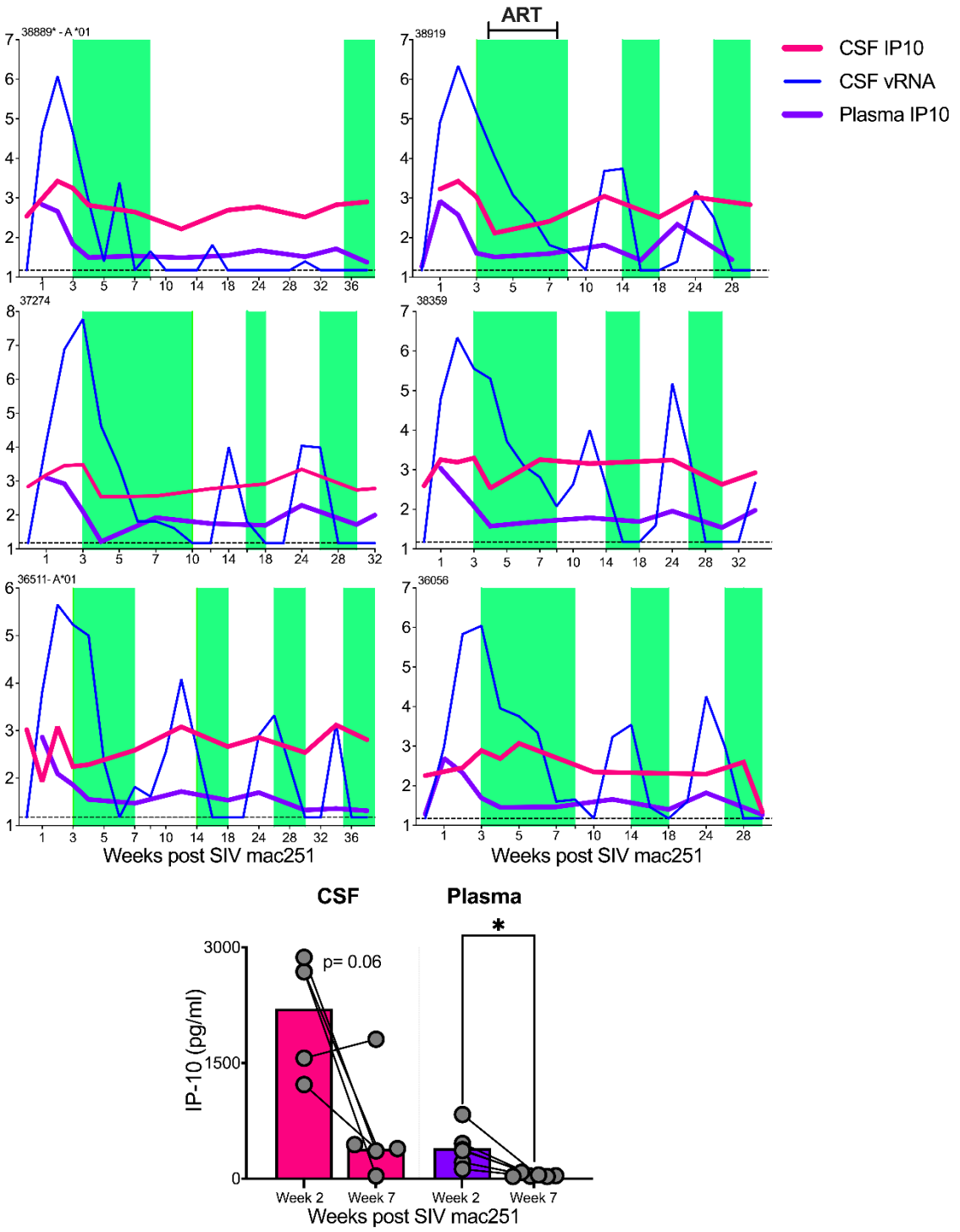

S11. Fig. Kinetics of plasma and CSF vRNA, plasma IP-10 and CSF IP-10. Green bar indicates duration of ART with FTC, TDF, and DTG. FTC = emtricitabine, TDF = tenofovir disoproxil fumarate (TDF), DTG = dolutegravir. Chronic 251(n = 6) cohort assessed.

Acknowledgements

The authors acknowledge several individuals whose contributions have been instrumental in the successful execution of the studies. The authors express their gratitude to Wilhelm Von Morgenland and Miles Christensen, as well as the CNPRC SAIDS team, for their coordination of macaque studies, animal care, and animal support. We also extend our appreciation to the CNPRC Veterinary Staff for their dedicated efforts in animal care and assistance. The authors are grateful to Yashavanth Shaan Lakshmanappa for his excellent technical assistance in preparation of ART, sample processing, and acquisition of flow cytometry data. The authors thank Chase Hawes, Jennifer Watanabe, and members of Koen Von Rompay's laboratory for valuable technical support during necropsies. We are thankful to Andradi Villabos for assistance provided during necropsies and for acquisition of flow cytometry data. The authors acknowledge funding support from NIAID, NIH K01OD023034 (SSI); NIA, RF1AG06001 (SSI, JHM); NIAID, NIH R56AI150409 (SSI) and support with federal funds from the National Cancer Institute, National Institutes of Health under contract number HHSN261201500003I and NCI contract 75N91019D00024 (JDL).

References

1. Survival of HIV-positive patients starting antiretroviral therapy between 1996 and 2013: a collaborative analysis of cohort studies. Lancet HIV. 2017;4(8):e349-e56. Epub 2017/05/16. doi: 10.1016/s2352-3018(17)30066-8. PubMed PMID: 28501495; PubMed Central PMCID: PMCPMC5555438.

2. Teeraananchai S, Kerr SJ, Amin J, Ruxrungtham K, Law MG. Life expectancy of HIV-positive people after starting combination antiretroviral therapy: a meta-analysis. HIV Med. 2017;18(4):256-66. Epub 2016/09/01. doi: 10.1111/hiv.12421. PubMed PMID: 27578404.

3. Trickey A, Sabin CA, Burkholder G, Crane H, d'Arminio Monforte A, Egger M, et al. Life expectancy after 2015 of adults with HIV on long-term antiretroviral therapy in Europe and North America: a collaborative analysis of cohort studies. Lancet HIV. 2023;10(5):e295-e307. Epub 2023/03/24. doi: 10.1016/s2352-3018(23)00028-0. PubMed PMID: 36958365; PubMed Central PMCID: PMCPMC10288029.

4. van Sighem AI, Gras LA, Reiss P, Brinkman K, de Wolf F, study Anoc. Life expectancy of recently diagnosed asymptomatic HIV-infected patients approaches that of uninfected individuals. AIDS. 2010;24(10):1527-35. Epub 2010/05/15. doi: 10.1097/QAD.0b013e32833a3946. PubMed PMID: 20467289.

5. Larsen A, Cheyip M, Tesfay A, Vranken P, Fomundam H, Wutoh A, et al. Timing and Predictors of Initiation on Antiretroviral Therapy Among Newly-Diagnosed HIV-Infected Persons in South Africa. AIDS Behav. 2019;23(2):375-85. Epub 2018/07/17. doi: 10.1007/s10461-018-2222-2. PubMed PMID: 30008050; PubMed Central PMCID: PMCPMC6331268.

6. Nicolau V, Cortes R, Lopes M, Virgolino A, Santos O, Martins A, et al. HIV Infection: Time from Diagnosis to Initiation of Antiretroviral Therapy in Portugal, a Multicentric Study. Healthcare (Basel). 2021;9(7). Epub 2021/07/03. doi: 10.3390/healthcare9070797. PubMed PMID: 34202051; PubMed Central PMCID: PMCPMC8306717.

7. Deeks SG. HIV infection, inflammation, immunosenescence, and aging. Annu Rev Med. 2011;62:141-55. Epub 2010/11/26. doi: 10.1146/annurev-med-042909-093756. PubMed PMID: 21090961; PubMed Central PMCID: PMCPMC3759035.

8. Deeks SG, Lewin SR, Havlir DV. The end of AIDS: HIV infection as a chronic disease. Lancet. 2013;382(9903):1525-33. Epub 2013/10/25. doi: 10.1016/S0140-6736(13)61809-7. PubMed PMID: 24152939; PubMed Central PMCID: PMCPMC4058441.

9. Ellis RJ, Badiee J, Vaida F, Letendre S, Heaton RK, Clifford D, et al. CD4 nadir is a predictor of HIV neurocognitive impairment in the era of combination antiretroviral therapy. AIDS. 2011;25(14):1747-51. doi: 10.1097/QAD.0b013e32834a40cd. PubMed PMID: 21750419; PubMed Central PMCID: PMCPMC3867631.

10. Heaton RK, Clifford DB, Franklin DR, Jr., Woods SP, Ake C, Vaida F, et al. HIV-associated neurocognitive disorders persist in the era of potent antiretroviral therapy: CHARTER Study. Neurology. 2010;75(23):2087-96. doi: 10.1212/WNL.0b013e318200d727. PubMed PMID: 21135382; PubMed Central PMCID: PMCPMC2995535.

11. Peluso MJ, Meyerhoff DJ, Price RW, Peterson J, Lee E, Young AC, et al. Cerebrospinal fluid and neuroimaging biomarker abnormalities suggest early neurological injury in a subset of individuals during primary HIV infection. J Infect Dis. 2013;207(11):1703-12. doi: 10.1093/infdis/jit088. PubMed PMID: 23460748; PubMed Central PMCID: PMCPMC3636785.

12. Wright EJ, Grund B, Cysique LA, Robertson KR, Brew BJ, Collins G, et al. Factors associated with neurocognitive test performance at baseline: a substudy of the INSIGHT Strategic Timing of AntiRetroviral Treatment (START) trial. HIV Med. 2015;16 Suppl 1:97-108. doi: 10.1111/hiv.12238. PubMed PMID: 25711328.

13. Antinori A, Arendt G, Becker JT, Brew BJ, Byrd DA, Cherner M, et al. Updated research nosology for HIV-associated neurocognitive disorders. Neurology. 2007;69(18):1789-99. Epub 2007/10/05. doi: 10.1212/01.WNL.0000287431.88658.8b. PubMed PMID: 17914061; PubMed Central PMCID: PMCPMC4472366.

14. Wang Y, Liu M, Lu Q, Farrell M, Lappin JM, Shi J, et al. Global prevalence and burden of HIV-associated neurocognitive disorder: A meta-analysis. Neurology. 2020;95(19):e2610-e21. Epub 2020/09/06. doi: 10.1212/WNL.0000000000010752. PubMed PMID: 32887786.

15. McArthur JC, Steiner J, Sacktor N, Nath A. Human immunodeficiency virus-associated neurocognitive disorders: Mind the gap. Ann Neurol. 2010;67(6):699-714. Epub 2010/06/03. doi: 10.1002/ana.22053. PubMed PMID: 20517932.

16. Nightingale S, Ances B, Cinque P, Dravid A, Dreyer AJ, Gisslen M, et al. Cognitive impairment in people living with HIV: consensus recommendations for a new approach. Nat Rev Neurol. 2023;19(7):424-33. Epub 2023/06/14. doi: 10.1038/s41582-023-00813-2. PubMed PMID: 37311873.

17. Wiley CA, Schrier RD, Nelson JA, Lampert PW, Oldstone MB. Cellular localization of human immunodeficiency virus infection within the brains of acquired immune deficiency syndrome patients. Proc Natl Acad Sci U S A. 1986;83(18):7089-93. Epub 1986/09/01. doi: 10.1073/pnas.83.18.7089. PubMed PMID: 3018755; PubMed Central PMCID: PMCPMC386658.

18. Wiley CA, Nelson JA. Role of human immunodeficiency virus and cytomegalovirus in AIDS encephalitis. Am J Pathol. 1988;133(1):73-81. Epub 1988/10/01. PubMed PMID: 2845792; PubMed Central PMCID: PMCPMC1880646.

19. Staprans S, Marlowe N, Glidden D, Novakovic-Agopian T, Grant RM, Heyes M, et al. Time course of cerebrospinal fluid responses to antiretroviral therapy: evidence for variable compartmentalization of infection. AIDS. 1999;13(9):1051-61. Epub 1999/07/09. doi: 10.1097/00002030-199906180-00008. PubMed PMID: 10397535.

20. Schnell G, Spudich S, Harrington P, Price RW, Swanstrom R. Compartmentalized human immunodeficiency virus type 1 originates from long-lived cells in some subjects with HIV-1-associated dementia. PLoS Pathog. 2009;5(4):e1000395. Epub 2009/04/25. doi: 10.1371/journal.ppat.1000395. PubMed PMID: 19390619; PubMed Central PMCID: PMCPMC2668697.

21. Sharer LR, Baskin GB, Cho ES, Murphey-Corb M, Blumberg BM, Epstein LG. Comparison of simian immunodeficiency virus and human immunodeficiency virus encephalitides in the immature host. Ann Neurol. 1988;23 Suppl:S108-12. Epub 1988/01/01. doi: 10.1002/ana.410230727. PubMed PMID: 2831797.

22. Clements JE, Mankowski JL, Gama L, Zink MC. The accelerated simian immunodeficiency virus macaque model of human immunodeficiency virus-associated neurological disease: from mechanism to treatment. J Neurovirol. 2008;14(4):309-17. Epub 2008/09/10. doi: 10.1080/13550280802132832. PubMed PMID: 18780232; PubMed Central PMCID: PMCPMC8797541.

23. Byrnes SJ, Angelovich TA, Busman-Sahay K, Cochrane CR, Roche M, Estes JD, et al. Non-Human Primate Models of HIV Brain Infection and Cognitive Disorders. Viruses. 2022;14(9). Epub 2022/09/24. doi: 10.3390/v14091997. PubMed PMID: 36146803; PubMed Central PMCID: PMCPMC9500831.

24. Williams K, Westmoreland S, Greco J, Ratai E, Lentz M, Kim WK, et al. Magnetic resonance spectroscopy reveals that activated monocytes contribute to neuronal injury in SIV neuroAIDS. J Clin Invest. 2005;115(9):2534-45. Epub 2005/08/20. doi: 10.1172/jci22953. PubMed PMID: 16110325; PubMed Central PMCID: PMCPMC1187930.

25. Matsuda K, Riddick NE, Lee CA, Puryear SB, Wu F, Lafont BAP, et al. A SIV molecular clone that targets the CNS and induces neuroAIDS in rhesus macaques. PLoS Pathog. 2017;13(8):e1006538. Epub 2017/08/09. doi: 10.1371/journal.ppat.1006538. PubMed PMID: 28787449; PubMed Central PMCID: PMCPMC5560746.

26. Letendre SL, Mills AM, Tashima KT, Thomas DA, Min SS, Chen S, et al. ING116070: a study of the pharmacokinetics and antiviral activity of dolutegravir in cerebrospinal fluid in HIV-1-infected, antiretroviral therapy-naive subjects. Clin Infect Dis. 2014;59(7):1032-7. Epub 2014/06/20. doi: 10.1093/cid/ciu477. PubMed PMID: 24944232; PubMed Central PMCID: PMCPMC4166983.

27. Calcagno A, Bonora S, Simiele M, Rostagno R, Tettoni MC, Bonasso M, et al. Tenofovir and emtricitabine cerebrospinal fluid-to-plasma ratios correlate to the extent of blood-brainbarrier damage. AIDS. 2011;25(11):1437-9. Epub 2011/06/30. doi: 10.1097/QAD.0b013e3283489cb1. PubMed PMID: 21712657.

28. Decloedt EH, Rosenkranz B, Maartens G, Joska J. Central nervous system penetration of antiretroviral drugs: pharmacokinetic, pharmacodynamic and pharmacogenomic considerations. Clin Pharmacokinet. 2015;54(6):581-98. Epub 2015/03/18. doi: 10.1007/s40262-015-0257-3. PubMed PMID: 25777740.

29. Letendre S, Marquie-Beck J, Capparelli E, Best B, Clifford D, Collier AC, et al. Validation of the CNS Penetration-Effectiveness rank for quantifying antiretroviral penetration into the central nervous system. Arch Neurol. 2008;65(1):65-70. Epub 2008/01/16. doi: 10.1001/archneurol.2007.31. PubMed PMID: 18195140; PubMed Central PMCID: PMCPMC2763187.

30. Hedlund G, Sandberg-Wollheim M, Sjogren HO. Increased proportion of CD4+CDw29+CD45R-UCHL-1+ lymphocytes in the cerebrospinal fluid of both multiple sclerosis patients and healthy individuals. Cell Immunol. 1989;118(2):406-12. Epub 1989/02/01. doi: 10.1016/0008-8749(89)90388-2. PubMed PMID: 2562931.

31. Margolick JB, McArthur JC, Scott ER, McArthur JH, Cohn S, Farzadegan H, et al. Flow cytometric quantitation of T cell phenotypes in cerebrospinal fluid and peripheral blood of homosexual men with and without antibodies to human immunodeficiency virus, type I. J Neuroimmunol. 1988;20(1):73-81. Epub 1988/11/01. doi: 10.1016/0165-5728(88)90116-6. PubMed PMID: 3263391.

32. Sharma V, Creegan M, Tokarev A, Hsu D, Slike BM, Sacdalan C, et al. Cerebrospinal fluid CD4+ T cell infection in humans and macaques during acute HIV-1 and SHIV infection. PLoS Pathog. 2021;17(12):e1010105. Epub 2021/12/08. doi: 10.1371/journal.ppat.1010105. PubMed PMID: 34874976; PubMed Central PMCID: PMCPMC8683024.

33. Goertz JE, Garcia-Bonilla L, Iadecola C, Anrather J. Immune compartments at the brain's borders in health and neurovascular diseases. Semin Immunopathol. 2023;45(3):437-49. Epub 2023/05/04. doi: 10.1007/s00281-023-00992-6. PubMed PMID: 37138042; PubMed Central PMCID: PMCPMC10279585.

34. Louveau A, Plog BA, Antila S, Alitalo K, Nedergaard M, Kipnis J. Understanding the functions and relationships of the glymphatic system and meningeal lymphatics. J Clin Invest. 2017;127(9):3210-9. Epub 2017/09/02. doi: 10.1172/jci90603. PubMed PMID: 28862640; PubMed Central PMCID: PMCPMC5669566 exists.

35. Lun MP, Monuki ES, Lehtinen MK. Development and functions of the choroid plexus–cerebrospinal fluid system. Nature Reviews Neuroscience. 2015;16(8):445-57. doi: 10.1038/nrn3921.

36. Zhou X, Yu S, Zhao DM, Harty JT, Badovinac VP, Xue HH. Differentiation and persistence of memory CD8(+) T cells depend on T cell factor 1. Immunity. 2010;33(2):229-40. Epub 2010/08/24. doi: 10.1016/j.immuni.2010.08.002. PubMed PMID: 20727791; PubMed Central PMCID: PMCPMC2928475.

37. Ram DR, Manickam C, Hueber B, Itell HL, Permar SR, Varner V, et al. Tracking KLRC2 (NKG2C)+ memory-like NK cells in SIV+ and rhCMV+ rhesus macaques. PLoS Pathog. 2018;14(5):e1007104. Epub 2018/06/01. doi: 10.1371/journal.ppat.1007104. PubMed PMID: 29851983; PubMed Central PMCID: PMCPMC5997355.

38. Sichien D, Scott CL, Martens L, Vanderkerken M, Van Gassen S, Plantinga M, et al. IRF8 Transcription Factor Controls Survival and Function of Terminally Differentiated Conventional and Plasmacytoid Dendritic Cells, Respectively. Immunity. 2016;45(3):626-40. Epub 2016/09/18. doi: 10.1016/j.immuni.2016.08.013. PubMed PMID: 27637148.

39. Jurczyszak D, Manganaro L, Buta S, Gruber C, Martin-Fernandez M, Taft J, et al. ISG15 deficiency restricts HIV-1 infection. PLoS Pathog. 2022;18(3):e1010405. Epub 2022/03/26. doi: 10.1371/journal.ppat.1010405. PubMed PMID: 35333911; PubMed Central PMCID: PMCPMC8986114 following competing interests: DB is founder and part owner of Lab11 Therapeutics Inc.

40. Hsu YL, Shi SF, Wu WL, Ho LJ, Lai JH. Protective roles of interferon-induced protein with tetratricopeptide repeats 3 (IFIT3) in dengue virus infection of human lung epithelial cells. PLoS One. 2013;8(11):e79518. Epub 2013/11/14. doi: 10.1371/journal.pone.0079518. PubMed PMID: 24223959; PubMed Central PMCID: PMCPMC3817122.

41. Berger G, Durand S, Fargier G, Nguyen XN, Cordeil S, Bouaziz S, et al. APOBEC3A is a specific inhibitor of the early phases of HIV-1 infection in myeloid cells. PLoS Pathog. 2011;7(9):e1002221. Epub 2011/10/04. doi: 10.1371/journal.ppat.1002221. PubMed PMID: 21966267; PubMed Central PMCID: PMCPMC3178557.

42. Dominguez CX, Amezquita RA, Guan T, Marshall HD, Joshi NS, Kleinstein SH, et al. The transcription factors ZEB2 and T-bet cooperate to program cytotoxic T cell terminal differentiation in response to LCMV viral infection. J Exp Med. 2015;212(12):2041-56. Epub 2015/10/28. doi: 10.1084/jem.20150186. PubMed PMID: 26503446; PubMed Central PMCID: PMCPMC4647261.

43. van der Leun AM, Thommen DS, Schumacher TN. CD8(+) T cell states in human cancer: insights from single-cell analysis. Nat Rev Cancer. 2020;20(4):218-32. Epub 2020/02/07. doi: 10.1038/s41568-019-0235-4. PubMed PMID: 32024970; PubMed Central PMCID: PMCPMC7115982.

44. Batterman KV, Cabrera PE, Moore TL, Rosene DL. T Cells Actively Infiltrate the White Matter of the Aging Monkey Brain in Relation to Increased Microglial Reactivity and Cognitive Decline. Front Immunol. 2021;12:607691. Epub 2021/03/06. doi: 10.3389/fimmu.2021.607691. PubMed PMID: 33664743; PubMed Central PMCID: PMCPMC7920950.

45. Stout JC, Ellis RJ, Jernigan TL, Archibald SL, Abramson I, Wolfson T, et al. Progressive Cerebral Volume Loss in Human Immunodeficiency Virus Infection: A Longitudinal Volumetric Magnetic Resonance Imaging Study. Archives of Neurology. 1998;55(2):161-8. doi: 10.1001/archneur.55.2.161.

46. Underwood J, Cole JH, Caan M, De Francesco D, Leech R, van Zoest RA, et al. Gray and White Matter Abnormalities in Treated Human Immunodeficiency Virus Disease and Their Relationship to Cognitive Function. Clin Infect Dis. 2017;65(3):422-32. Epub 2017/04/08. doi: 10.1093/cid/cix301. PubMed PMID: 28387814; PubMed Central PMCID: PMCPMC5850629.

47. Schnell G, Joseph S, Spudich S, Price RW, Swanstrom R. HIV-1 replication in the central nervous system occurs in two distinct cell types. PLoS Pathog. 2011;7(10):e1002286. Epub 2011/10/19. doi: 10.1371/journal.ppat.1002286. PubMed PMID: 22007152; PubMed Central PMCID: PMCPMC3188520.

48. Carvalhal A, Gill MJ, Letendre SL, Rachlis A, Bekele T, Raboud J, et al. Central nervous system penetration effectiveness of antiretroviral drugs and neuropsychological impairment in the Ontario HIV Treatment Network Cohort Study. J Neurovirol. 2016;22(3):349-57. Epub 2015/11/18. doi: 10.1007/s13365-015-0404-5. PubMed PMID: 26572786.

49. Hsiao F, Frouard J, Gramatica A, Xie G, Telwatte S, Lee GQ, et al. Tissue memory CD4+ T cells expressing IL-7 receptor-alpha (CD127) preferentially support latent HIV-1 infection. PLoS Pathog. 2020;16(4):e1008450. Epub 2020/05/01. doi: 10.1371/journal.ppat.1008450. PubMed PMID: 32353080; PubMed Central PMCID: PMCPMC7192375.

50. Parrish NF, Wilen CB, Banks LB, Iyer SS, Pfaff JM, Salazar-Gonzalez JF, et al. Transmitted/founder and chronic subtype C HIV-1 use CD4 and CCR5 receptors with equal efficiency and are not inhibited by blocking the integrin alpha4beta7. PLoS Pathog. 2012;8(5):e1002686. Epub 2012/06/14. doi: 10.1371/journal.ppat.1002686. PubMed PMID: 22693444; PubMed Central PMCID: PMCPMC3364951.

51. Gray JI, Farber DL. Tissue-Resident Immune Cells in Humans. Annu Rev Immunol. 2022;40:195-220. Epub 2022/01/20. doi: 10.1146/annurev-immunol-093019-112809. PubMed PMID: 35044795.

52. Sallusto F, Lenig D, Forster R, Lipp M, Lanzavecchia A. Two subsets of memory T lymphocytes with distinct homing potentials and effector functions. Nature. 1999;401(6754):708-12. Epub 1999/10/28. doi: 10.1038/44385. PubMed PMID: 10537110.

53. Smolders J, Heutinck KM, Fransen NL, Remmerswaal EBM, Hombrink P, ten Berge IJM, et al. Tissue-resident memory T cells populate the human brain. Nature Communications. 2018;9(1):4593. doi: 10.1038/s41467-018-07053-9.

54. Kumar BV, Ma W, Miron M, Granot T, Guyer RS, Carpenter DJ, et al. Human Tissue-Resident Memory T Cells Are Defined by Core Transcriptional and Functional Signatures in Lymphoid and Mucosal Sites. Cell Rep. 2017;20(12):2921-34. Epub 2017/09/21. doi: 10.1016/j.celrep.2017.08.078. PubMed PMID: 28930685; PubMed Central PMCID: PMCPMC5646692.

55. Eberlein J, Davenport B, Nguyen TT, Victorino F, Jhun K, van der Heide V, et al. Chemokine Signatures of Pathogen-Specific T Cells I: Effector T Cells. J Immunol. 2020;205(8):2169-87. Epub 2020/09/20. doi: 10.4049/jimmunol.2000253. PubMed PMID: 32948687; PubMed Central PMCID: PMCPMC7541659.

56. Zanoni M, Palesch D, Pinacchio C, Statzu M, Tharp GK, Paiardini M, et al. Innate, non-cytolytic CD8+ T cell-mediated suppression of HIV replication by MHC-independent inhibition of virus transcription. PLoS Pathog. 2020;16(9):e1008821. Epub 2020/09/18. doi: 10.1371/journal.ppat.1008821. PubMed PMID: 32941545; PubMed Central PMCID: PMCPMC7523993.

57. Sturdevant CB, Joseph SB, Schnell G, Price RW, Swanstrom R, Spudich S. Compartmentalized replication of R5 T cell-tropic HIV-1 in the central nervous system early in the course of infection. PLoS Pathog. 2015;11(3):e1004720. Epub 2015/03/27. doi: 10.1371/journal.ppat.1004720. PubMed PMID: 25811757; PubMed Central PMCID: PMCPMC4374811.

58. Lustig G, Cele S, Karim F, Derache A, Ngoepe A, Khan K, et al. T cell derived HIV-1 is present in the CSF in the face of suppressive antiretroviral therapy. PLoS Pathog. 2021;17(9):e1009871. Epub 2021/09/24. doi: 10.1371/journal.ppat.1009871. PubMed PMID: 34555123; PubMed Central PMCID: PMCPMC8509856 Ntshuba was unable to confirm their authorship contributions. On their behalf, the corresponding author has reported their contributions to the best of their knowledge.

59. Rustenhoven J, Drieu A, Mamuladze T, de Lima KA, Dykstra T, Wall M, et al. Functional characterization of the dural sinuses as a neuroimmune interface. Cell. 2021;184(4):1000-16.e27. Epub 2021/01/29. doi: 10.1016/j.cell.2020.12.040. PubMed PMID: 33508229; PubMed Central PMCID: PMCPMC8487654.

60. Cugurra A, Mamuladze T, Rustenhoven J, Dykstra T, Beroshvili G, Greenberg ZJ, et al. Skull and vertebral bone marrow are myeloid cell reservoirs for the meninges and CNS parenchyma. Science. 2021;373(6553). Epub 2021/06/05. doi: 10.1126/science.abf7844. PubMed PMID: 34083447; PubMed Central PMCID: PMCPMC8863069.

61. Herisson F, Frodermann V, Courties G, Rohde D, Sun Y, Vandoorne K, et al. Direct vascular channels connect skull bone marrow and the brain surface enabling myeloid cell migration. Nat Neurosci. 2018;21(9):1209-17. Epub 2018/08/29. doi: 10.1038/s41593-018-0213-2. PubMed PMID: 30150661; PubMed Central PMCID: PMCPMC6148759.

62. Tang Y, Chaillon A, Gianella S, Wong LM, Li D, Simermeyer TL, et al. Brain microglia serve as a persistent HIV reservoir despite durable antiretroviral therapy. J Clin Invest. 2023;133(12). Epub 2023/06/15. doi: 10.1172/jci167417. PubMed PMID: 37317962; PubMed Central PMCID: PMCPMC10266791.

63. Colton CA. Heterogeneity of microglial activation in the innate immune response in the brain. J Neuroimmune Pharmacol. 2009;4(4):399-418. Epub 2009/08/06. doi: 10.1007/s11481-009-9164-4. PubMed PMID: 19655259; PubMed Central PMCID: PMCPMC2773116.

64. Ta TT, Dikmen HO, Schilling S, Chausse B, Lewen A, Hollnagel JO, et al. Priming of microglia with IFN-gamma slows neuronal gamma oscillations in situ. Proc Natl Acad Sci U S A. 2019;116(10):4637-42. Epub 2019/02/21. doi: 10.1073/pnas.1813562116. PubMed PMID: 30782788; PubMed Central PMCID: PMCPMC6410786.

65. Colonna M, Butovsky O. Microglia Function in the Central Nervous System During Health and Neurodegeneration. Annu Rev Immunol. 2017;35:441-68. Epub 2017/02/23. doi: 10.1146/annurev-immunol-051116-052358. PubMed PMID: 28226226; PubMed Central PMCID: PMCPMC8167938.

66. Del Prete GQ, Smedley J, Macallister R, Jones GS, Li B, Hattersley J, et al. Short Communication: Comparative Evaluation of Coformulated Injectable Combination Antiretroviral Therapy Regimens in Simian Immunodeficiency Virus-Infected Rhesus Macaques. AIDS Res Hum Retroviruses. 2016;32(2):163-8. Epub 2015/07/08. doi: 10.1089/aid.2015.0130. PubMed PMID: 26150024; PubMed Central PMCID: PMCPMC4761795.

67. Hansen SG, Piatak M, Jr., Ventura AB, Hughes CM, Gilbride RM, Ford JC, et al. Immune clearance of highly pathogenic SIV infection. Nature. 2013;502(7469):100-4. Epub 2013/09/13. doi: 10.1038/nature12519. PubMed PMID: 24025770; PubMed Central PMCID: PMCPMC3849456.

68. Devanathan AS, Fallon JK, White NR, Schauer AP, Van Horne B, Blake K, et al. Antiretroviral Penetration and Drug Transporter Concentrations in the Spleens of Three Preclinical Animal Models and Humans. Antimicrob Agents Chemother. 2020;64(10). Epub 2020/07/15. doi: 10.1128/AAC.01384-20. PubMed PMID: 32661005; PubMed Central PMCID: PMCPMC7508597.

69. Hawes CE, Elizaldi SR, Beckman D, Diniz GB, Shaan Lakshmanappa Y, Ott S, et al. Neuroinflammatory transcriptional programs induced in rhesus pre-frontal cortex white matter during acute SHIV infection. J Neuroinflammation. 2022;19(1):250. Epub 2022/10/07. doi: 10.1186/s12974-022-02610-y. PubMed PMID: 36203187; PubMed Central PMCID: PMCPMC9535930.

70. Verma A, Schmidt BA, Elizaldi SR, Nguyen NK, Walter KA, Beck Z, et al. Impact of T(h)1 CD4 Follicular Helper T Cell Skewing on Antibody Responses to an HIV-1 Vaccine in Rhesus Macaques. J Virol. 2020;94(6). Epub 2019/12/13. doi: 10.1128/JVI.01737-19. PubMed PMID: 31827000; PubMed Central PMCID: PMCPMC7158739.

71. Ma ZM, Miller CJ. Immunophenotype of simian immunodeficiency virus-infected cells in the spleen of a rhesus monkey. AIDS Res Hum Retroviruses. 2015;31(4):359-60. Epub 2015/03/12. doi: 10.1089/aid.2014.0343. PubMed PMID: 25760311; PubMed Central PMCID: PMCPMC4378854.

CHAPTER 4: Chronic SIV-Induced neuroinflammation disrupts CCR7+ CD4+ T cell immunosurveillance in the rhesus macaque brain

****This work is pending publication in Journal of Clinical Investigation, accepted March 2024*

Presented in dissertation as will be published.

CHAPTER IV

Immune dysregulation underlies the neuroinflammatory process in HAND patients. As described in Section 3c of Chapter I, studies humans without neurological disorders have demonstrated that CCR7+ CD4+ T cells populate the CSF. In patients with MS, these subsets are reduced in the brain parenchyma, indicating a potential dysfunction of T cell subsets during neuroinflammation. Building upon this knowledge, our analysis in Chapter III demonstrated the presence of CCR7+ CCR5$^-$ CD4 T cells in all CNS compartments during homeostasis and following acute and chronic R5-T cell tropic SIVmac251 infection. A critical question that remained unanswered thus far is whether these CCR7+ CD4 T cells demonstrated canonical central memory attributes similar to their counterparts in the lymphoid compartment. In Chapter IV, we thoroughly investigate the transcriptional, epigenetic, and functional attributes of CCR7+ cells CD4 T cell in the brain parenchyma during homeostasis. Moreover, we investigate whether the frequencies of CCR7+ CD4 T cells are altered during chronic neuroinflammation by employing the macrophage tropic SIV strain widely used to model Neuro-HIV. Altogether, this Chapter provides insights into the role of CD4 T cells in both CNS immune surveillance and chronic neuroinflammation during SIV infection.

Chronic SIV-Induced neuroinflammation disrupts CCR7+ CD4+ T cell immunosurveillance in the rhesus macaque brain.

Sonny R. Elizaldi[1], Chase E Hawes[1], Anil Verma[2], Yashavanth Shaan Lakshmanappa[3], Ashok R. Dinasarapu[4], Brent T Schlegel[5], Dhivyaa Rajasundaram[5] Jie Li[6], Blythe P Durbin-Johnson[6], Zhong-Min Ma[3], Pabitra B. Pal[2], Danielle Beckman[3], Sean Ott[3], Reben Raeman[2], Jeffrey Lifson[7], John H. Morrison[3, 8], Smita S. Iyer [2,3,9]

[1]Graduate Group in Immunology, UC Davis, CA; [2]Department of Pathology, School of Medicine, University of Pittsburgh, PA; [3]California National Primate Research Center, UC Davis, CA; [4]Department of Neurology, School of Medicine, Emory University, Atlanta, GA 30322; [5] Department of Pediatrics, School of Medicine, University of Pittsburgh, PA, USA; [6]Bioinformatics Core, UC Davis, CA; [7]AIDS and Cancer Virus Program, Frederick National Laboratory, Frederick, MD, USA; [8]Department of Neurology, School of Medicine, UC Davis, CA;[9]Department of Pathology, Microbiology, and Immunology, School of Veterinary Medicine, UC Davis, CA.

ABSTRACT

CD4 T cells survey and maintain immune homeostasis in the brain, yet their differentiation states and functional capabilities remain unclear. Our approach, combining single-cell transcriptomic analysis, ATAC-seq, spatial transcriptomics, and flow cytometry, revealed a distinct subset of CCR7+ CD4 T cells resembling lymph node central memory (TCM) cells. We observed chromatin accessibility at the CCR7, CD28, and BCL-6 loci, defining molecular features of TCM. Brain CCR7+ CD4 T cells exhibited recall proliferation and interleukin-2 production ex vivo, showcasing their functional competence. We identified the skull bone marrow as a local niche for these cells alongside CNS border tissues. Sequestering TCM cells in lymph nodes using FTY720 led to reduced CCR7+ CD4 T cell frequencies in the cerebrospinal fluid, accompanied by increased monocyte levels and soluble markers indicating immune activation. In macaques chronically infected with SIVCL757 and experiencing viral rebound due to cessation of antiretroviral therapy, a decrease in brain CCR7+ CD4 T cells was observed, along with increased microglial activation and initiation of neurodegenerative pathways. Our findings highlight a role for CCR7+ CD4 T cells in CNS immune surveillance and their decline during chronic SIV highlights their responsiveness to neuroinflammation.

GRAPHICAL ABSTRACT

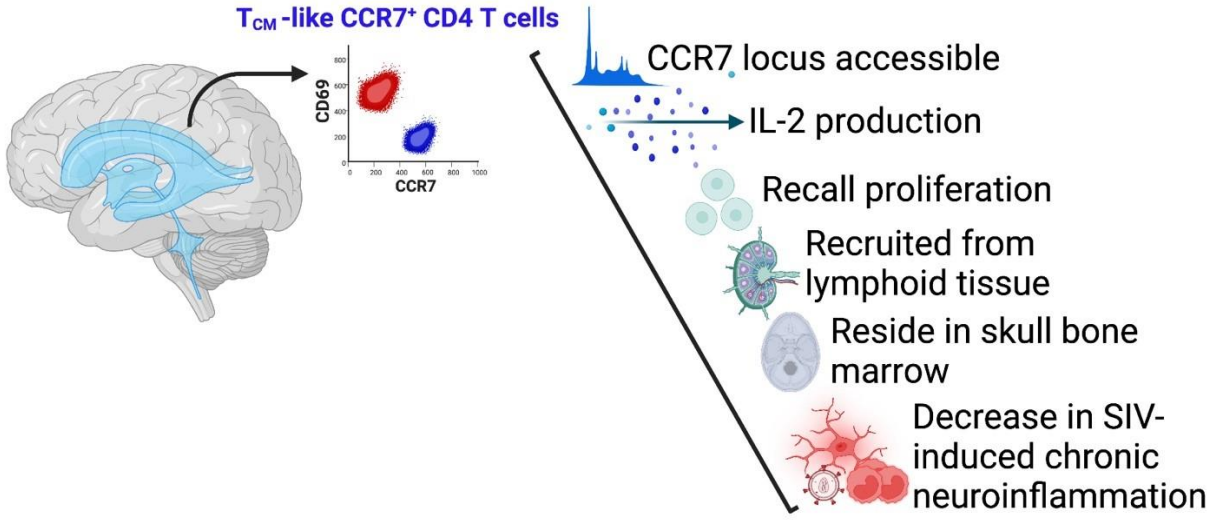

Keywords: central memory, tissue resident memory, choroid plexus stroma, brain parenchyma

INTRODUCTION

Antigen-experienced T lymphocyte subsets, encompassing central (T_{CM}), effector (T_{EM}), and tissue resident memory T cells (T_{RM}), actively survey and inhabit major organ systems, contributing to immune defense and tissue function (1). Lymphocyte surveillance of the central nervous system (CNS) primarily takes place at two barriers: the blood-cerebrospinal fluid barrier (BCSFB) and the blood-brain barrier (BBB). The CSF serves as a key site for T lymphocyte ingress into the CNS during homeostasis, functioning as an immunological equivalent of lymph (2). CSF CD4 T cells express markers such as CCR7, CD27, and CD45RO, characteristic of T_{CM} (3, 4). Beyond the CSF, recently, CD8 T_{RM} expressing CD69 and CD103 have been identified in human brain (5). While T cells reside in CNS niches during homeostasis, our understanding of specific CD4 T cell subsets in the CNS and its border tissues remains incomplete. Bridging this gap is important to understand underpinnings of immune dysregulation during neuroinflammation. This is particularly relevant in HIV infection, where CD4 T cells are primary targets, and chronic neuroinflammation persists in HIV-infected patients despite virological suppression (6).

We utilized a non-human primate model, the rhesus macaque, to study memory CD4 T cell subsets in the CNS. The rhesus macaque is particularly suited for CNS immunology research due to its close similarity to humans, including genetic diversity, a specialized neocortex, and complex meningeal structures (extensive dural and leptomeningeal layers). These features, along with a comprehensive spectrum of memory T cell differentiation states, make it an excellent model for exploring CNS T lymphocyte function. Additionally, perfusing the macaque brain enables precise identification of local brain immune populations while minimizing vascular contamination.

Diverging from the conventional distribution patterns of memory T cells in non-lymphoid tissues, we report that distinct CD69 and CCR7 CD4 T cell subsets populate the macaque brain parenchyma. CNS CCR7+ CD4 T cells exhibit phenotypic and functional features of T_{CM} including production of interleukin 2 and the capacity for rapid recall proliferation. Furthermore, CCR7+ CD4

T cells reside in the skull bone marrow. Our findings show decreased frequencies of this subset during SIV-induced chronic neuroinflammation, emphasizing responsiveness of CCR7+ CD4 T cells to CNS disruptions.

RESULTS

Single-cell transcriptomic analysis of CD45+ leukocytes identifies core T cell gene signatures in rhesus brain.

We previously identified T cell transcripts within synapse-dense brain regions through RNA sequencing (7). However, paucity of T cells amidst a predominance of neuronal and glial transcripts limited our assessment of T cell heterogeneity. To bridge this gap, we applied single-cell(sc) transcriptomics on cryopreserved CD45+ cells to elucidate transcriptional networks underlying memory T cell states in the non-inflamed brain parenchyma. T cells, distinguishable by flow cytometry, constituted an average of 20% of CD45+ cells with a CD4:CD8 ratio of 0.2:1 (**Figure S1**). Sc-RNA sequencing (seq) was performed on viably frozen CD45+ cells isolated from healthy macaque brain and spleen (**Figure 1A**). We enriched CD45+ cells for sequencing by positive selection and sorting for purity and viability (**Figures 1B-C**). A median of 4,952 and 3,151 CD45+ cells from the brain and spleen, respectively were sequenced, resulting in 19,000 single-cell transcriptomes passing quality control (**Figures S2A-E**). Marker gene analysis validated our approach, demonstrating high CD45 (*PTPRC*) expression (**Figure S2F**).

Transcriptome comparisons across tissues showed unique enrichment profiles. The spleen had a more pronounced B cell signature than the brain (**Figure 1D**), particularly in immunoglobulin-related genes (*ENSMMUG00000015202* [human orthologs IGHG1-4], *ENSMMUG00000002764* [human orthologs IGHA1 and IGHA2], *IGHM*, *IGKC*) and genes regulating B cell functions (*EBF1*, *BACH2*, *RelB*), antigen presentation (*CD74*, *HLADMB*, *HLADRA*), and signaling (*ALCAM*, *CD83*, *TRAF3*)(8). In contrast, CD45+ cells in the brain showed enriched T cell gene signatures. This included the T cell receptor α constant gene (*TRAC*), TCR signaling regulators (*TAOK3*, *Sos1*) (9), T cell metabolism-associated genes (*ERN1* and *TXNIP*)(10), and genes regulating effector and T_{CM} programs (*HSP70*, *DNAJB1*, *HSPH1*, *GZMA*, *ID2*, HELIOS (encoded by *IKZF2*), and *IL-7R* (11). We verified predominance of B cells in spleen

and T cells in brain through marker gene analysis and cell type cluster annotation (**Figures S2G-H**).

Non-inflamed brain harbors both effector memory (T_{EM}) and resident memory (T_{RM}) CD8 T cells.

We next pursued high-resolution unsupervised clustering with automated label transfer using blueprint_encode (12, 13). Ten cell clusters were identified, with manual inspection and marker gene analysis (14) confirming six as T cells (**Figures 1E, S3A**). These T cell clusters were isolated and independently reclustered, identifying three shared T cell subtypes between brain and spleen: Terminal effector memory CD8 T cells (T_{EM} 8 cluster; C0, C2, C3, C5), T_{CM} CD8 T cells (T_{CM} 8 cluster; C1, C4, C6) and T_{CM} CD4 cells (T_{CM} 4 cluster; C7 and C8) (**Figures 1F, S3B**).

The T_{EM}8 clusters (C0, C2, C3, C5) displayed varied gene expression (**Figures 2A, S3C-D**) highlighting functional diversity in brain CD8 T_{EM} cells. C0 showed genes typical of *effector memory* cells, such as S100 calcium- binding proteins (*S10010*, *S100A4*), *SH3BGRL3* expressed by T_h1 cells, regulatory receptor *CD52*, molecules driving T cell activation (*FLNA* and the scaffold protein *AHNAK*, cytolytic molecule *GZMB*, and transcription factors (TF) *KLF2* and *KLF3*. C2 was rich in *cytotoxic molecules* like *GZMA*, *GZMK*, *GZMB*, *GNLY*, *KLRC3*, *HELIOS*, and *HOPX* akin to human KIR+ CD8+ T cells (15). In contrast, C3 was enriched for DNAJ/Heatshock genes regulating memory T cell quiescence, Ikaros (encoded by *IKZF1*) and *TXNIP*, which suppress proliferation and inflammatory cytokines in T cells (16). C5 was characterized by genes linked to cell cycle progression and survival (*AKAP13*, *BABAM2*, *INPP4A*). Elevated expression of effector (*GZMA*, *KLRC2-3*, *CCL5*, *IFNG*), residency, and longevity genes (*ID2*, *AHR*, *IKZF2*, *HOPX*, *CD69*, *BCL2*) in the brain versus spleen (**Bar graph in 2A**) suggested that brain CD8 T_{EM} cell clusters encompassed resident and effector memory subsets, aligning with observations in mouse and human studies (5, 17).

Single-cell transcriptomic analysis reveals central memory CD4 and CD8 (T_{CM}) subsets in brain.

We shifted our focus to the remaining CD8 T cell clusters (C1, C4, C6) annotated as T_{CM}. There were notable gene expression differences between brain and spleen (**Figures 2B, S3E**). with brain C1 showing higher expression of memory-related genes (*IL-7R, JUN, FOSB, THEMIS*), along with anti-inflammatory regulators (*ATF3, ZFP36L2, NR4A2*). In addition, C1 expressed genes regulating mitochondrial function and memory cell maintenance (GLUT3, BTG1). C4 cells exhibited elevated levels of cytotoxicity and residency markers (*GAMM, GZMK, CRTAM*), and *NFκB*, with reduced *IL-7R* expression. Brain C4 also showed TCR activation markers (S*LC2A3, NR4A2)*, suggesting potential reactivation. C6 was distinguished by an abundance of *TNFAIP3*, which inhibits IFNγ and TNFα in CD8 T cells. These signatures of brain CD8 T_{CM} clusters indicate specialized roles in memory, effector, and regulatory functions.

Two CD4 T_{CM} clusters, C7 and C8 were discerned among CD4 T cells. C7 was characterized by abundance of co-stimulatory molecules (*CD28* and *ICOS*), *IL-7R* and survival-related TF, *BACH2*, quiescence-associated *FOXP1*, negative regulator of T cell activation, *PELI1*, memory-associated genes (*LTB*, *MAF*, *NFATC1*), and integrin *ITGβ1* (**Figures 2C, S3F**). C8, shared memory gene expression with C7 (*IL-7R*, *BACH2*, *LTB*), and expressed T_h17-associated genes (*CCR6*, *AHR*, *RORA*). Gene set enrichment analysis showed alignment with longevity and MAPK pathways, and downregulation of effector pathways such as NFκB, RIG-I and TNF signaling (**Figure 2D-E**). Overall, scRNA-seq analysis of CD45+ cells revealed a spectrum of T cell states in the brain and spleen.

T_{CM}/T_{RM} loci accessible in T cells within the brain.

To explore mechanisms regulating T_{CM} and T_{RM} differentiation and validate our scRNA-seq data, we profiled the transcriptome and epigenome in parallel. We isolated nuclei from CD45+

and CD45- cells extracted from brain (**Figure 3A**) and generated over 1.5 billion reads across 47,000 nuclei, with an average of 1378 genes/nuclei (**Figures S4A-D**). Transcriptome classification revealed distinct cell clusters, including glial cells (microglia, oligodendrocytes), neurons, endothelial cells, cancer cells, and T cells (**Figures 3B, S4E-F**). The largest immune cluster comprised of macrophages, microglia, and T cells, with each cluster expressing genes encoding proteins with known cell-type distinctions. Specifically, cells in the macrophage cluster expressed *CD86*, *TSPAN14*, and *TNFRSF21*. The microglia cluster expressed *ST6GALNAC3*, *ENTPD1*, and *P2RY12*, while T cell clusters expressed the T_h1 transcription factor [*STAT4*], T cell adaptor protein [*SKAP1*], as well as kinases and signaling molecules [*TNIK*, *ITK*, *FYN*]) (**Figures 3C, S4F**).

We identified expression of several key genes regulating T cell differentiation and function, including zinc finger TF (*ThPOK* and *GATA3*), Runx TF (*RUNX1* and *RUNX3*), T-box TF (*EOMES* and *TBX21*), inhibitor of DNA binding proteins (*ID2* and *ID3*), TF regulating cytokine production (*AHR* and *STAT4*), markers of antigen-experienced cells (*CD44*, *IFNG*, *ITGα4*, and *ITGβ1*), markers of T cell residency (*PRDM1*, *ITGα1*, *ITGαE*, *CD69*, *GZMB*, *KLRG1*, and *PRF1*), and markers of long-lived cells with T_{CM} features (*BCL2* and *BCL6*) (**Figure 3D**).

To quantitatively evaluate genes enriched in T cells, we conducted differential gene expression (DGE) analysis across T cell and microglial clusters. Within microglia, we discovered enrichment of canonical brain resident microglia transcripts, including *CX3CR1*, *ITGαM*, *TMEM*, and *SIGLEC* (18-20) (**Figure 3E**). In contrast, genes highly expressed by the T cell cluster included those regulating T cell signaling (*TRAC*, *ITK*, *THEMIS*, *TNIK*), TF controlling CD4 and CD8 T cell programs (*STAT4*, *RUNX3*), T cell migration (*CD44*, *ITGα4*), residency (*CD69*), and T cell survival (*BCLA11B*, *BCL2*), including the TF *ETS-1*, which regulates IL-7R expression (21) (**Figures 3E, S4G**). Genes involved in T_h17 function, *RORα* and *AHR* were also expressed in keeping with the transcriptome of $T_{CM}4$ C8. Furthermore, a similar T cell gene expression profile

was observed when comparing macrophages to T cells, with the IL-12-induced CD4 T_h1 TF, *STAT4* being the most highly expressed gene in T cells (**Figure S4H**). ATAC-seq analysis highlighted open chromatin in regulatory regions of STAT4, especially within the T cell cluster, aligning with high STAT4 expression (**Figure S4I**). Additionally, downstream targets of *STAT4*, including *IFNγ* and *ICOS*, were distinctively expressed in T cells, differing from patterns in innate immune cells (**Figure S4J**). These genes also featured as top markers in the T cell cluster in our sc RNA sequencing of CD45+ cells.

To formally ascertain whether T cell clusters expressed genes overlapping with our scRNA seq profiles, we examined 7798 transcripts from snRNA seq-derived immune clusters. We then used DGE p values for each expressed gene in T cells relative to macrophages and microglia. For comparison, we also included DGE p values of microglial transcripts relative to macrophages. Gene set enrichment analysis showed overlap with top 20 marker genes expressed by scRNA seq T cell clusters, including classical effector/memory transcripts such as *GZMB*, *CRTAM*, and *IL-7R*, among others (**Figure 3F**). Additionally, when aligning these DGE genes with known T cell signatures from mouse studies, we found that ITGαE (integrin receptor for T_{RM}) and TCF7 (TF critical for T_{CM} development) were notably present in T cells over macrophages/microglia (adjusted p value < 0.05).

To assess T_{CM} gene accessibility, we focussed on genes vital for T_{CM} function and survival - *CD28, IL-7R*, *and BCL2* - which macrophages and microglia also expressed. T cells exhibited increased ATAC peaks for *CD28* and *IL-7R*, suggesting an open chromatin configuration, especially in their promoter regions (**Figure 3G**), whereas *BCL2* accessibility was similar across immune cells (**Figure S4K**). Despite low expression, *CCR7* chromatin accessibility was higher in T cells, contrasting with CCR7 absence in innate immune cells. Additionally, our analysis of gene expression patterns and motif enrichment, using the HOMER database, revealed that TFs from

the bZIP, RUNT, and ATF families, pivotal in regulating T_{CM} genes, were significantly enriched, marking about 30% of target sequences in T cells.

To pinpoint genes controlling memory T cells states, we re-clustered 2,158 T cells, which revealed four distinct clusters (**Figure 3H**). Since CCR7 was expressed in < 1% of cells across all clusters, we probed the promoter accessibility within T_{RM} genes across three major T cell clusters (C0-C2). With *CD69* and *GZMB* marking T_{RMs} and their expression in C1, we anticipated and confirmed ATAC peaks for key T_{RM} genes in C1. Indeed, peak tracks showed increased chromatin accessibility for regulatory regions of *CD69, GZMB, and ITGαE* in C1 (**Figure 3I**). The sequencing outcomes indicate that the primate brain harbors T cells with diverse chromatin accessibility landscapes for genes that govern residency and migration, suggesting the presence of T cells with potential resident and central memory features.

CCR7^{+} CD4 T cells in CNS share phenotypic features with T_{CM} in blood and lymph nodes.

To validate and extend our sequencing observations, we investigated the immune makeup of the CSF. CSF samples were collected from the foramen magnum, alongside paired axillary lymph node aspirates and blood samples (**Figure S5A**). Unlike blood, CSF exhibited minimal B cell and monocyte presence and a preferential infiltration of T cells at steady state.

CSF T cells showed predominance of CD28^{high} CD4 memory T cells, with an absence of terminally differentiated (CD28- CD95+) and naive (CD28^{int} CD95-) subsets, consistent with human phenotypes (22). Relative to CD28^{high} subset in blood, approximately 50% of CSF CD28^{high} CD4 T cells expressed CCR7, compared to 20% in CD28^{high} CD8 T cells (**Figure S5B-C**).

We compared phenotype of CSF-derived T cells to those in matched CNS tissues and adjacent lymph nodes, spleen, and blood. Brain T cells showed distinct differentiation states: CD4 T cells were enriched for CD28, while CD8 T cells were mostly CD28- (**Figure 4A**). Like in the CSF, CD28^{high} CD4 T cells in the parenchyma showed varied CCR7 expression (**Figures 4B**). We

assessed CCR7+ CD4 T cells in the CNS (choroid plexus and brain parenchyma) to those in corresponding lymphoid compartments (deep cervical lymph nodes and spleen) to identify similarities to T_{CM}. Analysis of receptor expression revealed lower per cell CCR7 expression in the CNS than in lymphoid tissues. (**Figure 4C**).

CCR7+ CD4 T cells in each tissue were less likely to express CD69, a key T_{RM} marker (**Figure 4D**). PD-1 levels, indicative of TCR stimulation, were similar across subsets, aligning with findings in CD8 T_{RM} (23) (**Figure 4E**). Given known CCR5 expression in intestinal $CD69^{+}$ CD4 T_{RM} (24), we explored CCR7- CD4 T cells for increased CCR5 alongside higher CD69 levels. This pattern was confirmed in the CNS, but not in lymphoid tissues (**Figure 4F**). Thus, CD4 T cells within the non-inflamed brain parenchyma mainly show $CD28^{high}$ expression, bifurcating into subsets based on CD69 and CCR7, with CCR7+ T cells resembling their lymphoid counterparts.

We performed FLOW SOM clustering on CSF CD4+ T cells (n=4) to determine if CCR7+ and CCR7- subsets represent distinct clusters. Based on expression of specific T_h1 (CXCR3, CCR5), T_h17 (CCR6), activation and memory markers (CD95, PD-1, CD69), 5 metaclusters were defined with varying levels of CCR7 expression (**Figure S6A**). CCR7- and CCR7+ clusters showed enrichment of distinct surface markers; CCR5 and PD-1 were enriched in the CCR7- cluster, while CCR6 was enriched in the CCR7+ cluster (**Figure S6B**).

We then examined if CCR7+ CD4 T cells in the CSF resembled quiescent T_{CM}, and conversely, whether CCR7- CD4 T cells exhibited T_{RM} or activated effector memory cell features. Unlike blood CCR7- CD4 T cells in CSF predominantly expressed CD69, reflecting patterns in the brain (**Figure 4G, S7**). CSF CCR7- subset also showed higher expression of CCR5 and CXCR3, as well as activation markers like ICOS, EOMES, PD-1, and HLA-DR. Both subsets expressed CD127 and BCL-2. In summary, CCR7+ CD4 T cells in the CSF and brain display core T_{CM} traits, like those in lymphoid tissues. We postulated that these CNS CD4 T cells would exhibit functional

hallmarks of T_{CM} by producing IL-2. Upon PMA/Ionomycin stimulation, CSF CD4 T cells indeed demonstrated polyfunctionality, including IL-2 production (**Figure 4H**).

Sequestration of CD4 T_{CM} in lymphoid tissues reduces CCR7+ CD4 T cell frequencies in CSF and increases soluble inflammatory markers. To determine if CNS CCR7+ CD4 T cells displayed migration patterns to and from lymphoid tissue, a hallmark of T_{CM}, we explored the effect of FTY720, known to trap T_{CM} cells in lymph nodes, on T_{CM} frequencies in the CSF. We treated twelve rhesus macaques with FTY720 (30 µg/kg/day) for a month (**Figure 5A**) and analyzed paired blood and CSF T cells over eight weeks, tracking T cells within the subarachnoid space (SAS) through FTY720-induced lymphocyte depletion and the subsequent rebound post-treatment.

Analysis of blood T cells showed rapid decline in total CD4 T cells one week after FTY720, while CD4 T cell counts significantly decreased in CSF at week 4 post FTY720 (**Figure 5B**). Consistent with FTY720 mediated inhibition of S1PR-mediated T cell egress and retention of CCR7-expressing T cells in lymph nodes as documented in macaques (25), rapid sequestration of naive T cells, the subset exhibiting the highest per cell expression of CCR7 ensued. This was evidenced by a notable 4-fold reduction in the absolute counts of naive (CD28+ CD95-) T cells within week 1 of FTY720.

By week 4, there was an additional reduction in naive T cells, marked by a 100-fold decrease in CD4 T cells and an 80-fold decline in CD8 T cells compared to baseline (Figure S8A). The heightened CD4 T cell decline can be attributed to their shorter lymph node residency time, rendering them more susceptible to mechanisms impeding their egress (26). It took up to two weeks for a significant decrease in the peripheral CD4 T_{CM} pool to manifest, culminating in a 17-fold reduction by week 4. This decline was accompanied by a significant decrease in CSF CCR7+ CD4 T cells by week 4 indicating recruitment of CCR7+ CD4 T cells into the SAS from lymphoid tissues via the systemic compartment.

While blood CD8 T_{CM} frequencies fell (**Figure S8B**), CSF CD8 T cells remained stable, potentially due to CD28-CD95+ CD8 T cells in the CSF, which are mostly CCR7- and less affected by FTY720. This could also reflect their migration from non-lymphoid tissues. Consequently, the CSF CD4:CD8 ratio significantly dropped by week 4. The blood showed an increased frequency of CD28- T_{EM} early on, with CD4 and CD8 T cells CM:EM ratios shifting at weeks 1 and 4, consistent with the expected impact of CCR7- EM cells not being retained in lymph nodes. However, the CSF T cell CM:EM ratio remained unchanged throughout the four weeks, indicating a tight regulation that limits CD28- CD95+ CD4 T cells from entering the SAS (**Figure 5B**). Cytokine analysis showed a transient decrease in T_h1, T_h17, and regulatory cytokines in plasma after treatment, demonstrating extensive effects on CD4 helper subsets, although these cytokines were undetectable in the CSF (**Figure S8C**).

In mice, T cell depletion from meninges induces pro-inflammatory innate immune skewing (27). We therefore examined monocyte frequencies post FTY720 to gauge compensatory increase in the SAS. The data showed a net increase in monocytes in the CSF at week 4, significantly increasing monocyte/CD4 T cell ratio (**Figure 5C**). Significant elevation of CSF, but not blood, monocyte chemotactic protein-1 (MCP-1) at week 4 implied CSF monocyte influx was chemokine mediated. Moreover, CSF CCR5+ CD4 T cells significantly increased, and there was an inverse association ($r = -0.73$; $p < 0.01$) between CCR7+ and CCR5+ CD4 T cells (**Figure S8D**). In conclusion, the data suggest that CSF CCR7+ CD69- CD4 T cells are mainly recruited from lymphoid tissues. Moreover, immune activation linked to reduced CCR7+ CD4 T cells in the SAS suggests a role for these cells in neuroimmune homeostasis.

CCR7$^+$ CD4 T cells in CNS exhibit functional T_{CM} features and reside within skull bone marrow.

Recognizing the importance of bone marrow (BM), particularly within the skull (28, 29), for T_{CM} localization we explored presence of CD4 T cells with T_{CM} attributes in this niche. After

manually extracting BM cells from the skull, single-cell suspensions were stained to identify innate and adaptive immune cells. Like mouse brain findings, our analysis identified three immune subsets among CD3- CD45+ cells based on CD11b and HLA-DR expression (**Figure S9**). T cells comprised 71% of the CD45+ population in skull BM, echoing CSF T cell prevalence (**Figure 6A**), with a CD8 to CD4 T cell ratio mirroring that in brain tissue (**Figure 6B**). Like in the CNS, CCR7 expression in CD28+ CD4 T cells was variable, while CD28- CD4 T cells largely lacked CCR7 (**Figures 6C-D, S10**).

Phenotypic analysis revealed distinct profiles between CNS CD4 T cell subsets: CCR7+ cells showed higher integrin α4 and elevated CCR6, but lower CCR5 and CXCR3 expression compared to CD69+ cells, which had more pronounced PD-1 expression, in both skull BM and brain (**Figure 6E**). Functional characterization of memory CCR7- and CCR7+ CD4 subsets demonstrated that both brain CCR7- and CCR7+ CD4 T cells mounted recall proliferation ex vivo, while splenic CCR7+ CD4 T cells, and to a lesser extent CCR7- CD4 T cells were Ki67+ (**Figure 6F**). Analysis of cytokine production following PMA/I stimulation showed that CNS CCR7+ CD4 T cells produced a higher relative IL-2, while the CCR7- subset produced high levels of IL-2, IFNγ, and TNFα. This cytokine expression pattern was consistent with T_{CM} functionality, as exemplified by a similar cytokine pattern in splenic CD4 T_{CM} (**Figure 6G-I**). In summary, the data highlight the presence of a CCR7+ CD4 population in the brain and skull BM exhibiting T_{CM}-like characteristics, akin to T_{CM} in the spleen.

vRNA within frontal and temporal lobes during chronic SIV infection.

To better understand CD4 T_{CM} in the CNS, we investigated these cells in a model of chronic viral neuroinflammation (30). Aged rhesus macaques (17-20 years) were infected with neuropathogenic SIVCL757 to elicit chronic neuroinflammation and establish CNS virus presence. After the post-acute phase, to ensure CNS viral dissemination, suboptimal antiretroviral therapy (ART) was initiated during weeks 16 to 52 post-SIV when CSF and plasma viral RNA

(vRNA) levels exceeded the threshold of detection (> 15 vRNA copies/ml). This treatment was interrupted when vRNA levels fell below the threshold of detection (**Figure 7A**). We adopted this regimen to induce cycles of viral suppression and rebound within the CNS, simulating scenarios in individuals at risk for neurological co-morbidities due to chronic neuroinflammation (6). An exception to this protocol was followed in the case of 33191, which did not receive ART. This decision was made because CSF vRNA levels exceeded 15 copies/ml only at a single time point during week 6 and subsequently dropped below the threshold of detection. Longitudinal collections of CSF and matched blood from infected animals were conducted for up to 116 weeks, except for one SIV+ animal (34974) that was euthanized at 52 weeks due to health complications. Prior to necropsy, ART was interrupted in all animals (except ART-naive 33191) to induce viral rebound. At necropsy, CNS and peripheral lymphoid tissues were collected for analysis. Age-matched control group of SIV-unexposed animals (n=5) was also assessed.

Following infection, viremic animals (n=4) exhibited median plasma viral loads of 165,000 copies/mL at week 3, with CSF viral RNA (vRNA) reaching a median of 19,750 vRNA copies/mL (**Figure S11**). Plasma and CSF vRNA exhibited a lower magnitude and variable pattern when compared to viral loads observed following SIVmac251 (31). Like SIVmac251, there was plasma-CSF concordance during acute SIVCL757 infection before ART initiation. An exception was observed in one TRIM5α-restrictive animal (32967), which displayed transient plasma viral discordance up to week 6 post-infection. Of note, 2 animals (33191 and 34996) demonstrated sporadic and minimal vRNA in CSF, despite plasma vRNA after the acute phase. ART initiation between sixteen to forty-six weeks post-infection led to viral suppression (vRNA copies <15) in plasma as early as 4 weeks and as late as 6 weeks post ART initiation. Throughout chronic infection, viral loads in CSF were consistently 3 log-fold lower than those in plasma (median viral loads/ml at week 108: plasma, 50,000; CSF, 65), aligning with our findings in acute SHIV.C.CH505 (**Figure 7B**) (25).

At necropsy, 3mm post-mortem punch biopsies were collected to assess vRNA and vDNA in various brain regions, border tissues, CNS-draining lymph nodes, and peripheral lymphoid tissues (**Figure 7C**). The frontal lobe, linked to cognition, displayed vRNA positivity in both gray and white matter across all animals tested. However, vDNA was undetectable. The detection of vRNA and vDNA exhibited variability in the temporal lobe, limbic system, and other brain and border tissues. While the CNS-draining lymph nodes and peripheral lymphoid tissues showed vRNA in all animals, vDNA was not consistently detected across CNS tissues in certain animals. The presence of widespread vRNA within the CNS coupled with low levels of vDNA, may be attributed to ineffective viral integration of SIVCL757 within CNS myeloid and CD4 T cells.

CSF lymphocyte analysis showed trend for CD4 T cell reduction during the first 12 weeks of infection (not significant), while CD8 T cells exhibited an increase ($p<0.05$; fold change: 13). Both CD4 and CD8 T cell frequencies stabilized during the chronic phase (**Figure 7D**). These findings highlight widespread vRNA in the CNS, low vDNA levels, and acute changes in CD4 and CD8 T lymphocyte populations within the CSF following SIVCL757 infection.

Spatial profiling of hippocampus shows induction of neuroinflammatory and neurodegenerative gene programs during chronic SIV infection.

To assess the extent of neuroinflammatory responses during chronic SIV infection, we utilized two complementary methods: spatial transcriptomics on the hippocampus and single-cell analysis of CD45-enriched cells derived from brain parenchyma. Initially, we examined T cell distribution in the human brain by performing immunohistochemistry (IHC) analysis on hippocampal sections from both glioblastoma patients (GBM-01) and non-demented individuals from the Netherlands Brain Bank. We aimed to identify neurons (NeuN), myeloid cells (CD11b, IBA1), and lymphocytes (CD45, CD3, CD4). Healthy tonsil sections showed abundant T cells and myeloid cells and lacked neuron-specific staining. In contrast, hippocampal sections from non-demented patients displayed microglia, neurons, T cells, and monocytes, primarily around blood

vessels (**Figure S12**). Glioblastoma patient-derived hippocampal tissue exhibited a pronounced distribution of T cells throughout the brain parenchyma.

With the presence of T cells in the human brain established by IHC, we analyzed hippocampal tissue from chronically SIV-infected macaques (one healthy control, 33980, and one SIV+ animal, 35595) using the Nanostring Digital Spatial Profiler (DSP) platform. Using CD3, CD45, and NeuN as morphological markers to identify T cells, leukocytes, and neurons, we selected 24 regions of interest (ROIs) with varying CD45 expression levels, covering distinct spatial zones within the hippocampus. These zones included areas around CA1, small and large blood vessels, and parenchymal regions (**Figure 8A**). The expression of CD45, CD3, and NeuN proteins showed heterogeneity across the selected 24 ROIs. Using the fluorescence signal of CD3 and CD45, we identified T cells primarily within blood vessels. Subsequently, these 24 ROIs underwent comprehensive 147-plex antibody profiling and whole transcriptomic analysis (WTA). The data showed higher *CD3ε* RNA counts and lower CD3ε protein counts in SIV-infected ROIs, suggestive of possible CD3 protein internalization due to activation (**Figure 8B**). Antibody profiling revealed the expected enrichment of signals corresponding to glial cells (oligodendrocytes [myelin basic protein], astrocytes [GFAP, APOE, S100B, amyloid β, Vimentin], microglia [TMEM119, CD11b, IBA1, P2RY12] neuronal proteins (synaptophysin, neurofilament light chain, Tau, NCAM [CD56], Calbindin), endothelial and muscle cells [CD31, CD34, Fibronectin]. With respect to immune proteins, we detected myeloid cell markers (CD14, CSF1R, CD11c, HLA-DR, CD40, CD68), memory T_{CM} markers (CD127, BCL-2, BCL-6), effector/resident cell marker (GZMB), and transcriptional regulators (BCL-6, FOXP3) (**Figure 8C**).

Activation of neurodegenerative and metabolic gene programs in SIV infected hippocampus.

DGE analysis across control and SIV-infected ROIs (n =12 control; n=12 SIV) demonstrated altered expression of numerous neurodegenerative and metabolic KEGG pathway

genes in response to SIV; specifically, 52 metabolic and 25 neurodegenerative KEGG pathways were disrupted with SIV (**Figure 8D-E**). We saw decreased expression of ETC genes (*NDUFB7*, *NDUFB11*, and *COX4I1*) and a decrease in inositol polyphosphate phosphatase 4A (*INPP4A*), a suppressor of glutamate excitotoxicity in the CNS linked to neurodegeneration in the striatum. Additionally, we identified increase in *BST1*, a risk factor for neurodegenerative diseases (ND). Downregulation of *HSP5*, *CTNNB1*, *COX4I1*, *KLC1*, *DCTN1*, and *PSMB7* linked to various neurodevelopmental and ND was also observed (32). The upregulation of the mitochondrial calcium uniporter, located on the inner mitochondrial membrane, is noteworthy, as disturbances in calcium homeostasis are linked to ND (33-37).

Single cell analysis identifies activated inflammatory macrophage population in SIV infected brain.

As spatial transcriptomics does not offer single-cell resolution, we complemented our analysis with single-cell gene expression of CD45+ enriched brain cells from control animals (33980, 33994), as described in Figure 2, in conjunction with SIV+ animal 32967. To delineate myeloid cell activation at a deeper resolution, we subclustered the myeloid cluster (macrophages and microglia) into eight distinct subclusters. Utilizing established microglial markers (*PTPRC, ITGαM, CX3CR1, and P2RY12*), cluster 3 and cluster 5 were designated microglia-like (**Figure 8F**), while clusters 0, 1, 2, 4, and 7 expressed definitive macrophage markers *CD68* and *FCGR1A.* HLA genes *B2M* and *CD74* were primarily expressed in clusters 0, 2, 4, and 6. Genes related to anti-viral responses (*IFIT2, IFIT3, IRF3, MAVS, STING1, TNF*) and chemokine trafficking (*CCL5, CCL19, CCL21, CCR5, CXCR3*) showed variability but were generally expressed at low levels. Noteworthy was cluster 4, which was enriched in SIV-brain. Cluster 4 displayed a gene signature of activated inflammatory macrophages, featuring high expression of MHC genes, and *IL-1β*. Assessment DGEs in total CD45+ cells showed alterations in chemokine, T cell receptor, MAPK signaling pathways due to chronic SIV infection. Key genes linked to T cell function (*STAT4*,

PTPN6, *NFATC3*, *NFκB1*, *JAK3*, etc.) and MAPK signaling pathway (*EPHA2*, *PTPRR*, *TRAF2*, *NFATC3*) (*SPI1*, *NFATC3 etc.*) were altered (**Figure 8G**). In summary, spatial and single-cell analyses unveiled significant alterations in genes governing neuroinflammatory processes in both myeloid and T cells during chronic SIV infection.

CCR7+ CD4 T cell frequencies decreased during SIV-induced neuroinflammation.

After uncovering a complex interplay of genes involved in the initiation and progression of neuroinflammation in response to viral presence in the brain, we examined cellular and soluble markers in the CNS. We assessed myeloid populations (microglia [CD11b+CD45lo/int], macrophages, monocytes [CD45+CD14/CD16+]), and lymphoid populations (CD4 and CD8 T cells) from single cell suspensions. We observed a significant increase in brain monocytes, indicative of active recruitment to CNS during chronic SIV (**Figure 9A**). Correspondingly, there was a significant increase in plasma levels of CCL2, a monocyte chemoattractant (data not shown). We also investigated microglial activation in the brain and found that overall, HLA-DR expression on microglia was not significantly different (**Figure 9B**). To explore the potential for active recruitment of monocytes and/or lymphocytes to the brain, we examined a panel of inflammatory analytes. Interferon protein 10 (IP-10), a chemoattractant for monocytes and T cells, was significantly increased in the CSF at weeks 70-93 post-infection, suggesting ongoing recruitment (**Figure 9C**). While the total CD4 T cell population in the brain remained unchanged during chronic SIV (**Figure 9D**), a significant increase in the frequency of CD4 T cells expressing PD-1 was noted, indicative of immune activation (**Figure 9E**).

Importantly, the CCR7+ CD69- CD4 subset was decreased in the brain during chronic SIV (**Figure 9F**), an effect not observed in adjacent CNS compartments (**Figure S13**). To determine if the decrease in the CCR7+ CD4 subset was a consequence of virus mediated depletion, we examined expression of chemokine receptors CXCR3 and CCR5 expressed by target cells. The data showed that, on average, CD4 CD69+ cells in the CNS expressed higher relative levels of

CXCR3+CCR5+ arguing against virus mediated depletion of CCR7+ CD4 T cells (**Figure 9G**). In sum, the data emphasize the CNS immune surveillance role of CCR7+ CD4 T cells and their potential to counter neuroinflammatory processes during chronic neuroinflammation.

DISCUSSION

Our data show that T cells in the non-inflamed CNS exhibit diverse differentiation states, characterized by unique chromatin accessibility patterns corresponding to T_{CM} and T_{EM}/T_{RM} profiles. Beyond their presence in CSF and brain parenchyma, we also identify T_{CM} cells occupying the skull BM niche, potentially poised to replenish adjacent CNS compartments. Notably, impeding T cell egress from lymph nodes using FTY720 led to reduced CCR7+ CD4 T cells within the CSF, suggesting potential migration of T_{CM} from lymph nodes to the CSF, likely through vascular routes. Lastly, in a chronic HIV infection model, we observed a specific decline in CCR7+ CD4 T cells in the brain parenchyma.

While the presence of CCR7+ CD4 T cells in the brain challenges established paradigms of memory T cell distribution in non-lymphoid tissues, there is precedence for our observations. For instance, 90% of CSF T cells express CCR7 (4, 38), and CCR7+ T cells populate non-lymphoid tissues including the skin, gut, colon, and cervix (39-41). Moreover, ligands for CCR7, namely CCL19 and CCL21, are present in human CNS (42-44). In rodent models, CCL19 and CCL21 production in the CNS is linked to CCR7+ CD8 T cell recruitment (45). The reduction in CCR7+ CD4 T cells during chronic SIV infection could stem from multiple mechanisms: (a) CCR7 binding with CCL19 triggering its internalization, (b) Diminished CCR7 expression might result from the influx of SIV-specific CCR7- effector cells or the effector differentiation of herpes-virus specific CD4 memory cells in the brain parenchyma (38, 46-48). Notably, within the SAS, activated CCR7- T cells enter the brain parenchyma, while quiescent CCR7+ T cells migrate out of the CNS (49). (c) CCR7+ cells might migrate to lymph nodes through nasal lymphatics (50), and (d) The HIV-1 viral protein U (Vpu) could downregulate CCR7, though this assumes widespread productive infection and likely does not fully account for the observed changes (51). Conclusively establishing the relative contributions of these factors holds significant implications for neuroinflammation.

Currently, it remains unclear whether increased neuroinflammation is a cause or results from the loss of CCR7+ CD4 T cells in the brain, or if these cells are direct targets of the virus. Thus, several key questions need to be addressed to establish the underlying mechanisms, and pathological outcomes of this reduction. Firstly, the co-localization of virus with CD4 T cells, as observed in the brain parenchyma with SIV mac251 (31, 52), still needs confirmation with SIVCL757. Secondly, increased PD-1+ CD4 T cell frequencies in the chronic SIV-infected brain align with observed immune activation indices. However, there is a need for a more in-depth exploration of associated pathways of immune dysregulation, such as T_h17/Treg imbalance and their potential pathogenic consequences (53).This is particularly relevant as CCR7+ CD4 T cells exhibit features of T_h17 and T regulatory cells. Finally, our FTY720 studies suggest broad immune activation, raising questions about effects on CD4 helper subsets like T regulatory cells (54), and connection to CNS immune activation.

In summary, we demonstrate that CD4 T cells with T_{CM} features reside within the primate CNS. Taken together, these data support a model of CNS immunosurveillance by CCR7+ T_{CM}-like population. During chronic viral infection, T_{CM}-like cell frequencies are perturbed likely due to egress to the draining deep cervical lymph node or differentiation to T_{EM} in response to local antigen. Further studies defining their migration potential and functional features will advance our understanding of neuroimmune surveillance during homeostasis and dysregulation in disease.

MATERIALS AND METHODS

Sex as a biological variable.

Animals of both sexes were included in the study, except for the chronic SIV study, which consisted only of females. This decision was made because females are at a higher risk for neurodegenerative diseases, and we aimed to reduce variability in our infection studies.

Rhesus Macaques.

Colony bred Rhesus Macaques (*Macaca Mulatta*) were sourced and housed at the California National Primate Research Center (CNPRC) and maintained in accordance with American Association for Accreditation for Laboratory Animal Care (AAALAC) and Animal Welfare Act guidelines. All procedures were approved by the Institutional Animal Care and Use Committee (IACUC) at UC Davis. Animals (total n=47) consisted of both males (n=17) and females (n=30) with ages ranging from 8 months – 29 years. Select animals were utilized for FTY720 treatment studies (n=12) and SIV infection studies (n=5). Additional tissues were obtained from uninfected opportunistic medical culls for unrelated conditions (n=9; 4 males, 5 females; ages: 0.8-19.7 [years. months]) to bolster analyses with low sample sizes. Animal details are in Table S1 and S2.

FTY720 Treatment.

Fingolimod (FTY720) was obtained from Millipore Sigma and given orally daily by mixing with animal feed. Animals (n=12, 10 males, 2 females; ages 3.5-5.6 [years. months]) received 30 μg/kg of FTY720 daily over four weeks.

SIV Infection.

Animals were infected with SIVsm804e-CL757 strain (SIVCL757) donated by Hirsch and colleagues (NIAID, NIH, Bethesda, MD)(30) . Viral stocks were thawed at 4C and diluted 16.7-fold in HBSS to a final volume of 0.5 mL and stored on ice prior to administration. Animals (n=6;

6 females; ages 17.6-20.8 were intravenously infected with 500 $TCID_{50}$. Animals were treated with ART regimen consisting of Emtricitabine [40 mg/kg], Tenofovir Disproxil Fumarate [5.1 mg/kg] and Dolutegravir [2.5 mg/kg]) administered as previously described(31).

Specimen Collection and Processing.

Animals were anesthetized with 10mg/kg of ketamine hydrochloride administered intramuscularly for routine collections and with pentobarbital at necropsy. Collection of plasma, serum, and PBMCs were performed as previously described (55). Cerebrospinal fluid (CSF) was collected via the foramen magnum and examined for blood contamination by both visual inspection and Hemastix™ testing strips (Siemens) in accordance with manufacturer instructions. Lymphoid tissues and CNS-associated tissues were obtained at necropsy following cardiac saline perfusion and immediately processed for isolation of mononuclear cells using collagenase IV digestion and a 21/75% Percoll gradient.

Flow Cytometry.

Whole blood, CSF, and fine needle lymph node aspirates (FNA) were freshly stained and acquired on the same day following collection. Mononuclear cells obtained from necropsy tissues were either freshly stained and acquired the same day or stained following cryopreservation, with identical methods used for all comparisons. Antibody information can be found in Table S3. Sample acquisition and fluorescence measurements were performed on a BD Bioscience FACSymphony utilizing FACSDiva software (Version: 8.0.1). Sample compensation, population gating, and analysis was performed using FlowJo (Version 10.8.1)

Intracellular Cytokine Stimulation Assay.

Aliquots of 2 million freshly collected PBMCs and CSF cells were stimulated with PMA/Ionomycin (eBioscience Cell Stimulation Cocktail) and incubated for 1 hour at 37°C. Brefeldin A (BD GolgiPlug) and monensin (BD GolgiStop) was added to cell suspensions and

incubated at 37°C for an additional 4 hours. The remainder of the procedure was carried out as previously described (56).

FlowSOM.

Clustering of cells and construction of a minimum spanning tree of relationships between clusters was conducted using FlowSOM, version 2.4.0 (57) with logicle transformation (58). Clustering was based on CXCR3, CD95, PD-1, CD69, CCR5, and, with CCR7 expression used to define groups within metaclusters. Numbers of metaclusters were selected dynamically by the FlowSOM algorithm. Data from each panel was analyzed separately with a cluster defined as overrepresented in the CCR7+ or CCR7- group, if the corresponding adjusted standardized residual from the chi-square test performed on the table of cluster cell counts by CCR7 status was greater than 3. Analyses were conducted using R version 4.2.1.

Viral RNA Quantification.

Quantification of plasma and CSF viral RNA (vRNA) was performed as previously described, using a quantitative reverse transcriptase polymerase chain reaction (qRT-PCR) assay for the detection of SIV gag (59).

Cell Preparation for Sequencing Studies.

Cryopreserved mononuclear cells from rhesus brain and splenic tissues were thawed at room temperature, placed in fresh complete media (For splenic cells: RPMI supplemented with 10% HI-FBS, 1% L-glutamine, 1% penicillin-streptomycin; For brain tissue derived cells: DMEM supplemented with 10% HI-FBS, 1% L-glutamine, 1% penicillin-streptomycin) and treated with 2 units/mL of DNase I (Roche Diagnostics) for 15 minutes at 37°C. Cells were washed in complete media and CD45+ cells were isolated using CD45 microbeads for non-human primates (Miltenyi Biotech) in accordance with the manufacturer's protocol. Enriched CD45+ cells were stained for CD45 and a live dead marker for subsequent flow cytometric sorting. Live CD45+ cells were

characterized and quantified on a BD FACSymphony cell analyzer and sorted utilizing a FACS Aria and suspended in DMEM for single cell RNA sequencing studies.

Single Cell RNA sequencing.

Sample processing, including barcoding, gel-bead assembly in emulsion (GEM), GEM reverse transcription, cDNA amplification, and library construction, followed the Chromium Next GEM single cell 3' v3.1 protocol by 10X Genomics. Sequencing and bioinformatic analysis was performed as previously described (31). Differential gene expression (DGE) analysis across different cell types and conditions was conducted using Seurat functions, employing a threshold of (adjusted P-value < 0.05, |log2 FC| > 0.25) with Benjamini-Hochberg correction. Gene-set enrichment analysis and functional annotation were carried out using clusterProfiler 4.0 and visualized through custom scripts. Pathways represented by DGE genes were visualized with a chord plot utilizing the 'circlize' package in R. All subsequent data analysis was performed in R v4.2.0.

Single nuclei RNA-seq and ATAC.

Nuclei were isolated from brain derived live CD45+ and CD45- cells using the Chromium Nuclei Isolation Kit (10X Genomics) using manufacture instructions. Following isolation, nuclei were stored on ice and used immediately for subsequent library preparation. Barcoded 3' single cell gene expression library and ATAC library were prepared from single nuclei suspensions using the Chromium Single Cell Multiome kit (10X Genomics) following the manufacturer's instruction. The libraries were quantified by fluorometry on a Qubit instrument (LifeTechnologies) and by qPCR with a Kapa Library Quant kit (Kapa Biosystems-Roche) prior to sequencing. The libraries were sequenced on a NovaSeq 6000 sequencer (Illumina) with paired-end 150 bp reads with approximately 35,000 reads pairs per nuclei for gene expression and 25,000 read pairs per nuclei for ATAC libraries.

Single nuclei RNA-seq and ATAC quantification and statistical analysis.

The raw single-cell multiome (ATAC + Gene Expression) sequencing data was pre-processed using Cell Ranger ARC pipeline (10X Genomics). This step involves the demultiplex of cells using cell barcodes, the alignment of reads to Mmul10 reference genome, removal of empty droplets, cell debris and low-quality cells. The filtered gene expression data was imported to Seurat (60) (v4.3.0) for further quality control. Cells were required to have between 250 and 5000 genes, 500 and 12000 unique transcripts, and 1000 and 70000 ATAC peaks. Cell doublets were removed using DoubletFinder (61). Gene expression data and chromatin accessibility data were normalized, and dimensionality reduced individually using LogNormalize method in Seurat with a scale factor of 10000. Chromatin accessible peak data produced by Cell Ranger was processed using Signac (62) (v1.8.0) and normalized using term frequency-inverse document frequency (TF-IDF) in RunTFIDF function, selecting the top features and then dimension reduced using singular value decomposition on the TF-IDF matrix. After dimension reduction, the two modalities were integrated using the weighted nearest neighbor method in Seurat. The integrated graph was then used for UMAP visualization and clustering. Cell type identification was carried out on clusters generated at resolution 2.25, using the R package scType (63). Differential expression analysis was done using a linear model in limma (64), adjusting for cell cycle scores and the number of genes expressed.

Spatial Transcriptomics Profiling.

Paraformaldehyde-fixed, paraffin-embedded hippocampal brain tissues were profiled using GeoMx® DSP (65). 5 µm tissue sections were prepared according ƒto manufacturer's recommendations for GeoMx-NGS RNA BOND RX slide preparation (manual no. MAN-10131-02). Tissue morphology was visualized using fluorescent antibodies specific to lymphocyte and

neuron specific markers (anti-CD45 [Novus], anti-CD3 [Primary, Bio-Rad], Secondary anti-Rat IgG, [ThermoFisher], and anti-NeuN [Millipore Sigma], and nucleic acid stain Cyto83 [ThermoFisher]). Twelve regions of interest (ROIs) of 660 x 785 μm geometric shapes (squares) were created and localized to brain blood vessels and neuron rich areas. After ROI selection, UV light was utilized to release and collect oligonucleotides from each ROI. For Whole Transcriptome analysis, Illumina i5 and i7 dual-indexing primers were added to each area of illumination (AOI) during PCR. Library concentration was measured using a Qubit fluorometer (Thermo Fisher Scientific), and quality assessed using a Bioanalyzer (Agilent). The Illumina NextSeq 2000 was used for sequencing, and the resulting FASTQ files were mapped to the Hs_R_NGS_WTA_v1.0 reference (Nanostring) using the NanoString GeoMx NGS pipeline v2.1 to generate raw count data/ each target probe AOIs. Raw counts were processed using the same NanoString GeoMx NGS pipeline and converted to digital count conversion (DCC) files. For protein analysis, oligos were enumerated on the nCounter platform. Protein data was normalized to ERCC-sequence specific probes followed by area normalization, and lastly to control IgG (rabbit and mouse) to control for background signal.

DCC files were further processed using Geomxtools (66) R package (Bioconductor version 3.2.0, Nanostring, Seattle, WA, USA). Data were quality controlled per individual AOI. AOIs were excluded from the dataset if they met any of the following conditions: less than 80% reads aligned to the reference, less than 40% sequencing saturation, or less than 1000 raw reads. Limit of quantification (LoQ) calculated for raw data based on the distribution of the negative control probes (“NegProbe”) and used as an estimate for the quantifiable limit of gene expression per AOI (67). A gene was considered detected if its expression is above the LoQ for that AOI. Genes were included in the analysis if they were detected above the LoQ in > 5% of AOIs. Then, the data was normalized using the third quantile (Q3) to account for differences in cellularity and ROI size. The Linear Mixed Model (LMM) was used to calculate the significant differences

between the two groups, and genes were considered significantly expressed when adj.p < 0.1 (677 DGEs). The differentially expressed genes were used to create heatmaps of selected KEGG pathways. The heatmaps were created using ComplexHeatmap (version 2.13.1) R package (68).

Immunohistochemistry.

De-identified formalin-fixed paraffin embedded human hippocampal tissues from non-demented patients (n=3) and a patient with glioblastoma (n=1) were obtained from the Netherlands Brain Bank and human tonsil tissues (n=1) was obtained from the UC Davis Cancer Center Repository. Rabbit polyclonal anti-CD3 (Agilent), mouse monoclonal anti-CD4 (Novus), rabbit polyclonal anti-CD45 (Novus), rabbit monoclonal anti-IBA1 (Invitrogen), rabbit polyclonal anti-CD11b (Invitrogen), and rabbit monoclonal anti-NeuN (Abcam) were used for subsequent immunohistochemical staining. All 4 μm paraffin sections were subjected to a heat antigen retrieval step before application of primary antibodies by treating slides with AR-10 (Biogenex) for 2 minutes at 125^{o}C in a Digital Decloaking Chamber (Biocare), followed by cooling to 90^{o}C for 10 minutes, or by treating slides with H-3300 (Vector) for 20 minutes at 100^{o}C. Following primary staining, samples were incubated with anti-mouse and anti-rabbit EnVision+ system secondary antibodies (Agilent), followed by treatment with AEC chromogen (Agilent) and counterstained with Gill's hematoxylin I (StatLab). Primary antibodies were replaced by mouse or rabbit isotype controls and ran with each staining series as negative controls. Slides were visualized with a Zeiss Imager Z1 (Carl Zeiss) and images captured using a Zeiss Axiocam (Carl Zeiss).

Statistical Analyses.

Wilcoxon signed rank test were used for paired analyses (i.e., longitudinal and within group comparisons). Mann-Whitney U-test were used for unpaired comparison between animal cohorts/treatment groups. Tests were performed in GraphPad Prism (Version 9.5.1) with significance values denoted as follows: * $p < 0.05$, ** $p < 0.01$, *** $p < 0.001$, **** $p < 0.0001$.

Study Approval.

All nonhuman primates were maintained according to the guidelines of the IACUC of University of California, Davis, based on the approved protocol (#22379, 22261, 22787, 22033, 23363)

Data and materials availability.

RNA-seq dataset is accessible at GSE221815. All data are provided in the Supporting data values file.

Study Approval.

All nonhuman primates were maintained according to the guidelines of the IACUC of University of California, Davis, based on the approved protocol (#22379, 22261, 22787, 22033, 23363)

REFERENCES

1. Schenkel JM, and Masopust D. Tissue-resident memory T cells. *Immunity.* 2014;41(6):886-97.
2. Ransohoff RM, Kivisäkk P, and Kidd G. Three or more routes for leukocyte migration into the central nervous system. *Nature Reviews Immunology.* 2003;3(7):569-81.
3. de Graaf MT, Smitt PA, Luitwieler RL, van Velzen C, van den Broek PD, Kraan J, and Gratama JW. Central memory CD4+ T cells dominate the normal cerebrospinal fluid. *Cytometry B Clin Cytom.* 2011;80(1):43-50.
4. Kivisakk P, Mahad DJ, Callahan MK, Trebst C, Tucky B, Wei T, et al. Human cerebrospinal fluid central memory CD4+ T cells: evidence for trafficking through choroid plexus and meninges via P-selectin. *Proc Natl Acad Sci U S A.* 2003;100(14):8389-94.
5. Smolders J, Heutinck KM, Fransen NL, Remmerswaal EBM, Hombrink P, Ten Berge IJM, et al. Tissue-resident memory T cells populate the human brain. *Nat Commun.* 2018;9(1):4593-.
6. Nightingale S, Ances B, Cinque P, Dravid A, Dreyer AJ, Gisslen M, et al. Cognitive impairment in people living with HIV: consensus recommendations for a new approach. *Nat Rev Neurol.* 2023;19(7):424-33.
7. Hawes CE, Elizaldi SR, Beckman D, Diniz GB, Shaan Lakshmanappa Y, Ott S, et al. Neuroinflammatory transcriptional programs induced in rhesus pre-frontal cortex white matter during acute SHIV infection. *J Neuroinflammation.* 2022;19(1):250.
8. Staupe RP, Lodge KE, Thambi N, Toole D, Tamburino AM, Chang D, et al. Single cell multi-omic reference atlases of non-human primate immune tissues reveals CD102 as a biomarker for long-lived plasma cells. *Communications Biology.* 2022;5(1):1399.
9. Poltorak M, Meinert I, Stone JC, Schraven B, and Simeoni L. Sos1 regulates sustained TCR-mediated Erk activation. *Eur J Immunol.* 2014;44(5):1535-40.
10. Kokubo K, Hirahara K, Kiuchi M, Tsuji K, Shimada Y, Sonobe Y, et al. Thioredoxin-interacting protein is essential for memory T cell formation via the regulation of the redox metabolism. *Proc Natl Acad Sci U S A.* 2023;120(2):e2218345120.
11. Hetemaki I, Kaustio M, Kinnunen M, Heikkila N, Keskitalo S, Nowlan K, et al. Loss-of-function mutation in IKZF2 leads to immunodeficiency with dysregulated germinal center reactions and reduction of MAIT cells. *Sci Immunol.* 2021;6(65):eabe3454.
12. Dunham I, Kundaje A, Aldred SF, Collins PJ, Davis CA, Doyle F, et al. An integrated encyclopedia of DNA elements in the human genome. *Nature.* 2012;489(7414):57-74.
13. Martens JHA, and Stunnenberg HG. BLUEPRINT: mapping human blood cell epigenomes. *Haematologica.* 2013;98(10):1487-9.
14. Franzen O, Gan LM, and Bjorkegren JLM. PanglaoDB: a web server for exploration of mouse and human single-cell RNA sequencing data. *Database (Oxford).* 2019;2019.
15. Li J, Zaslavsky M, Su Y, Guo J, Sikora MJ, van Unen V, et al. KIR(+)CD8(+) T cells suppress pathogenic T cells and are active in autoimmune diseases and COVID-19. *Science.* 2022;376(6590):eabi9591.
16. Lyon de Ana C, Arakcheeva K, Agnihotri P, Derosia N, and Winandy S. Lack of Ikaros Deregulates Inflammatory Gene Programs in T Cells. *J Immunol.* 2019;202(4):1112-23.
17. Urban SL, Jensen IJ, Shan Q, Pewe LL, Xue H-H, Badovinac VP, and Harty JT. Peripherally induced brain tissue-resident memory CD8(+) T cells mediate protection against CNS infection. *Nature immunology.* 2020;21(8):938-49.
18. Sousa C, Biber K, and Michelucci A. Cellular and Molecular Characterization of Microglia: A Unique Immune Cell Population. *Front Immunol.* 2017;8:198.
19. Friess L, Cheray M, Keane L, Grabert K, and Joseph B. Atg7 deficiency in microglia drives an altered transcriptomic profile associated with an impaired neuroinflammatory response. *Molecular Brain.* 2021;14(1):87.

20. Lee E, Eo JC, Lee C, and Yu JW. Distinct Features of Brain-Resident Macrophages: Microglia and Non-Parenchymal Brain Macrophages. *Mol Cells.* 2021;44(5):281-91.
21. Grenningloh R, Tai TS, Frahm N, Hongo TC, Chicoine AT, Brander C, et al. Ets-1 maintains IL-7 receptor expression in peripheral T cells. *J Immunol.* 2011;186(2):969-76.
22. Kivisäkk P, Mahad DJ, Callahan MK, Trebst C, Tucky B, Wei T, et al. Human cerebrospinal fluid central memory CD4⁺ T cells: Evidence for trafficking through choroid plexus and meninges via P-selectin. *Proceedings of the National Academy of Sciences.* 2003;100(14):8389-94.
23. Scholler AS, Nazerai L, Christensen JP, and Thomsen AR. Functionally Competent, PD-1(+) CD8(+) Trm Cells Populate the Brain Following Local Antigen Encounter. *Front Immunol.* 2020;11:595707.
24. Woodward Davis AS, Roozen HN, Dufort MJ, DeBerg HA, Delaney MA, Mair F, et al. The human tissue-resident CCR5(+) T cell compartment maintains protective and functional properties during inflammation. *Sci Transl Med.* 2019;11(521).
25. Pino M, Paganini S, Deleage C, Padhan K, Harper JL, King CT, et al. Fingolimod retains cytolytic T cells and limits T follicular helper cell infection in lymphoid sites of SIV persistence. *PLoS Pathog.* 2019;15(10):e1008081.
26. Mandl JN, Liou R, Klauschen F, Vrisekoop N, Monteiro JP, Yates AJ, et al. Quantification of lymph node transit times reveals differences in antigen surveillance strategies of naive CD4+ and CD8+ T cells. *Proc Natl Acad Sci U S A.* 2012;109(44):18036-41.
27. Derecki NC, Cardani AN, Yang CH, Quinnies KM, Crihfield A, Lynch KR, and Kipnis J. Regulation of learning and memory by meningeal immunity: a key role for IL-4. *J Exp Med.* 2010;207(5):1067-80.
28. Herisson F, Frodermann V, Courties G, Rohde D, Sun Y, Vandoorne K, et al. Direct vascular channels connect skull bone marrow and the brain surface enabling myeloid cell migration. *Nat Neurosci.* 2018;21(9):1209-17.
29. Mazzitelli JA, Smyth LCD, Cross KA, Dykstra T, Sun J, Du S, et al. Cerebrospinal fluid regulates skull bone marrow niches via direct access through dural channels. *Nat Neurosci.* 2022;25(5):555-60.
30. Matsuda K, Riddick NE, Lee CA, Puryear SB, Wu F, Lafont BAP, et al. A SIV molecular clone that targets the CNS and induces neuroAIDS in rhesus macaques. *PLoS pathogens.* 2017;13(8):e1006538-e.
31. Elizaldi SR, Verma A, Ma ZM, Ott S, Rajasundaram D, Hawes CE, et al. Deep analysis of CD4 T cells in the rhesus CNS during SIV infection. *PLoS Pathog.* 2023;19(12):e1011844.
32. Zhuang W, Ye T, Wang W, Song W, and Tan T. CTNNB1 in neurodevelopmental disorders. *Frontiers in Psychiatry.* 2023;14.
33. Liao Y, Dong Y, and Cheng J. The Function of the Mitochondrial Calcium Uniporter in Neurodegenerative Disorders. *Int J Mol Sci.* 2017;18(2).
34. O'Neill C, Cowburn RF, Bonkale WL, Ohm TG, Fastbom J, Carmody M, and Kelliher M. Dysfunctional intracellular calcium homoeostasis: a central cause of neurodegeneration in Alzheimer's disease. *Biochem Soc Symp.* 2001(67):177-94.
35. Pfeiffer RF. Parkinson disease: calcium channel blockers and Parkinson disease. *Nat Rev Neurol.* 2010;6(4):188-9.
36. Lim D, Fedrizzi L, Tartari M, Zuccato C, Cattaneo E, Brini M, and Carafoli E. Calcium homeostasis and mitochondrial dysfunction in striatal neurons of Huntington disease. *J Biol Chem.* 2008;283(9):5780-9.
37. Tradewell ML, Cooper LA, Minotti S, and Durham HD. Calcium dysregulation, mitochondrial pathology and protein aggregation in a culture model of amyotrophic

lateral sclerosis: mechanistic relationship and differential sensitivity to intervention. *Neurobiol Dis.* 2011;42(3):265-75.
38. Kivisäkk P, Mahad DJ, Callahan MK, Sikora K, Trebst C, Tucky B, et al. Expression of CCR7 in multiple sclerosis: implications for CNS immunity. *Ann Neurol.* 2004;55(5):627-38.
39. Campbell JJ, Murphy KE, Kunkel EJ, Brightling CE, Soler D, Shen Z, et al. CCR7 expression and memory T cell diversity in humans. *J Immunol.* 2001;166(2):877-84.
40. Kim CH, Rott L, Kunkel EJ, Genovese MC, Andrew DP, Wu L, and Butcher EC. Rules of chemokine receptor association with T cell polarization in vivo. *J Clin Invest.* 2001;108(9):1331-9.
41. Unsoeld H, and Pircher H. Complex memory T-cell phenotypes revealed by coexpression of CD62L and CCR7. *J Virol.* 2005;79(7):4510-3.
42. Krumbholz M, Theil D, Steinmeyer F, Cepok S, Hemmer B, Hofbauer M, et al. CCL19 is constitutively expressed in the CNS, up-regulated in neuroinflammation, active and also inactive multiple sclerosis lesions. *J Neuroimmunol.* 2007;190(1-2):72-9.
43. Pashenkov M, Söderström M, and Link H. Secondary lymphoid organ chemokines are elevated in the cerebrospinal fluid during central nervous system inflammation. *J Neuroimmunol.* 2003;135(1-2):154-60.
44. Giunti D, Borsellino G, Benelli R, Marchese M, Capello E, Valle MT, et al. Phenotypic and functional analysis of T cells homing into the CSF of subjects with inflammatory diseases of the CNS. *J Leukoc Biol.* 2003;73(5):584-90.
45. Alt C, Laschinger M, and Engelhardt B. Functional expression of the lymphoid chemokines CCL19 (ELC) and CCL 21 (SLC) at the blood-brain barrier suggests their involvement in G-protein-dependent lymphocyte recruitment into the central nervous system during experimental autoimmune encephalomyelitis. *Eur J Immunol.* 2002;32(8):2133-44.
46. Lanzavecchia A, and Sallusto F. Understanding the generation and function of memory T cell subsets. *Current Opinion in Immunology.* 2005;17(3):326-32.
47. McMenamin PG. Distribution and phenotype of dendritic cells and resident tissue macrophages in the dura mater, leptomeninges, and choroid plexus of the rat brain as demonstrated in wholemount preparations. *Journal of Comparative Neurology.* 1999;405(4):553-62.
48. Schnittman SR, and Hunt PW. Clinical consequences of asymptomatic cytomegalovirus in treated human immunodeficency virus infection. *Curr Opin HIV AIDS.* 2021;16(3):168-76.
49. Schlager C, Korner H, Krueger M, Vidoli S, Haberl M, Mielke D, et al. Effector T-cell trafficking between the leptomeninges and the cerebrospinal fluid. *Nature.* 2016;530(7590):349-53.
50. Cupovic J, Onder L, Gil-Cruz C, Weiler E, Caviezel-Firner S, Perez-Shibayama C, et al. Central Nervous System Stromal Cells Control Local CD8(+) T Cell Responses during Virus-Induced Neuroinflammation. *Immunity.* 2016;44(3):622-33.
51. Ramirez PW, Famiglietti M, Sowrirajan B, DePaula-Silva AB, Rodesch C, Barker E, et al. Downmodulation of CCR7 by HIV-1 Vpu results in impaired migration and chemotactic signaling within $CD4^+$ T cells. *Cell Rep.* 2014;7(6):2019-30.
52. Mohammadzadeh N, Roda W, Branton WG, Clain J, Rabezanahary H, Zghidi-Abouzid O, et al. Lentiviral Infections Persist in Brain despite Effective Antiretroviral Therapy and Neuroimmune Activation. *mBio.* 2021;12(6):e0278421.
53. Favre D, Mold J, Hunt PW, Kanwar B, Loke P, Seu L, et al. Tryptophan catabolism by indoleamine 2,3-dioxygenase 1 alters the balance of TH17 to regulatory T cells in HIV disease. *Sci Transl Med.* 2010;2(32):32ra6.

54. Liu Y, Jiang J, Xiao H, Wang X, Li Y, Gong Y, and Huang Y. The sphingosine-1-phosphate receptor agonist FTY720 and its phosphorylated form affect the function of CD4+CD25+ T cells in vitro. *Int J Mol Med.* 2012;30(1):211-9.
55. Verma A, Hawes CE, Lakshmanappa YS, Roh JW, Schmidt BA, Dutra J, et al. Monoclonal antibodies protect aged rhesus macaques from SARS-CoV-2-induced immune activation and neuroinflammation. *Cell Reports.* 2021;37(5):109942.
56. Verma A, Schmidt BA, Elizaldi SR, Nguyen NK, Walter KA, Beck Z, et al. Impact of T(h)1 CD4 Follicular Helper T Cell Skewing on Antibody Responses to an HIV-1 Vaccine in Rhesus Macaques. *J Virol.* 2020;94(6).
57. Van Gassen S, Callebaut B, Van Helden MJ, Lambrecht BN, Demeester P, Dhaene T, and Saeys Y. FlowSOM: Using self-organizing maps for visualization and interpretation of cytometry data. *Cytometry A.* 2015;87(7):636-45.
58. Parks DR, Roederer M, and Moore WA. A new “Logicle” display method avoids deceptive effects of logarithmic scaling for low signals and compensated data. *Cytometry Part A.* 2006;69A(6):541-51.
59. Hansen SG, Jr MP, Ventura AB, Hughes CM, Gilbride RM, Ford JC, et al. Immune clearance of highly pathogenic SIV infection. *Nature.* 2013;502(7469):100-4.
60. Hao Y, Hao S, Andersen-Nissen E, Mauck WM, 3rd, Zheng S, Butler A, et al. Integrated analysis of multimodal single-cell data. *Cell.* 2021;184(13):3573-87.e29.
61. McGinnis CS, Murrow LM, and Gartner ZJ. DoubletFinder: Doublet Detection in Single-Cell RNA Sequencing Data Using Artificial Nearest Neighbors. *Cell Syst.* 2019;8(4):329-37.e4.
62. Stuart T, Srivastava A, Madad S, Lareau CA, and Satija R. Single-cell chromatin state analysis with Signac. *Nat Methods.* 2021;18(11):1333-41.
63. Ianevski A, Giri AK, and Aittokallio T. Fully-automated and ultra-fast cell-type identification using specific marker combinations from single-cell transcriptomic data. *Nature Communications.* 2022;13(1):1246.
64. Ritchie ME, Phipson B, Wu D, Hu Y, Law CW, Shi W, and Smyth GK. limma powers differential expression analyses for RNA-sequencing and microarray studies. *Nucleic Acids Res.* 2015;43(7):e47.
65. Merritt CR, Ong GT, Church SE, Barker K, Danaher P, Geiss G, et al. Multiplex digital spatial profiling of proteins and RNA in fixed tissue. *Nat Biotechnol.* 2020;38(5):586-99.
66. Ortogero N YZ, Vitancol R, Griswold M, Henderson D 2022.
67. Zimmerman SM, Fropf R, Kulasekara BR, Griswold M, Appelbe O, Bahrami A, et al. Spatially resolved whole transcriptome profiling in human and mouse tissue using Digital Spatial Profiling. *Genome Res.* 2022;32(10):1892-905.
68. Gu Z. Complex heatmap visualization. *iMeta.* 2022;1(3):e43.

FIGURES.

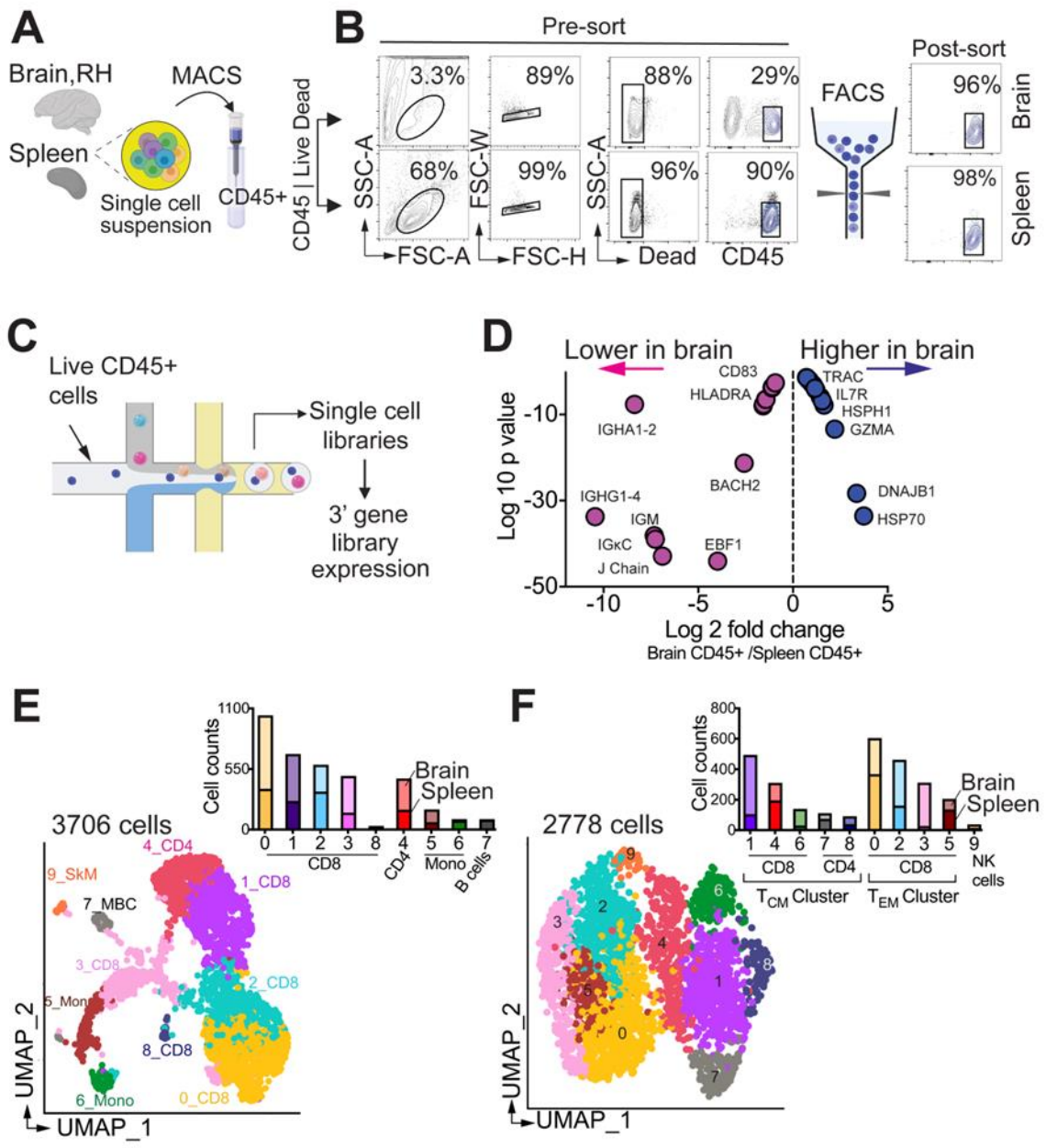

Figure 1. Single-cell transcriptomic analysis of CD45+ leukocytes identifies core T cell gene signatures in the rhesus brain. (A-C) Schematic of single CD45+ cell profiling in brain, right hemisphere (RH) and spleen. **(D)** Differences in B and T cell transcripts in brain versus spleen. **(E)** UMAP of scRNA-seq transcriptional profiles from brain and spleen identifies 10 clusters. Cell clusters are color-coded based on cell identity assigned using Single R. SkM,

skeletal muscle; MBC, memory B cells; Mono, monocytes. Inset shows cell proportions in each cluster split by tissue type (bottom, spleen; top, brain)**. (F)** UMAP shows 10 sub-clusters from T cell clusters in E.

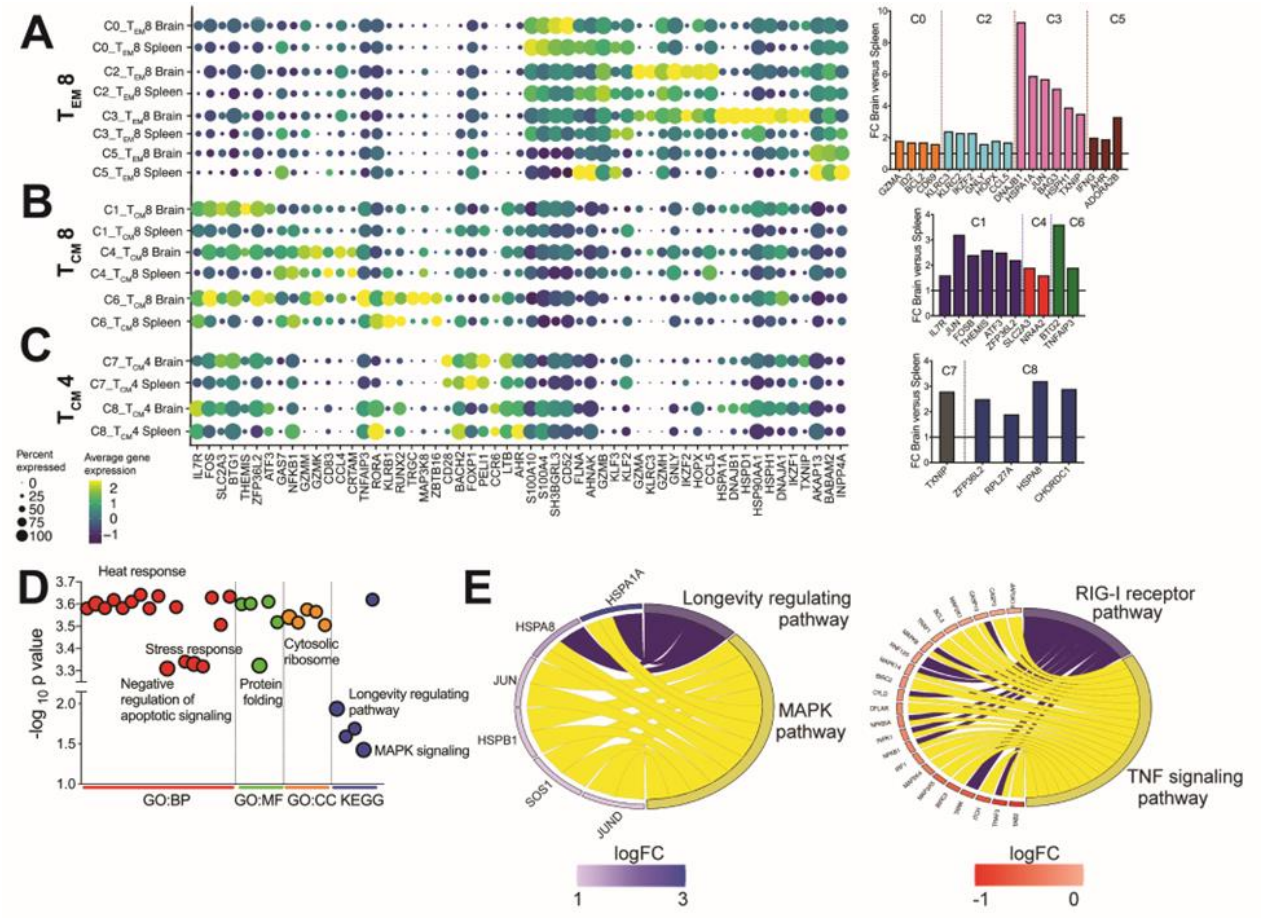

Figure 2. T cell clusters in rhesus brain. (A-C) Select marker genes of cell clusters. Dot size represents proportion of cells expressing gene and color designates expression level with bar graphs representing genes significantly higher in brain relative to spleen for indicated clusters. **(D)** Dot plot displays link between genes and pathways from GO biological processes (GO:BO), GO molecular functions (GO:MF), and GO cellular component (GO:CC) and KEGG. **(E)** Chord plots show pathways and corresponding genes enriched versus underrepresented in $T_{CM}4$ cell clusters.

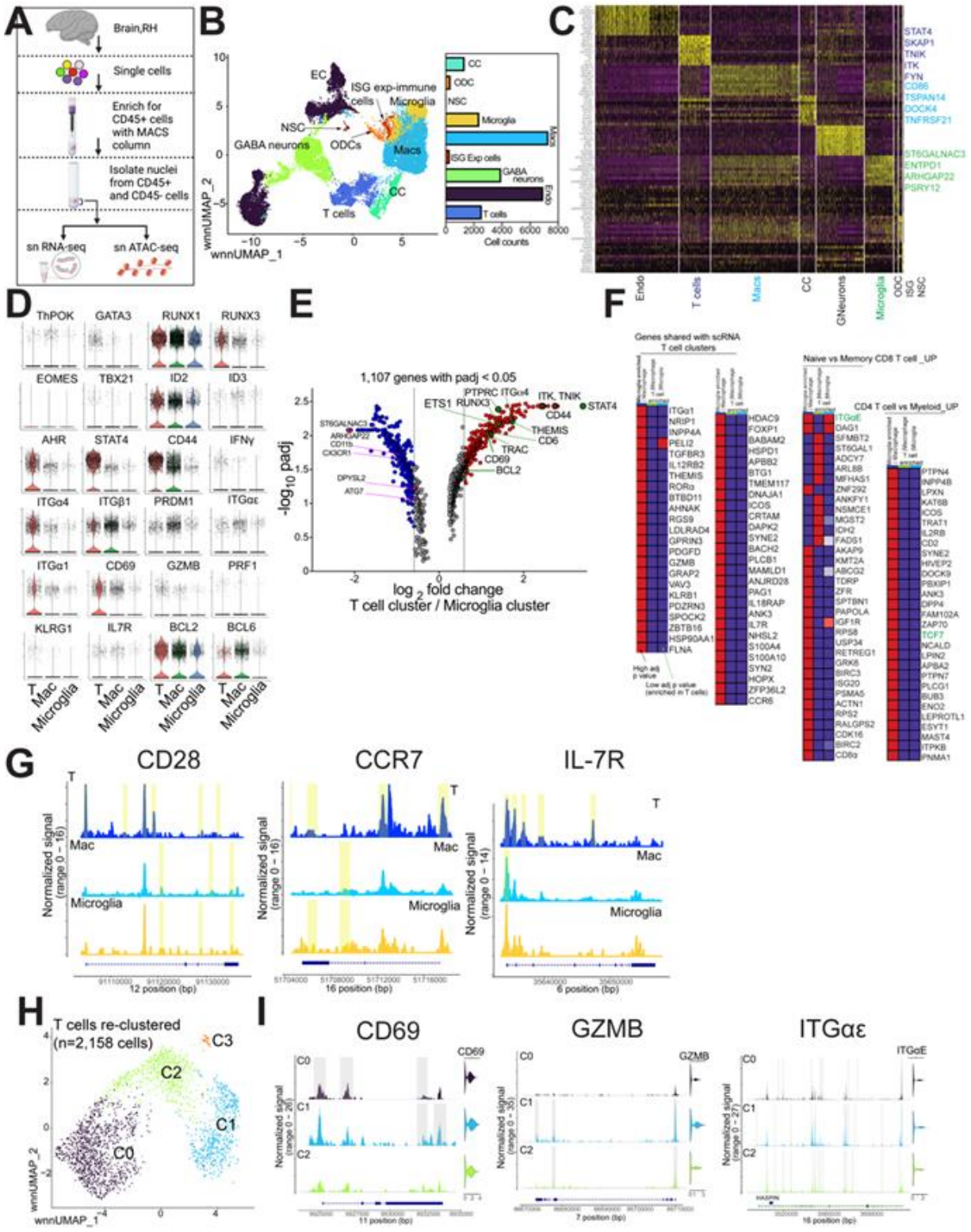

Figure 3. T_{CM}/T_{RM} loci accessible in T cells within the brain. (A) Schematic of sn RNA analysis. **(B)** UMAP projection of 25,321 snRNA-seq profiles. Dots represent individual cells, and colors

indicate cluster identity (labelled on right). EC, endothelial cells; NSC, neural stem cells; CC, cancer cells; Macs, macrophages; ODC, oligodendrocyte precursor cells; ISG exp cells, interferon stimulated gene expressing cells. **(C)** Heat map representation of RNA-seq of cluster-specific marker genes across all clusters. **(D)** Violin plots show expression of key genes across immune clusters. **(E)** Gene expression differences between T cell and microglial cell clusters. **(F)** GSEA of shared genes across sn and sc analysis. **(G)** Genomic regions showing snATAC-seq tracks of chromatin accessibility of T_{CM} genes across T cell, microglia, and macrophage immune clusters. **(H)** UMAP projection of 3 major T cell subclusters (2,158 T cells). **(I)** Genomic regions showing snATAC-seq tracks of chromatin accessibility of $T_{RM/EM}$ genes across 3 major T cell clusters (C0-C2) in H.

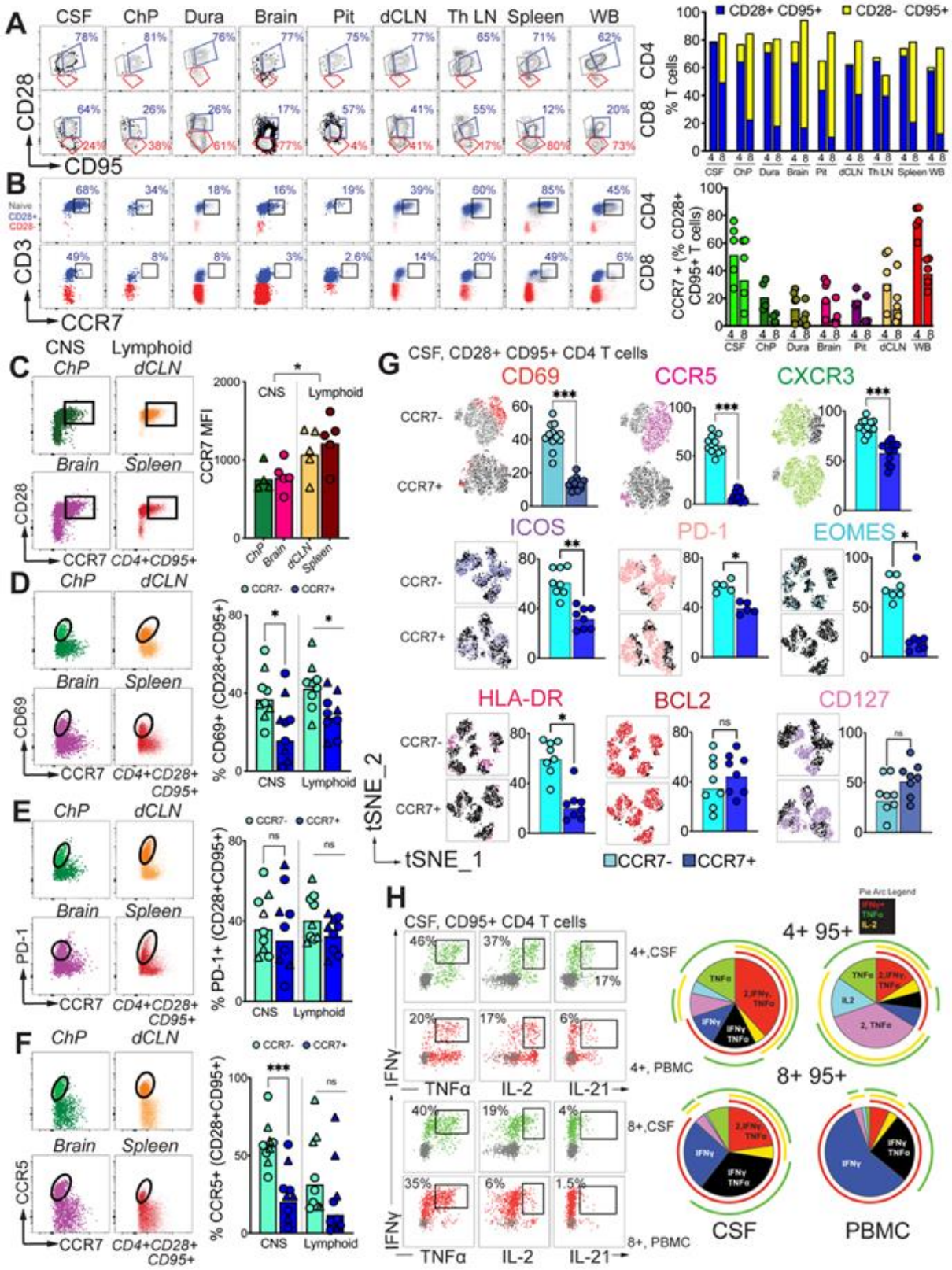
A
CSF
ChP
Dura
Brain
Pit
dCLN
Th LN
Spleen
WB
CD28
CD95
CD4
CD8
% T cells
CD28+ CD95+
CD28- CD95+
B
Naive
CD28+
CD28-
CD3
CCR7
CCR7 + (% CD28+ CD95+ T cells)
C
CNS
Lymphoid
ChP
dCLN
Brain
Spleen
CD28
CCR7
CD4+CD95+
CCR7 MFI
D
CD69
CD4+CD28+ CD95+
% CD69+ (CD28+CD95+)
E
PD-1
% PD-1+ (CD28+CD95+)
F
CCR5
% CCR5+ (CD28+CD95+)
G
CSF, CD28+ CD95+ CD4 T cells
CD69
CCR5
CXCR3
ICOS
PD-1
EOMES
HLA-DR
BCL2
CD127
CCR7-
CCR7+
tSNE_1
tSNE_2
H
CSF, CD95+ CD4 T cells
4+,CSF
4+, PBMC
8+,CSF
8+, PBMC
IFNγ
TNFα
IL-2
IL-21
4+ 95+
8+ 95+
CSF
PBMC

Figure 4. CCR7^{+} CD4 T cells in CNS share phenotypic features with T_{CM} in blood and lymph nodes. (A) Representative flow plots illustrate CD28 and CD95 expression on CD4 and CD8 T cells; frequencies of CD28+CD95+ (blue) and CD28-CD95+ (yellow) in CD4 T cells and CD8 T cells. **(B)** Representative flow plots illustrate CCR7 expression on CD28^{High} CD4 (top row) and CD28^{High} CD8 (bottom row) T cells; frequencies of CCR7 expression on CD28^{High} CD4 and CD28^{High} CD8 T cells. **(C)** Representative flow plots illustrate CD28 expression and CCR7 expression on CD4+CD95+ T cells in CNS and lymphoid tissues; CCR7 MFI of CD4+CD95+. **(D-F)** Representative flow plots indicating CD69, PD-1, CCR5 and CCR7 expression on CD4+CD28+CD95+ T cells in CNS and lymphoid tissues; frequency of CD69+, PD-1+, and CCR5+ on CD4+CD28+CD95+ CCR7-/+ T cells. **(G)** Representative tSNE plot illustrating expression of T cell markers on CD4+CD28+CD95+ CCR7-/+ T cells in the CSF; frequencies for each population. **(H)** Representative flow plots illustrating cytokine production in the CSF and PBMCs. CSF, cerebrospinal fluid; ChP, choroid plexus; Pit, pituitary; dCLN, deep cervical lymph nodes; Th LN, thoracic lymph node. WB, whole blood; PBMC, peripheral blood mononuclear cell

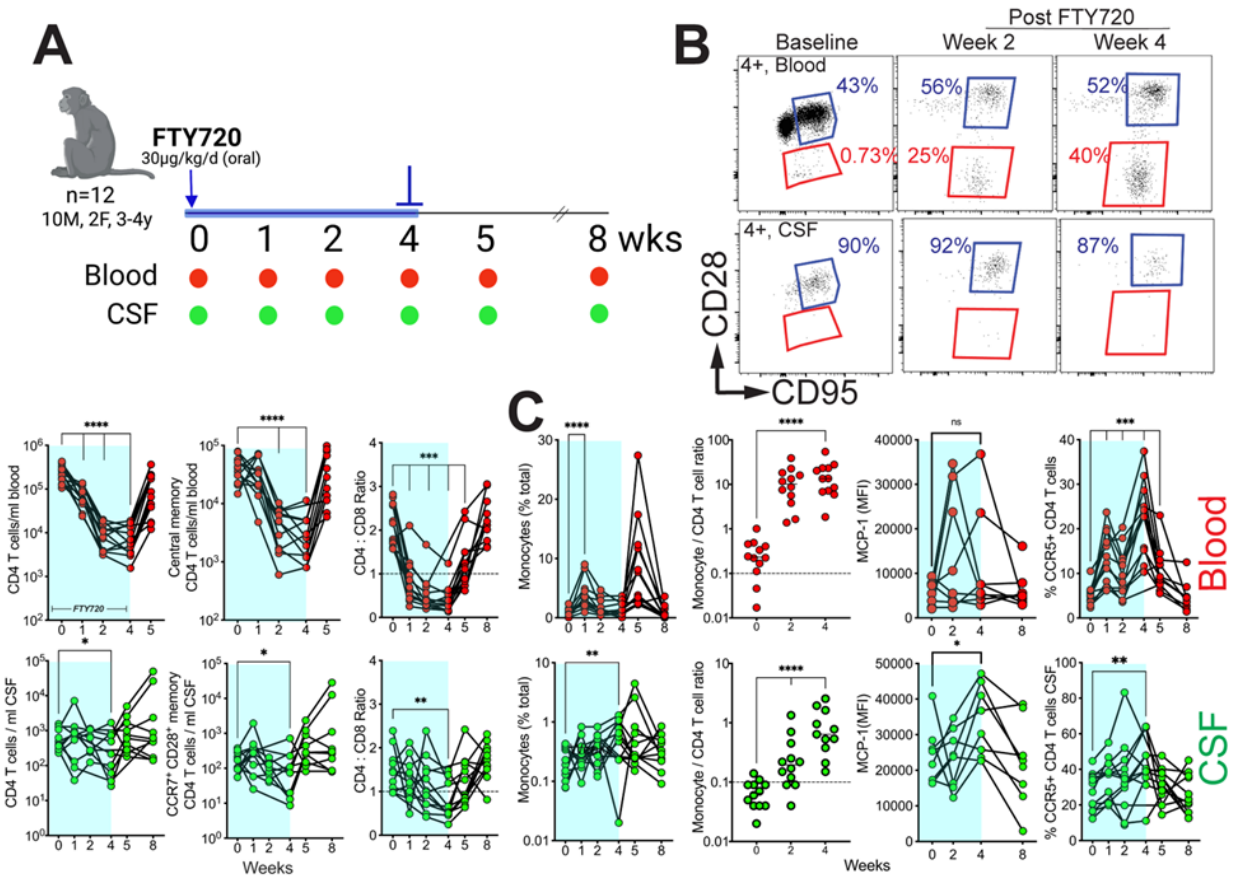

Figure 5. Sequestration of CD4 T_{CM} in lymphoid tissues reduces CCR7^{+} CD4 T cell frequencies in CSF. (A) Study schematic: n= 12 rhesus macaques (age,3-4 years) were administered an oral dose of 30 µg/kg per day of FTY720 for the first four weeks of the study. CSF taps and blood draws were performed at indicated timepoints. **(B)** Representative flow plots indicating CD28 and CD95 expression on CD4 T cells from the blood (top row) or the CSF (bottom row) (Left); CD4 T cell counts/ml, Central memory CD4 T cells and CCR7+CD28+ memory CD4 T cells/ ml blood or CSF, and CD4:CD8 Ratio for Blood and CSF (Right). **(C)** Frequencies of Monocytes, Monocyte to CD4 T cell ratio, Median Fluorescent Intensity (MFI) of Monocyte Chemoattractant Protein-1 (MCP-1), and CCR5 expression of CD4 T cells in the blood and CSF over the course of the study.

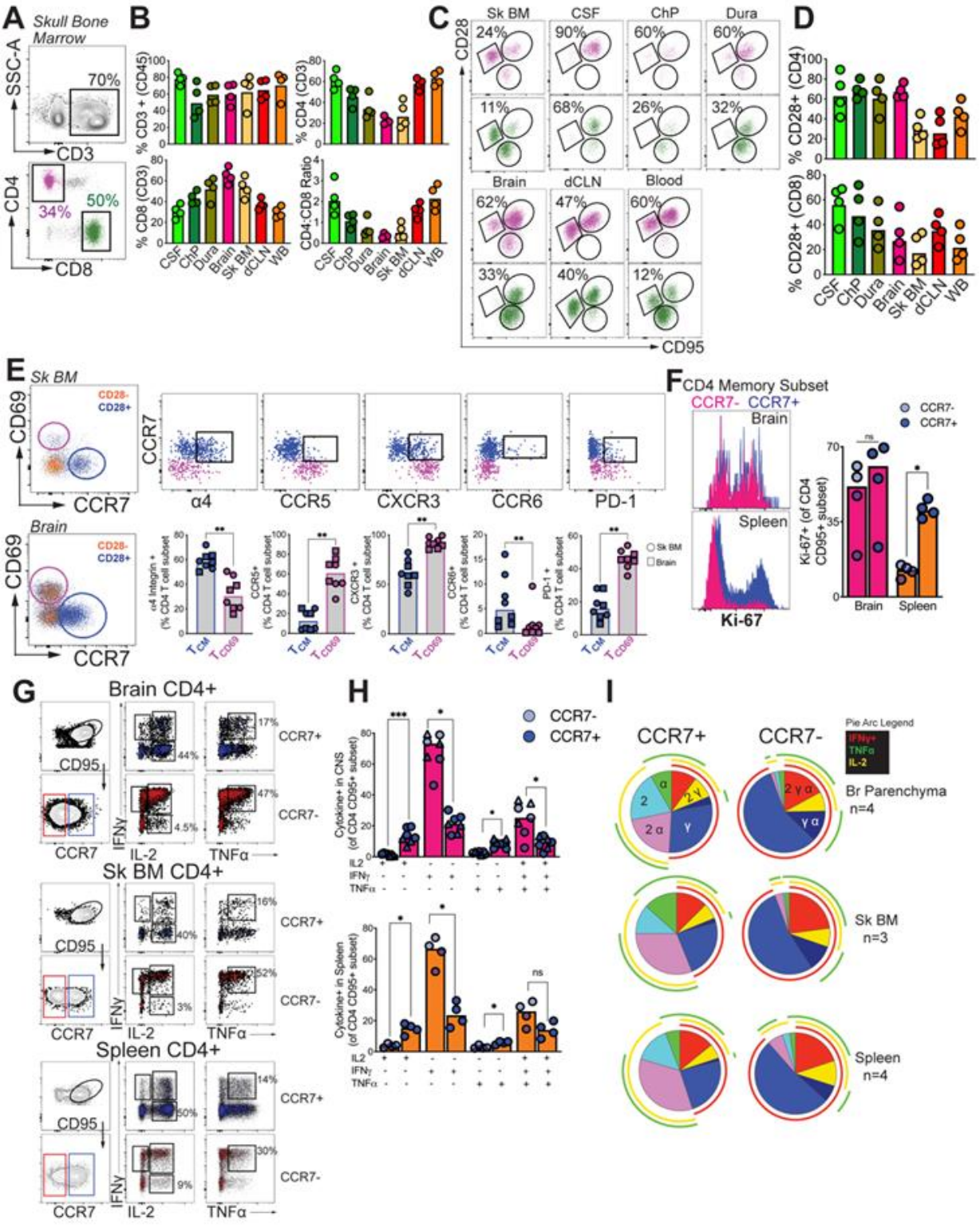

Figure 6. CCR7+ CD4 T cells in CNS exhibit functional T_{CM} features and reside within skull bone marrow. (A) Representative gating for T cells within the skull BM and **(B)** corresponding

frequencies of CD3, CD4 (top), CD8 T cells, and CD4/CD8 ratios (bottom) across tissue compartments. **(C)** Population gates for CD4 (purple) and CD8 (green) subsets with **(D)** corresponding frequencies of CD28+ subsets across tissue compartments**. (E)** Phenotypic characterization of T_{CM}-like (CCR7+; blue) and tissue resident (CD69+; purple) CD4 T-cells from brain and skull BM. **(F)** Ki67 MFI and frequencies on CCR7- and CCR7+ CD4 T cells after T cell activation using anti-CD3 and anti-CD28. **(G-I)** Representative gating for CD95+ CCR7+ CD4 T cells and CD95+ CCR7- CD4 T cells and bar charts illustrating cytokine production after stimulating with PMA/Ionomycin in Brain, Skull BM, and Spleen. **(I)** Pie Charts indicating cytokine functionality after PMA/Ionomycin treatment. **(A-F)** Data points indicate individual tissue samples. **(F)** Symbols indicate skull BM (circle) or brain tissue (square) samples. Bars indicate medians.

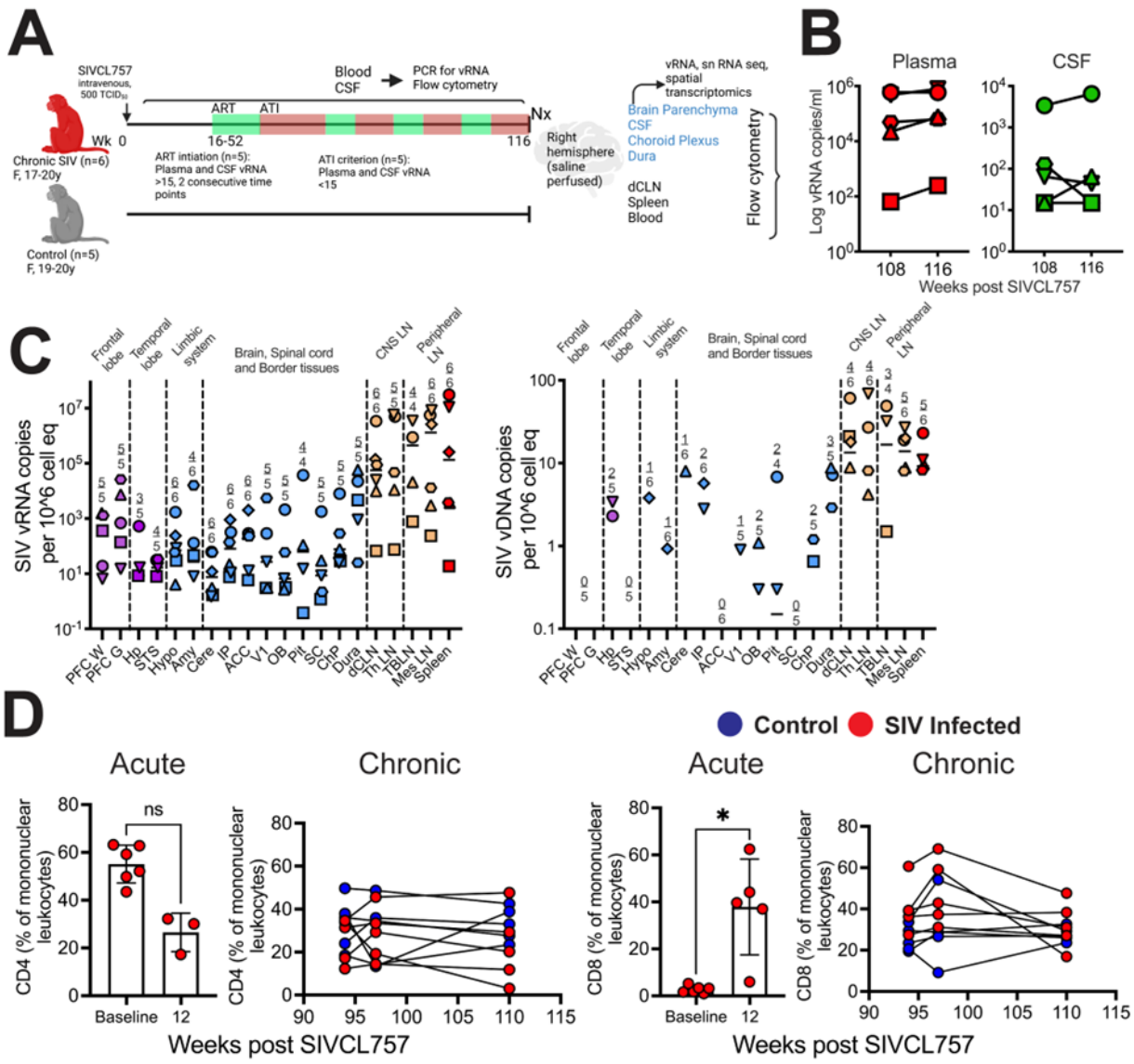

Figure 7. vRNA within frontal and temporal lobes during chronic SIV infection. (A) Study schematic: rhesus macaques were infected with SIVCL757 intravenously and longitudinally assessed for systemic and CNS viral burden, single nuclei (sn) RNA sequencing, spatial transcriptomics and immune responses by flow cytometry. **(B)** Kinetics of plasma (red) and CSF (green) viral loads during the chronic phase (wk108 – 116) of SIVCL757. **(C)** vRNA and vDNA in various brain regions, dura mater, deep cervical lymph nodes, and PBMCs. **(D)** CSF CD4 and CD8 frequencies during the acute phase (week 12) and chronic phase (week 92-110) of SIVCL757 infection. PFC W, pre-frontal cortex white matter; PFC G, PFC gray matter; Hp;

hippocampus; STS, superior temporal sulcus; Hypo, Hypothalamus; Amy, Amygdala; Cere, Cerebellum; IP, inferior/intra parietal; ACC, anterior cingulate cortex; V1, primary visual cortex; OB, olfactory bulb; Pit, pituitary; SC, spinal cord (near base of skull); ChP, choroid plexus; dCLN, deep cervical lymph node; Th LN, thoracic lymph node; TBLN, tracheobronchial lymph nodes; Mes LN, mesenteric lymph nodes.

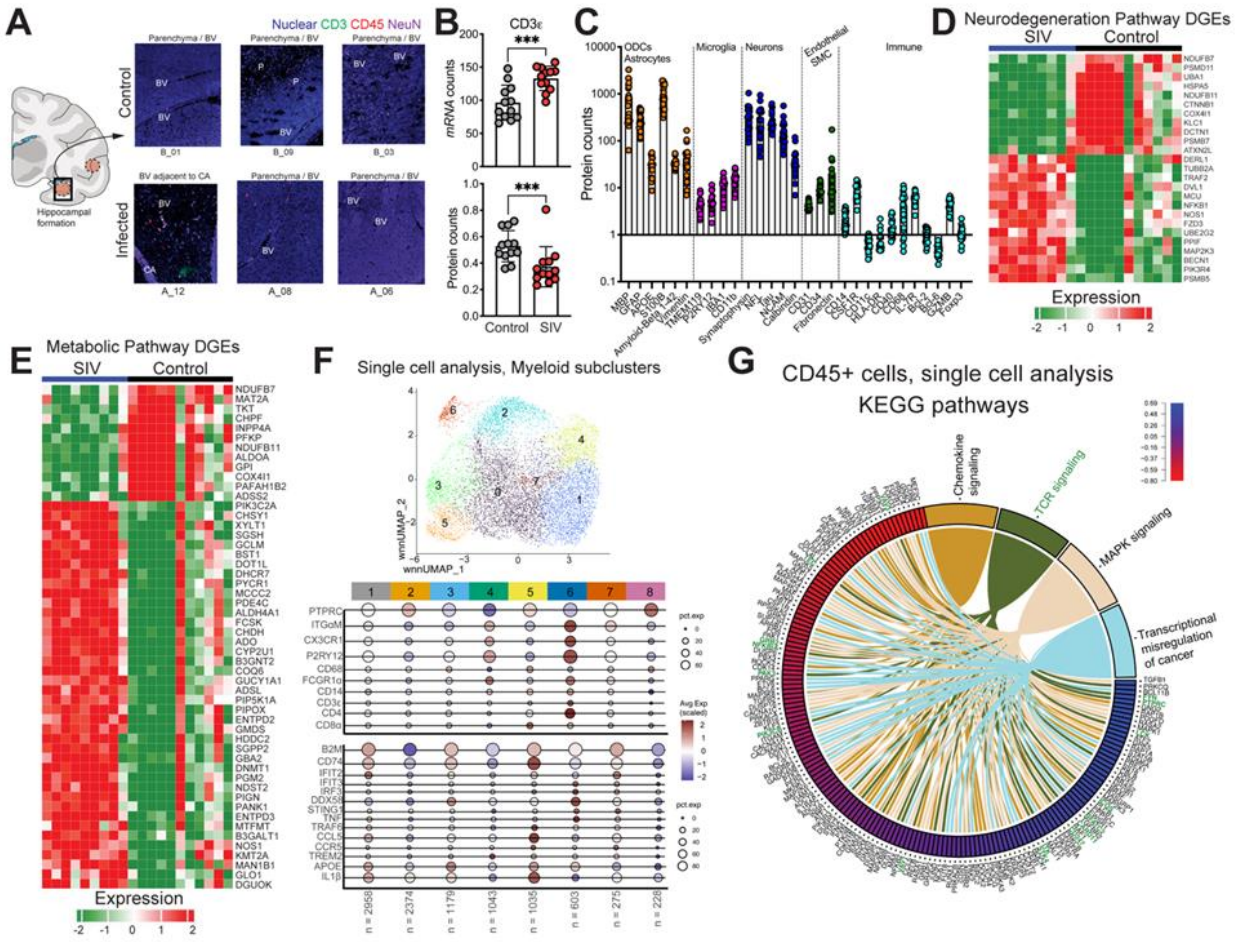

Figure 8. Induction of neuroinflammatory and neurodegenerative gene programs during chronic SIV infection. (A) Representative illustration for ROI selection within the hippocampal region of control (top) and SIVCL757 infected (bottom) animals; Nuclear (blue), CD3 (green), CD45 (red), and NeuN (Purple) for Nanostring whole transcriptome analysis (WTA) and proteomics pipeline. **(B)** CD3ε *mRNA* and protein counts for ROIs. **(C)** Protein counts for all ROIs. **(D)** Differentially expressed neurodegenerative genes across control and SIV infected ROIs. **(E)** Differentially expressed metabolic genes across control and SIV infected ROIs. **(F)** UMAP plot shows cell annotation for myeloid specific gene clusters from sc data. Dot plots depict average gene expression of canonical microglia, monocyte, macrophage, antiviral and inflammatory response genes across 8 distinct myeloid clusters. **(G)** Chord plot of differentially expressed

genes across control and SIV infected CD45-enriched cells from single cell transcriptomics. Genes related to TCR signaling pathway are colored in green for clarity.

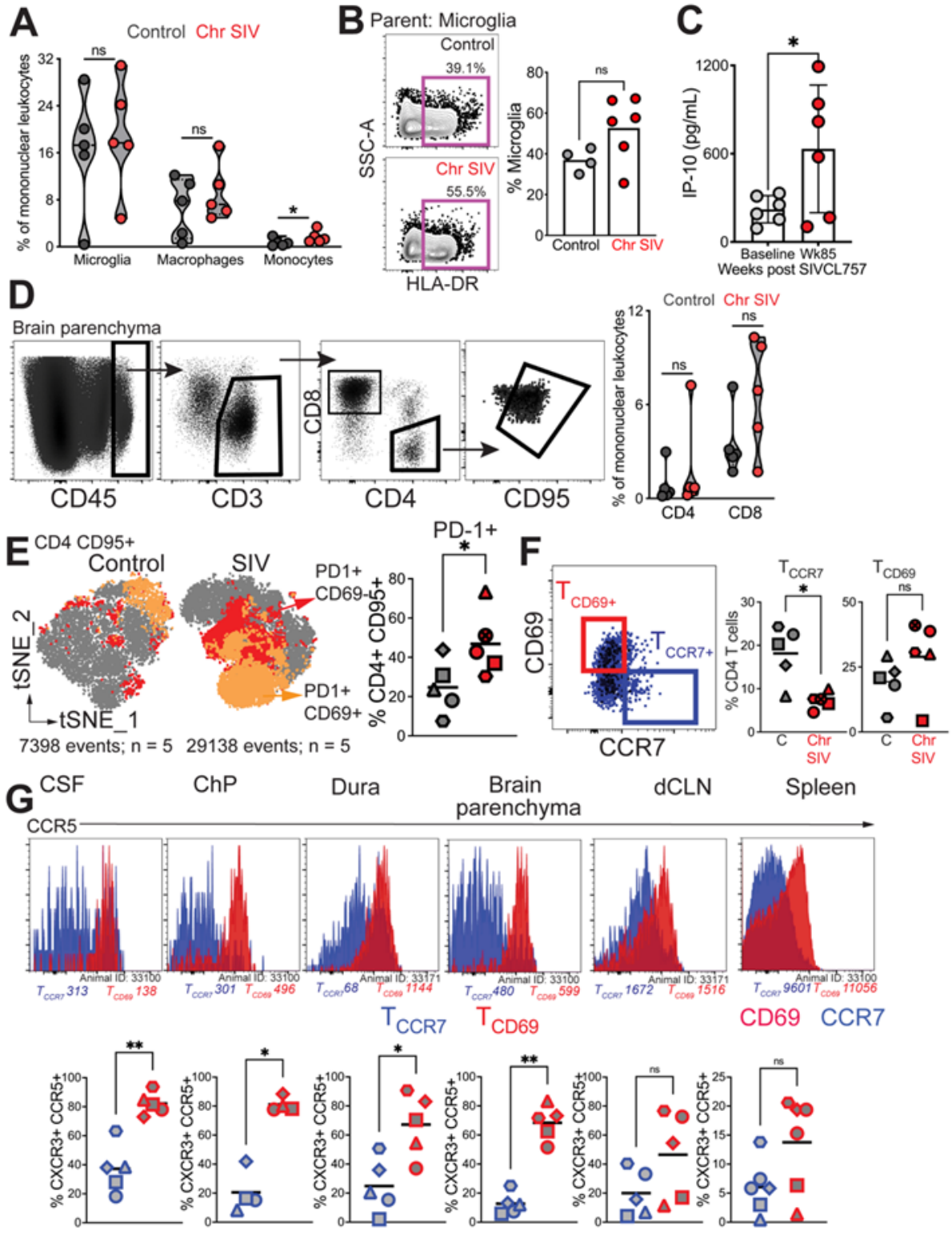

Figure 9. CCR7+ CD4 T cell frequencies decreased during SIV-induced neuroinflammation.

(A) Frequencies of Myeloid (microglia, macrophage, and monocytes) within the control (black)

and chronically infected SIV brain (red). **(B)** Representative flow plot illustrating HLA-DR expression on microglia cells (left); Frequency of HLA-DR expression (right). **(C)** IP-10 concentration within the rhesus CSF between baseline (grey) and chronic SIV CL757 infection (red; week 85). **(D)** Representative flow plots show CD4 and CD8 T cells in brain (left) and scatter plot shows frequencies (right). (**E**) t-SNE plot shows distribution of PD-1+ cells control and SIV brain (left) and scatter plot shows significantly higher PD-1+ frequencies with chronic SIV (right). **(F)** Representative flow plots depict gating strategy for T_{CD69+}(red gate) and T_{CCR7+} (blue gate) populations (left); Frequencies of T_{CCR7} and T_{CD69} populations (right) in the control (grey) and chronic SIV CL757 (red) infected brain. (**G**) Histogram plots indicating CCR5 expression and MFI (top) on T_{CCR7} (blue) and T_{CD69} (red); Frequencies of CXCR3+CCR5+ within T_{CCR7} and T_{CD69} across the CSF, Choroid plexus (ChP), Dura, Brain Parenchyma, deep cervical lymph node (dCLN) and spleen.

S1 Table. NHP cohort for chronic SIV study (SIVCL757)

Animal ID	Infection status	Age at Euthanasia(years:months:day)	Sex	Weight (kg)	TRIM5	ART regimen
33100	Uninfected	20:07:09	**F**	**12.32**	TFP/Q	N/A
33171	Uninfected	20:06:27	F	9.27	TFP/TFP	N/A
33980	Uninfected	19:06:26	F	9.6	TFP/TFP	N/A
33994	Uninfected	19:06:16	F	10.31	TFP/TFP	N/A
34194	Uninfected	19:06:16	F	11.84	TFP/TFP	N/A
35886	SIVCL757	17:05:27	F	9.11	TFP/Q	FTC/TDF/DTG
35595	SIVCL757	17:07:17	F	11.9	Q/CypA	FTC/TDF/DTG
34974	SIVCL757	17:08:22	F	8.94	TFP/Q	FTC/TDF/DTG
32967	SIVCL757	20:07:21	F	13.06	TFP/TFP	FTC/TDF/DTG
33191	SIVCL757	20:07:02	F	11.06	TFP/TFP	FTC/TDF/DTG
34996	SIVCL757	18:06:20	F	11.46	N/A	FTC/TDF/DTG

SIV: Simian Immunodeficiency Virus; ART: Anti-Retroviral Therapy; FTC: Emtricitabine; TDF: Tenofovir disoproxil fumarate; DTG: Dolutegravir.

S2 Table. Nonhuman primate cohort for tissue assessment during medculls/necropsies

Animal ID	Sex	Age (years.months)	Weight (kg)	Infection status	Study Treatments	Euthanasia timepoint at weeks post-infection	Medcull Condition
38163	F	15.07	7.48	Uninfected	N/A	N/A	N/A
40691	M	12.08	12.18	Uninfected	N/A	N/A	N/A
38691	F	14.11	13.56	Uninfected	N/A	N/A	N/A
40499	F	12.11	9.79	Uninfected	N/A	N/A	N/A
45721	M	5.06	14.75	Uninfected	FTY720	N/A	N/A
45781	M	5.06	8.66	Uninfected	FTY720	N/A	N/A
46235	M	4.07	14	Uninfected	FTY720	N/A	N/A
46354	M	4.06	10.96	Uninfected	FTY720	N/A	N/A
46410	M	4.06	12.7	Uninfected	FTY720	N/A	N/A
46548	M	4.05	8.25	Uninfected	FTY720	N/A	N/A
46551	M	4.05	8.59	Uninfected	FTY720	N/A	N/A
47081	F	3.06	5.28	Uninfected	FTY720	N/A	N/A
47154	M	3.06	8.63	Uninfected	FTY720	N/A	N/A
47161	M	3.06	9.32	Uninfected	FTY720	N/A	N/A
47387	F	3.05	7.85	Uninfected	FTY720	N/A	N/A
47466	M	3.04	7.04	Uninfected	FTY720	N/A	N/A
34051	F	20.00	6.97	Uninfected	N/A	N/A	N/A
35488	F	18.01	8.54	Uninfected	N/A	N/A	N/A
36798	F	16.11	10.31	Uninfected	N/A	N/A	N/A
37164	F	16.01	10.83	Uninfected	N/A	N/A	N/A
40234	F	12.11	8.72	Uninfected	N/A	N/A	N/A
40742	M	12.00	11.81	Uninfected	N/A	N/A	N/A
41217	F	11.11	10.77	Uninfected	N/A	N/A	N/A
41812	F	11.00	6.51	Uninfected	N/A	N/A	N/A
25888	F	29.01	9.92	Uninfected	N/A	N/A	N/A
33374	F	19.08	6.64	Uninfected	N/A	N/A	N/A
35328	M	17.03	11.22	Uninfected	N/A	N/A	N/A
47862	M	0.08	1.27	Uninfected	N/A	N/A	CHRONIC DIARRHEA
42318	F	10.11	8.25	Uninfected	N/A	N/A	NX (UNRELATED PROJECT)
39157	F	11.08	8.88	Uninfected	N/A	N/A	BILATERAL RENAL FAILURE
35115	M	16.08	12.12	Uninfected	N/A	N/A	BILATERAL ARTHRITIS STIFLES
44003	F	5.11	5.5	Uninfected	N/A	N/A	BILATERAL ARTHRITIS STIFLES
44510	M	5.09	7.47	Uninfected	N/A	N/A	REGENERATIVE JOINT DISEASE - STIFLES
44288	F	5.01	4.9	Uninfected	N/A	N/A	TRICHOBEZOAR; CHRONIC ULCERATIVE GASTRITIS
41647	M	8.11	9.18	Uninfected	N/A	N/A	HEPATIC AMYLOID
46078	F	19.07	6.19	Uninfected	N/A	N/A	HEMOABDOMEN
33100	F	20.07	12.32	Uninfected	N/A	N/A	N/A
33171	F	20.07	9.27	Uninfected	N/A	N/A	N/A
33980	F	19.07	9.6	Uninfected	N/A	N/A	N/A
33994	F	19.06	10.31	Uninfected	N/A	N/A	N/A
34194	F	19.06	11.84	Uninfected	N/A	N/A	N/A
35886	F	17.06	9.11	SIVCL757	Embicitrabine, Tenofovir Disproxil Fumarate, Dolutegravir (ART)	121	N/A
35595	F	17.08	11.9	SIVCL757	Embicitrabine, Tenofovir Disproxil Fumarate, Dolutegravir (ART)	121	N/A
34974	F	17.09	8.94	SIVCL757	Embicitrabine, Tenofovir Disproxil Fumarate, Dolutegravir (ART)	78	BICAVITARY EFFUSION
32967	F	20.08	13.06	SIVCL757	Embicitrabine, Tenofovir Disproxil Fumarate, Dolutegravir (ART)	121	N/A
33191	F	20.07	11.06	SIVCL757	Embicitrabine, Tenofovir Disproxil Fumarate, Dolutegravir (ART)	121	N/A
34996	F	18.07	11.46	SIVCL757	Embicitrabine, Tenofovir Disproxil Fumarate, Dolutegravir (ART)	121	N/A

S3 Table. Key reagents and resources

REAGENT or RESOURCE	SOURCE	IDENTIFIER
Antibodies		
Mouse anti-Human CXCR3 (Clone:1C6/CXCR3) - APC	BD Biosciences	Cat# 550967; RRID: AB_398481
Mouse anti-Human CD16 (Clone:3G8) - APC	BD Biosciences	Cat# 561248; RRID: AB_10612010
Mouse anti-Human CD49d (Clone: HP2/1) - APC	Beckman Coulter	Cat# B01682; RRID: AB_398681
Mouse anti-Human CD28 (Clone: 28.2) - APC-Cy7	BioLegend	Cat# 302966; RRID: AB_2800753
Mouse anti-Human CD3 (Clone: SP34-2) - APC-Cy7	BD Biosciences	Cat# 557757; RRID: AB_396863
Mouse anti-Human CD20 (Clone: 2H7) - APC-Cy7	BioLegend	Cat# 302314; RRID: AB_314262
Mouse anti-Human KI-67 (Clone: B56) - Alexa Fluor 488	BD Biosciences	Cat#558616; RRID: AB_10611866
Mouse anti- Non-Human Primate CD45 (Clone: D058-1283) - Alexa Fluor 488	BD Biosciences	Cat# 557803; RRID: AB_396879
Mouse anti-Human BCL2 (Clone: Bcl-2/100) - Alexa Fluor 647	BD Biosciences	Cat# 563600; RRID: AB_2738306
Mouse anti-Human IL-21 (Clone:3A3-N2.1) - Alexa Fluor 647	BD Biosciences	Cat# 560493; RRID: AB_1645421
Mouse anti-Human CD3 (Clone: SP34-2) - Alexa Fluor 700	BD Biosciences	Cat#557917; RRID: AB_396938
Mouse anti-Human CD14 (Clone: M5E2) - Alexa Fluor 700	BioLegend	Cat# 301822; RRID: AB_493747
Rat anti-Human CCR7 (Clone:3D12) - PE	BD Biosciences	Cat# 552176; RRID: AB_394354
Mouse anti-Human CD163 (Clone: GHI/61) - PE	BioLegend	Cat# 333606; RRID: AB_1134002
Mouse anti-Human IL-21 (Clone:3A3-N2.1) - PE	BD Biosciences	Cat# 562042; RRID: AB_10896123
Mouse anti-Human CD21 (Clone: Bly-4) - PE-Cy7	BD Biosciences	Cat# 561374; RRID: AB_10681717
Mouse anti-Human CD103 (Clone: Ber-Act8) - PE-Cy7	BioLegend	Cat# 350212; RRID: AB_10782579
Mouse anti-Human CD11C (Clone: 3.9) - PE-Cy7	Invitrogen	Cat# 25-0116-42; RRID: AB_1582274
Mouse anti-Human EOMES (Clone: WD1928) - PE-Cy7	ThermoFisher	Cat# 25-4877-42; RRID: AB_2573456
Mouse anti-Human CD127 (Clone: eBioRDR5) - PE-Cy7	ThermoFisher	Cat# 25-1278-42; RRID: AB_1659672
Mouse anti-Human IFN-g (Clone: B27) - PE-Cy7	BioLegend	Cat# 506518; RRID: AB_2123321
Mouse anti-Human CCR6 (Clone: G034E3) - PE-CF594	BioLegend	Cat# 353430; RRID: AB_2564233
Mouse anti-Human CD40 (Clone: 5C3) - PE-CF594	BioLegend	Cat# 334342; RRID: AB_2566457
Mouse anti-Human IL-2 (Clone:MQ1-17H12) - PE-CF594	BioLegend	Cat# 500344; RRID: AB_2564091
Mouse anti-Human TNFA (Clone: MAb11) - FITC	BioLegend	Cat# 502906; RRID: AB_315258
Mouse anti-Human CXCR3 (Clone: 1C6/CXCR3) - BV421	BD Biosciences	Cat# 562558; RRID: AB_2737653
Mouse anti-Human FOXP3 (Clone: 206D) - BV421	Biolegend	Cat# 320124; RRID: AB_2565972
LIVE/DEAD Fixable Aqua Dead Cell Stain Kit - BV510	Life Technologies	Cat# L34966; RRID: N/A
Mouse anti-Human CD11b (Clone: ICRF44) - BV510	BD Biosciences	Cat# 563088; RRID: AB_2737996
Mouse anti-Human CD8 (Clone: SK1) - BV510	BD Biosciences	Cat# 563919; RRID: AB_2722546
Mouse anti-Non-Human Primate CD45 (Clone: D058-1283) - BV605	BD Biosciences	Cat# 564098; RRID: AB_2738590
Mouse anti-Human CCR4 (Clone: 1G1) - BV605	BD Biosciences	Cat# 562906; RRID: AB_2737882
Mouse anti-Human CD4 (Clone: L200) - BV650	BD Biosciences	Cat# 563737; RRID: AB_2687486
Mouse anti-Human CCR5 (Clone: 3A9) - BV650	BD Biosciences	Cat# 564999; RRID: AB_2739037
Mouse anti-Human CD69 (Clone: FN50) - BV711	BioLegend	Cat# 310944; RRID: AB_2566466
Rat anti-Human CX3CR1 (Clone:2A9-1) - BV711	BioLegend	Cat# 341630; RRID: AB_2814256
Mouse anti-Human CD95 (Clone: DX2) - BUV737	BD Biosciences	Cat# 564710; RRID: AB_2738907

Rat anti-Human CX3CR1 (Clone:2A9-1) - BV711	BioLegend	Cat# 341630; RRID: AB_2814256
Mouse anti-Human CD95 (Clone: DX2) - BUV737	BD Biosciences	Cat# 564710; RRID: AB_2738907
Armenian Hamster anti-Human/Mouse/Rat ICOS (Clone: C398.4A) - BV785	BioLegend	Cat# 313534; RRID: AB_2629729
Mouse anti-Human CCR5 (Clone: 3AG) - BV786	BD Biosciences	Cat# 565001; RRID: AB_2739039
Mouse anti-Human HLA-DR (Clone: L243) - BV786	BioLegend	Cat# 307642; RRID: AB_2563461
Mouse anti-Human CD8 (Clone: SK1) - BUV805	BD Biosciences	Cat# 564913; RRID: AB_2833078
Mouse anti-Human PD-1 (Clone: EH12.2H7) - Pacific Blue	BioLegend	Cat# 329916; RRID: AB_2283437
LIVE/DEAD Fixable Near-IR Dead Cell Stain Kit	Life Technologies	Cat# L34976; RRID: N/A
Mouse anti-Human CD45 (Clone: 2B11+PD7/26)	Novus	Cat# NBP2-34528AF647; RRID: AB_960384
Rat anti-Human CD3 (Clone: CD3-12)	Bio-Rad	Cat# MCA1477; RRID: AB_321245
Rabbit anti-NeuN (Clone: polyclonal)	Millipore Sigma	Cat# ABN78; RRID: AB_10807945
Goat anti-Rat IgG (H+L) Crossed Adsorbed secondary Antibody, Alexa Fluor 594	ThermoFisher	Cat# A-11007; RRID: AB_10561522
Syto83	ThermoFisher	Cat# S11364; RRID: N/A
Rabbit anti-Human CD3 (Clone: polyclonal)	Agilent	Cat# A045229-2; RRID: AB_2335677
Mouse anti-Human CD4 (Clone: OTI5D9)	Novus	Cat# NBP2-46149; RRID: N/A
Rabbit anti-Human CD11b (polyclonal)	Invitrogen	Cat# PA5-29633; RRID: AB_2547108
Rabbit anti-Human CD45 (Clone: polyclonal)	Abcam	Cat# ab10558; RRID: AB_442810
Rabbit anti-Human IBA1 (Clone: HL22)	Invitrogen	Cat# MA5-36257; RRID: AB_2890455
Rabbit anti-Human NeuN (Clone: EPR12763)	Abcam	Cat# ab177487; RRID: AB_2532109
Purified NA/LE Mouse anti-Human CD49d (Clone: 9F10)	BD Biosciences	Cat# 555501; RRID: AB_2130052
Purified NA/LE Mouse anti-Human CD28 (Clone: CD28.2)	BD Biosciences	Cat# 555725; RRID: AB_396068

Bacterial and virus strains

SIVsm804e-CL757	Dr. Vanessa Hirsch, NIAID	doi: 10.1371/journal.ppat.1006538

Biological samples

Rhesus macaque biological fluids (Blood and Cerebrospinal Fluid)	CNPRC, UC Davis	N/A
Rhesus macaque tissues (Brain tissue, pituitary gland, dura mater, choroid plexus, skull bone marrow, draining cervical lymph node, thoracic lymph node, fine needle axillary lymph node aspirates, spleen)	CNPRC, UC Davis	N/A
Formalin fixed and paraffin embedded human hippocampal tissue from non-demented anonymous human patients	Netherlands Brain Bank	N/A
Formalin fixed and paraffin embedded human hippocampal tissue from an anonymous human patient with glioblastoma	Netherlands Brain Bank	
Formalin Fixed and paraffin embedded human tonsil tissue	Cancer Center Repository, UC Davis	N/A

Chemicals, peptides, and recombinant proteins		
Brilliant Stain Buffer plus	BD Biosciences	Cat# 566385
BD FACS Lysing Solution	BD Biosciences	Cat# 349202
BD Cytofix/CytoPerm	BD Biosciences	Cat# 51-2090KZ
BD Perm/Wash	BD Biosciences	Cat# 51-2091KZ
eBioscience Foxp3/Transcription staining buffer set	Invitrogen	Cat# 00-5523-00
Protein Transport Inhibitor Containing Brefeldin A (BD GolgiPlug)	BD Biosciences	Cat# 555029
Protein Transport Inhibitor Containing Monensin (BD GolgiStop)	BD Biosciences	Cat# 554724
Gill's Hemotoxylin I	StatLab	Cat# HXGH1LT
Collagenase Type 4 (265 u/mg dw)	Worthington Biochemical Corporation	Cat# LS004188
DNase I Recombinant, RNase-free	Roche Diagnostics	Cat# 04716728001
Embicitrabine	Gilead Sciences	Cat# GS-9019
Tenofovir Disproxil Fumarate	Gilead Sciences	Cat# GS-4331
Dolutegravir (GSK Comet)	GSK plc	Cat# GSK1349572A
Hydroxypropylbetadex (Kleptose HPB)	Roquette	Cat# 346113102B
FTY720	Millipore Sigma	Cat# SMLO700
Critical commercial assays		
T cell activation/Expansion Kit, non-human primate	Miltenyi Biotec	Cat# 130-092-919
eBioscience Cell Stimulation Cocktail	Invitrogen	Cat# 00-4970-93
LEGENDplex NHP Inflammation Panel (13-plex)	BioLegend	Cat# 740389
CD45 microbeads, non-human primate	Miltenyi Biotec	Cat# 130-091-899
Chromium Next GEM Single Cell 3' GEM, Library & Gel Bead Kit v3.1	10X Genomics	Cat# PN-1000121
Chromium Nuclei Isolation Kit with RNase Inhibitor	10X Genomics	Cat# PN-1000494
Chromium Next GEM Single Cell Multiome ATAC + Gene Expression Reagent Bundle	10X Genomics	Cat# PN-1000283
Deposited data		
Single Cell RNA Sequencing Results	This paper	GEO Accession: GSE221815
Experimental models: Organisms/strains		
Rhesus macaque (Macaca Mulatta)	CNPRC, UC Davis	N/A
Oligonucleotides		
Software and algorithms		
GraphPad Prism (Version 9.5.1)	GraphPad	https://www.graphpad.com/
FACS Diva (Version 8.0.1)	BD Biosciences	https://www.bdbiosciences.com/en-us/products/software/instrument-software
FlowJo (Version 10.8.1)	FlowJo LLC	https://www.flowjo.com/
FlowSOM (Version 2.4.0)	Van Gassen et al. (doi: 10.1002/cyto.a.22625.)	https://bioconductor.org/packages/release/bioc/html/FlowSOM.html
R (Version 4.2.1)	R Core Team	https://www.r-project.org/
CellRanger (Version 7.0.1)	10X Genomics	https://support.10xgenomics.com/single-cell-gene-expression/software/pipel
Seurat (Version 4.3.0)	Hao et al. (doi: 10.1016/j.cell.2021.04.048.); Stuart et al. (doi: 10.1016/j.cell.2019.05.031)	https://satijalab.org/seurat/

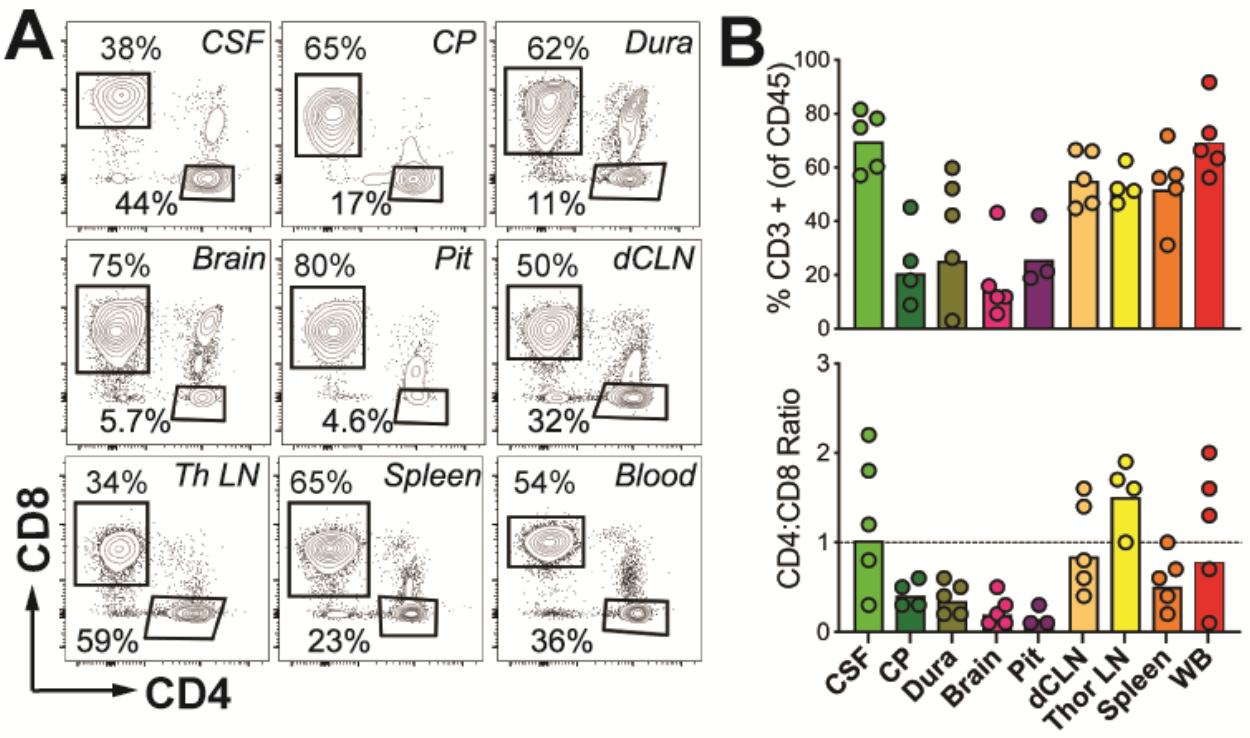

Figure S1. Distribution of CD4 and CD8 T cells in brain parenchyma and its border tissues, **Related to Figure 1** (**A**) Illustrates CD4 and CD8 T cell frequencies (gated on CD3+ cells) in various tissues as indicated. CSF, cerebrospinal fluid; CP, choroid plexus; Dura, Dura mater; Pit, Pituitary; dCLN, deep cervical lymph nodes, Th LN, thoracic lymph nodes. (**B**) bar graphs show % CD3+ T lymphocytes and CD4: CD8 ratios across CNS and lymphoid tissues.

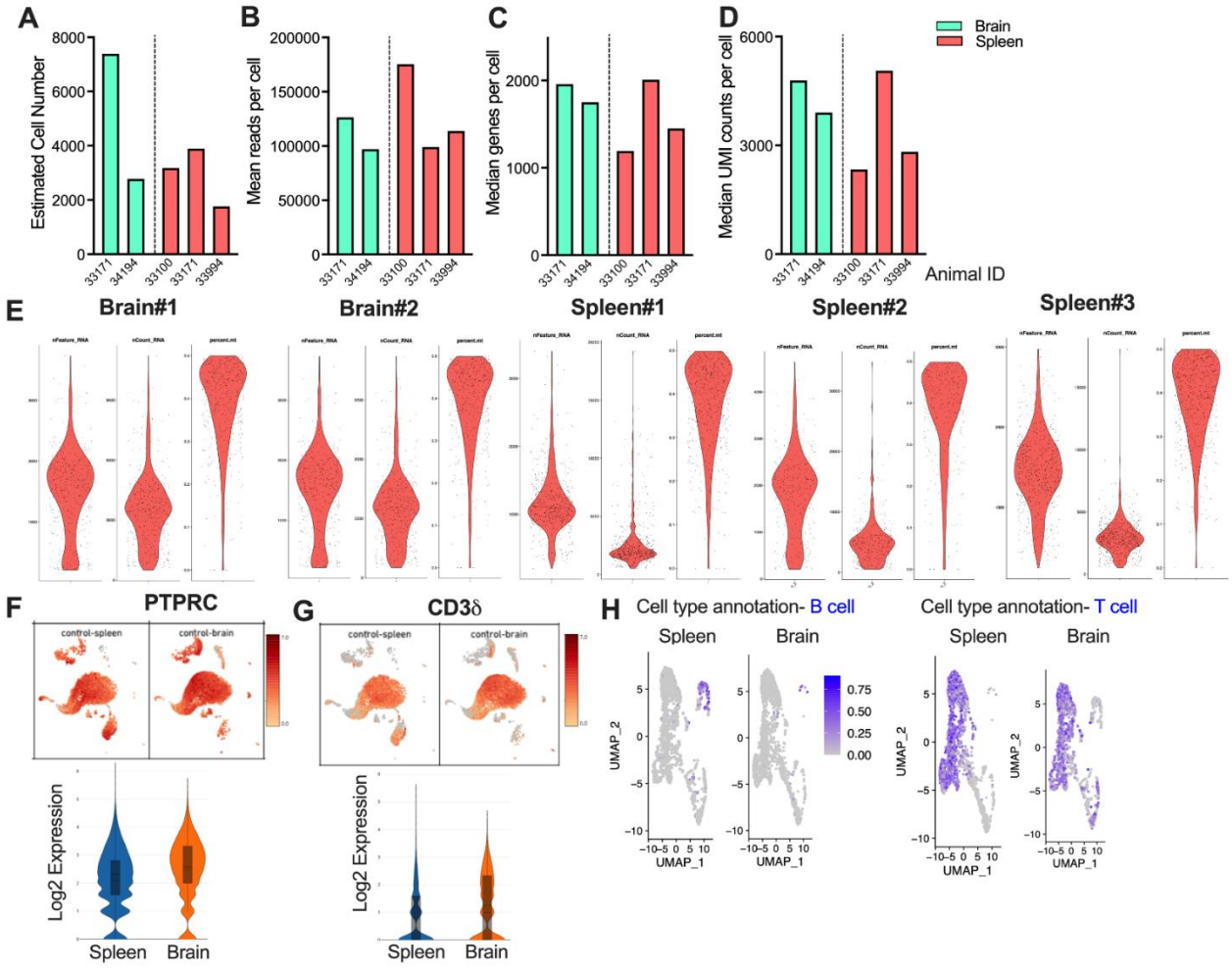

Figure S2. Single-cell transcriptomic analyses of CD45+ immune cells reveal presence of core T cell molecular programs in brain, related to Figure 1. (**A**) lists cell numbers sequenced for each sample. (**B-D**) Mean, median reads per cell and UMI counts per cell. (**E**) quality metrics on each sample. (**F**) Expression profile of PTPRC shown in UMAPs and violin plots. (**G**) Expression profile of CD3δ subunit shown in UMAPs and violin plots. (**H**) UMAP plots show cell type annotation for B cells and T cells across tissue types.

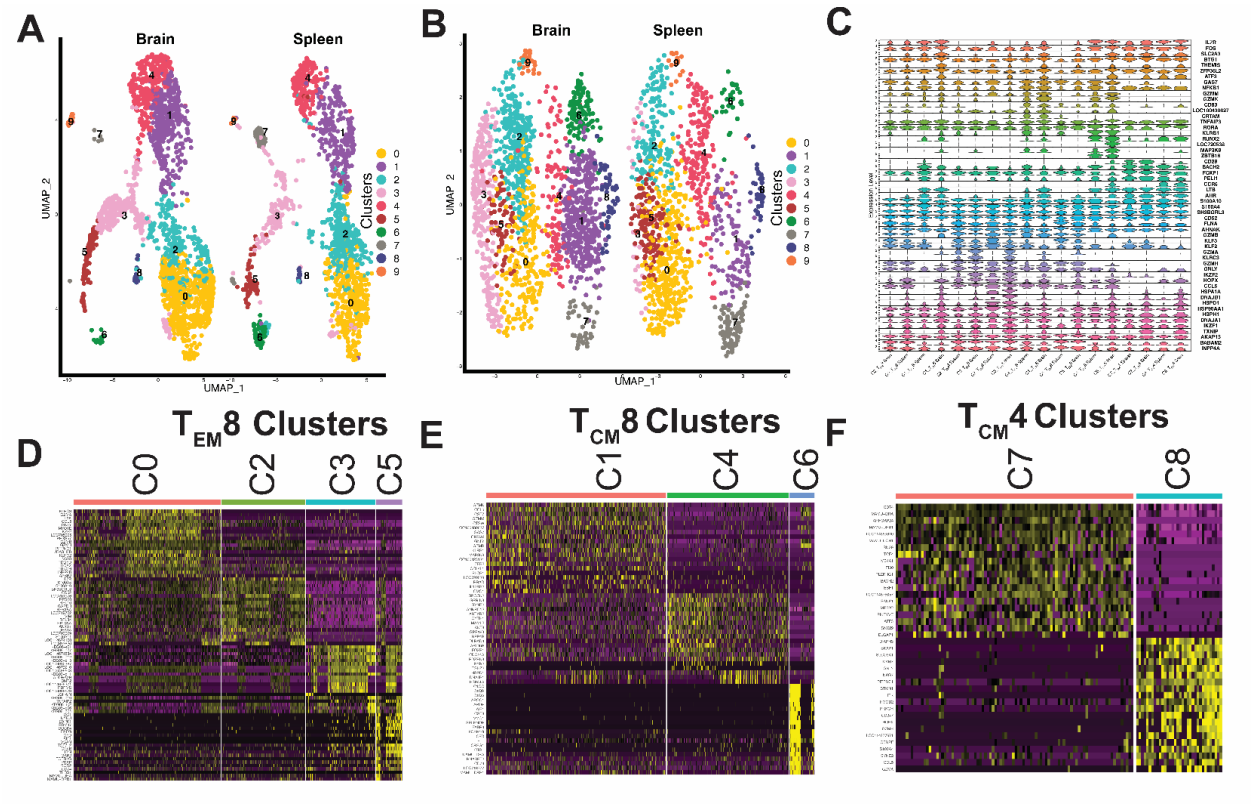

Figure S3. Single-cell transcriptomic analyses of CD45+ immune cells reveal presence of core T cell molecular programs in brain, related to Figure 1. (**A**) UMAP of scRNA seq transcriptome profiles color coded according to assigned cell types by tissue- brain (2137 cells) and spleen (1569 cells). (**B**) UMAP of T cell subclusters color coded according to assigned cell types by tissue - brain (1619 cells) and spleen (1159 cells). (**C**) Expression of top marker genes in each T cell cluster. (**D-F**) heat maps of gene expression within clusters demonstrate differential expression across clusters.

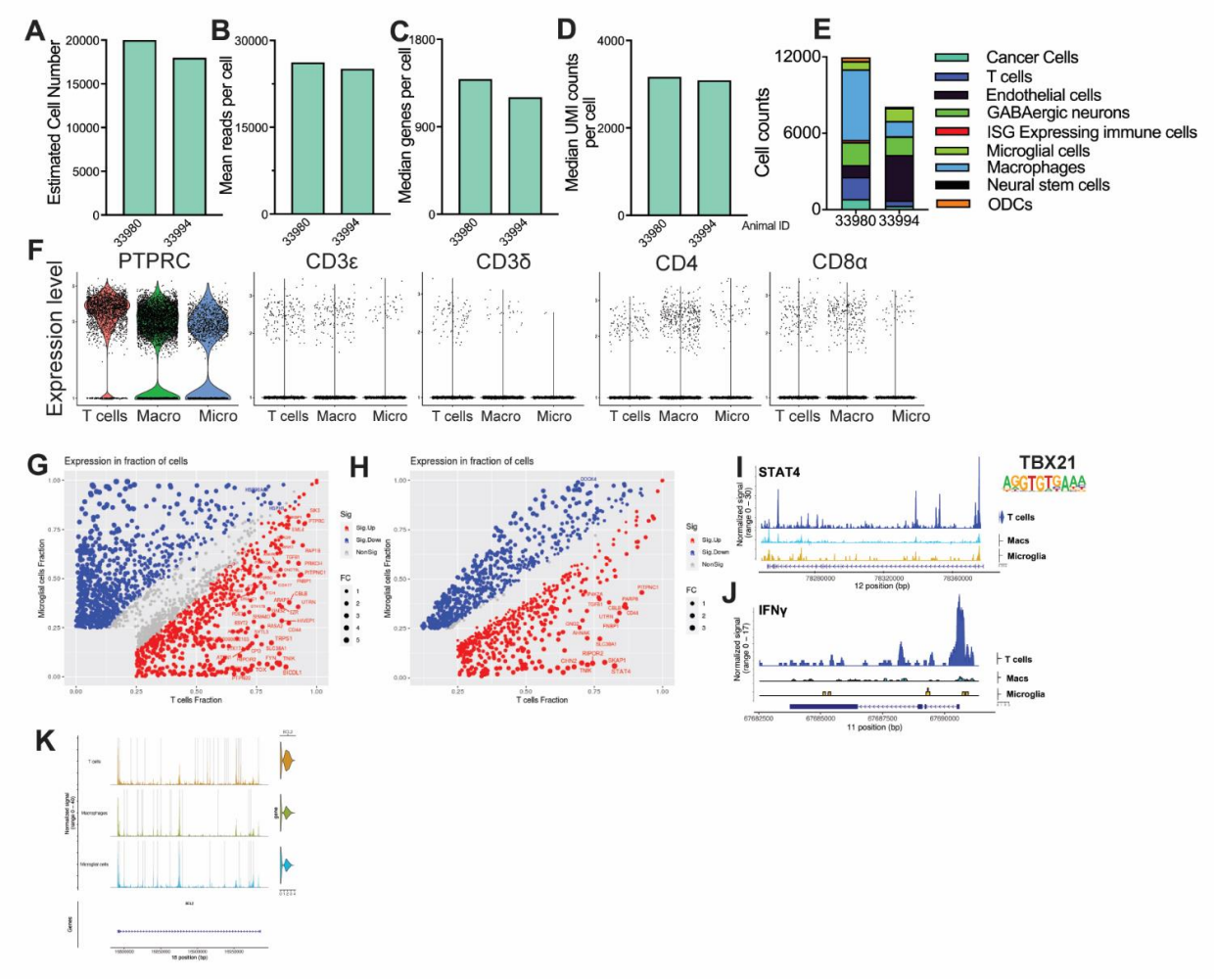

Figure S4. Single cell regulatory landscape of T cells and brain resident microglia, related to Figure 2. (**A**) lists cell numbers sequenced for each sample. (**B-D**) Mean, median reads per cell and UMI counts per cell. (**E**) Cell counts for each cluster shown per sample. (**F**) Expression profile of PTPRC shown in UMAPs and violin plots. Scatter plots show proportion and intensity of gene expression comparing (**G**) Microglia to T cells. (**H**) Macrophage to T cells. (**I-K**) Genomic regions showing snATAC-seq tracks of chromatin accessibility of STAT4, IFN-γ, and BCL-2.

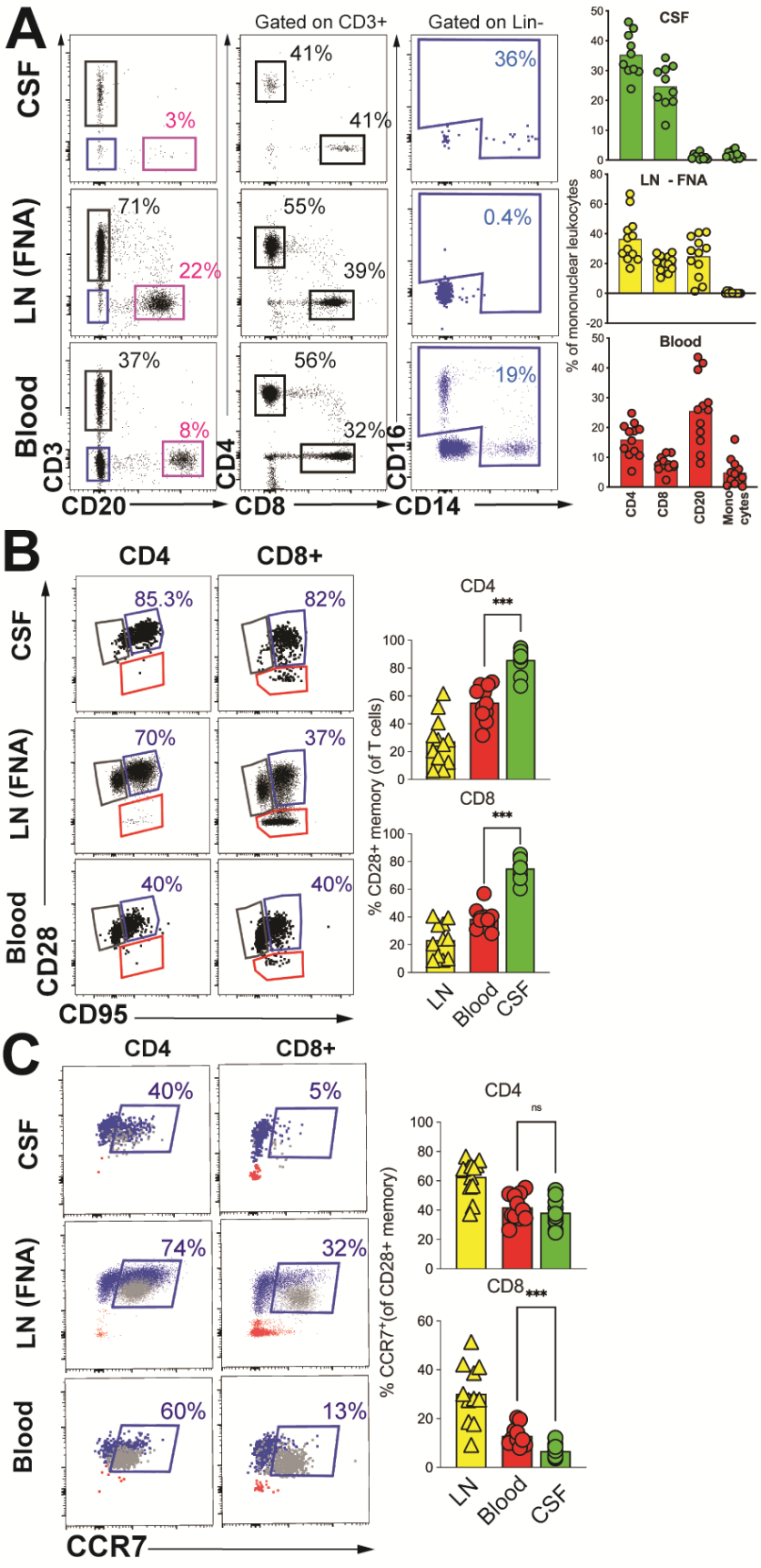
A
Gated on CD3+
Gated on Lin-
CSF
LN (FNA)
Blood
CD3
CD20
CD4
CD8
CD16
CD14
41%
41%
36%
3%
71%
55%
0.4%
22%
39%
37%
56%
19%
8%
32%
CSF
LN - FNA
Blood
% of mononuclear leukocytes
CD4
CD8
CD20
Monocytes
B
CD4
CD8+
CSF
LN (FNA)
Blood
CD28
CD95
85.3%
82%
70%
37%
40%
40%
CD4
CD8
***
% CD28+ memory (of T cells)
LN
Blood
CSF
C
CD4
CD8+
CSF
LN (FNA)
Blood
CCR7
40%
5%
74%
32%
60%
13%
CD4
ns
CD8
***
% CCR7+(of CD28+ memory)
LN
Blood
CSF

Figure S5. CCR7^{+} CD4 T cells in the CNS share phenotypic features with T_{CM} in blood and lymph nodes, related to Figure 3. (A) Representative flow plots identifying CD3 T cells, CD20 B cells, CD4 T cells, CD8 T cells and Monocytes (Left) and their frequencies (Right) in the CSF, Lymph node Fine Needle Aspirate (LN FNA), and Blood of healthy rhesus macaques. CSF: n=10; LN-FNA: n =12; Blood: n=12 **(B)** Representative flow plots identifying expression of CD28 and CD95 on CD4 and CD8 T cells (Left) and their frequencies (Right) from the CSF, LN (FNA), and Blood. **(C)** Representative flow plots identifying CCR7 expression on CD28+ CD4 and CD28+ CD8 T cells (Left) and their frequencies in the CSF, Lymph node Fine Needle Aspirate (LN FNA), and Blood.

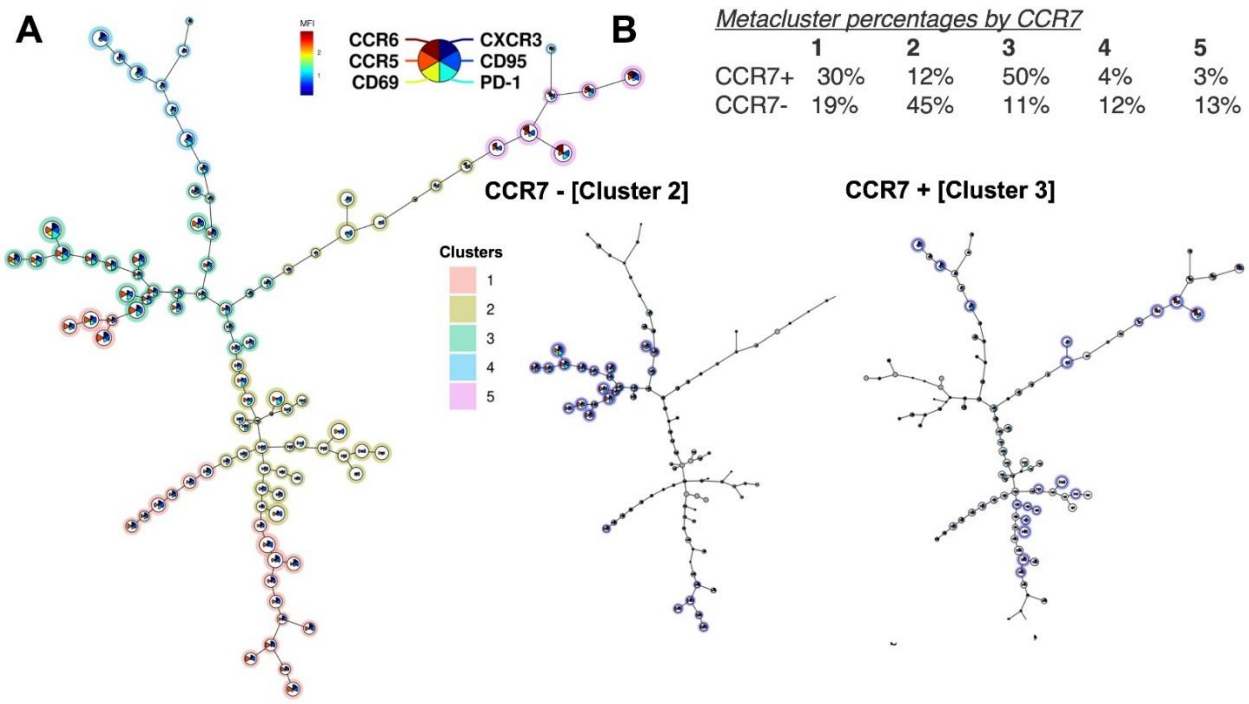

Figure S6. CCR7⁺ CD4 T cells in the CNS share phenotypic features with T_{CM} in blood and lymph nodes, related to Figure 3. (A) Minimal spanning tree constructed using the FlowSOM (self-organizing map) tool to map phenotypic relationships between live CD4 T cell isolated from healthy rhesus CSF. Star chart wedges denote expression of each indicated marker in cluster. Nodes indicate cellular cluster which are grouped into 5 larger Metaclusters indicated by color (metacluster 1: pink; metacluster 2; yellow; metacluster 3: green; metacluster 4: blue; metacluster 5: purple) which share similar phenotypes. Connections indicate phenotypically related cellular clusters. Nodes are represented as pie charts representing relative expression of chemokine and activation markers (CCR6, CCR5, CD69, CXCR3, CD95, PD-1) within a given cluster. **(B)** Minimal spanning trees highlighting in blue, clusters that contain CCR7- (top) and CCR7+ (bottom) CD4 T cell populations.

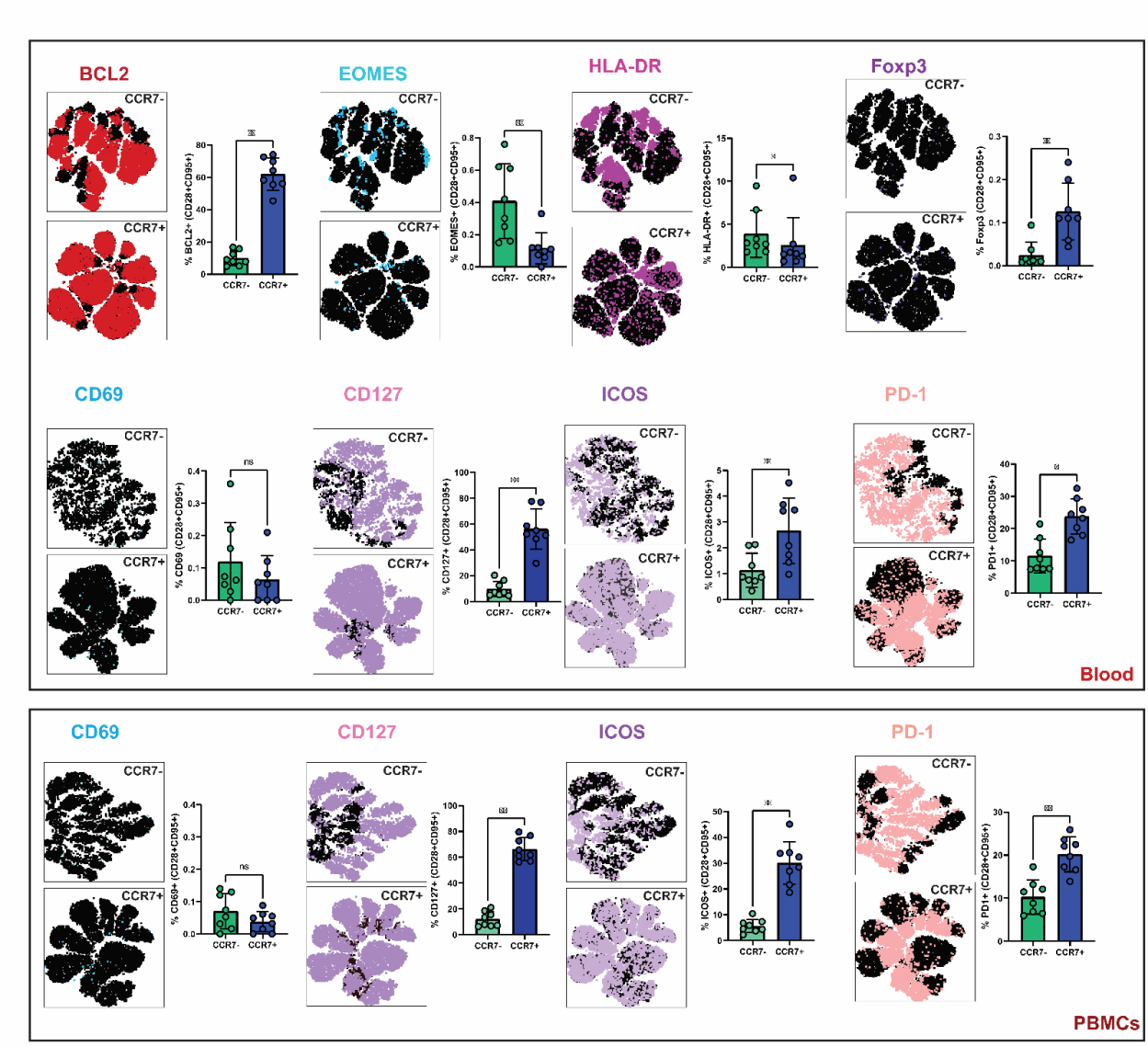

Figure S7. CCR7⁺ CD4 T cells in the CNS share phenotypic features with T_{CM} in blood and lymph nodes, related to Figure 3. Representative tSNE plot illustrating CD69, BCL2, CD69 (column 1), CCR5, EOMES, CD127 (Column 2), HLA-DR, ICOS (Column 3) , and CXCR3, Foxp3, PD-1 (Column 4) expression on CD4+CD28+CD95+ CCR7-/+ T cells in the CSF, Blood and PBMCs; frequencies for each population are expressed to the right of the tSNE plots.

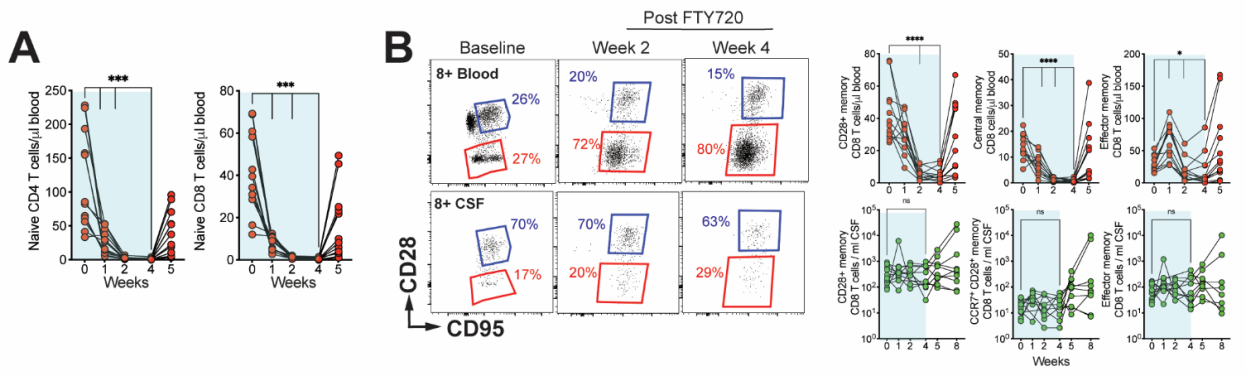

Figure S8. FTY720 mediated sequestration of CD4 T_{CM} in lymphoid tissues decreases CCR7^{+} CD4 T cell frequencies in CSF, related to Figure 4.(**A**) Frequencies of Naïve CD4 T cells and Naive CD8 T cells in the blood over the course of the study (**B**) Representative longitudinal flow plots indicating CD28 and CD95 expression on CD4 T cells from the blood (top row) or the CSF (bottom row) (Left); Frequencies of CD28+ memory CD8 T cells, Central Memory CD8 T cells, CCR7+CD28+ memory CD8 T cells, and Effector CD8 T cells in the blood and CSF over the course of the study

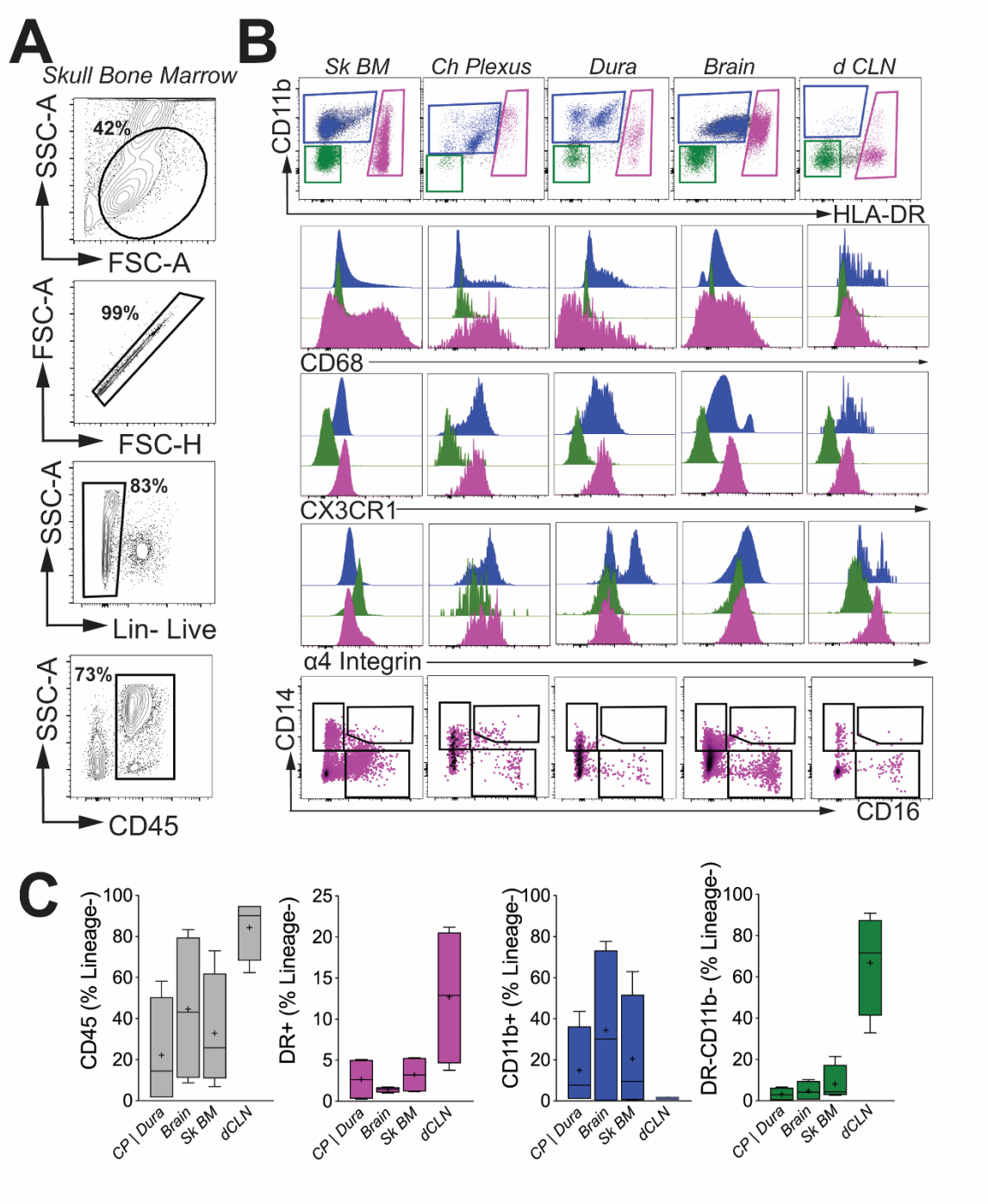

Figure S9. CCR7+ CD4 T cells in CNS exhibit functional T_{CM} features and reside within skull BM, related to Figure 5. Frequencies of Lineage (CD20/CD3/Dead) negative CD45+ cells (gray), MHC-II+ (DR) (pink), CD11b+ (blue), and DR-CD11b- cells within the choroid plexus (CP)/dura

mater (Dura), brain, skull BM (Sk BM), and draining cervical lymph node (dCLN). Box and whisker plots indicate medians with quartiles.

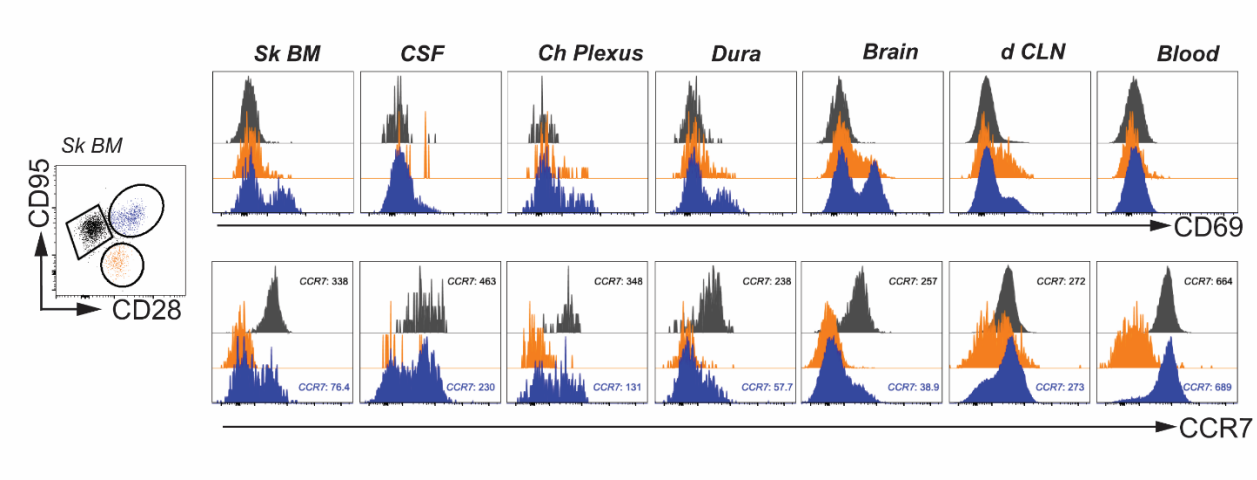

Figure S10. CD28+ CD4 T cells exhibit heterogeneity in the expression of CCR7 and CD69 in T_{CM} cells across the tissues, related to Figure 5. Representative flow plot of CD4+; CD95+CD28- (black), CD95+CD28+ (blue), and CD95-CD28+ (orange) cells from the skull BM; expression of CD69 and CCR7 shown by histogram for all 3 CD4 T cell subsets in the Skull BM, CSF, Choroid Plexus, Dura, Brain, Deep cervical lymph node, and blood.

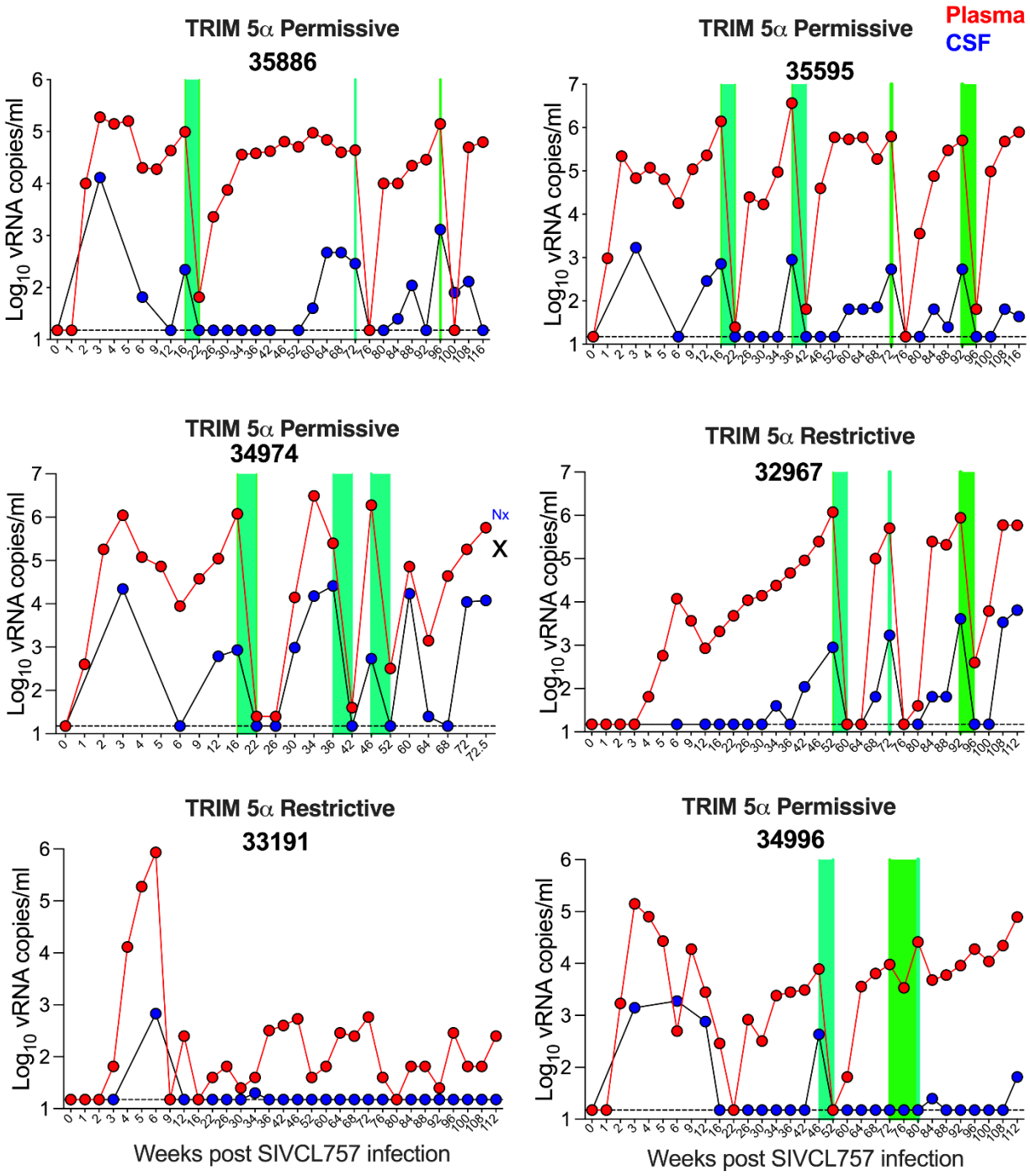

Figure S11. Longitudinal Plasma and CSF viral loads, related to Figure 6. Kinetics of vRNA in Plasma (red line) and CSF (blue) following SIVCL757 infection. Green bars indicate timing of antiretroviral therapy.

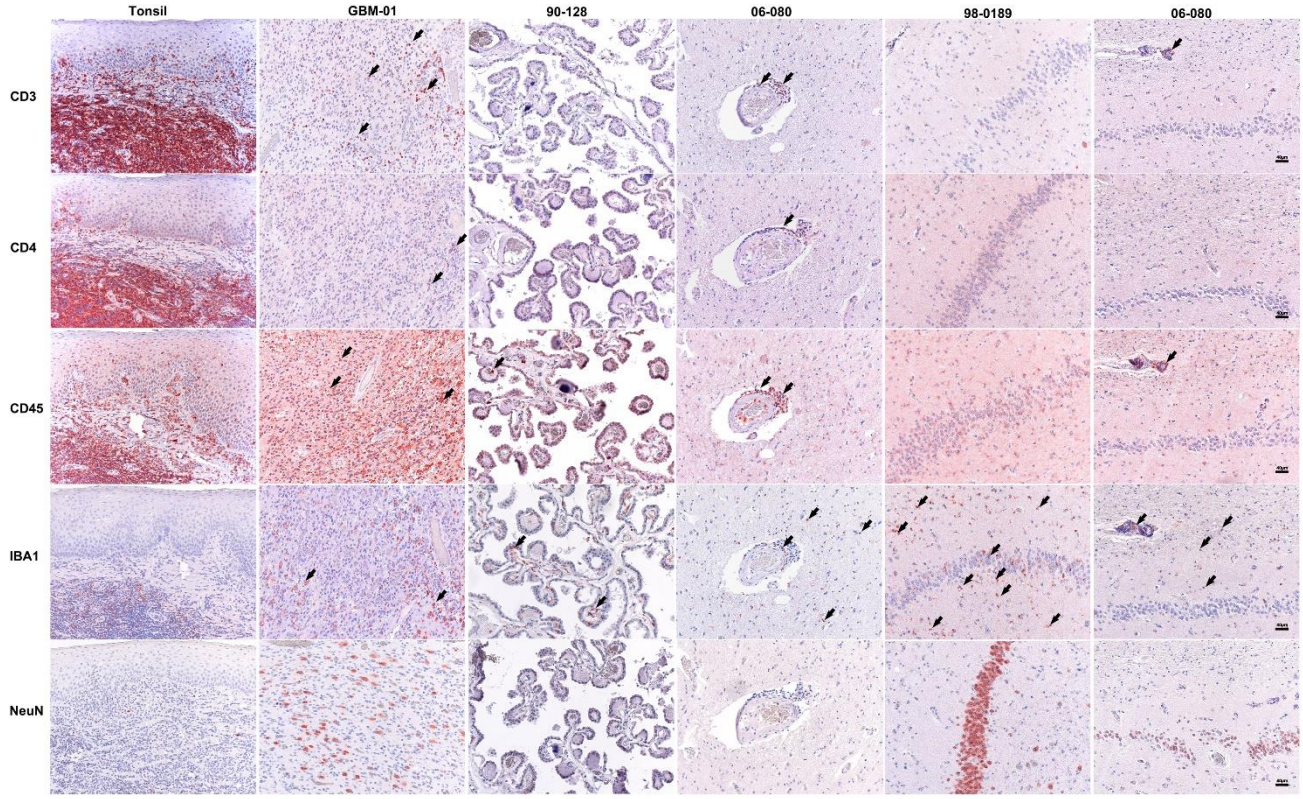

Figure S12. IHC reveals presence of T cells within the human brain, related to Figure 7. T lymphocytes are localized to blood vessel in the non-demented human brain. H&E with immunohistochemical staining of lymphocyte specific markers (CD3, CD4), myeloid/leukocyte specific markers (CD11b, CD45, IBA1) and neuron-specific markers (NeuN) from paraffin embedded human tonsil and brain tissues derived from either a patient with glioblastoma (Sample ID: GBM-01) or non-demented patients (Sample IDs: 90-128, 06-080, 98-0189, 06-080). Tissue/patient samples are organized by columns and immunohistochemical markers by row.

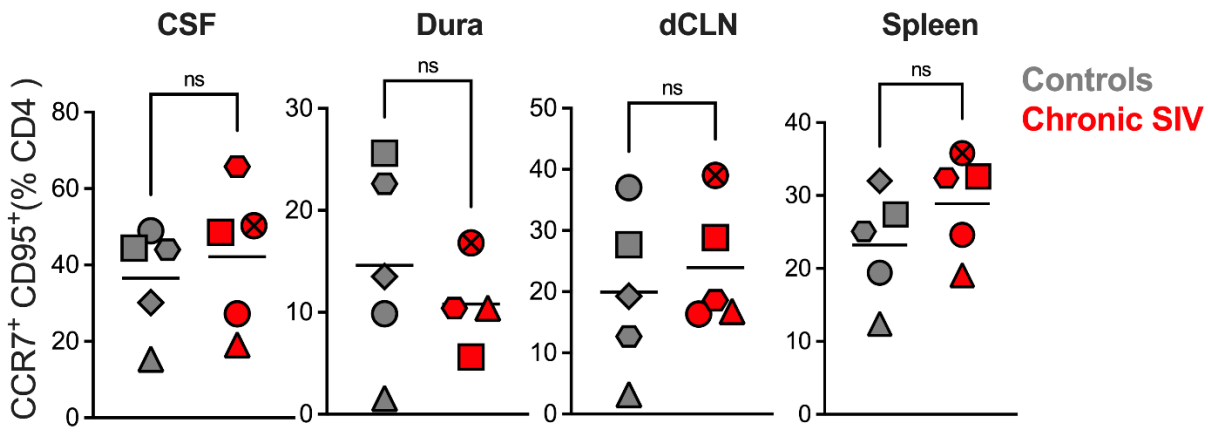

Figure S13. Preferential depletion of parenchymal CCR7+ CD4 T cells in chronic SIV infection, related to Figure 9. CCR7+ memory T cells in control (grey) and Chronic SIV infected (red) in the CSF, Dura, DCLN, and Spleen (left to right).

Conclusions and Future Directions

Historically, the HAND field concentrated on the involvement of myeloid cells in the development of HAND, due to early clinical observations of HIV+ myeloid cells in postmortem brain tissue of AIDS patients. These findings led researchers to recapitulate this etiology in SIV non-human primate models, primarily the rhesus macaque model. However, these early models had limitations, as they involved the experimental depletion of CD8 or CD4 T cells utilizing antibodies. This approach resulted in models that rapidly progressed to AIDS, with a high incidence of encephalitis and myeloid infection, all common hallmarks of HAND in the pre-ART era.

Today in 2024, the incidence of HAND remains just as high as it was in the pre-ART era (~50%). However, now PLWH experience milder forms of disease, likely attributable to the reduction in viral burden in the blood and CSF due to ART. When embarking on this project, our goal was to understand HAND in today's HIV patient. So, what has changed since the identification of the first case of HIV in 1981? One, today's PLWH on ART now maintain stable CD4 T cell counts. This is crucial to consider because CD4 T cells are primary targets for HIV infection, especially for transmitted/founder viruses which utilize CD4 as the primary receptor and CCR5 as a co-receptor for entry. Moreover, in the past two decades our understanding of how the immune system interphases with the brain has evolved dramatically. Noteworthy discoveries include the re-discovery of the meningeal lymphatics, highlighting the potential to generate immune responses to antigens derived from the CNS (2). Two, tissue resident memory T cells have been shown to localize to the human brain, suggestive of immune memory in a tissue once thought to be an immune privileged site (3). Third, T cells have been found to localize to other border tissues of the CNS such as the skull bone marrow, highlighting that not only the brain but other CNS tissues are surveyed and protected by T cells (4). Fourth, SIV infected T cells have been identified within the rhesus macaque CSF and these cells can infiltrate the brain during an

R5 tropic infection, setting a new precedent for T cell involvement in HIV-related neuroinflammation (5). Altogether, these insights set the stage for my focus on the role of CD4 T cells in neuroinflammation and HAND.

We first aimed to address the role of CD4 T cells in HAND by identifying a suitable model. Intravenous infection of rhesus macaques with SIVmac251 results in robust viral replication and systemic infection that naturally disseminates into both peripheral and CNS tissues causing pathology and neuropathology similar to that observed in humans. As previously mentioned, prior models utilized SIVmac251 infection paired with CD4/CD8 depletion antibodies to study HAND, however we and others note that T cell depletion is not necessary to establish viral replication in the CSF and CNS. We have identified viral dissemination throughout the brain parenchyma as early as 3 weeks post SIVmac251 infection without T cell depletion. Our major findings are graphically denoted in **Figure 1** below.

A major strength of this dissertation is the examination of lymphocytes within the non-human primate brain. Thanks to exceptional efforts of the pathology staff at the CNPRC, we were to conduct trans-cardiac saline perfusions, which enabled the precise isolation and identification of lymphocytes from the NHP brain without blood contamination. Moreover, our collaboration with the Dr. John Morrison and his Laboratory at the CNPRC has allowed us to expand our research to include lymphocytes in less studied CNS border tissues, including the dura mater, choroid plexus, and the skull bone marrow.

The research presented in this dissertation represents several achievements, notably conducting the first comprehensive analysis of lymphocytes in the primate CNS using advanced techniques such as flow cytometry, single cell RNA sequencing, and Nanostring Digital Spatial Profiling. Additionally, it marks the first thorough evaluation of CNS border tissues in the non-human primate brain. In Chapter II, we utilized bulk RNA sequencing and multi-parameter flow cytometry to identify gene and protein signatures consistent with innate (microglia, monocytes,

macrophages) and adaptive (T lymphocyte) cell signatures in discrete regions of the rhesus macaque brain, namely the prefrontal cortex and synapse-dense regions of the brain. This chapter also demonstrated the R5 tropic T/F viruses (SHIV.CH.505) can acutely establish viral infection of the CNS paired with gene signatures consistent with effector responses and neuroinflammation.

Chapter III demonstrates the presence of HIV target CD4+ CCR5+ T cells within the brain, choroid plexus, dura, and skull bone marrow at homeostasis in non-human primates. These findings are suggestive of a population of T cells within the CNS that are vulnerable to infection, may play a role in initiating neuroinflammation and potentially serve as long term reservoirs in chronic disease. Utilizing SIVmac251, another R5 tropic virus, we observed similarly to SHIVCH505 infection, an induction of acute viral dissemination to the brain parenchyma and adjacent border tissues. These findings revise our conceptual understanding of HIV dissemination to the CNS; they indicate that viral and inflammatory events are not confined to the brain alone. Rather, interactions between the brain and its surrounding border tissues may play a crucial role in regulating CNS inflammation and viral persistence. Moreover, this chapter shows that HIV transcripts can be identified in CD4 T cells within the brain during acute infection, despite their rarity in the brain, alluding to their ability to transmigrate into the brain across the BBB. Lastly, this chapter delves into the role of CD4 T cells in chronic SIV infection, revealing that acute depletion of CD4 T cells from the CNS continues well into the chronic phase of infection. The long-term depletion of CD4 T cells in the is concerning, given their importance in mice for learning behavior and controlling latent CNS viruses, highlighting potential complications in managing chronic SIV/HIV infection (6, 7).

Chapter IV advances the research presented in the previous chapters by comprehensively characterizing the T lymphocyte populations in the CNS during homeostasis and SIV infection, employing emerging technologies such as single cell and spatial transcriptomics. A key finding of

this chapter is the identification of CCR7+ CD4 T cells in the CNS, that are characteristic of a T_{CM} phenotype. These cells exhibit chromatin accessibility of T_{CM} gene loci (CCR7, CD28, and BCL6), recall proliferation/IL-2 production, and their surface protein expression (CD95+, CCR7+, CD69-) is consistent with T_{CM} found in peripheral tissues. Notably, we observed a depletion of these T_{CM} like cells in the brain during chronic infection with the neurotropic virus SIVCL757. These observations were paired with evidence of microglial activation and neurodegenerative gene signatures.

Future research should prioritize several areas. First, it is essential to employ T-cell receptor (TCR) sequencing to identify the specific antigens that T cells in the NHP brain respond to during both normal conditions and SIV infection. Although it is known that T-cell activation, regardless of the antigen's specificity, can drive T-cell migration to the brain, the exact nature of these antigens, particularly whether T cells target SIV or other viruses like herpesviruses, remains unclear (9). Previous studies have found Epstein-Barr Virus (EBV)-specific T cells in the CSF of patients with Alzheimer's Disease, suggesting that the CNS TCR pool could comprise a variety of potential antigenic targets (10).

Another critical area of focus is improving our understanding of how these T cells are distributed within the brain under both homeostasis and during infection. One key difficulty when visualizing T cells within the primate CNS via IHC is that they are rare and are difficult to find in the absence of inflammation or infection. Enhancements in staining methods, development of RNA-based microscopy technologies, and RNA seq platforms are all great approaches to enhance our understanding of homeostatic T lymphocytes within the CNS. At homeostasis, we identified that CD8 T cells are more prominent that CD4 T cells within the CNS tissues globally, in future studies it would be interesting to identify if there are any differences in localization of these two populations across the CNS tissues by employing flow and histology-based techniques.

By addressing these focal points, future studies can significantly advance our understanding of T cell behavior in the CNS during health and disease.

Future studies using mouse models could help unravel the mechanistic questions behind HIV infection and HIV pathology of the CNS. Established models, such as NSG (NOD SCID IL2R gamma null mice), are extremely immunodeficient and often commonly utilized as transplant recipients for human bone marrow, liver, and thymus, often dubbed BLT mice. These mice host human lymphocytes, making them susceptible to HIV infection. BLT mice have previously shown that T cells, in the absence of myeloid cells establish HIV infection within the mouse brain (11). This model offers a valuable platform for testing therapeutic antibodies designed to inhibit T cell migration to the CNS. The mouse model provides an opportunity to explore strategies for controlling T cell movement to the CNS. This can be achieved by targeting integrins (e.g. LFA-1) or chemokines (such as CXCR3, CCR5, CCR6) that facilitate their trafficking. However, a major challenge in this approach is to selectively inhibit CD4 T cell migration to prevent the virus from seeding in the CNS, without hindering CD8 T cell movement, which is crucial for immune surveillance and protection against latent viruses, including herpesviruses, within the CNS.

The CNS is a complex network of various cell types that interact closely with each other. Among these, astrocytes play a crucial role in supporting neuronal differentiation and homeostasis, contributing to the blood-brain barrier's formation, and forming the glia limitans. As the most abundant cell type in the CNS, astrocytes have the ability to either mitigate or exacerbate neuroinflammation and frankly have been ignored in favor of microglia. Astrocytes can dampen microglia activation by secreting anti-inflammatory agents such as transforming growth factor B and prostaglandin E (12, 13). Additionally, astrocytes can induce FasL mediated apoptosis of T cells (14-16). Conversely, astrocytes are a major source of proinflammatory cytokines IL-1β and IL-6, contributing to the neuroinflammatory process (17, 18). In other models of neuroinflammation such as Alzheimer's and Parkinson’s disease, astrocytes are commonly found to be activated (19-

21). Furthermore, in the presence of IFN-γ, typically produced by Th1 cells, astrocytes become activated secreting chemokines such as CCL3, CCL5, CXCL8, and CXCL10 to drive the neuroinflammatory process (22). The role of astrocytes in blood brain barrier integrity and their interphase/interaction with T cells warrants further investigation in animal models and in HAND patients.

In summary, my dissertation emphasizes the need for a deeper understanding of the role of CD4 T cells in the neuropathogenesis of HAND.

REFERENCES

1. Nightingale S, Winston A, Letendre S, Michael BD, McArthur JC, Khoo S, et al. Controversies in HIV-associated neurocognitive disorders. *Lancet Neurol.* 2014;13(11):1139-51.
2. Louveau A, Smirnov I, Keyes TJ, Eccles JD, Rouhani SJ, Peske JD, et al. Structural and functional features of central nervous system lymphatic vessels. *Nature.* 2015;523(7560):337-41.
3. Smolders J, Heutinck KM, Fransen NL, Remmerswaal EBM, Hombrink P, Ten Berge IJM, et al. Tissue-resident memory T cells populate the human brain. *Nat Commun.* 2018;9(1):4593-.
4. Cugurra A, Mamuladze T, Rustenhoven J, Dykstra T, Beroshvili G, Greenberg ZJ, et al. Skull and vertebral bone marrow are myeloid cell reservoirs for the meninges and CNS parenchyma. *Science.* 2021;373(6553).
5. Sharma V, Creegan M, Tokarev A, Hsu D, Slike BM, Sacdalan C, et al. Cerebrospinal fluid CD4+ T cell infection in humans and macaques during acute HIV-1 and SHIV infection. *PLOS Pathogens.* 2021;17(12):e1010105.
6. Kipnis J, Cohen H, Cardon M, Ziv Y, and Schwartz M. T cell deficiency leads to cognitive dysfunction: implications for therapeutic vaccination for schizophrenia and other psychiatric conditions. *Proc Natl Acad Sci U S A.* 2004;101(21):8180-5.
7. Ai S, and Klein RS. Update on T cells in the virally infected brain: friends and foes. *Curr Opin Neurol.* 2020;33(3):405-12.
8. Kivisäkk P, Mahad DJ, Callahan MK, Sikora K, Trebst C, Tucky B, et al. Expression of CCR7 in multiple sclerosis: Implications for CNS immunity. *Annals of Neurology.* 2004;55(5):627-38.
9. Schläger C, Körner H, Krueger M, Vidoli S, Haberl M, Mielke D, et al. Effector T-cell trafficking between the leptomeninges and the cerebrospinal fluid. *Nature.* 2016;530(7590):349-53.
10. Gate D, Saligrama N, Leventhal O, Yang AC, Unger MS, Middeldorp J, et al. Clonally expanded CD8 T cells patrol the cerebrospinal fluid in Alzheimer's disease. *Nature.* 2020;577(7790):399-404.
11. Honeycutt JB, Liao B, Nixon CC, Cleary RA, Thayer WO, Birath SL, et al. T cells establish and maintain CNS viral infection in HIV-infected humanized mice. *J Clin Invest.* 2018;128(7):2862-76.
12. Font-Nieves M, Sans-Fons MG, Gorina R, Bonfill-Teixidor E, Salas-Pérdomo A, Márquez-Kisinousky L, et al. Induction of COX-2 enzyme and down-regulation of COX-1 expression by lipopolysaccharide (LPS) control prostaglandin E2 production in astrocytes. *J Biol Chem.* 2012;287(9):6454-68.
13. Vincent VA, Tilders FJ, and Van Dam AM. Inhibition of endotoxin-induced nitric oxide synthase production in microglial cells by the presence of astroglial cells: a role for transforming growth factor beta. *Glia.* 1997;19(3):190-8.
14. Bechmann I, Lossau S, Steiner B, Mor G, Gimsa U, and Nitsch R. Reactive astrocytes upregulate Fas (CD95) and Fas ligand (CD95L) expression but do not undergo programmed cell death during the course of anterograde degeneration. *Glia.* 2000;32(1):25-41.
15. Choi C, Park JY, Lee J, Lim JH, Shin EC, Ahn YS, et al. Fas ligand and Fas are expressed constitutively in human astrocytes and the expression increases with IL-1, IL-6, TNF-alpha, or IFN-gamma. *J Immunol.* 1999;162(4):1889-95.
16. Bechmann I, Mor G, Nilsen J, Eliza M, Nitsch R, and Naftolin F. FasL (CD95L, Apo1L) is expressed in the normal rat and human brain: evidence for the existence of an immunological brain barrier. *Glia.* 1999;27(1):62-74.

17. Aloisi F, Carè A, Borsellino G, Gallo P, Rosa S, Bassani A, et al. Production of hemolymphopoietic cytokines (IL-6, IL-8, colony-stimulating factors) by normal human astrocytes in response to IL-1 beta and tumor necrosis factor-alpha. *J Immunol.* 1992;149(7):2358-66.
18. Luo C, Jian C, Liao Y, Huang Q, Wu Y, Liu X, et al. The role of microglia in multiple sclerosis. *Neuropsychiatr Dis Treat.* 2017;13:1661-7.
19. Akiyama H, Arai T, Kondo H, Tanno E, Haga C, and Ikeda K. Cell mediators of inflammation in the Alzheimer disease brain. *Alzheimer Dis Assoc Disord.* 2000;14 Suppl 1:S47-53.
20. Xia MQ, Bacskai BJ, Knowles RB, Qin SX, and Hyman BT. Expression of the chemokine receptor CXCR3 on neurons and the elevated expression of its ligand IP-10 in reactive astrocytes: in vitro ERK1/2 activation and role in Alzheimer's disease. *J Neuroimmunol.* 2000;108(1-2):227-35.
21. Hirsch EC, Breidert T, Rousselet E, Hunot S, Hartmann A, and Michel PP. The role of glial reaction and inflammation in Parkinson's disease. *Ann N Y Acad Sci.* 2003;991:214-28.
22. Jehs T, Faber C, Juel HB, and Nissen MH. Astrocytoma cells upregulate expression of pro-inflammatory cytokines after co-culture with activated peripheral blood mononuclear cells. *Apmis.* 2011;119(8):551-61.

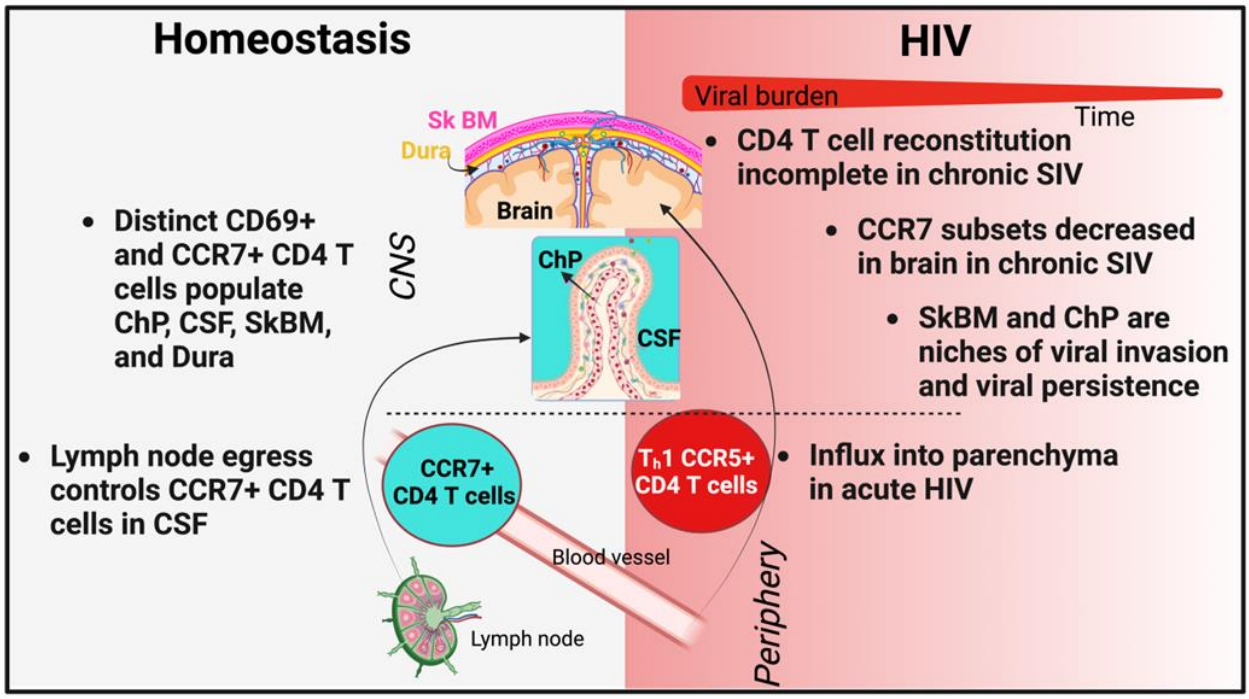

Figure 1. Dynamics of CNS T Lymphocyte Populations at homeostasis and during SIV Infection. A visualization of the dissertation's central findings, focused on the observed T lymphocyte populations in the rhesus macaque CNS at homeostasis (left; grey) and the phenotypic changes observed in CNS T lymphocytes during acute viral dissemination (right; red).